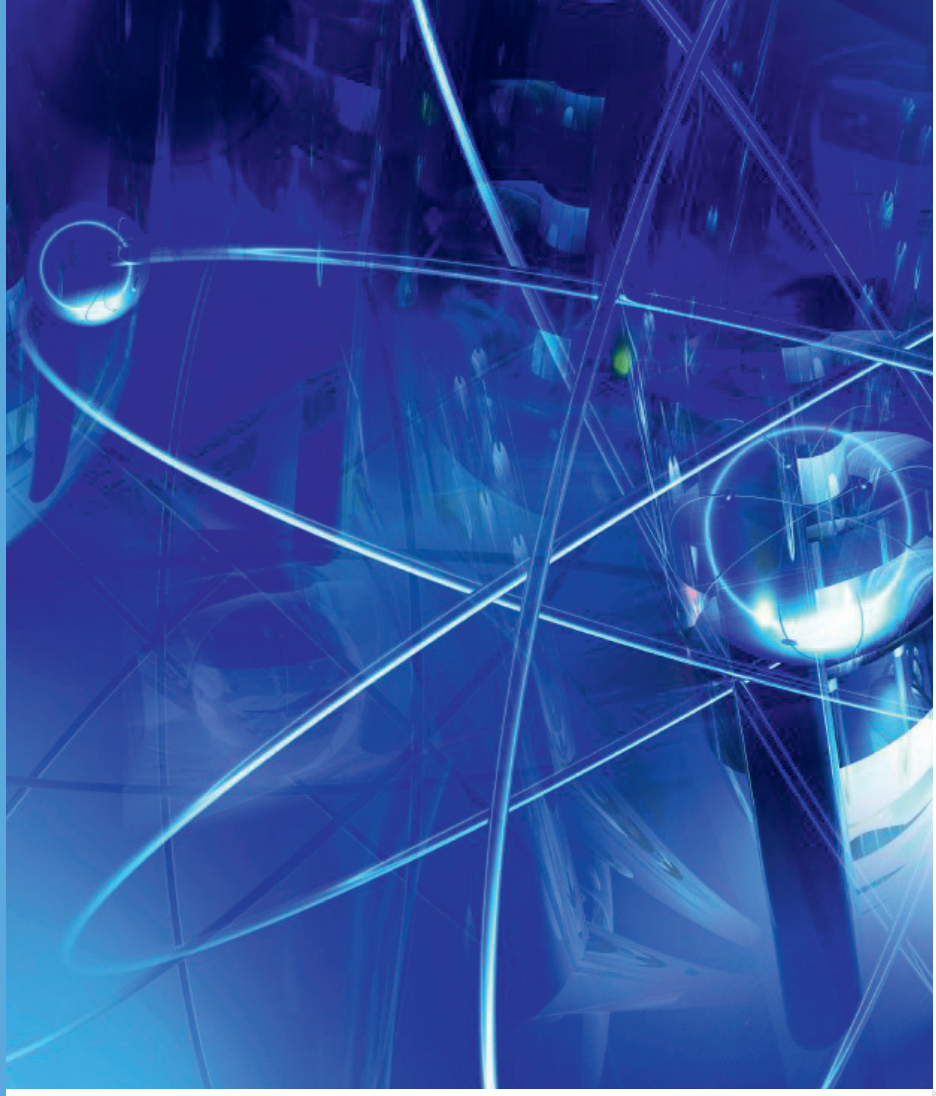

SCIENCE • TECHNOLOGY • RESEARCH HIGHLIGHTS • VISIONS •

Dissertation
42

Simplifying solute transport modelling of the geological multi-barrier disposal system

Antti Poteri

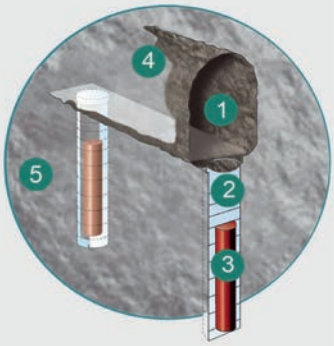

VTT SCIENCE 42

Simplifying solute transport modelling of the geological multi-barrier disposal system

Antti Poteri

Thesis for the degree of Doctor of Science in Technology to be presented with due permission for public examination and criticism in Auditorium F239a, Otakaari 3, at Aalto University (Espoo, Finland) on the 29th of November 2013 at 12 o'clock noon.

ISBN 978-951-38-8097-2 (Soft back ed.)
ISBN 978-951-38-8098-9 (URL: http://www.vtt.fi/publications/index.jsp)

VTT Science 42

ISSN-L 2242-119X
ISSN 2242-119X (Print)
ISSN 2242-1203 (Online)

JULKAISIJA – UTGIVARE – PUBLISHER

VTT
PL 1000 (Tekniikantie 4 A, Espoo)
02044 VTT
Puh. 020 722 111, faksi 020 722 7001

VTT
PB 1000 (Teknikvägen 4 A, Esbo)
FI-02044 VTT
Tfn +358 20 722 111, telefax +358 20 722 7001

VTT Technical Research Centre of Finland
P.O. Box 1000 (Tekniikantie 4 A, Espoo)
FI-02044 VTT, Finland
Tel. +358 20 722 111, fax + 358 20 722 700

Kopijyvä Oy, Kuopio 2013

Simplifying solute transport modelling of the geological multi-barrier disposal system

Moniesteperiaatteeseen perustuvan geologisen loppusijoitusjärjestelmän yksinkertaistettu kulkeutumismalli. **Antti Poteri.** Espoo 2013. VTT Science 42. 63 p. + app. 141 p.

Abstract

A simplified model was developed to represent radionuclide migration from a deep geological nuclear waste repository system to the biosphere. The modelled repository system is based on the concept of multiple nested transport barriers. The model can be used to assess migration and migration properties of single nuclides (no decay chains) through the repository system. Radionuclide transport processes included to the model are diffusion and sorption in the repository near-field and advection, matrix diffusion and sorption in the geosphere. A simplified approach to handle solubility limited release of the nuclide from the waste canister is included into the model.

The model treats transport barriers as well-mixed volumes. It is also assumed that radionuclide outflow from a barrier can be calculated by neglecting radionuclide concentration in the target barrier. Radionuclide transport through the simplified system can be calculated by applying formal analogy of the model to the mathematical model of the radioactive decay chain.

Simplifying the barriers as well-mixed volumes suggests that they can be characterised by simple performance measures. Radionuclide outflow from the barrier can be represented by an equivalent flow rate, which is an apparent volumetric flow rate that combined with the radionuclide concentration in the barrier gives the outflow rate of the nuclide. Temporal behaviour of the release rate can be described by two time constants: i) compartment half-life of the nuclide concentration calculated by dividing capacity of the barrier (the total pore volume multiplied by the retardation factor) with the equivalent flow rate and ii) delay time for start of the outflow from barrier after beginning of the inflow to barrier.

Performance of the simplified approach to produce actual release rates for different nuclides was tested by modelling C-14, I-129 and Pu-239 using data from the RNT-2008 radionuclide migration analysis. Accuracy of the simplified approach is challenged if the nuclide's half-life is not long compared to the time required for the development of perfectly mixed solute concentration field in the barrier. The nuclide and barrier combinations that are prone to this behaviour can be identified by comparing the estimated compartment delay time with the nuclide's radioactive half-life. The simplified model performed well for the C-14 and I-129, as expected based on the measures above. Early transients of the concentration field in the buffer and in the geosphere are important for the transport of Pu-239 in the calculated case. The simplified model gave results for Pu-239 that were roughly of the same order of magnitude than the corresponding numerical results.

Keywords nuclear waste, repository system, migration, modelling

Moniesteperiaatteeseen perustuvan geologisen loppusijoitusjärjestelmän yksinkertaistettu kulkeutumismalli

Simplifying solute transport modelling of the geological multi-barrier disposal system.
Antti Poteri. Espoo 2013. VTT Science 42. 63 s. + liitt. 141 s.

Tiivistelmä

Tässä työssä on kehitetty yksinkertaistettu malli kuvaamaan radionuklidien kulkeutumista geologisesta loppusijoitustilasta maanpinnalle. Mallinnettu loppusijoitusjärjestelmä perustuu moniesteperiaatteeseen. Mallin avulla on mahdollista arvioida yksittäisen nuklidin kulkeutumista ja kulkeutumisominaisuuksia loppusijoitussysteemissä. Kulkeutumisprosesseista malli sisältää loppusijoitustilan lähialueella diffuusion ja sorption sekä geosfäärissä kulkeutumisen pohjaveden virtauksen mukana, matriisidiffuusion ja sorption. Malliin on lisätty myös yksinkertaistettu kuvaus nuklidin liukoisuusrajoitteiselle vapautumiselle loppusijoituskapselista.

Vapautumisesteet kuvataan mallissa hyvin sekoitettuina tilavuuksina ja massasiirron vapautumisesteestä ulos oletetaan riippuvan konsentraatiosta vain tarkasteltavassa vapautumisesteessä. Tällainen systeemi on matemaattisesti analoginen radioaktiivisen hajoamisketjun kanssa. Tätä analogiaa käytetään hyväksi laskettaessa radionuklidien kulkeutuminen loppusijoitussysteemin läpi.

Hyvin sekoitetun tilavuuden malli mahdollistaa vapautumisesteen toiminnan kuvaamisen muutamalla tunnusluvulla. Nuklidin vapautumisnopeus loppusijoitusjärjestelmän vapautumisesteestä voidaan esittää ekvivalentin virtaaman avulla. Ekvivalentti virtaama on näennäinen tilavuusvirtaama, joka pitoisuuteen yhdistettynä antaa aineen massavirran. Vapautumisnopeuden aikakehitystä voidaan kuvata kahdella vapautumiseste- ja nuklidikohtaisella aikavakiolla: i) nuklidin pitoisuuden puoliintumisaika, joka voidaan laskea jakamalla vapautumisesteen nuklidikohtainen kapasiteetti (huokostilavuuden ja nuklidikohtaisen pidätyskertoimen tulo) nuklidin ekvivalentilla virtaamalla ulos vapautumisesteestä sekä ii) massan siirron viipymäaika vapautumisesteessä.

Yksinkertaistetun mallin kykyä arvioida radionuklidien vapautumisnopeuksia testattiin mallintamalla nuklidien C-14, I-129 ja Pu-239 aktiivisuusvirrat yhdelle RNT-2008 kulkeutumisanalyysin laskentatapaukselle. Mallin tarkkuus heikkenee, jos nuklidin radioaktiivinen puoliintumisaika ei ole pitkä verrattuna aikaan, joka vaaditaan hyvin sekoitetun pitoisuuden saavuttamiseen vapautumisesteessä. Tällaiset nuklidit ja vapautumisesteparit on kuitenkin mahdollista tunnistaa vertaamalla nuklidin radioaktiivista puoliintumisaikaa ja massan siirron viivettä vapautumisesteessä. Malli tuotti vertailuna käytetyn numeerisen mallin kanssa yhtenevät tulokset nuklideille C-14 ja I-129, kuten edellä mainitun vertailun perusteella oli odotettavissa. Pu-239:n puoliintumisajan ja kulkeutumisnopeuden perusteella sen vapautumisnopeudet lasketussa tapauksessa sekä sijoitusreiän täyteaineesta että geosfääristä voivat määräytyä pitoisuuskentän transienttisesta käyttäytymisestä vapautumisesteessä. Mallin tuottamat tulokset vapautumisnopeudelle ovat kuitenkin tässäkin tapauksessa suunnilleen samaa suuruusluokkaa kuin numeerisen mallin tulokset.

Avainsanat nuclear waste, repository system, migration, modelling

Preface

This study was conducted at VTT Technical Research Centre of Finland, as a part of the nuclear waste management studies financed by Posiva Oy. The work was carried out under a number of separate projects over a period of several years. I am most grateful to Professor Rainer Salomaa of Aalto University School of Science for his patience and encouragement during this time. His comments to the manuscript of this thesis were very valuable.

The starting point of this work came about through discussions with Dr. Aimo Hautojärvi at Posiva Oy on alternative modelling approaches that could be used to describe the essence of the geological multi-barrier system. I am very grateful to Dr. Hautojärvi for his numerous suggestions and advice, which helped to keep the work focused on the essentials and which also considerably improved the manuscript. I also like to thank Dr. Kari Rasilainen and Professor Markus Olin for their comments to the manuscript.

This work would have not been possible without the contributions of the co-authors of the publications. Besides Dr. Aimo Hautojärvi, I am indebted to Henrik Nordman and Veli-Matti Pulkkanen at VTT, Dr. Pirkko Hölttä, Dr. Marja Siitari-Kauppi, Dr. Nina Huittinen and Martti Hakanen of the University of Helsinki and Dr. Pekka Kekäläinen of the University of Jyväskylä.

I am also grateful to Lasse Koskinen at Posiva Oy, Jari Löfman and other present and former colleagues at VTT for our inspiring and interesting discussions, which created an enjoyable working environment. I would also like to thank Dr. Paul Smith at SAM Ltd. and Dr. José Luis Cormenzana at ENRESA for their comments and suggestions during the early stages of the project. I am sincerely grateful to Professor Jussi Timonen and Mikko Nykyri for thorough reviewing of the manuscript of the Publication [I].

Espoo, October 2013 Antti Poteri

Academic dissertation

Supervisor
Prof. Rainer Salomaa
Department of Applied Physics
Aalto University, Finland

Reviewers
Prof. Markku Kataja
Department of Physics
University of Jyväskylä, Finland

Prof. Dr. Klaus-Jürgen Röhlig
Institut für Endlagerforschung
TU Clausthal, Germany

Opponent
Prof. Anders Wörman
Kunglika Tekniska Högskolan
Institutionen för Byggvetenskap
Teknikringen 76
100 44 Stockholm, Sverige

List of publications

This thesis is based on the following original publications which are referred to in the text as [I–V]. The publications are reproduced with kind permission from the publishers

I Poteri, A., Nordman, H., Pulkkanen, V.-M., Hautojärvi, A. and Kekäläinen, P. Representing solute transport through the multi-barrier disposal system by simplified concepts. Posiva report series, Posiva Oy, Olkiluoto, Finland, 2012. Report Posiva 2012-20. 90 p. + app. 4 p.

II Poteri, A. Retention properties of flow paths in fractured rock, Hydrogeology Journal. Vol. 17 (2009) No: 5, pp. 1081–1092. doi: 10.1007/s10040-008-0414-y.

III Hölttä, P., Poteri, A., Siitari-Kauppi, M. and Huittinen, N. Retardation of mobile radionuclides in granitic rock fractures by matrix diffusion, 2008. Physics and Chemistry of the Earth. Vol. 33 (2008) No: 14–16, pp. 983–990. doi: 10.1016/j.pce.2008.05.010

IV Hölttä, P., Poteri, A., Hakanen, M. and Hautojärvi, A. Fracture flow and radionuclide transport in block-scale laboratory experiments. Radiochimica Acta Vol. 92 (2004), pp. 775–779.

V Hölttä, P., Siitari-Kauppi, M., Huittinen, N. and Poteri, A. Determination of matrix diffusion properties of granite, Materials Research Society Symposium Proceedings. Vol. 985 (2007), pp. 557–562.

Author's contributions

Most of the publications included in this thesis were produced jointly by a group of co-authors. Publication [I] is based on discussions with Dr. Aimo Hautojärvi to simplify and clarify the role of the different transport barriers in a geological repository of nuclear waste. The studied hypothesis was that the transport barrier system could be modelled as a chain of barriers described by response functions that limit and delay transport through them. Such a system could be further greatly simplified and components compared with each other by representing the transport barriers as well-mixed volumes. This would lead to a straightforward and concise representation of the whole repository system analogously to the radioactive decay chain. The author's contribution was to develop the calculation system and tools, to study the validity of the simplified modelling concept. The author wrote the whole Publication [I], he conducted all of the modelling work presented in the Publication [I], except the numerical verification of the transport through the barrier system and diffusion through the bentonite buffer, which were carried out by co-authors Henrik Nordman and Veli-Matti Pulkkanen. Dr. Pekka Kekäläinen checked and advised on the mathematical formulation of the transport equations.

Publication [II] is based on the modelling work carried out by the task force on groundwater flow and transport of solutes of the Äspö Hard Rock Laboratory in Sweden. The modelling task studied solute transport in fractured rock under different flow conditions. Modelling issues were discussed between the different modelling groups during the course of the work. The author was solely responsible for the modelling work and writing of the Publication [II].

Publications [III–V] present studies on tracer and hydraulic testing of crystalline rock in laboratory. All modelling of these tests was conducted by the author excluding the I-131 modelling in Publication [III], which was carried out by Dr. Pirkko Hölttä. The author has also contributed to the planning of the tests and writing of the modelling parts of the publications. In addition to the publications included to this thesis, the author has also contributed to the studies on migration in the geosphere in the context of the in-situ tracer tests [26, 27, 28, 29, 30, 31 and 32] and in the context of the performance assessment of the nuclear waste repository [33].

Contents

List of symbols and abbreviations

KBS	Nuclear Fuel Safety Project (KBS – kärnbränslesäkerhet) of Swedish power companies in late 1970s
KBS-3	Geological final repository concept developed within the KBS project in Sweden
KBS-3V	KBS-3 repository concept based on vertical deposition holes and vertical emplacement of the waste canisters
PA	Performance assessment of nuclear waste repository using models to simulate the long-term behaviour of different barriers
RNT-2008	An interim safety case report of Posiva Oy on the radionuclide release and transport analysis, reported in the year 2008
SC	Site characterisation.
c-b-f	Release path via canister-buffer-facture
c-b-t-f	Release path via canister-buffer-tunnel-fracture
cb	Notation for the canister to buffer interface
bf	Notation for the buffer to fracture interface
bt	Notation for the buffer to tunnel interface
tf	Notation for the tunnel to fracture interface
f	Notation for the fracture to biosphere interface
m_c	Solute mass in the canister [M]
m_b	Solute mass in the buffer [M]
m_t	Solute mass in the section of tunnel above the deposition hole [M]
m_f	Solute mass in the geosphere [M]
$\dot{m}_{out}$	Solute mass flow to the biosphere [M/T]

λ	Mass transfer coefficient [1/T]
λ_c	Mass transfer coefficient from canister to buffer [1/T]
λ_{bf}	Mass transfer coefficient from buffer to fracture [1/T]
λ_{bt}	Mass transfer coefficient from buffer to tunnel [1/T]
λ_{tf}	Mass transfer coefficient from tunnel to fracture [1/T]
λ_f	Mass transfer coefficient from fracture to geosphere [1/T]
t_d	Delay time [T]
t_{dc}	Delay time from canister to buffer [T]
t_{dbf}	Delay time from buffer to fracture [T]
t_{dbt}	Delay time from buffer to tunnel [T]
t_{dtf}	Delay time from buffer to fracture [T]
t_{df}	Delay time in geosphere [T]
δ	Dirac Delta function $\delta(t)$ [1/T]
δ_τ	$\delta(t-\tau)$ [1/T]
q	Equivalent flow rate [L^3/T]
q_c	Equivalent flow rate from canister to buffer [L^3/T]
q_{bf}	Equivalent flow rate from buffer to fracture [L^3/T]
q_{bt}	Equivalent flow rate from buffer to tunnel [L^3/T]
q_{tf}	Equivalent flow rate from tunnel to fracture [L^3/T]
q_f	Equivalent flow rate in geosphere [L^3/T]
$T_{1/2}$	Compartment half-life [T]
$T_{1/2}^c$	Compartment half-life in the canister [T]
$T_{1/2}^{bf}$	Compartment half-life for the release path from buffer to fracture [T]
$T_{1/2}^{bt}$	Compartment half-life for the release path from buffer to tunnel [T]
$T_{1/2}^t$	Compartment half-life in the section of tunnel above the deposition hole [T]
$T_{1/2}^f$	Compartment half-life in geosphere [T]
R	Retardation factor [-]
V_p	Pore volume [L^3]

1. Introduction

Spent nuclear fuel from Finnish nuclear power plants is planned to be disposed of in a geological repository hosted in deep crystalline bedrock [34]. The planned repository system has the objective to ensure that the spent nuclear fuel is reliably contained until its radioactivity has decayed to a harmless level.

Performance of the repository system is based on two functions. First, it should provide stable and predictable conditions for the waste canisters. This facilitates canisters to maintain the tightness. The repository system is based on multiple nested barriers that prevent possible future disturbances to impair waste canisters, or it will at least significantly attenuate the possible disturbances in the proximity of the waste canisters. This decreases significantly the probability that waste canisters will fail in the near future when the radioactivity of the waste is still high.

The second function of the repository system is to limit radionuclide release rates in case there is a leaking waste canister. This safety function of the repository performance is handled in the repository performance assessment by considering sufficiently complete set of different radionuclide release and transport scenarios, that is alternative sequences of possible events or processes connected to the radionuclide release and transport. A defective waste canister that is leaking radionuclides to the groundwater is one of the key scenarios analysed in the past performance assessments of the repository system [10, 22 and 35]. The canister may be, for example, initially defective due to the flaw in manufacturing. Corrosion of the canister could then penetrate the wall of the canister. A small hole is created through which the release of the radionuclides can take place. The repository system should retard and limit migration of the radionuclides from the repository to the biosphere, such that the radiological effects in the biosphere will be insignificant. This thesis focuses on this second safety function of the repository system to limit radionuclide release rates in case of a leaking waste canister. The scenario considered in detail is based on release from canister through a small hole. However, the simplified approach is not limited to this scenario.

Performance of the final repository system that is suitable for the granitic crystalline rock has been studied already for a few decades [10, 22, 18, 35, 36, 37, 38, 39, 40, 41 and 42]. The plans in Finland are based on the Swedish KBS-3 concept [18], in which the waste is encapsulated into corrosion resistant copper canisters that are disposed of at about 400–500 m depth in the bedrock. Flow and transport

of solutes in the vicinity of the canister is limited by low permeable bentonite clay buffer around the canisters. Each canister contains about 2 tons of the spent nuclear fuel and the present plans for the repository comprises about 4 500 canisters. Radionuclide release and transport for this kind of system has been analysed in a number of Finnish performance assessments [10, 22, and 35]. Similar systems have also been analysed for example in Sweden [18, 38 and 40], Switzerland [41], France [36], Canada [39] and Japan [42]. These assessments have been based on detailed numerical analysis of the radionuclide releases and transport for varying scenarios of the future events and conditions. The present simplified approach aims not to replace the detailed numerical analysis. The aim is to provide a complementary approach to characterise the different components of the repository system so that the importance of the different barriers for the overall performance of the system to limit radionuclide transport can be easily and transparently identified.

1.1 The multi-barrier system

The performance of the geological repository is based on nested transport barriers that form a multi-barrier system to hinder transport of radionuclides from the waste canisters to the biosphere. The repository system studied in this thesis is based on the KBS-3V concept [18] illustrated in Figure 1.

The planned performance of the repository system aims to long-term containment of the waste in the waste canisters [21]. Engineered barriers are designed to support this function of the repository under the expected conditions in the host rock. However, as noted earlier the present thesis concentrates on the second function of the repository that is to limit radionuclide release rates in case there is a leaking waste canister. In this concept, the transport barriers and their main safety functions with respect to radionuclide transport are the following [21]:

- Canister: a copper waste canister with iron insert built to withstand expected mechanical loads. The canister is resistant to corrosion and, under the expected evolution of conditions, should remain intact for at least 100,000 years [14, 43 and 44]. There have been claims on much quicker corrosion [46], but these results are considered controversial [45]. In the KBS-3V concept, the canisters will be emplaced in vertical deposition holes drilled in the floors of the disposal tunnels.
- Buffer: protects the canister against minor rock movements and prevents groundwater flow in the immediate vicinity of the canister. Experiments have shown that hydraulic conductivity of water in bentonite is very low, about 10^{-13} m/s or less [e.g. 47, 48 and 49]. This ensures that transport of solutes in the buffer takes place by diffusion only. The buffer surrounds the waste canister in the deposition hole such that the canister becomes isolated from the bedrock.
- Tunnel backfill: prevents significant groundwater flow in the tunnels. Hydraulic conductivity of the backfill depends on the bentonite content of the

backfill. The design basis is a hydraulic conductivity that is less than 10^{-10} m/s under the expected conditions [50]. The backfill also provides mechanical stability for the tunnels and for the buffer in the deposition hole.

- Bedrock: provides predictable conditions and isolates the repository against surface and near-surface processes. The block structure of the crystalline bedrock dissipates stress along the fracture zones and the rock mass between the zones is geologically stabile [51]. The geochemistry of the deep groundwater, e.g. salinity, indicates slow movement and exchange of solutes of the groundwater [51 and 53]. Lately, it has been noted that even the influences of the possibly violent hydraulic disturbances on the surface caused by the glacial cycle are likely to be strongly attenuated inside the block of rock surrounded by the major fracture zones [52]. This indicates that in the repository scale the bedrock is able to limit both inflow of the harmful substances to the repository and possible releases of radionuclides from the repository to the biosphere. However, it is not impossible that a future shear movement of the rock affects transport properties around a single or a few canister locations. Function of the repository system under these kinds of events is commonly handled by separate considerations [c.f. 10 and 40].

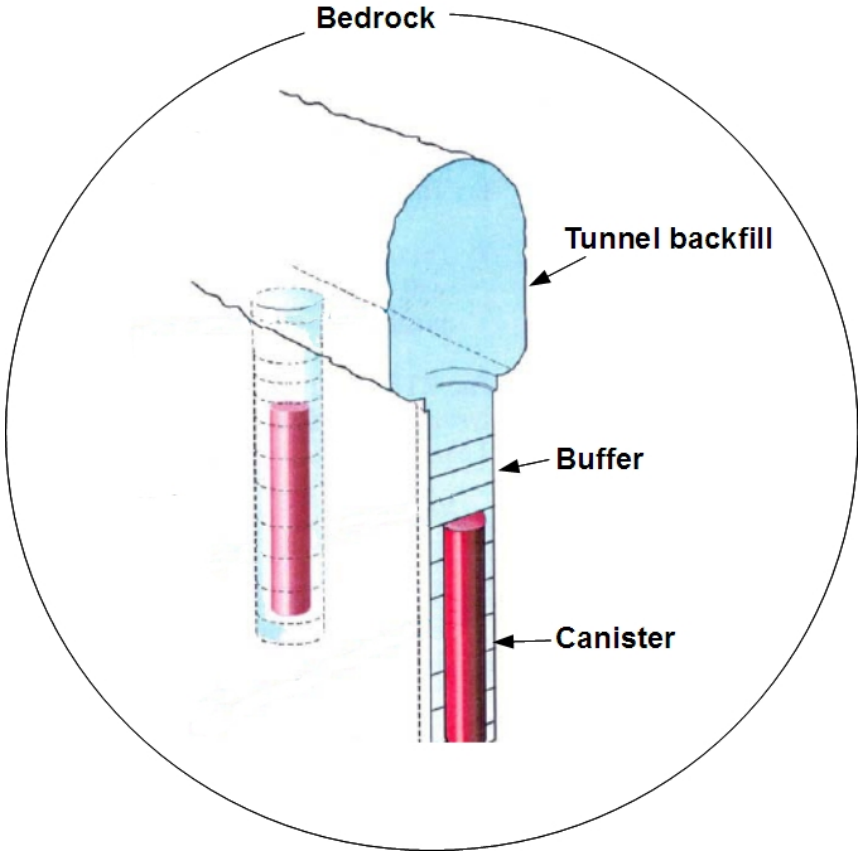

Figure 1. The main transport barriers in the KBS-3V disposal concept (based on [21]).

Transport and retention processes considered in the present model include advection, molecular diffusion and sorption. Sorption is represented by linear equilibrium sorption, in which a fixed distribution coefficient (K_d) gives the ratio of sorbed and non-sorbed phases of the nuclide concentration. A retardation factor, R in Equation (1), is calculated to measure retention caused by the sorption

$$R = 1 + \frac{1-\varepsilon}{\varepsilon}\rho K_d, \quad (1)$$

where $\boldsymbol{\varepsilon}$ is porosity and $\boldsymbol{\rho}$ is bulk density.

1.2 Radionuclide release paths

The release paths of radionuclides from the waste canister must pass the transport barriers introduced in the previous section and illustrated in Figure 1.

Schematically, the topology of the release paths can be represented by the flow chart given in Figure 2.

Release and transport of radionuclides from the repository to the biosphere is possible if the waste canister loses its integrity and becomes filled with groundwater. This process would involve the following stages of radionuclide migration:

- Radionuclides are released from the fuel matrix into the water in the canister. Part of the inventory of some nuclides could be released instantaneously when leaking commences. Remaining part of the inventory is released through degradation of the fuel matrix and metal parts [54 and 55]. In the present thesis, the release of radionuclides is considered as a source of radionuclides and not as a transport barrier.

- Nuclides escape from the water-filled canister via the same hole through which groundwater penetrated the canister. The hole may e.g. result from an initial defect in the canister that develops into a penetrating hole due to corrosion [56 and 57]. In the cases dealt within this study, there is no advection from the canister to the buffer. A part of the inventory could be released from canister in gas phase immediately after integrity of the canister is lost. The gas mediated transport is not considered in the present thesis.

- The waste canister is isolated from the surrounding rock and from the deposition tunnel above by the buffer material. The possibility that canister sinks such that the transport barrier function of the buffer is lost is considered to be low, because conventional soil-mechanical calculations indicate a maximum sinking of 1 to 5 mm in 10 000 years with decreasing rate of sinking with time [c.f. 78]. Nuclides must pass the buffer to reach the outflow locations on the outer boundary of the buffer. The buffer material is compacted bentonite clay that swells when saturated. This prevents formation of continuous flow paths inside the deposition hole. The saturated buffer material becomes hydraulically impermeable and mass transfer through it takes place only by molecular diffusion [e.g. 58]. The background rock matrix that hosts the deposition hole is in practice impermeable as well [1 and 65] and solute can migrate through the rock matrix only by molecular diffusion. This makes the transport path directly through the background rock mass extremely slow and negligible from the safety point of view. More efficient transport routes are established from the buffer to the tunnel backfill and from the buffer to a flowing fracture intersecting the deposition hole, in case such a fracture exists. The approach taken in this work is that transport of radionuclides is divided between the path from the buffer to the tunnel and from the buffer to a sub horizontal fracture which, conservatively assumed, intersects the deposition hole at the location of the hole in the canister.

- Deposition holes are drilled in the floor of the tunnels [e.g. 18 and 21]. The tunnel is filled with a backfill material that has a low hydraulic conductivity in order to limit the advectional mass transport [54 and 77]. The hydraulic

conductivity of the backfill is aimed to be low enough, below 10^{-10} m/s, so that diffusion is the dominant transport process [54]. This hydraulic conductivity is about in the same order of magnitude as the average hydraulic conductivity of the rock mass at the depth of the repository [59]. This means that the tunnel is not likely to collect water over large volumes of the rock mass or provide fast flow paths for the radionuclides, assuming that the tunnel backfill performs as planned. A fracture intersecting the tunnel is the only feasible outflow location from the tunnel, following to the same reasoning as above for the fracture intersecting the deposition hole.

- Crystalline bedrock plays a central role in geological disposal regarding the KBS-3 concept. Groundwater flow and radionuclide migration through the bedrock takes place through a network of interconnected water conducting fractures [e.g. 1, 6, 12, 64 and 65]. The deposition holes and disposal tunnels will be excavated into rock at a depth of several hundreds of metres. The deep repository indicates sparse fracturing and low groundwater flow rates around the repository, and long transport distances from the repository to the biosphere. Migration through the geosphere involves processes that may prevent or delay radionuclide migration by advection and diffusion causing retention of the radionuclide migration [84]. In the present work the geosphere retention processes considered are matrix diffusion and sorption.

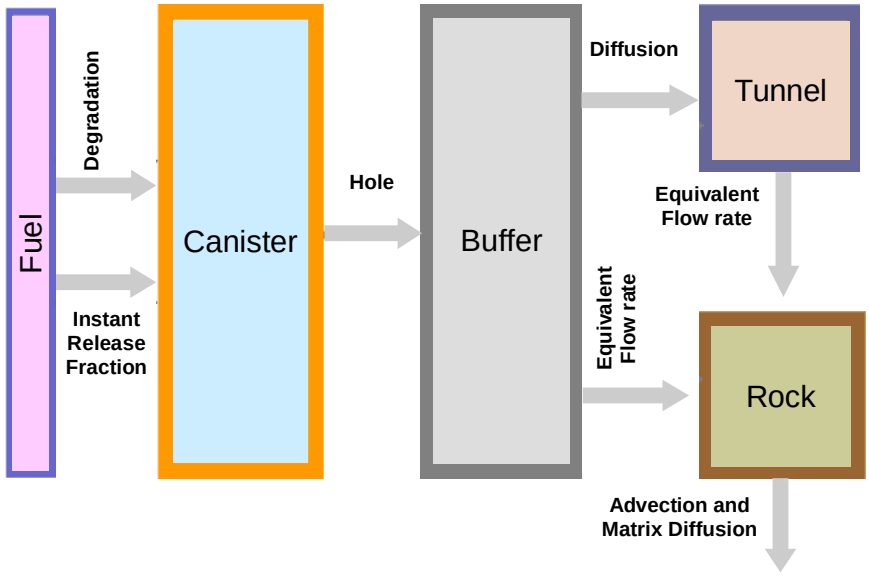

Figure 2. Release paths through the different transport barriers (based on Publication [I]).

Radionuclide release paths outlined above are based on the assumption that the different components of the repository barrier system perform as planned. Physical and chemical changes to the properties of the transport barriers during the evolution of the site cannot be completely ruled out. For example, those changes could lead to degradation of the buffer material. In this case the buffer is not able to fulfil the planned performance to prevent groundwater flow in the vicinity of the buffer [e.g. 40]. The present simplified approach provides a straightforward way to assess influences of these kinds of disturbances to the performance of the whole repository system. For example, severely degraded buffer can be conservatively removed from the system by allowing no significant retention or attenuation of the radionuclide migration in the buffer.

1.3 Radionuclide migration modelling

Radionuclide migration from the repository to the biosphere has been recently analysed as a part of the safety analysis of the underground repository, e.g. [10, 17 and 22]. Radionuclide migration in these analyses has been largely based on the application of numerical models. In many cases the repository system is handled by a suit of nested numerical codes, e.g. applying separate codes for the repository near-field and far-field analysis [e.g. 10]. Detailed numerical compartment models have also been developed to represent the whole repository system [e.g. 68] and novel numerical transport modelling approaches, e.g. based on probabilistic interpretations [69]. Numerical models are a necessity when geometrically, physically and chemically detailed and complicated systems are modelled. A drawback of numerical models, however, is the difficulty in evaluating and elucidating the role and importance of individual barriers to hinder radionuclide migration as well as key processes and parameters with regard to the performance of the system as a whole.

Representation of the repository system using simplified concepts has been studied in the past to some extent [8, 16, 66 and 67]. An analytical steady-state model based on a network of resistances has been presented by Nilsson et al. [8]. Their model focuses on transport by diffusion through the repository near field from the defective canister into a fracture that intersects the deposition hole, whereas the present model considers the whole multi-barrier system including the repository far field. In addition, their model is a steady-state model and the present model includes the time evolution of the system.

A sophisticated analytical model representing the repository near field and geosphere has been presented by Hedin [67]. His model is also able to handle nuclide ingrowth from its parent nuclide in the fuel matrix and in the canister, and longitudinal dispersion in the geosphere. These processes are not considered in the model presented in this thesis. However, at least in the cases analysed by Hedin, the ingrowth of the nuclides in the buffer or geosphere appeared not to be an important phenomenon [67]. Nuclides in the decay chains can be simulated as single nuclides and the result is used as an indicator for the efficiency of the different

transport barriers to hinder migration of these nuclides. Hedin's model handles both the waste canister and the buffer as well-mixed volumes, but gives a lumped contribution for the near field system or combined near-field and far-field system. In the present model the assumption of perfect mixing is extended for all barriers. The back coupling in mass transport between the successive barriers is neglected. The performance of the individual barriers is then given by the barrier specific characteristic times and the equivalent flow rates. The approach applied in this thesis lends itself for modifications of the release paths. Changing or adding a transport barrier in the model requires only determination of the time constant for the updated barrier and it's coupling with the neighbouring barriers.

A simplified compartment model of the repository near field system has been previously developed by Romero et al. [16 and 66]. While their model very closely resembles the present model, there are also clear differences between them. The Romero's model is based on integrated finite differences for the geometry that is represented by compartments. The model is supplemented by analytical and semi-analytical solutions at the critical points of the release paths, such as the hole in the canister and the intersection of the fracture and the buffer. The model includes decay chains and the main near field migration processes. As noted above, the present model simplifies description of the transport barrier system even further, by describing all barriers as single compartments with well-mixed solute concentration, applying analytical coupling between all compartments and neglecting the back-coupling of the mass transfer between the successive barriers.

The approach presented in this thesis does not consider radioactive decay chains. In principle, it is possible to model decay chains using the present approach. It requires that separate nuclide specific "sub-compartments" are defined into the barrier compartments. However, the main advantage of the present approach is the compact and informative description of the nuclide specific barrier properties that would have been partly lost if the decay chains were implemented to the model. Nuclides in the decay chains can be treated as single nuclides in the present approach to collect indicative information, the barrier time constants, on the efficiency of different barriers to limit transport of the nuclide.

For a single radionuclide the present approach leads to a description of the transport barrier system that is formally analogous to a branching radioactive decay chain. To author's knowledge this analogy has not been utilised earlier for modelling of the solute transport through the repository multi-barrier system. In practice, this means that the solute transport for a single radionuclide through the multi-barrier system can be represented by the Bateman's equation [62]. Solutions to this equation have also been extended to branching chains, and for longer chains than were explicitly offered in the Bateman's original work [e.g. 60 and 63]. Publication [I] applied solution for an arbitrarily long branching chain that was readily available in conjunction of another earlier work by the author [61]. Performances of the individual barriers, i.e. the barrier specific compartment half-lives of the nuclide concentration, can be approximated by simple analytical equations (Sections 3.2, 4.4 and [I]).

2. Purpose of this study

Safety analysis of the deep underground repository needs to consider the possible release of radionuclides from the waste canister and the potential for subsequent migration of the radionuclides from the repository to the biosphere. These analyses involve uncertainties due to long time-scales, parameter uncertainties and evolving conditions. Commonly these uncertainties need to be handled by applying conservative assumptions in the simulations. However, radionuclide migration analysis is not merely a computational issue. It should also demonstrate the main characteristics of the repository system that affect its performance.

The purpose of this study was to seek a simplified concept that represents the repository system as a whole as well as the role of individual barriers with respect to repository system's performance to limit radionuclide release rates. The starting points of the work were to characterise individual barriers by their response functions of mass transfer and to investigate possibility to treat the barriers as well-mixed compartments. For time invariant linear processes the total system response for any kind of barrier response functions is calculated by convolution of the individual barrier response functions. Transport properties of the barrier system can be assessed by directly comparing barrier response functions, assuming that transient phenomena, like rock shear movements or chemical changes, do not occur during the analysed period of time.

The present approach represents transport barriers of the repository system by exponential response function that in case of the repository near-field barriers is equivalent with assumption of well-mixed radionuclide concentration within the pore volume of the barrier. This offers an efficient way to characterise and analyse radionuclide migration through the barrier system. Novel features of the present approach can be summarised by following points:

- Performance of each individual transport barrier is represented by characteristic time constants derived from the capacity of the barrier and the transfer rate from that barrier to the next. The characteristic time constants are based on the assumption of well-mixed solute concentration in the barrier (Section 3.2 below).
- Performance of the repository barrier system can be assessed based on the characteristic time constants of the individual barriers. This comparison

directly indicates the main transport barriers that will govern radionuclide release rates.

- Migration of a single radionuclide through the simplified barrier system is formally analogous to the radioactive decay chain. The system behaviour can be represented by the Bateman's equation and its solutions [e.g. 60, 62 and 63].

Performance of the simplified approach to estimate nuclide specific release rates depends on the accuracy of representing mass transfer through the barrier for a given nuclide by the assumed exponential response function (well-mixed conditions). Applicability of the assumption of well-mixed conditions for the different barriers when the repository system is functioning as planned is discussed later in Section 3.2. Mass transfer through a barrier can be faster than it is determined by the well-mixed model if the performance of the barrier as a transport barrier is deteriorated. This can happen, for example, due to disturbed conditions. In the near-field barriers the faster mass transfer can take place if the total pore volume in the barrier is not easily accessible for the radionuclides compared to the outflow from the barrier. This means that there is less resistance for outflow from the barrier than for mixing inside the barrier. An example for this kind of situation is chemical or mechanical deterioration of the buffer at the fracture intersection that may also lead to advection in the buffer.

Influence of the disturbed conditions to the mass transport properties through the barriers is highly uncertain. In the repository performance assessments these uncertainties are commonly handled by making conservative assumptions, i.e. choosing parameter values that very likely overestimate the mass transfer rates. The same approach can be easily applied in the present model. As noted above, performance of the transport barriers in the present approach is represented by the characteristic time constants. The time constants depend on the mass outflows from the barrier and capacities of the barriers (total pore volume multiplied by the nuclide's retardation factor). Thus, the effect of conservative assumptions on the time constants can be easily assessed. As an ultimate conservative assumption it is also possible to "short circuit" an individual barrier by associating very short duration time constants with the barrier.

Basically, the present approach is developed for analysis of the KBS-3 type repository system assuming that the transport characteristics of the barriers follow the designed behaviour. Detailed calculations applying the present approach for this kind of system have been carried out in [I]. The calculated case is handled as a base scenario of the expected future evolution of the repository system in most of the recent performance assessments of the underground repository [10, 17, 22, 40 and 42].

3. Transport characteristics of the repository system

3.1 Geosphere as a host for the repository

Fractured rock can be conceived as a hydrologically heterogeneous, dual-porosity medium that is composed of water filled pore space in the water-conducting fractures and still standing water in the pore space of the rock matrix between the fractures [e.g. 1, 65 and 70]. Odling and Roden [11] have carried out a numerical study of fractured rock where both the background rock matrix and fractures were water conducting. Their conclusions were that fractures increase the heterogeneity of the flow field even if the fractures are not interconnected, and that fractures are important for transport also in cases where the rock matrix is water conducting. Generally, the hydraulic conductivity of the background rock matrix is low compared to the equivalent hydraulic conductivity of the fractures; therefore groundwater flow in fractured rock takes place predominantly along water-conducting fractures [c.f. 1 and 65].

The properties of the flow field in fractured rock are characterised by high heterogeneity as the fracture sizes and their hydraulic transmissivities vary considerably. Internal heterogeneity in fractures gives rise to channelling of the groundwater flow [83]. These preferential flow paths not only influence the properties of the flow field but also solute transport and retention properties. Experiments have indicated that distinct flow paths or channelled flow are needed to explain tracer transport in fractured rock, because tracer experiments have shown multiple peaks in breakthrough curves, quick initial arrival times and long tailings [2, 19 and 72].

Fracture network simulations of flow and transport through fractured rock have indicated the existence of preferential flow paths. Transit times between successive segments along trajectories are usually correlated. A particle that is in a high-velocity segment is more likely to indicate high-velocity in the subsequent segment due to conservation of flux at the fracture intersections [12]. A similar conclusion has also been reached based on particle tracking simulations using a stochastic continuum model [23].

The majority of the total pore volume in fractured rock lies in the rock matrix between fractures [e.g. 1, 15 and 70], although the flow is dominated by water-

conducting fractures. The still-standing pore water in the rock matrix plays an important role in the transport of solutes, as solute molecules can enter pore spaces in the rock mass by molecular diffusion. This rock matrix diffusion can cause significant retention in solute transport [4, 6 and 24].

In the performance assessment simulations geosphere transport from a leaking canister is usually conservatively simplified by considering only the quickest channel. This is also consistent with the observed tendency of preferential flow paths. In the present approach the geosphere response function is represented by a lumped parameter model of combined exponential-plug flow that has been applied to simulate transport of environmental tracers in the hydrological systems [e.g. 79, 80 and 81]. Approximation of the advection-matrix diffusion transport in geosphere by the exponential lumped parameter model is mathematically similar to the well-mixed model for the engineered barriers. It is also conservative in sense that it maintains the level of the maximum release rate. Release rate in the very early part of the breakthrough is overestimated and the tailing of the approximated breakthrough curve is shorter than in the advection-matrix diffusion model.

Characteristic to the fractured rock is that large hydraulic features are, on average, better hydraulic conductors than smaller ones. The flow rate in large features is also larger, because they collect flow from smaller features. This creates preferential flow paths that run over long distances. The simulations in [II] indicated that the segments at the beginning of flow paths, starting from sparsely fractured rock intended to host deposition holes, are more favourable to the matrix diffusion. This leads to greater retention in the solute migration at the beginning than later parts of the release paths. This becomes evident for accumulation of the hydrodynamic control of retention (β) along the flow paths in Figure 3 [II]. The total β accumulates in very early parts for most of the paths. The effect of matrix diffusion is weaker in larger hydraulic features mainly due to the larger flow rates. Hydrodynamic control of retention is a grouped parameter that couples the properties of the flow field with the retention by matrix diffusion [85 and 86]. This parameter can be written as $\beta = 2WL/Q$, in which W is the average width of the transport channel, Q is the flow rate and L is path length [82, 87 and 88]. For example, time of arrival of a cumulative mass fraction ϕ for an instantaneous source when the matrix diffusion takes place to an infinite matrix is $t_\phi = \tau + \eta\,\beta^2$ [82], in which τ is the water residence time, η depends on the rock matrix properties, together with the selected mass fraction, and the hydrodynamic control of retention, β. Thus, in this case the delay caused by matrix diffusion is proportional to the inverse of the square of the flow rate.

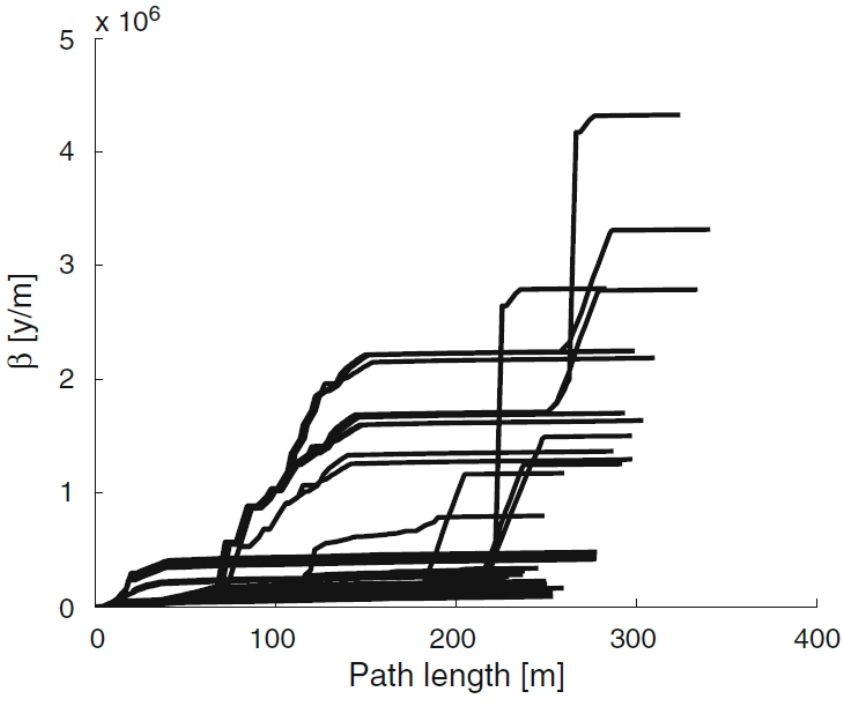

Figure 3. Hydrodynamic control of the retention (β) plotted as a function of the path length for one hundred paths under the natural flow conditions (from [II]).

Results of the modelling study of flow and transport in a generic fracture network in Publication [II] supports the simplified representation of the geosphere release path applied in this thesis. Transport processes involved in [II] were advection, matrix diffusion and sorption. Simulations were performed both for typical experimental flow conditions that are applied in the characterisation of the site scale transport properties in geosphere and for natural flow conditions that are assumed to prevail around the closed repository. The present simplified approach represents geosphere release paths by a single transport channel that is surrounded by an infinite and homogenous rock matrix. These simplifications are discussed below based on the results of the Publication [II].

Solute transport in fractured rock was studied in [II] in case the flow path branches off to two parallel paths. Figure 4 shows modelling results for migration of iodine in case the flow is divided between two different type fractures. The contribution of both paths in the output is significant only in a very rare case of evenly distributed flow rate between the paths. This indicates that solute transport through the system of interconnected fractures is easily dominated by one of the parallel routes. The reason for this behaviour is that the delay and attenuation of the solute transport caused by the matrix diffusion that depends strongly on the flow rate, as noted also above.

It can be concluded from the results above that retention along a release path starting from a potential deposition location is likely to be dominated by a few first fractures. Thus, it is adequate to simplify modelling of the geosphere release path from a deposition hole by representing the release path by a single transport channel.

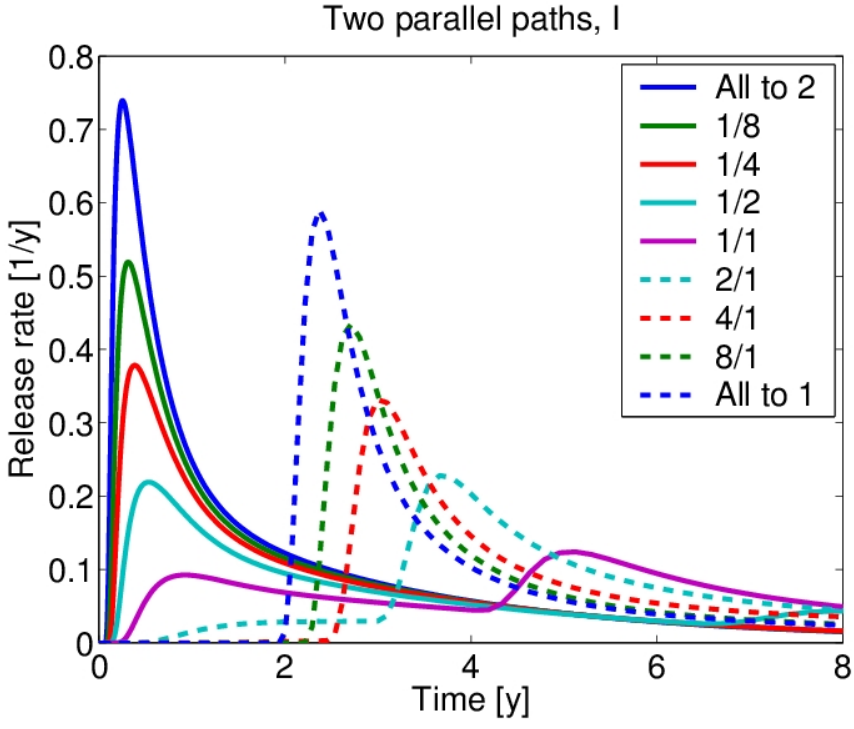

Figure 4. Breakthrough curves for I-129 through the system of two parallel fractures. The numbers in the legend indicate division of the total flow rate between the type 1 and type 2 fracture (Q1/Q2) (from [II]).

Retention properties of the rock matrix are heterogeneous. Due to the past geological processes the fracture wall may be coated by different minerals and the layer of the rock matrix closest to the transport channel could have altered properties compared to the rock matrix further away from the fracture wall. The influence of the heterogeneous properties of the rock matrix to the solute transport has also been studied in [II] under typical site characterisation (SC) and performance assessment (PA) flow conditions. Simulations indicated that the detailed heterogeneity of the rock matrix properties is not as important for solute transport under the natural flow conditions that prevail around the closed repository, than it is under the typical experimental flow conditions applied in the site investigations. This can be recognised from the simulation results, because the approach applied in [II]

provides means to separate contributions of the different immobile zones from the overall retention such that the solute breakthrough curve can be calculated as a convolution between the contributions of the individual immobile zones [II] (cf. Figure 5).Typical to the PA flow condition is that contributions of the limited volume immobile pore spaces are narrow pulses. This indicates that those immobile pore spaces are fully saturated by the tracer and that the tracer concentration in those pore spaces is in equilibrium with the tracer concentration in the fracture. A consequence of this is that the characteristics of the breakthrough curve in PA conditions are determined by the very thick layer of unaltered rock.

Figure 5 shows a summary of the simulation results for solute transport in case of heterogeneous rock matrix. The heterogeneity of rock matrix is represented by successive layers of geological materials with different retention properties: the coating mineral, fracture gouge, cataclasite, altered rock matrix and unaltered rock matrix. Site characterisation (SC) flow conditions and the studied flow path in Figure 5 is modelled using typical in-situ tracer test set-up. Similarly, performance assessment (PA) flow conditions and studied flow path in Figure 5 is modelled using typical value of the natural hydraulic gradient in the repository depth (0.5%) and the same fractures, but over a longer travel distance, that were applied in the corresponding SC simulations. Figure 5 shows contributions of the individual layers of the rock matrix to the solute breakthrough curve. In case of typical PA flow conditions (figures c and d) the breakthrough curve (black line) is well represented by the unaltered rock matrix only (purple line). This indicates that it is reasonable to represent the rock matrix along the geosphere release path by applying effective retention properties of the unaltered rock matrix, as it is done in the present thesis.

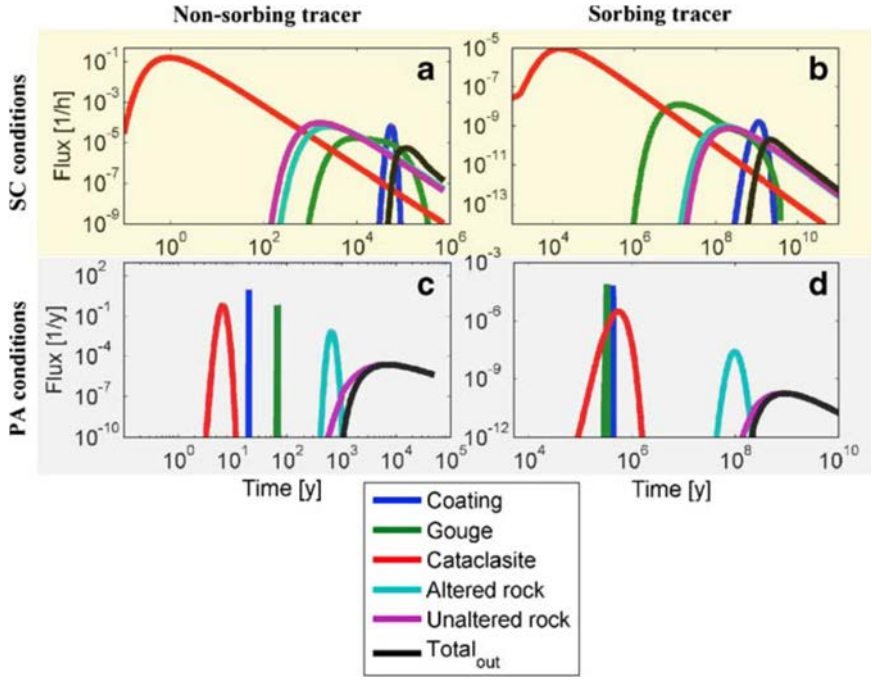

Figure 5. Contributions of the individual layers of the pore space to the retention of the iodine and americium in the typical site characterisation (SC) and performance assessment (PA) flow conditions: a) Iodine in SC flow field, b) Americium in SC flow field, c) Iodine in PA flow field and d) Americium in PA flow field. Tracer breakthrough curves are indicated by black lines (from [II]).

Tracer experiments and their interpretation in Publications [III–V] link the migration model applied in [II] with the actual solute transport properties along a fracture in rock. The tracer tests were carried out in the laboratory, which enabled better characterisation of the tested rock volume, easier control of the flow field and more complete tracer recovery than in the in-situ tests. The aim of these tests was to study transport and retention processes, rather than to characterise the transport properties of the studied rock volume.

The studied piece of rock was a 0.9 m × 0.9 m × 0.7 m block of non-foliated, fine-grained and equigranular granitic rock [IV]. A natural horizontal fracture was identified at about 17 cm from the top of the block. This fracture was penetrated by a grid of 9 core drilled holes. The experiments to investigate solute transport in this block of rock were organised such that the hydraulic properties and flow channels of the fracture were studied in Publication [IV], a series of tracer tests carried out using the drill cores were analysed in Publication [V] and tracer tests performed in the natural fracture of the block were studied in Publication [III]. The Publication [III] also summarised results of the tracer tests that were executed both using the drill cores [V] and along the flow channels on the fracture plane [III].

Hydraulic properties of the fracture were characterised and a first set of tracer tests were analysed in Publication [IV]. Flow rates in the first tests were too high for matrix diffusion to be a significant retention process. Tracer tests showed that solute transport in the fracture plane took place along distinct channels and that it was feasible to perform more detailed tracer tests along these channels.

Tracer tests were performed in parallel using the drill core samples from the holes drilled to rock block [V] and testing the transport channels across the fracture [III]. The drill core samples were glued one after the other in order to create three longer samples. These core samples were emplaced inside tubes, such that 0.5 mm artificial flow channels were created between the walls of the tubes and the drill core samples inside the tubes. Tracer tests were executed by applying different flow rates for the water flow through the artificial flow channel and using different tracers. Modelling indicated that matrix diffusion can explain the differences between breakthrough curves for different flow rates and for non-sorbing uranine and sorbing sodium tracers [V].

Another set of tracer tests carried out in the fracture was analysed in Publication [III]. The same tracers were applied in the fracture experiments that were applied in the experiments with the drill core samples. Uranine and sodium were injected simultaneously as a cocktail of two tracers in order to ensure that the same flow field applies to transport of both tracers. Modelling of the tracer tests assumed that advection, dispersion and matrix diffusion were the active transport processes in both tests. Consistent parameterisations were applied for the flow fields of both tracers in the same test and for the rock properties between the drill core and fracture experiments. Distribution coefficient for the sorption of sodium was taken from independent batch measurement data. It was observed that: i) matrix diffusion and sorption in the rock matrix can explain the observed difference between the uranine and sodium breakthrough curves within the same test configuration and ii) matrix diffusion and sorption can explain results from the drill core experiment and from the fracture experiment with very similar rock matrix properties; the interpreted porosity of the rock matrix was only slightly increased from 0.4% to 0.5% in the model of the fracture experiment.

The series of experiments [III–V] increased confidence on the model predictions of the solute retention in groundwater flow, and thereby also on the modelling results in [II].

3.2 The repository as a multi-barrier system

The KBS-3V repository concept is based on successive barriers such that the majority of barriers are enveloped by the subsequent barrier. This assures that all barriers are utilized to their full capacity in limiting the consequences of a possible release. Detailed assessment of the performance of the barrier system is a complicated task that must be based on numerical radionuclide migration analysis. Understanding the main characteristics of the system is better achieved by the use of simplified concepts.

The inherent nature of the barriers, and thus the barrier system as a whole, is here assumed to be governed by linear processes of Gaussian diffusion, advection, matrix diffusion and linear equilibrium sorption. These processes are also time invariant in a sense that a shift in time of the input leads to the same shift in time of the output, assuming that transient phenomena, like rock shear movements or chemical changes, do not occur during the analysed period of time. Output from a linear time invariant system can be represented by a convolution integral between the input and the system response [71]

$$y(t) = \int_0^t h(\tau)g(t-\tau)d\tau, \tag{2}$$

where $h(t)$ is the input and $g(t)$ is the system response function, i.e., output from the system for an instantaneous unit input at time $t = 0$. The system is completely defined by its response function. The response function in Equation (2) could represent the whole repository system, but the equation applies also in the case of individual barriers. This means that the output from an individual barrier is the convolution between the input into the barrier and the barrier's response function. This shows that the response function of the whole repository system is a series of convolutions between the individual barrier response functions. A useful property of the convolution from the repository system analysis point of view is that [e.g. 13]

$$\begin{aligned} \eta_y &= \eta_h + \eta_g \\ \sigma_y^2 &= \sigma_h^2 + \sigma_g^2, \end{aligned} \tag{3}$$

in which $\eta_n = \int_{-\infty}^{\infty} t\, n(t)dt$, $\sigma_n^2 = \int_{-\infty}^{\infty} t^2 n(t)dt - \eta_n^2$, and $n(t)$ is a response function, i.e. $\int_{-\infty}^{\infty} n(t)dt = 1$. Thus, the average release time for convolution of two response functions is sum of the average release times of the two convoluted response functions, and the variance of the release time for the convolution of the two response functions is sum of the variances of the release times of the two convolute response functions.

These properties of Equation (2) support a simple analysis of the system. The temporal width of a barrier response function is directly coupled with the release rate out from the barrier, and thus, limitation of the release rate. The summation of the variances, i.e. temporal width squared, in convolution leads to dominance of the temporally broadest response function in the convoluted combined response function of the successive barriers. In Publication [I] this is illustrated by very simple examples showing that, in most cases, one of the barriers will dominate the attenuation of the release rates through a system of dissimilar barriers. This property alone is essential in characterising the repository system. It indicates that the response of the system as a whole is easily governed by a single, the longest, characteristic time.

Characterisation of the barrier system can be developed further by finding suitable measures for the performance of the individual barriers. Figure 6 illustrates

the interfaces between the individual barriers in the KBS-3V disposal concept as analysed in this study. The resistance against solute transport through the barrier interfaces, i.e. transfer between the barriers, appears to be considerable compared to the resistances within the barriers for the following reasons:

- Release from the canister takes place through a small hole (Figure 6a, c→b). The mass transfer mechanism into and out of the canister is molecular diffusion. The mass flow from the canister depends on the diameter of the hole (d in Figure 6a). The mass flow mixing radionuclide concentration inside the canister depends roughly on the effective cross-sectional area of the about 700 litre water volume inside the canister. For about 5 meter long canister this gives an effective cross-sectional area of about 0.14 m^2. Safety assessments have typically assumed that initial defects in the size scale of millimetres will be identified in the inspection of the canister [e.g. 40]. Thus, the effective cross-sectional area for mixing inside the canister is several orders of magnitude larger than the size of the possible hole in the canister. Well-mixed conditions can be expected inside the canister although the concentration gradient is probably steeper over the hole than inside the canister. Other mechanisms enhancing mixing, e.g. thermal convection [54], in addition to diffusion may also occur inside the canister.
- Release from the buffer can take place to a potential fracture intersecting the deposition hole (Figure 6b, b→f) or to the tunnel above the deposition hole (Figure 6c, b→t). Mass transfer inside the buffer takes place by molecular diffusion. Mass transfer from the buffer surface to a potential fracture is also usually assumed to take place by diffusion. It appears that the diffusion resistance from the buffer to the fracture dominates the total diffusion resistance from the canister surface to the fracture [e.g. 25]. Calculating diffusion resistance for the mixing inside the ring of the buffer material around the canister and assuming a vertical concentration gradient over the thickness of the buffer (l_b in Figure 6b, here l_b = 35 cm) shows an equivalent flow rate for the mass transfer of about 30 L/a. The corresponding equivalent flow rate is about 1 L/a for diffusional mass transfer (Equation 1 in [25]) to a 0.2 mm fracture ($2b_v$ in Figure 6b, here $2b_v$ = 0.2 mm) with a rather high groundwater flow rate of 10 L/a across the deposition hole. In performance assessments this measure of the mass transfer has been estimated for a wide range of different conditions showing typically variability from about 0.2 L/a to 5 L/a [22]. This shows that diffusional mixing inside the buffer is much stronger than the outflow to the fracture. Mixing of the nuclides inside the buffer before the nuclides reach the outflow location is also enhanced if the fracture does not intersect the deposition hole exactly at the location of the defect in the canister. The mass flow rate along the release pathway from the buffer to the tunnel is in the order of the mixing mass flow rate inside the buffer, as the whole cross-sectional area is available for diffusion from the buffer to the tunnel. However, the top of the canister will be 2–3 metres below the tunnel floor (S_c in Figure 6c), i.e. at

almost 1/3 of the depth of the deposition holes. This means that radionuclides will spread nearly over the entire buffer before release to the tunnel begins. In summary, a well-mixed concentration field over the buffer is a reasonable assumption. Validity of the assumption for well-mixed conditions in the buffer has also been noted by Hedin [67].

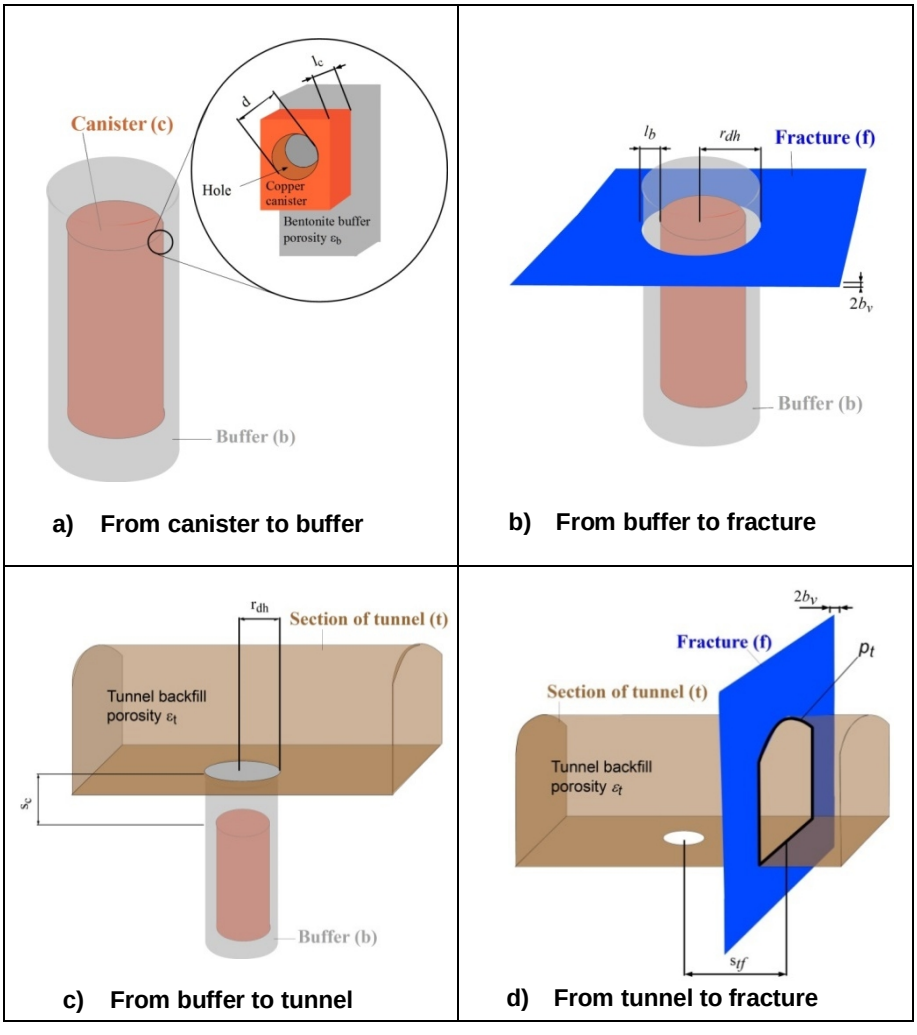

Figure 6. Interfaces between individual transport barriers in the KBS-3V disposal concept (based on [l]).

- Release from the tunnel backfill takes place to a fracture intersecting the tunnel (Figure 6d, t→f). A fracture intersecting the tunnel may have a larger aperture ($2b_v$ in Figure 6d) than a fracture that is allowed to intersect a

deposition hole. However, it is not allowed that a significant fracture intersects the tunnel very close to the deposition hole. This means that the radionuclides need to travel along the tunnel before they reach the outflow location. Migration along the tunnel causes efficient mixing of the radionuclides in the tunnel. In addition, the design basis of the tunnel backfill aims to limit groundwater flow in the backfilled tunnel. Permeability of the backfill is designed to be low enough ($K<10^{-10}$ m/s) such that molecular diffusion is a dominant migration process [50]. This means that well-mixed nuclide concentration in the tunnel backfill is a reasonable assumption. In many performance assessments no diffusion resistance have been assigned to the tunnel [10, 22 and 35] or it has turned out to be small [17].

- The main mass transfer processes in radionuclide migration through the interconnected network of water conducting fractures in the geosphere are advection, matrix diffusion and sorption [10, 17, 22, 41, 42 and 54]. The performance of the geosphere release path is different from the other transport barriers, as it does not have an inherent well-mixed character as the other transport barriers. However, validity of the assumption, that the geosphere release path is conservatively approximated by the exponential lumped parameter model that is mathematically similar to a well-mixed volume approximation, has been studied in [I, 81]. The model for geosphere is selected such that it captures the maximum level and the temporal spread of the main part of the geosphere response function. However, this model is not able to reproduce the extended long tailing of the advection-matrix diffusion breakthrough curve. Also, the early time behaviour of the geosphere response is ignored by the exponential model. The objective of this approximation is to facilitate handling of the whole barrier system with the same simplified model and to facilitate using the same characteristic parameters for all transport barriers.

The barrier response functions do not, however, fully comply with well-mixed systems. In practice, there is a delay between the start of inflow to the barrier and the outflow from the barrier that could be of importance for short-lived nuclides. The delay time between the start of the inflow to the barrier and the start of the outflow from the barrier can be incorporated to the group of Equations (4) [I] describing the simplified barrier system.

$$\begin{aligned}
&\frac{dm_c}{dt} + \lambda_c m_c = \delta_0 \\
&\frac{dm_b}{dt} + (\lambda_{bf} + \lambda_{bt}) m_b = \lambda_c m_c * \delta_{t_{dc}} \\
&\frac{dm_t}{dt} + \lambda_{tf} m_t = \lambda_{bt} m_b * \delta_{t_{dbt}} \\
&\frac{dm_f}{dt} + \lambda_f m_f = \lambda_{tf} m_t * \delta_{t_{dtf}} + \lambda_{bf} m_b * \delta_{t_{dbf}}
\end{aligned} \quad , \qquad (4)$$

where $*$ means convolution $y(t) = h(t) * g(t) = \int_0^t h(\tau)g(t-\tau)d\tau$, $\delta_\tau = \delta(t-\tau)$, with δ as the Dirac delta function, δ_0 is an instantaneous release of a unit mass at $t = 0$, $\delta_{t_{dc}}$ is an instantaneous release of a unit mass at the delay time in the canister, $\delta_{t_{dbt}}$ an instantaneous release of a unit mass at the delay time from the buffer to the tunnel, $\delta_{t_{dbf}}$ an instantaneous release of a unit mass at the delay time from the buffer to the fracture, and $\delta_{t_{dtf}}$ an instantaneous release of a unit mass at the delay time from the tunnel to the fracture. Other notations in Equation (4) include mass transfer constants: λ_c from the canister to the buffer, λ_{bf} from the buffer to the fracture, λ_{bt} from the buffer to the tunnel, λ_{tf} from the tunnel to the fracture, and λ_f along the geosphere path. Solute masses are noted as: m_c in the canister, m_b in the buffer, m_t in the tunnel and, $\mathrm{m_f}$ in the geosphere. The solute mass flow out of the multi-barrier system will be $\dot{m}_{out} = \lambda_f m_f * \delta_{t_{df}}$, where $\delta_{t_{df}}$ is an instantaneous release of a unit mass at the delay time in the geosphere.

As noted earlier, the response function of the repository barrier system can be determined as a convolution between the individual barrier response functions. The approach applied in Publication [I] separates delay time from the barriers' response functions in Equations (4) by idealising the delay time as a pure translation in time. The system response function is determined by representing barriers as idealised well-mixed volumes without any delay times. Under this assumption Equations (4) take the form of Bateman equations with known solutions [e.g. 60, 62 and 63]. Delay times in different barriers are determined separately and summed up to give the total delay time of the repository system. The total delay is then applied as a translation in time of the whole system response function. Separation of the delay times from the attenuation and spreading of the solute pulse simplifies the computation of the response function, and also facilitates uncertainty analysis of the system by separating the different barrier properties in the overall performance of the system.

The concept presented above is used to characterise the performance of the individual barriers using systematic measures that are directly comparable between the different barriers (Figure 2). Useful measures for description of mass transfer through the barrier system that is represented as a simplified multi-compartment model (Figure 7) include:

i. Equivalent flow rate (q): The mass transfer out from the barrier can be expressed as the equivalent flow rate discharging the barrier in question [7]. The equivalent flow rate is an apparent volumetric flow rate that combined with the solute concentration in the compartment gives the outflow of the solute mass. The equivalent flow rate is a convenient quantity for measuring the mass transfer capacity out of the barrier, as it enables easy comparison of the diffusive mass fluxes from buffer and backfill to the flowing water in fracture, both with each other and with the flow rates in the hydraulic environment deep in the rock. Mass transfer in the repository near field as represented by equivalent flow rates has recently been considered by

Neretnieks et al. [7]. That study confirmed that the simple concept of equivalent flow rate is accurate enough compared to uncertainties in the actual flow rates and properties of the transport barriers.

ii. Compartment half-life ($T_{1/2} = \ln(2)\, R\, V_p/q$): The equivalent flow rates (q) together with the pore volumes (V_p) of the barriers and retardation factors of the nuclides in the barriers (R) give the time constants of the different barriers. The half-life of the solute concentration in the compartment is the only parameter needed to describe an ideal system of perfect mixing tanks. The inverse of the compartment half-life is proportional to the mass transfer coefficient out of the barrier. In the case of the geosphere, the active total pore volume for matrix diffusion is not well known and the geosphere half-life is based on the estimated mass transfer coefficient $T_{1/2} = \ln(2)/\lambda$, where λ is the mass transfer coefficient.

iii. Delay time (t_d): In reality there is a delay between the start of the inflow to the barrier and the outflow from the barrier, as the solute must reach the outlet location before the outflow begins. This delay time is treated as a time shift of the solute release rate out of the barrier. In practice, it significantly affects the duration and level of the breakthrough curve only for strongly sorbing nuclides that have a short radioactive half-life.

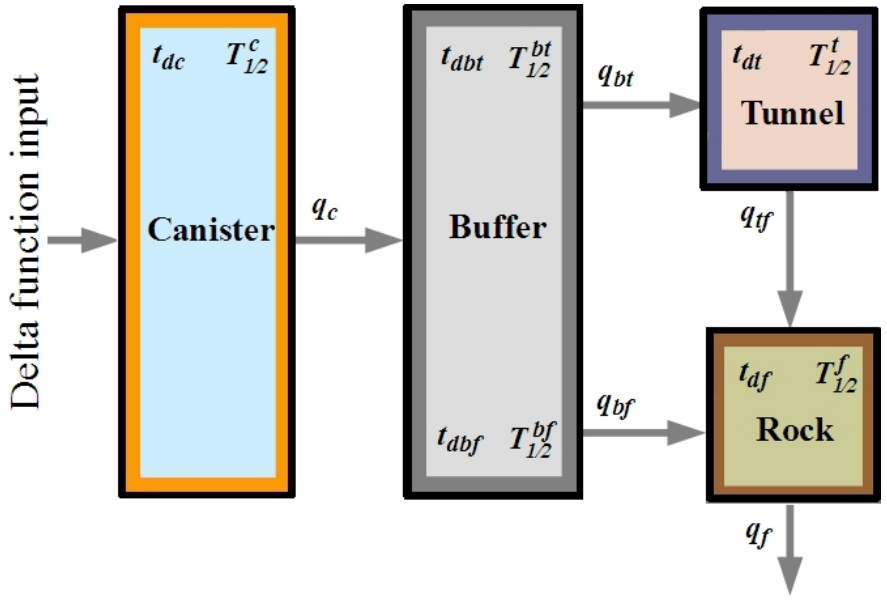

Figure 7. Repository system as represented by the simplified multi-compartment model. The system response function can be determined by characterising each barrier with a single mass transfer coefficient and taking the delays into account.

The present approach focuses only on migration of the dissolved radionuclides. For example, gas mediated and colloidal transports are not discussed in this context. There is a consensus on the main transport processes that dominate the radionuclide migration through the barrier system. Molecular diffusion, advection, sorption and solubility limitation are the main processes affecting the radionuclide transport through the repository system [54, 55 and 58]. Advection in the buffer is insignificant when the full swelling pressure of the buffer material has been achieved [58]. This means that transport in the buffer is dominated by diffusion and sorption. Solubility limitation and corresponding precipitation and co-precipitation are not considered to be important for the buffer due to the low concentrations of the radionuclides [58]. The same as for the buffer applies largely also for the tunnel backfill. The backfill of the tunnel is designed to have low hydraulic conductivity in order to prevent advection along the tunnel. This indicates that diffusion and sorption may dominate solute transport also in the tunnel backfill. However, it is straightforward to include advective release from the backfilled tunnel to the equivalent flow rate out of the tunnel, and use the present approach as long as the assumption for well-mixed concentration in the backfill is justified. The simplified model for the geosphere is based on the advection, sorption and matrix diffusion that are generally agreed to be the main transport processes in the geosphere [54]. This indicates that the simplified approach covers the main transport processes of the multi-barrier system.

An important assumption for the performance of the simplified model is that the mixing inside the barrier is sufficiently efficient compared to the mass outflow from the barrier. This leads to dynamic behaviour of the solute migration, in which the outflow from the barrier is proportional to the mass in the barrier. The discussion above shows that this seems to be generally an appropriate assumption; at least when the barriers are assumed to function as planned.

4. Discussion

The present model is based on characterisation of the migration properties of the transport barriers using simplified concepts of compartment half-life and delay time, which are derived for each nuclide using material and geometrical properties of the barrier (porosity, geometrical dimensions, location and dimension of the outflow point), and transport characteristics of the nuclide (diffusivity, sorption). The mass transfer rate can be determined as an equivalent flow rate, which has long been used to describe solute transport properties in the underground repository context and is still currently considered to be sufficiently accurate and an adequate practical approach [7]. The present model has similarities with the compartment model of Romero et al. [16] and the analytical model of Hedin [67]. However, in the present model the simplified description of the transport barrier system is reduced to a single compartment per each transport barrier. This gives a simplified but complete representation of the migration properties for different transport barriers of the repository system by their compartment half-lives. This alone offers a straightforward way to compare performance of the different barriers and the barrier system. In addition, using the present approach the time evolution of the radionuclide mass in the different barriers for a single nuclide is formally analogous to the evolution of radioactive decay chain.

The simplified approach, as implemented in the present model, can be applied only to single nuclides, although spent nuclear fuel also involves decay chains. This is not a major restriction of the model, because single nuclides, such as I-129 and C-14, have been shown to have a dominant role in most performance assessments carried out for geological repositories in crystalline rock [e.g. 10, 17 and 22]. Nuclides that are members of the decay chains can also partly be analysed as single nuclides, as Pu-239 in [I]. This gives indication of the migration properties of these nuclides in the different barriers, which can then be compared with other nuclides. Many of the nuclides in the chains are also present or produced in significant amounts already in the spent fuel matrix.

4.1 Compartment half-lives

As a test of the simplified model, compartment half-lives are calculated for the repository system in [I] using radionuclides and data from an interim safety case report of Posiva Oy on the radionuclide release and transport analysis, the RNT-2008 analysis, [10]. The calculated case considered here, and in [I], is the RNT-2008 calculation case Sh1Fd defined by: a small diameter (1 mm) hole in the canister (existing from t = 0), default flow conditions of equivalent flow rates of 0.2 L/a from buffer to fracture, 10 L/a from tunnel to fracture and transport resistance of 50 000 a/m over the geosphere path and increased fuel degradation rate of 10^{-6} 1/a. RNT-2008 analysis considered a two layer rock matrix along the geosphere release paths. The present analysis is simplified from the RNT-2008 analysis such that the rock matrix in geosphere is composed of one infinite layer only and properties of the one layer rock matrix are selected based on the properties of the two layer matrix by applying porosity of the first layer and effective diffusivity of the second layer. The release path from buffer to the excavation damaged zone beneath the deposition tunnel was not calculated in this test case.

Figure 8 shows the compartment half-lives for different nuclides ordered by the maximum of the compartment half-lives for different transport barriers. A few interesting conclusions can be made based on the figure. The main transport barriers, i.e. those having the longest compartment half-life, are the canister (cb) and the buffer (bf). Geosphere (f) is not a major transport barrier for the repository system due to the relatively low geosphere transport resistance (WL/Q) assumed in the analysis [10 and I]. For the non-sorbing nuclides (C-14, Cl-36 and I-129) the contribution of the geosphere is insignificant, especially for the anionic nuclides (Cl-36 and I-129). The small hole in the canister is the main barrier for the nuclides which have a low sorption or for the cationic species (Cs-135 and Cs-137). The buffer is the main barrier for the sorbing nuclides. Nuclides radioactive half-lives are also indicated in Figure 8 by the colour coding of the nuclide names, so that they can be compared with the compartment half-lives. Short radioactive half-life compared to the compartment half-life indicates very efficient attenuation of the release rate. This is the case for most of the americium, curium and plutonium isotopes.

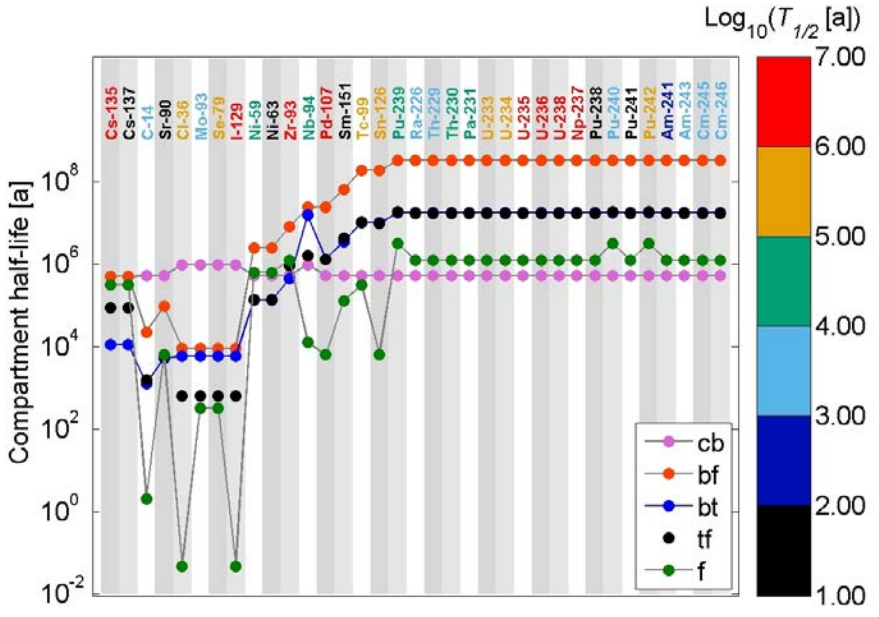

Figure 8. Compartment half-lives for the different nuclides in the RNT-2008 calculation case Sh1Fd [10 and I]. Nuclides are ordered by the maximum compartment half-life. Nuclide names are colour-coded by their radioactive half-life as indicated by the colour scale on the right.

4.2 Performance of the simplified model

The actual release rates of the radionuclides from the repository system depend on several other properties than the nuclide specific compartment half-lives. These features include at least i) the source term from spent fuel, ii) radioactive decay and in-growth, iii) delay time from the inflow start to the barrier to the outflow start from the barrier and iv) solubility limitations of the element of the radionuclide. Only the solubility limitation, among the features i-iv above, directly affects the compartment half-life by eliminating dependence between the compartment's capacity and the release rate from the compartment (i.e. release of the nuclide from the compartment does not affect the nuclide's water phase concentration). In practice the solubility limitation affects only the first compartment (canister) and it can be handled by omitting the first compartment and representing the solubility limited release from the first compartment as a source term to the second compartment. Other features i-iii do not directly change the compartment half-life and they can be taken into account as a post-processing step of the modelling. Thus, the compartment half-life can be regarded as a barrier's property that limits the transport of nuclides by distributing the releases over a longer period of time. This leads to attenuation of the release rates that affects all nuclides regardless of the

radioactive half-life or the source term. Another mechanism of restricting the nuclides release rates is based on the radioactive decay and long travel times of the nuclides over the release paths. Therefore, in order to estimate the actual release rates of the nuclides the delay times need to be taken into account.

The early evolution of the release rate from the barrier is in many cases not following the assumption of well-mixed solute concentration. Characteristics of the nuclide release rate can be dominated by this early transient phase of the concentration field, especially if the nuclide's radioactive half-life is short. The accuracy of the simplified approach is limited when the transient behaviour is important to the overall performance of the system. However, this behaviour also indicates that the nuclide's release rate is strongly attenuated by the radioactive decay in the barrier in question.

4.3 Barrier delay times

Nuclides and barriers that need additional attention due to the early time behaviour can be identified by considering the radionuclides half-lives and the different barrier delay times. If this ratio is small, i.e. the delay time is short compared to the nuclide's half-life, the nuclide's response function for the barrier will become fully developed and the influence of the early time transient in the concentration field is not likely to be important.

The nuclide dependent behaviour of the delay time in the barrier is demonstrated for the RNT-2008 case Sh1Fd in Figure 9. The figure shows ratios between the nuclide's estimated barrier delay times based on [I] and the radioactive half-lives. Figure 9 indicates that the model should work well in this calculation case for the non-sorbing and cationic nuclides, because the ratio between the compartment delay time and nuclide's half-life is small. There are also a number of sorbing nuclides that show long barrier delay times compared to the nuclides' half-lives. This indicates that these nuclides are efficiently retained in the barrier. Finally, there are some sorbing nuclides that have similar barrier delay time to their radioactive half-life. This indicates that the nuclide is not completely retained in the barrier and the maximum release rate could be determined by the early transient phase before the well-mixed concentration field has been developed. One of these nuclides, Pu-239, shows delay time in the buffer and in the geosphere that is comparable to its radioactive half-life. This nuclide was selected for the more detailed analysis in [I].

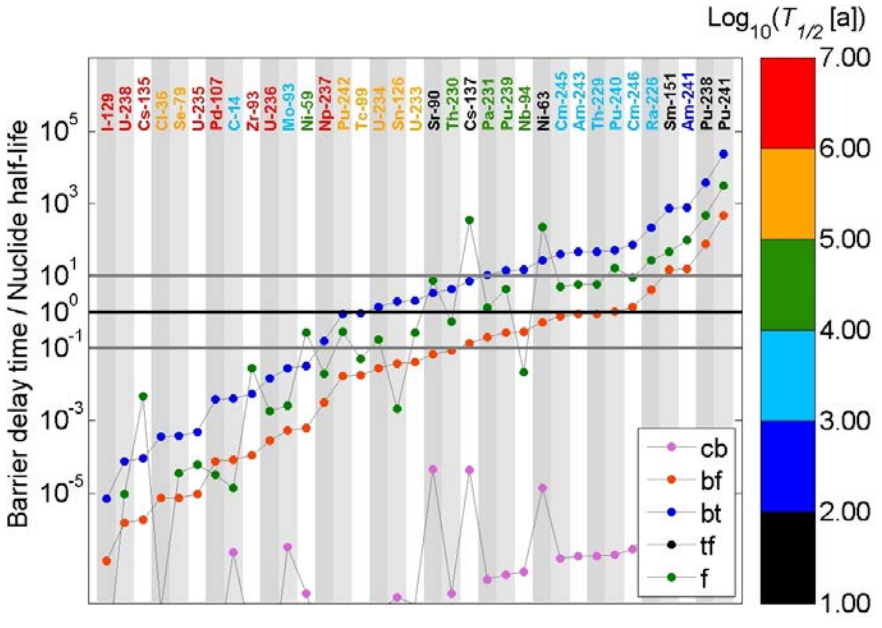

Figure 9. Barrier delay time divided by the nuclide radioactive half-life plotted for different barriers in the RNT-2008 calculation case Sh1Fd [10 and I]. Different barriers are indicated by the legend (cb – from canister to buffer, bf – from buffer to fracture, bt – from buffer to tunnel, tf – from tunnel to fracture, f – fracture in geosphere). Nuclides are sorted by delay in the buffer (barrier bf). Colour coding of the nuclide names indicates logarithm of the nuclide's radioactive half-life. Black horizontal line indicates equal barrier delay time and nuclide half-life. Gray horizontal lines indicate one order of magnitude differences in the ratio of barrier delay time to nuclide half-life.

4.4 Response functions

The performance of the simplified model to reproduce nuclide specific release rates has been tested with regard to three key representative nuclides. These include the sorbing and solubility limited nuclide Pu-239, Pu-239NS defined as Pu-239 without solubility limitation to represent generally a sorbing nuclide, the non-sorbing neutral nuclide C-14, and the non-sorbing anionic nuclide I-129 [I]. The response functions of the simplified approach are assumed to be exponential. This means that they have a functional form given in Equation (5).

$$h(t) = \begin{cases} 0, & t < t_d \\ \lambda\, e^{-\lambda(t-t_d)}, & t \geq t_d \end{cases}, \qquad (5)$$

where t_d is the barrier delay time and $\lambda = q/(R\,V_p)$ is the mass transfer coefficient out from the barrier, calculated using the equivalent flow rate (q), pore volume (V_p) and retardation factors of the nuclides in the barrier (R) as explained in Section 3.2. The mass transfer coefficients that define the response functions for different transport barriers in Publication [I], and also in the examples of the present section, are shown in Table 1.

Table 1. Characteristics of the mass transfer coefficients for the inter-barrier transport (from [I]).

From To	→ Canister	Buffer	Tunnel	Fracture
↓ Buffer	$q_{ch} = \frac{\pi\, r_h^2\, D_w}{l_c}$ $q_{hm} = \frac{r_h r_u}{r_h + r_u} 2\,\pi\, D_{eb}$ $q_c = \frac{q_{ch}\, q_m}{q_{ch} + q_m}$ $\lambda_c = \frac{q_c}{V_c}$			
Tunnel		$q_{bt} = \frac{\pi\, r_{dh}^2 D_{eb}}{s_c}$ $\lambda_{bt} = \frac{q_{bt}}{R_{pb}\varepsilon_b V_b}$		
Fracture		$q_{bf} = 2\,\pi r_{dh} 2b_v \sqrt{\frac{4\, D_w v_{dh}}{\pi^2 r_{dh}}}$ $\lambda_{bf} = \frac{q_f}{R_{pb}\varepsilon_b V_b}$	$q_{tf} = p_t 2b_v \sqrt{\frac{4\, D_w v_t}{\pi\, p_t/2}}$ $\lambda_{tf} = \frac{q_{tf}}{R_{pt}\varepsilon_t V_t}$	
Biosphere				$u = \sqrt{\varepsilon_m R_{pm} D_{em}}\, WL/Q$ $\lambda_f = \frac{1}{4.3\, u^2}$

The notations used in Table 1 are the following.

For the canister	
q_{ch}	the equivalent flow rate through the hole
q_{hm}	the equivalent flow rate on the bentonite side of the hole
q_c	the equivalent flow rate through the hole and bentonite side of the hole
r_h	the radius of the hole
r_u	the outer radius of the hole in the side of the buffer
D_w	the molecular diffusion coefficient in free water
D_{eb}	the effective molecular diffusion coefficient in the buffer
l_c	the thickness of the canister wall
V_c	the volume of the canister
λ_c	the decay constant of the solute for the mass transfer from canister to buffer
For the buffer	
q_{bf}	equivalent flow rate from buffer to fracture
q_{bt}	equivalent flow rate from buffer to tunnel
r_{dh}	radius of the deposition hole
$2b_v$	volume aperture of the fracture
D_w	molecular diffusion coefficient in free water
v_{dh}	flow velocity of groundwater in the fracture
ε_b	porosity of the buffer
V_b	volume of the buffer
R_{pb}	retardation factor in the buffer
λ_{bf}	decay constant of the solute in mass transfer from buffer to fracture
λ_{bt}	decay constant of the solute in mass transfer from buffer to tunnel
For the tunnel	
q_{tf}	equivalent flow rate from tunnel to fracture
p_t	length of the intersection of the fracture and the tunnel wall
$2b_v$	volume aperture of the fracture
D_w	molecular diffusion coefficient in free water
v_t	flow velocity of graoundwater in the fracture
R_{pt}	retardation factor in the tunnel backfill
λ_{tf}	decay constant of the solute in the mass transfer from tunnel to fracture
ε_t	porosity of the tunnel backfill
V_t	volume of the tunnel section
For the fracture	
u	transport resistance through the flow path
ε_m	porosity of the rock matrix
R_{pm}	retardation factor in the rock matrix
D_{em}	effective diffusion coefficient in the rock matrix
WL/Q	hydrodynamic control of retention
λ_f	decay constant of the solute in mass transfer along the flow path

The response functions of the individual barriers and the whole multi-barrier system for these nuclides were compared in Publication [I] against the numerical results calculated for the near-field by REPCOM [9] and for the geosphere by FTRANS [74]. Geosphere transport is also compared against the analytical solution. The near-field model REPCOM is a compartment model, as the present one. However, it is based on dense discretisation, numerical estimation of the mass exchange rates and it includes all near-field migration processes. In addition to REPCOM also COMSOL multiphysics [3] was applied to the buffer to fracture and buffer to tunnel pathways. The response function for the release from the tunnel to the fracture was not tested in the present work, as the approach of the earlier performance assessments [10, 22 and 35] was followed and a well-mixed solute concentration in the tunnel section was assumed already in the first place.

Barrier and nuclide specific response functions were first calculated without considering the radioactive decay. The following observations were concluded from the comparisons of the simplified model with numerical models [I]:

- The pathway from canister to buffer shows good agreement with the numerically calculated response function. This is to be expected, because both the numerical model and the simplified model are based on the assumption of well-mixed conditions inside the canister.
- The pathway from the buffer to the fracture has been modelled by assuming conservatively that the fracture is adjacent to the hole in the waste canister. This configuration is prone to early transients of the radionuclide discharge from the buffer to the fracture. This is especially true for radionuclides that have a short radioactive half-life compared to the diffusion delay time through the buffer. This has been the case for Pu-239 among the calculated nuclides, as noted above. Numerical modelling with COMSOL multiphysics also indicated that the very early time transient of diffusion through the buffer to flowing groundwater in the fracture is more complicated than the compartment models, such as REPCOM, are generally able to reproduce [75 and I].
- The pathway from the buffer to the tunnel also shows some transient behaviour, as the hole in the canister is assumed to be on the top of the canister, i.e. close to the tunnel. However, the distance from the top of the canister to the tunnel is about 2.5 m compared to about 0.35 m from the canister to the fracture. This means that the time scale for the early transients along the tunnel pathway is about 50 times longer than for the buffer to fracture pathway.
- The pathway through the geosphere to the biosphere has been approximated by the exponential response function in order to introduce the same temporal characteristics for geosphere as for the other barriers and to facilitate handling of the whole repository system by analogy to the radioactive decay chain. Geosphere is assumed to consist of a single thick homogeneous layer of unaltered rock, so the approximation of the geosphere response function can easily been compared with the known analytical solutions of

the advection and matrix diffusion along fractures [e.g. 73]. These comparisons show that the main part and peak level of the response function can be represented by the exponential response function. The very early rise of the breakthrough curve is easily significantly overestimated by the well-mixed approximation, which may influence the accuracy of the model for strongly sorbing and short lived nuclides.

All information on the performance of the barrier system in the present simplified approach is given by the response function of the barrier system. As an example, the response functions for the three nuclides studied in Publication [I] are shown in Figure 10. They are presented without radioactive decay in order to facilitate comparison of the transport properties between the different barriers. Clear differences can be observed between the different nuclides and different barriers. For example, the following observations can be made from the response functions:

- The tunnel to fracture pathway (c-b-t-f) and the buffer to fracture pathway (c-b-f) are almost equally important for non-sorbing anionic species (I-129).
- The tunnel pathway is not important for sorbing species (Pu-239).
- The tunnel pathway is the dominating path for non-sorbing neutral species (C-14).
- The response function from the canister to the buffer (cb) dominates the total response function for non-sorbing species (C-14 and I-129).
- Retention in the geosphere is not important for non-sorbing species (C-14 and I-129).
- The transport of sorbing species (Pu-239) is strongly attenuated by the barrier system, mainly due to the strong retention in the buffer.
- Retention in the geosphere is also important for sorbing species (Pu-239).

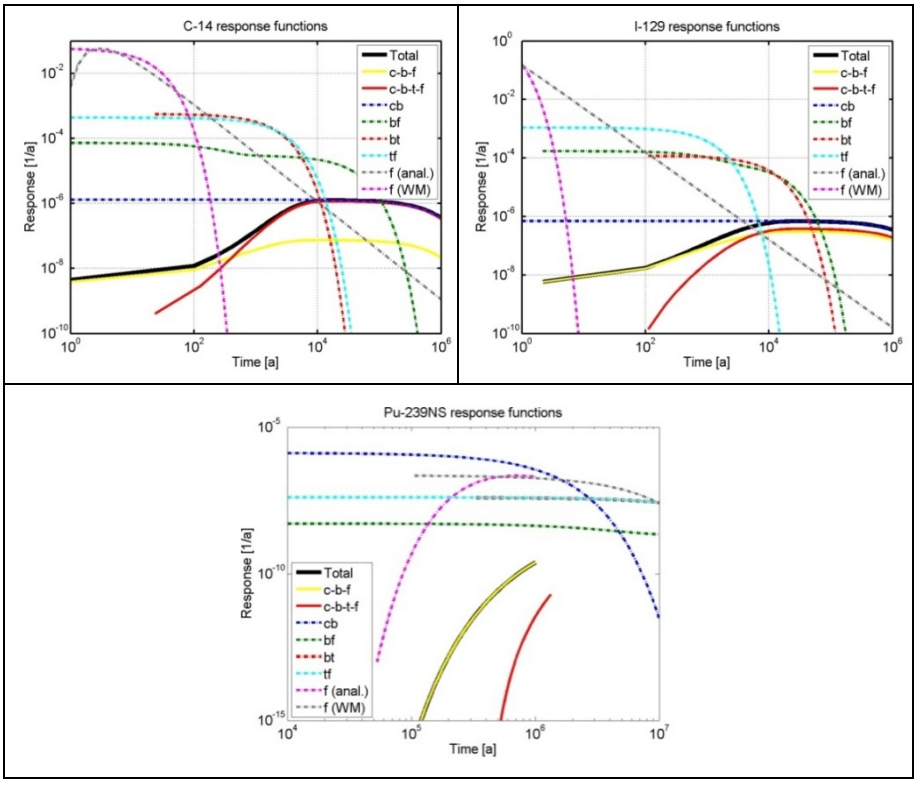

Figure 10. Response functions for individual barriers (cb: from canister to buffer, bf: from buffer to fracture, bt: from buffer to tunnel, tf: from tunnel section to fracture and f: geosphere), different pathways (c-b-f: pathway canister-buffer-fracture and c-b-t-f: pathway canister-buffer-tunnel section-fracture) and the total response function of the whole system (black line). Radioactive decay and possible solubility limitations are not taken into account. The geosphere response function is shown both for the simplified solution (WM, the exponential-plug flow model as an analogy of the well-mixed model) and for the analytical advection-matrix diffusion model (anal.) as described in [I].The buffer to fracture (bf) responses function include approximation of the early time transient in the nuclide concentration field.

Response functions calculated using the simplified concept of the repository system and without radioactive decay can be used to identify the main transport barriers also for the actual radionuclides. I-129 has a long radioactive half-life and the response function calculated without radioactive decay (Figure 10) should be an accurate representation of the I-129 transport properties. The response function for C-14, calculated without radioactive decay in Figure 10, is fully developed after a few thousands of years. The radioactive half-life of C-14 is about 5,700 years indicating that the early transients of the response functions, being of short duration, will not be of importance to the overall performance of the system for C-14.

Pu-239 is a relatively short-lived and strongly sorbing nuclide. Figure 9 above already indicated potential influences of the early transient to outflow from buffer to fracture and for the geosphere path. This can be studied further by looking at the response function in Figure 10. The total response function of the barrier system is dominated by the buffer to fracture pathway (c-b-f) indicating an early transient lasting at least up to a few hundred thousands of years. This is a long time compared to the 24,000-year radioactive half-life of Pu-239. Clearly, the Pu-239 release rate will be attenuated by several orders of magnitude due to the combined action of the barrier system and radioactive decay. In practice, this means that the early transient phase of the diffusion through the buffer to the fracture, the main transport barrier for Pu-239, will be important for the release rates of Pu-239, as is also observed in the Publication [I].

The early rising phase of the geosphere response function for Pu-239 lasts longer than the radioactive half-life of Pu-239. This can be seen by comparing exponential (well-mixed) model approximation (dotted grey line) and analytical response functions (dotted magenta line) for the geosphere in Figure 10. In the case of Pu-239, the geosphere provides considerable retention. The delay and peak level of the geosphere response function are quite well approximated by the exponential model, but the release rates regarding the early rise of the response function are clearly over-estimated by the exponential model (dotted grey line vs. dotted magenta line in Figure 10). This affects the accuracy of the exponential model approximation of the geosphere response function, as the duration of the transient is much longer than the radioactive half-life of Pu-239. The same applies also to the buffer to fracture response function, although the influence is opposite to the geosphere, and the exponential model underestimates the response function during the early phase. Note, that the response functions from the buffer to the fracture (bf, dotted green lines) in Figure 10 include approximation of the early transient. This can be seen as a step at about 1,000 years for C-14, before 10,000 years for I-129, and before 10^7 years for Pu-239.

4.5 Time constants of the barrier system

The model is able to rank the importance of individual transport barriers to hinder radionuclide migration with respect to the performance of the repository system as a whole. This can be used to focus further improvement of the model on the most important barriers.

The main characteristics of the barrier system can be condensed to performance indicators for each barrier type, as suggested in Section 3.2. The compartment half-life is calculated from the equivalent flow rate and the storage capacity of the barrier. The storage capacity for a non-sorbing neutral species is equal to the pore volume of the barrier. The storage capacity and effective diffusivities for anions in the buffer material [e.g. 5] and in the rock matrix [e.g. 20] have been observed to be smaller than for neutral species. This phenomenon can be easily incorporated into the present model by applying appropriate capacity factors

and equivalent flow rates. The sorbed solute mass of the sorbing species is also taken into account in the capacity factor by multiplying the pore volume by the retardation factor [I].

As an example, Table 2 presents the characteristics of the I-129 response functions shown in Figure 10. Comparing the compartment half-lives, delay times, storage capacities and equivalent flow rates in Table 2 shows that there is a great variability in performance between the different barriers. Characteristics for the buffer to fracture and buffer to tunnel pathways are quite similar, indicating that these alternative pathways are equally important for I-129. Finally, the variability between equivalent flow rates is clearly larger than between the storage capacities. The compartment half-life for the canister is much longer than those of the other barriers, because the discharge (equivalent flow rate) from canister to buffer is significantly choked by the small size of the hole in canister. Based on compartment half-life the canister is the dominating transport barrier for I-129. This is also clearly seen by plotting the I-129 response functions on a linear scale (Figure 11). The total response function of the barrier system in practice equals with the canister response function.

Table 2. Characteristics of the different transport barriers for I-129 based on the simplified approach [I].

Parameter	**Canister**	**Buffer to fracture**	**Buffer to tunnel**	**Tunnel section**	**Geo-sphere**
Equivalent flow rate [L/a]	$0.5 \cdot 10^{-3}$	0.2	0.31	10	N/A*)
Storage capacity [L]	700	2 600	2 600	9 200	N/A*)
$T_{1/2}$ **[a]**	980 000	9000	5900	640	0.23
Delay time [a]	0.0013	2.2	110	0**)	0.008

*) Geosphere half-life is calculated directly from the mass transfer coefficient through the geosphere path. This means that only the quotient of the equivalent flow rate and storage capacity is determined.

**) Well-mixed condition is assumed for the tunnel, following definitions in the RNT-2008 definitions.

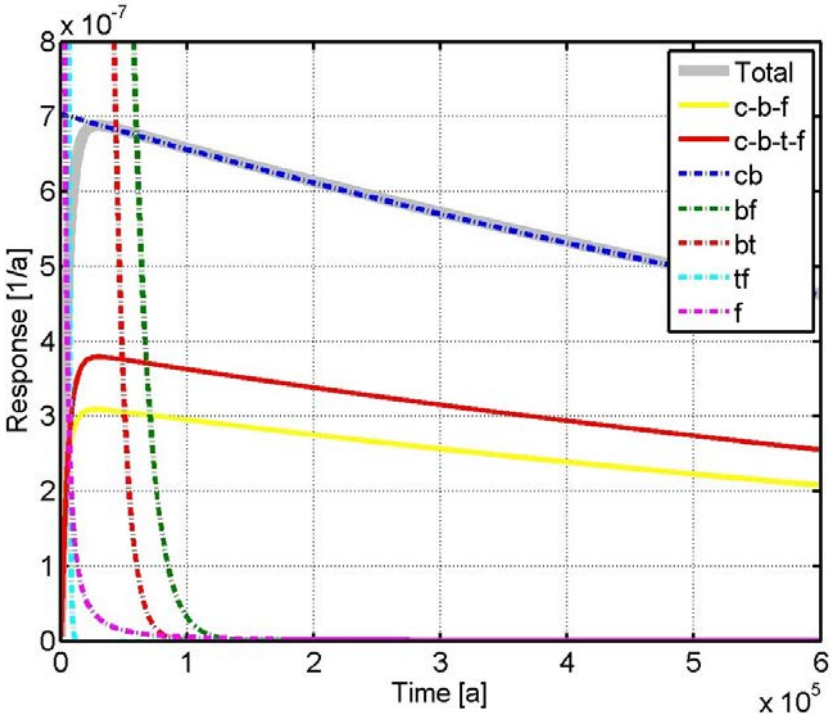

Figure 11. I-129 response functions for individual barriers (cb: from canister to buffer, bf: from buffer to fracture, bt: from buffer to tunnel, tf: from tunnel section to fracture and f: geosphere), for different pathways (c-b-f: pathway canister-buffer-fracture and c-b-t-f: pathway canister-buffer-tunnel section-fracture). The total response function of the whole system is indicated by the thick grey line. The geosphere's response function is represented by the analytical matrix diffusion model (f) described in [I]. Radioactive decay is not taken into account in the response functions.

4.6 Release rates

The objective of the simplified model was to assess the performance of the barrier system in limiting radionuclide migration from repository to biosphere. The actual radionuclide release rates to the biosphere will also depend on the source terms of the different nuclides. The source terms are not considered as a transport barrier in this study, but for calculation of the nuclide specific release rates they need to be implemented to the model. In practice, two kinds of sources exist: gradual leaching of the radionuclides, which is usually assumed to take place at a constant rate, and an instantaneous release of nuclides [e.g. 76]. The radionuclide release rate from a barrier or a set of barriers is calculated as a convolution integral between the total response function of the barrier system and the source term (Equation 2).

This indicates that the influence of the source term on the characteristics of the release rate can be roughly estimated on the same basis as the importance of the individual barriers are estimated for the performance of the whole repository system. In case of an instantaneous or very short source term, the release rate into the biosphere can be approximated by directly scaling the total system response function with the released inventory, because the temporally wider response function will dominate the convolution of the source and response functions. The opposite case is that the duration of the source is long compared to the response function of the barrier system. In this case the source term determines temporal spreading of the inventory. All calculations above can be done without radioactive decay, because no decay chains are involved in the model. The radioactive decay can be taken into account as a final step of the calculation by multiplying the time series of the release rate by the decay factor $\exp(-\lambda t)$.

Some radionuclides have low solubility in groundwater, which could affect release rate of the radionuclide. Publication [I] shows a simple and straightforward approach to approximate the solubility-limited release of a radionuclide from the canister. Possible onset of the solubility limitation is estimated by comparing the release rates of the source terms for gradual leaching and the solubility-limited release at the beginning of the release. If the release rate for gradual leaching exceeds the solubility limited release, then the solubility limited release should be used and the release rate from the canister is determined by the equivalent flow rate and the solubility-limited nuclide concentration. The duration of the solubility-limited release can be estimated based on the release rate from the canister, radioactive half-life of the nuclide and inventory of the nuclide [I].

The performance of the simplified model to reproduce the release rates for migration over the whole barrier system is shown in Figure 12 for the three nuclides calculated in [I] using data from the RNT-2008 analysis [10]. Four different model alternatives have been calculated: i) the simplified model without correction for early transient in the buffer (blue curve), ii) an additional sub-compartment in the buffer for the early transient in the buffer to fracture path, iii) repository near field compartments by simplified model without correction of early transient in the buffer convoluted with the analytical geosphere response and iv) the repository near field with the simplified model using an additional sub-compartment in the buffer for the early transient in the buffer to fracture path convoluted with the analytical geosphere response. It can be noted that C-14 and I-129 agree well with the corresponding numerical results, as it had been expected based on Figure 9. For Pu-239 an alternative model without solubility limitation (Pu-239NS) has also been calculated as a generic example of a sorbing nuclide. Release rates for both Pu-239 and Pu-239NS are within an order of magnitude from the corresponding numerical results. The initial inventory in a canister for Pu-239 has been about 2×10^{13} Bq, which gives source rate of about 2×10^{7} Bq/a (at the beginning of the release) using the spent fuel degradation rate of 10^{-6} 1/a. Thus, the attenuation of the Pu-239 and Pu-239NS release rates is several orders of magnitude and the relative accuracy of the present approach is reasonable. Naturally a considerable part of the attenuation comes from the radioactive decay due to the slow migra-

tion. However, response functions in Figure 10 show that a lot of attenuation takes place also due to the temporal spreading of the releases from the barriers. The early transient in the buffer for the buffer to fracture path and in the geosphere were studied more closely as suggested by Figures 9 and 10. Results in Figure 12 indicate that the main part of the discrepancy between the simplified approach and the numerical model comes from the geosphere response function, in agreement with the response function in Figure 10. The deviations of the early time behaviour in the simplified model response functions for the buffer and the geosphere are in the opposite directions. Comparing the simplified model calculated with the analytical geosphere response (red curve) with the numerical result (black curve) shows that the release rate estimated by the simplified model for the repository near field only is within a half of an order of magnitude from the numerical result. It also shows that conservatism of the model cannot be guaranteed if the early transient phase of the nuclide concentration field in the barrier is important for the release rates. However, inevitably this also means that the half-life of the nuclide cannot be longer than duration of the transient, implying implicitly that the release rates are considerably attenuated.

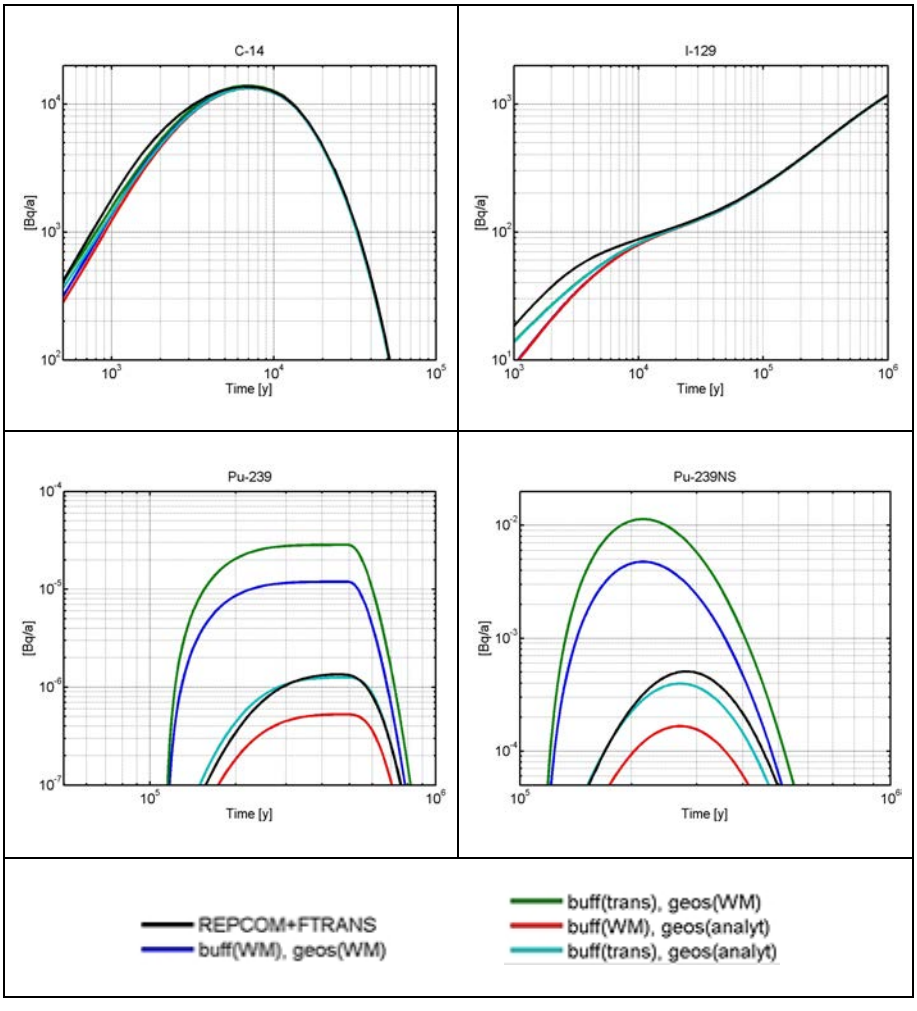

Figure 12. Calculated release rates for the nuclides C-14, I-129, Pu-239 and Pu-239NS (non-solubility limited Pu-239 representing a generic sorbing nuclide) through the repository system using data from the RNT-2008 analysis [10]. Four alternative cases have been calculated for each nuclide: i) the simplified model without corrections for early transient in the buffer (blue curves), ii) sub-compartment in the buffer for an early transient from the buffer to the fracture path (green curves), iii) the simplified model for the near field without corrections for early transient in the buffer and the analytical response function for the geosphere (red curves) and iv) sub-compartment in the buffer for an early transient from the buffer to the fracture path and the analytical response function for the geosphere (cyan curves). Numerical modelling results are shown by black curves. Figure is based on the results in Publication [I].

5. Summary and conclusions

A simplified model has been developed to represent radionuclide migration from a deep geological underground repository system to the biosphere. The modelled repository system is based on the KBS-3V concept. This concept is founded on a series of transport barriers that, in case of a leaking waste canister, should limit and retard the release and transport of radionuclides. The transport barriers include the waste canister, the bentonite buffer around the waste canister in the deposition hole, the backfilled disposal tunnel above the deposition holes, and the geosphere surrounding the whole repository.

Under the expected future conditions, there is estimated to be a considerable transport resistance between the barriers surrounding a potentially leaking canister. Low mass transfer rates between the barriers suggest that each transport barrier could be treated as a well-mixed volume. The system of interconnected well-mixed compartments without significant back-coupling of the mass flow is mathematically analogous to a radioactive decay chain. Application of this analogy provides a straightforward way to solve the total response function of the barrier system. It also suggests a familiar way to characterise the transport properties of the different barriers based on their compartment half-lives of the nuclide concentration. The present approach enables analysis of the repository system by introducing following transport barriers characteristics:

- Performance of each individual transport barrier is represented by characteristic time constants derived from the properties of the barrier and the transfer rate from that barrier to the next. The characteristic time constants are based on the assumption of well-mixed solute concentration in the barrier.
- Performance of the repository barrier system can be assessed based on the characteristic time constants of the individual barriers. This comparison directly indicates the main transport barriers, which have the longest characteristic times and are governing radionuclide release rates.
- Migration of a single radionuclide through the simplified barrier system is formally analogous to the radioactive decay chain. The system behaviour can be represented by the Bateman's equation and its well-known solutions.

In addition to compartment half-life, it is useful to characterise the barriers based on the delay time of mass transfer in the barrier and equivalent flow rate out of the

barrier. The delay time is the period of time required after the onset of inflow to a transport barrier before the outflow may start. The equivalent flow rate is an apparent volumetric flow rate that combined with the solute concentration in the barrier gives the outflow of the solute mass.

The simplified approach has been tested by modelling three nuclides that have different transport characteristics and which have also proven to be important in the past performance assessments carried out for a geological repository hosted in crystalline fractured rock [e.g. 10, 17 and 22]. Breakthrough curves for non-sorbing C-14 and I-129 were in good agreement with the results of the corresponding numerical simulations. The simplified model correctly considerably attenuates the release rate for the strongly sorbing and short-lived Pu-239, but the model is not as accurate as for the other tested nuclides. The calculated Pu-239 release rate is roughly of the same order of magnitude from the corresponding numerical results. Early transients of the barrier response functions in the buffer and geosphere are important for Pu-239 due to its short radioactive half-life compared to the compartment half-lives of these barriers. Approximation of the advection–matrix diffusion in the geosphere based on the response function of the lumped parameter model of combined exponential-plug flow model is fairly inaccurate, but a conservative estimate, for the early time behaviour. Replacing the exponential geosphere response function with the analytical advection-matrix diffusion solution improves the performance of the model. Additional improvement of the model can be achieved by also considering the early transient in radionuclide diffusion through the buffer.

Extension of the calculations to other nuclides than the tested three nuclides above is straightforward. The compartment half-lives for different transport barriers and different radionuclides can be determined by dividing the storage capacity of the compartment by the equivalent flow rate out of the barrier. Capacity of the barrier is defined as the total pore volume multiplied by the retardation factor of the nuclide in the barrier. The equivalent flow rate out of the barrier depends on the barrier, and possibly on the calculation case, that is analysed. Typically, the equivalent flow rate is calculated from the mass flux by diffusion (from canister to buffer or from buffer to tunnel) or applying diffusive boundary layer to the flowing water (from buffer to fracture or from tunnel to fracture). A collection of the equations for both equivalent flow rates and barrier capacities are presented in [I]. Compartment half-lives and delay times for all nuclides in one of the calculation case of the RNT-2008 analysis [10] are also presented respectively in Figures 8 and 9 of this thesis.

Characterisation of the transport barriers based on the compartment half-lives and delay times provides a transparent approach of identifying the main transport barrier for different nuclides. This information can be used to understand the essential safety functions of the repository system. It can also help to guide model improvement and uncertainty analysis of the transport barrier system.

The simplified approach, as implemented here, is applicable only to single nuclides. However, this is not likely to pose a major restriction on the application of the model, since single nuclides such as I-129 and C-14, have been found to have

a dominant role in most of the recent performance assessments of the repositories in crystalline fractured rock [e.g. 10, 17 and 22]. Modelling of the nuclides in the decay chains as single nuclides gives information on their migration behaviour through the barrier system that could be also helpful in understanding and interpreting actual numerical radionuclide migration simulations.

References

[1] Bear, J., 1993. Modeling flow and contaminant transport in fractured rocks. Published in flow and contaminant transport in fractured rock, edited by Bear, J., Tsang, C.-F. and de Marsily, G. Academic Press Inc., 1993. ISBN 0-12-083980-6.

[2] Becker, M.W. and Shapiro, A.M., 2000. Tracer transport in fractured crystalline rock: evidence of nondiffusive breakthrough tailing. Water Resources Research, Vol. 36, No. 7, pp. 1677–1686.

[3] COMSOL, 2012. COMSOL Multiphysics webpage. http://www.comsol.com.

[4] Grisak, G.E. and Pickens, J.F., 1980. Solute transport through fractured media. 1. The effect of matrix diffusion. Water Resources Research, Vol. 16, No. 4, pp. 719–730.

[5] Muurinen, A., 1994. Diffusion of anions and cations in compacted sodium bentonite. VTT Technical Research Centre of Finland. Espoo, Finland. VTT Publications 168.

[6] Neretnieks, I., 1980. Diffusion in the Rock Matrix: An Important Factor in Radionuclide Retardation? Journal of Geophysical Research, Vol. 85, No. B8, pp. 4379–4397.

[7] Neretnieks, I., Liu, L. and Moreno, L., 2010. Mass transfer between waste canister and water seeping in rock fractures. Revisiting the Q-equivalent model. Swedish nuclear fuel and waste management Co., Stockholm, Sweden. SKB Technical Report TR-10-42.

[8] Nilsson, L., Moreno, L., Neretnieks, I. and Romero, L., 1991. A resistance network model for radionuclide transport into the near field surrounding a repository for nuclear waste (SKB, Near Field Model 91). Swedish Nuclear Fuel and Waste Management Co., Stockholm, Sweden. SKB Technical Report 91-30.

[9] Nordman H. and Vieno T., 1994. Near-field model REPCOM. Nuclear Waste Commission of Finnish Power Companies (YJT), Helsinki, Finland. Report YJT-94-02.

[10] Nykyri, M., Nordman, H., Marcos, N., Löfman, J., Poteri, A., and Hautojärvi, A., 2008. Radionuclide Release and Transport – RNT-2008. Posiva Oy, Olkiluoto, Finland. Report Posiva 2008-06.

[11] Odling, N.E. and Roden, J.E., 1997. Contaminant transport in fractured rocks with significant matrix permeability, using natural fracture geometries. Journal of Contaminant Hydrology, Vol. 27, pp. 263–283.

[12] Painter, S. and Cvetkovic, V., 2005. Upscaling discrete fracture network simulations: An alternative to continuum transport models. Water Resources Research, Vol. 41, No. 2, W02002, doi: 10.1029 /2004WR003682.

[13] Yarlagadda, R.K. Rao., 2010. Analog and digital signals and systems. Springer Science. ISBN 978-1-4419-0033-3.

[14] Raiko, H., 2005. Disposal canister for spent nuclear fuel – design report. Posiva Oy, Olkiluoto, Finland. Report Posiva 2005-02.

[15] Rasilainen, K., 1997. Matrix diffusion model, In situ tests using natural analogues. Technical Research Centre of Finland, Espoo, Finland. VTT Publications 331.

[16] Romero, L., Moreno, L. and Neretnieks, I., 1991. A compartment model for solute transport in the near field of a repository for radioactive waste (Calculations for Pu-239) Swedish Nuclear Fuel and Waste Management Co., Stockholm, Sweden. SKB Technical Report 91-48.

[17] SKB, 2010. Radionuclide transport report for the safety assessment SR-Site. Swedish Nuclear Fuel and Waste Management Co, Stockholm, Sweden. SKB Report TR-10-50.

[18] SKBF/KBS, 1983. Final storage of spent nuclear fuel — KBS-3, Vol. I–IV. Swedish Nuclear Fuel Supply Co/Division KBS, Stockholm, Sweden.

[19] Tsang, C.F., Tsang, Y.W. and Hale, F.V., 1991. Tracer transport in fractures: Analysis of field data based on a variable-aperture channel model. Water Resources Research, Vol. 27, No. 12, pp. 3095–3106.

[20] Valkiainen, M., Aalto, H., Lindberg, A., Olin, M. and Siitari-Kauppi, M., 1995. Diffusion in the matrix of rocks from Olkiluoto – The effect of anion exclusion. Nuclear Waste Commission of Finnish Power Companies, Helsinki, Finland. Report YJT-95-20.

[21] Vieno, T. and Ikonen, A., 2005. Plan for safety case of spent fuel repository at Olkiluoto. Posiva Oy, Olkiluoto, Finland. Report Posiva 2005-01.

[22] Vieno, T., and Nordman, H., 1999. Safety assessment of spent fuel in Hästholmen, Kivetty, Olkiluoto and Romuvaara – TILA-99. Posiva Oy, Olkiluoto, Finland. Report Posiva 99-07.

[23] Öhman, J., Niemi A. and Tsang, C.-F., 2005. A regional-scale particle-tracking method for nonstationary fractured media, Water Resources Research, Vol. 41, No. 3, W03016, doi: 10.1029/2004WR003498.

[24] Tang, D.H., Frind, E.O. and Sudicky, E.A., 1981. Contaminant transport in fractured porous media: Analytical solution for a single fracture. Water Resources Research, Vol. 17, No. 3. pp. 555–564.

[25] Neretnieks, I., 1982. Leach rates of high level waste and spent fuel – Limiting rates as determined by backfill and bedrock conditions. Elsevier Science Publishing Company Inc., New York, USA. Scientific Basis for Nuclear Waste Management V. Pp. 559–568.

[26] Andersson, P., Byegård, J., Billaux, D., Cvetkovic, V., Dershowitz, W., Doe, T., Hermansson, J., Poteri, A., Tullborg, E.-L. and Winberg, A., 2007. TRUE Block Scale Continuation Project, Final Report, Swedish nuclear fuel and waste management Co, Stockholm, Sweden. SKB Technical Report TR-06-42.

[27] Poteri, A., Cvetkovic, V., Dershowitz, W., Billaux, D. and Winberg, A., 2006. Illustration of Uncertainties in Assessments of Flow and Transport in a Block Scale Fracture Network – an Example from the Äspö Hard Rock Laboratory. American Geophysical Union, Fall Meeting 2006, abstract #H12A-07.

[28] Poteri, A., 2005. TRUE Block Scale continuation project. Evaluation of the BS2B sorbing tracer tests using the Posiva stream tube approach. Swedish Nuclear Fuel and Waste Management, Stockholm, Sweden. SKB International Progress Report IPR-05-36. Stockholm, Sweden.

[29] Poteri, A., Billaux, D., Dershowitz, W., Gómez-Hernández, J., Cvetkovic, V., Hautojärvi, A., Holton, D., Medina, A. and Winberg, A., 2002. Final report of the TRUE Block Scale project 3. Modelling of flow and transport. Swedish Nuclear Fuel and Waste Management, Stockholm, Sweden. SKB Technical Report TR-02-15.

[30] Winberg, A., Andersson, P., Byegård, J., Poteri, A., Cvetkovic, V., Dershowitz, W., Doe, T., Hermanson, J., Gómez-Hernándéz, J., Hautojärvi, A., Billaux, D., Tullborg, E.-L., Holton, D., Meier, P. and Medina, A., 2002. Final

report of the TRUE Block Scale project. 4. Synthesis of flow, retention in the block scale. Swedish Nuclear Fuel and Waste Management, Stockholm, Sweden. SKB Technical Report TR-02-16.

[31] Poteri, A., 2008, Solute transport and retention in fractured rock. Technical Research Centre of Finland VTT, Espoo, Finland. VTT Research Notes 2464. http://www.vtt.fi/inf/pdf/tiedotteet/2009/T2464.pdf.

[32] Poteri, A., 2003. Retention processes discrimination for various assumptions of fracture heterogeneity. Swedish Nuclear Fuel and Waste Management, Stockholm, Sweden. SKB International progress report IPR-03-42.

[33] Löfman, J. and Poteri, A., 2008. Groundwater flow and transport simulations in support of RNT-2008 analysis. Posiva Oy, Olkiluoto, Finland, Posiva Working Report 2008-52.

[34] Posiva Oy, 2008. Safety Case Plan 2008. Posiva Oy, Olkiluoto, Finland. Report Posiva 2008-05.

[35] Vieno, T. and Nordman, H., 1996. Interim report on safety assessment of spent fuel disposal, TILA-96. Posiva Oy, Olkiluoto, Finland. Report Posiva 96-17.

[36] Andra, 2005. Dossier 2005, Granite. Safety analysis of a geological repository. Agence nationale pour la gestion des déchets radioactifs, Châtenay-Malabry, France. Andra Report Series, 287 VA. ISSN 1772-2136.

[37] SKBF/KBS, 1978. Handling and final storage of Unprocessed spent nuclear fuel, Volumes I–II. Nuclear Fuel Safety Project (KBS) of the Swedish power utilities.

[38] SKB, 1999. Deep repository for spent nuclear fuel. SR 97 – Post-closure safety, Volumes I–II. Swedish Nuclear Fuel and Waste Management, Stockholm, Sweden. SKB Technical Report TR-99-06.

[39] Gierszewski, P., Avis, J.,Calder, N., D'Andrea, A., Garisto, F., Kitson, C., Melnyk, T., Wei, K. and Wojciechowski, L., 2004. Third Case Study – Postclosure Safety Assessment. Ontario Power Generation, Toronto, Ontario, Canada. Report No: 06819-REP-01200-10109-R00.

[40] SKB, 2011. Long-term safety for the final repository for spent nuclear fuel at Forsmark. Main report of the SR-Site project, Volumes I–III. Swedish Nuclear Fuel and Waste Management, Stockholm, Sweden. SKB Technical Report TR-11-01.

[41] Nagra, 1994. Kristallin – I, Safety Assessment Report. Die Nationale Genossenschaft für die Lagerung radioaktiver Abfälle (Nagra), Wettingen, Switzerland. Report NAGRA NTB-93-22.

[42] JNC, 2000. H12: Project to Establish the Scientific and Technical Basis for HWL Disposal in Japan. Japan Nuclear Cycle Development Institute (JNC), Ibaraki, Japan. Report JNC TN1410 2000-001.

[43] King, F., Ahonen, L., Taxén, C., Vuorinen, U. and Werme, L., 2001. Copper corrosion under expected conditions in a deep geological repository. Swedish Nuclear Fuel and Waste Management, Stockholm, Sweden. SKB Technical TR-01-23.

[44] Kwong, G.M., 2011. Status of Corrosion Studies for Copper Used Fuel Containers Under Low Salinity Conditions. Nuclear Waste Management Organization (NWMO), Toronto, Ontario, Canada. Report NWMO TR-2011-14.

[45] Swedish National Council for Nuclear Waste Report, 2010. Nuclear Waste State-of-the-Art Report 2010 – challenges for the final repository programme. Swedish Government, Stockholm, Sweden. Official Reports SOU 2010:6.

[46] Szakálos, P., Hultqvist. G. and Wikmark, G., 2007. Corrosion of copper by water. The Electrochemical Society. Electrochemical and Solid-State Letters, Vol. 10, No. 11, pp. C63-C67.

[47] Villar, M.V., Sánchez, M. and Gens, A., 2008. Behaviour of a bentonite barrier in the laboratory: Experimental results up to 8 years and numerical simulation. Elsevier, Ltd. Physics and Chemistry of the Earth Vol. 33. Pp. S476–S485.

[48] Pusch, R., 1980. Permeability of highly compacted bentonite. Nuclear Fuel Safety Project (KBS) of the Swedish power utilities. SKBF/KBS Technical Report 80-16.

[49] Komine, H., 2008. Theoretical equations for evaluating hydraulic conductivities of bentonite based buffer and backfill. Journal of Geotechnical and Geoenvironmental Engineering. doi: 10.1061/(ASCE)1090-0241(2008) 134:4(497).

[50] Börgesson, L., Dixon, D., Gunnarsson, D., Hansin, J., Jonsson, E. and Keto, P., 2009. Assessment of backfill design for KBS-3V repository. Posiva Oy, Olkiluoto, Finland. Posiva Working Report 2009-115.

[51] Ahonen, L., Hakkarainen, V., Kaija, J., Kuivamäki, A. Lindberg, A., Paananen, M., Paulamäki, S. and Ruskeeniemi, T., 2011. Geological safety aspects of nuclear waste disposal in Finland. Geoscience for Society 125th Anniversary Volume. Ed. Nenonen K. and Nurmi P. A. Geological Survey of Finland, Special Paper 49. Pp. 145–152.

[52] Vidstrand, P., Follin, S., Selroos, J.-O., Näslund, J.-O. and Rhén, I., 2012. Modeling of groundwater flow at depth in crystalline rock beneath a moving ice-sheet margin, exemplified by the Fennoscandian Shield, Sweden. Springer-Verlag. Hydrogeology Journal, DOI 10.1007/s10040-012-0921-8.

[53] Pitkänen, P., Luukkonen, A. and Partamies, A., 2007. Buffering against intrusion of groundwater of undesirable composition. In: OECD/NEA workshop proceedings, Manchester, United Kingdom, 13–15 November 2007. NEA No. 6362.

[54] Miller, B. and Marcos, N., (Eds.), 2007. Process Report – FEPs and scenarios for a spent fuel repository at Olkiluoto. Posiva Oy, Olkiluoto, Finland. Report Posiva 2007-12.

[55] SKB, 2010. Fuel and Canister process report for the safety assessment SR-Site. Swedish Nuclear Fuel and Waste Management, Stockholm, Sweden. SKB Technical Report TR-10-46.

[56] Posiva, 2006. Expected evolution of a spent nuclear fuel repository at Olkiluoto. Revised October 2007. Posiva Oy, Olkiluoto, Finland. Report Posiva 2006-05.

[57] SKB, 1999. SR 97. Processes in the repository evolution. Swedish Nuclear Fuel and Waste Management, Stockholm, Sweden. SKB Technical Report TR-99-07.

[58] SKB, 2010. Buffer, backfill and closure process report for the safety assessment SR-Site. Swedish Nuclear Fuel and Waste Management, Stockholm, Sweden. SKB Technical Report TR-10-47.

[59] Vaittinen, T., Ahokas, H., Nummela, J. and Paulamäki, S., 2011. Hydrogeological structure model of the Olkiluoto site – Update in 2011. Posiva Oy, Olkiluoto, Finland. Posiva Working Report 2011-65.

[60] Yuan, D. and Kernan, W., 2007. Explicit solutions for exit-only radioactive decay chains. American Institute of Physics. Journal of Applied Physics 101. 094907 (2007). doi: 10.1063/1.2715785.

[61] Poteri, A. and Vieno, T., 1989. Probabilistic system assessment code SYVAC/FI for safety analysis of nuclear waste disposal. Technical Research Centre of Finland, Espoo, Finland. VTT Research Notes 1018. (In Finnish).

[62] Bateman, H., 1910. Solution of a system of differential equations occurring in the theory of radio-active transformations. Proceedings of the Cambridge Philosophical Society Vol. 15, pp. 423–427.

[63] Amaku, M., Pascholati, P.R. and Vanin, V.R., 2010. Decay chain differential equations: Solution through matrix algebra. Elsevier B.V. Computer Physics Communications Vol. 181, pp. 21–23. doi: 10.1016/j.cpc.2009.08.011.

[64] Berkowitz, B., 2002. Characterizing flow and transport in fractured geological media: A review. Elsevier Science Ltd. Advances in Water Resources Vol. 25, pp. 861–884.

[65] Fetter, C.W., 1988. Applied Hydrogeology, Second Edition. Merrill Publishing Company. Columbus, Ohio, USA. ISBN 0-675-20887-4.

[66] Romero, L., Thompson, A., Moreno, L., Neretnieks, I., Widen, H. and Boghammar, A., 1999. Comp23/Nuctran User's guide. Proper version 1.1.6. Swedish Nuclear Fuel and Waste Management, Stockholm, Sweden. SKB Report R-99-64.

[67] Hedin, A., 2001. Integrated analytic radionuclide transport model for a spent nuclear fuel repository in saturated fractured rock. Nuclear Technology Vol. 138, No. 2, pp.179–205.

[68] Lee, Y.-M., Kang, C.-H. and Hwang, Y.-S., 2007. Nuclide release from an HLW repository: Development of a compartment model. Elsevier Ltd. Annals of Nuclear Energy Vol. 34, pp. 782–791.

[69] Murakami, H. and Ahn, J., 2011. Development of compartment models with Markov-chain processes for radionuclide transport in repository region. Elsevier Ltd. Annals of Nuclear Energy Vol. 38, pp. 511–519.

[70] Tsang, C.-F. and Neretnieks, I., 1998. Flow channeling in heterogeneous fractured rocks. American Geophysical Union. Reviews of Geophysics, Vol. 36, No. 2, pp. 275–298. Paper number 97RG03319.

[71] Chen, C.-T., 1999. Linear System Theory and Design (3rd Edition). Oxford University Press. ISBN 978-0-19-511777-6, Electronic ISBN 978-1-61344-115-2.

[72] Nordqvist, A.W., Tsang, Y.W., Tsang, C.F., Dverstorp, B. and Andersson J., 1996. Effects of high variance of fracture transmissivity on transport and sorption at different scales in a discrete model for fractured rocks. Journal of Contaminant Hydrology Vol. 22, pp.39–66.

[73] Kekäläinen, P., Voutilainen, M., Poteri, A., Hölttä, P., Hautojärvi, A. and Timonen, J., 2011. Solutions to and validation of matrix-diffusion models. Springer. Transport in Porous Media Vol. 87, pp.125–149. doi: 10.1007/s11242-010-9672-y.

[74] FTRANS, 1983. A two-dimensional code for simulating fluid flow and transport of radioactive nuclides in fractured rock for repository performance assessment. Intera Environmental Consultants Inc., Houston, Texas, USA. Report ONWI-426.

[75] Pulkkanen, V.-M. and Nordman, H., 2011. Effect of bedrock fractures on radionuclide transport near a vertical deposition hole for spent nuclear fuel. Posiva Oy, Olkiluoto, Finland. Report Posiva 2011-03.

[76] Werme, L.O., Johnson, L.H., Oversby, V.M., King, F., Spahiu, K., Grambow, B. and Shoesmith, D.W., 2004. Spent fuel performance under repository conditions: A model for use in SR-Can. Swedish Nuclear Fuel and Waste Management, Stockholm, Sweden. SKB Technical Report TR-04-19.

[77] Hansen, J., Korkiala-Tanttu, L., Keski-Kuha, E. and Keto, P., 2010. Deposition tunnel backfill design for a KBS-3V repository. Posiva Oy, Olkiluoto, Finland. Posiva Working Report 2009-129.

[78] Smith, P. and Curti, E., 1995. Some variations of the Kristalline-I near-field model. Die Nationale Genossenschaft für die Lagerung radioaktiver Abfälle (Nagra), Wettingen, Switzerland. Nagre Technical Report 95-09.

[79] Maloszewski, P. and Zuber, A., 1996. Lumped parameter models for the interpretation of environmental tracer data. In: Manual on Mathematical Models in Isotope Hydrogeology. IAEA (International Atomic Energy Agency), Vienna, pp. 9–58.

[80] Isam, E.A. and Campana, M.E., 1996. A general lumped parameter model for the interpretation of tracer data and transit time calculation in hydrologic systems. Journal of Hydrology, Vol. 179, pp. 1–21.

[81] Maloszewski, P. and Zuber, A., 1996. A general lumped parameter model for the interpretation of tracer data and transit time calculation in hydrologic systems (Journal of Hydrology 179 (1996) 1-21) Comments. Journal of Hydrology, Vol. 204, pp. 297–300.

[82] Painter, S., Cvetkovic, V. and Selroos, J.-O., 1998. Transport and retention in fractured rock: Consequences of a power-law distribution for fracture lengths. Physical Review E, Vol. 57, No. 6, pp. 6917–6922.

[83] Neretnieks, I. (2006), Channeling with diffusion into stagnant water and into a matrix in series, Water Resour. Res., 42, W11418, doi: 10.1029/2005WR004448.

[84] NEA, 2002. Radionuclide retention in geological media. Workshop Proceedings, Oskarshamn, Sweden, 7–9 May 2001. Nuclear Energy Agency, Organisation for Economic Co-operation and Development. Report NEA No. 3061.

[85] Cvetkovic, V. Cheng, H., Byegård, J., Winberg, A., Tullborg, E.L. and Widestrand, H., 2010. Transport and retention from single to multiple fractures in crystalline rock at Äspö (Sweden): 1. Evaluation of tracer test results and sensitivity analysis. Water Resources Research, Vol. 46, W05505, doi: 10.1029/2009WR008013.

[86] Cvetkovic, V., Solroos, J.O. and Cheng, H., 1999. Transport of reactive tracers in rock fractures. Journal of Fluid Mechanics, Vol. 378, pp. 335–356.

[87] Cvetkovic, V. and Cheng, H., 2008. Sorbing tracer experiments in a crystalline rock fracture at Äspö (Sweden): 3. Effect of microscale heterogeneity. Water Resources Research, Vol. 44, W12447, doi: 10.1029/2007WR006797.

[88] RETROCK project, 2004. RETROCK Project (2004), Treatment of geosphere retention phenomena in safety assessments: Scientific basis of retention processes and their implementation in safety assessment models (WP2), Report SKB R-04-48, Swedish Nuclear Fuel and Waste Management Co., Stockholm, Sweden.

PUBLICATION I

Representing solute transport through the multi-barrier disposal system by simplified concepts

In: Posiva report series, Posiva Oy, Olkiluoto, Finland. Report Posiva 2012-20.

POSIVA 2012-20

Representing Solute Transport Through the Multi-Barrier Disposal System by Simplified Concepts

Antti Poteri
Henrik Nordman
Veli-Matti Pulkkanen
Aimo Hautojärvi
Pekka Kekäläinen

February 2012

POSIVA OY
Olkiluoto
FIN-27160 EURAJOKI, FINLAND
Phone (02) 8372 31 (nat.), (+358-2-) 8372 31 (int.)
Fax (02) 8372 3809 (nat.), (+358-2-) 8372 3809 (int.)

POSIVA 2012-20

Representing Solute Transport Through the Multi-Barrier Disposal System by Simplified Concepts

Antti Poteri, Henrik Nordman
Veli-Matti Pulkkanen
VTT

Aimo Hautojärvi
Posiva Oy

Pekka Kekäläinen
University of Jyväskylä
Department of Physics

February 2012

POSIVA OY
Olkiluoto
FI-27160 EURAJOKI, FINLAND
Phone (02) 8372 31 (nat.), (+358-2-) 8372 31 (int.)
Fax (02) 8372 3809 (nat.), (+358-2-) 8372 3809 (int.)

ISBN 978-951-652-201-5
ISSN 1239-3096

Posiva-raportti – Posiva Report

Posiva Oy
Olkiluoto
FI-27160 EURAJOKI, FINLAND
Puh. 02-8372 (31) – Int. Tel. +358 2 8372 (31)

Raportin tunnus – Report code
POSIVA 2012-20

Julkaisuaika – Date
February 2012

Tekijä(t) – Author(s)
Antti Poteri, Henrik Nordman, Veli-Matti Pulkkanen, VTT
Aimo Hautojärvi, Posiva Oy
Pekka Kekäläinen, University of Jyväskylä, Department of Physics

Toimeksiantaja(t) – Commissioned by
Posiva Oy

Nimeke – Title

REPRESENTING SOLUTE TRANSPORT THROUGH THE MULTI-BARRIER DISPOSAL SYSTEM BY SIMPLIFIED CONCEPTS

Tiivistelmä – Abstract

The repository system chosen in Finland for spent nuclear fuel is composed of multiple successive transport barriers. If a waste canister is leaking, this multi-barrier system retards and limits the release rates of radionuclides into the biosphere. Analysis of radionuclide migration in the previous performance assessments has largely been based on numerical modelling of the repository system. The simplified analytical approach introduced here provides a tool to analyse the performance of the whole system using simplified representations of the individual transport barriers. This approach is based on the main characteristics of the individual barriers and on the generic nature of the coupling between successive barriers.

In the case of underground repository the mass transfer between successive transport barriers is strongly restricted by the interfaces between barriers leading to well-mixed conditions in these barriers. The approach here simplifies the barrier system so that it can be described with a very simple compartment model, where each barrier is represented by a single, or in the case of buffer, by not more than two compartments. This system of compartments could be solved in analogy with a radioactive decay chain. The model of well mixed compartments lends itself to a very descriptive way to represent and analyse the barrier system because the relative efficiency of the different barriers in hindering transport of solutes can be parameterised by the solutes half-times in the corresponding compartments. In a real repository system there will also be a delay between the start of the inflow and the start of the outflow from the barrier. This delay can be important for the release rates of the short lived and sorbing radionuclides, and it was also included in the simplified representation of the barrier system.

In a geological multi-barrier system, spreading of the outflowing release pulse is often governed by the typical behaviour of one transport barrier, because the reservoir capacities of and mass transfer coefficients between adjacent barriers may differ significantly. Characterisation of these properties of the repository system by the simplified approach is straightforward. The relative efficiency of the different barriers in attenuating transport of radionuclides can be determined by comparing the solute's half-times in the barriers. Solute's half-times in different barriers can also be compared with the radioactive half-lives of the nuclides. Already the first barrier along the release path in which the solute's half-time is longer than the nuclide's radioactive half-life will be an efficient transport barrier for that nuclide, although the barrier with longest solute half-time will be the most efficient barrier.

The release rates of radionuclides from a leaking waste canister may also be dominated by their source term instead of the barrier system of the repository. Spent nuclear fuel is a ceramic material that dissolves slowly into groundwater. Waste dissolution can also be treated as a barrier in which the dissolution time (or half of it) corresponds to a solute's half-times in a barrier, and can be readily compared with the other barriers.

The validity of the simplified description was tested against numerical transport simulations for three representative nuclides: C-14, I-129 and Pu-239. The results of these simulations showed reasonable agreement with those of the simplified approach.

Avainsanat - Keywords

Radionuclide migration, repository, multibarrier system, performance assessment.

ISBN	ISSN
ISBN 978-951-652-201-5	ISSN 1239-3096
Sivumäärä – Number of pages: 92	Kieli – Language: English

Posiva-raportti – Posiva Report

Posiva Oy
Olkiluoto
FI-27160 EURAJOKI, FINLAND
Puh. 02-8372 (31) – Int. Tel. +358 2 8372 (31)

Raportin tunnus – Report code
POSIVA 2012-20

Julkaisuaika – Date
Helmikuu 2012

Tekijä(t) – Author(s)
Antti Poteri, Henrik Nordman, Veli-Matti Pulkkanen, VTT
Aimo Hautojärvi, Posiva Oy
Pekka Kekäläinen, University of Jyväskylä, Department of Physics

Toimeksiantaja(t) – Commissioned by
Posiva Oy

Nimeke – Title

LOPPUSIJOITUSTILAN VAPAUTUMISESTEIDEN KUVAAMINEN YKSINKERTAISTETTULA MALLILLA

Tiivistelmä – Abstract

Suomeen suunniteltu ydinjätteiden loppusijoituslaitos rakentuu useista sisäkkäisistä vapautumisesteistä. Vapautumisesteiden tarkoituksena on pidättää ja rajoittaa radionuklidien leviämistä biosfääriin, jos jätekanisteri alkaa vuotaa. Radionuklidien kulkeutumisen mallinnus on aiemmissa turvallisuusselvityksissä perustunut loppusijoitussysteemin numeeriseen mallintamiseen. Tässä raportissa esitettävä lähestymistapa tarjoaa keinon arvioida koko loppusijoitussysteemin toimintaa kuvaamalla yksittäisten vapautumisesteiden toiminta yksikertaisella analyyttisellä mallilla.

Geologisen loppusijoitustilan luonteesta johtuen massan siirto peräkkäisten vapautumisesteiden välillä on voimakkaasti rajoitettu, mikä johtaa hyvin sekoitettuun pitoisuusjakaumaan vapautumisesteiden sisällä. Tässä raportissa esiteltävässä yksinkertaistetussa mallissa vapautumisesteistä rakennetaan yksinkertainen kompartmenttimalli. Jokainen vapautumiseste kuvataan yhdellä kompartmentilla, lukuun ottamatta kahdella kompartmentilla kuvattavaa sijoitusreiän bentoniittipuskuria. Aineiden kulkeutuminen kompartmenttimallin läpi voidaan ratkaista analogisesti radioaktiivisen hajoamisketjun kanssa.

Hyvin sekoitettujen kompartmenttien malli on tehokas tapa kuvata vapautumisesteiden toimintaa. Vapautumisesteen toiminta on mallissa kuvattu kahdella aikavakiolla: pitoisuuden puoliintumisaika vapautumisesteessä ja viiveaika kulkeutumiselle vapautumisesteen yli. Pitoisuuden puoliintumisaika kuvaa vapautumisesteen kykyä levittää ja vaimentaa pitoisuusvuota. Nimensä mukaisesti viiveaika kuvaa vapautumisesteen läpi kulkevan pitoisuus pulssin siirtymistä ajassa. Pulssin viivästyminen ei sinänsä laimenna tai levitä aineiden pitoisuuksia, mutta lyhytikäisillä radioaktiivisilla aineilla viivästyminen voi johtaa merkittävään pitoisuusvuon vaimenemiseen.

Vapautumisesteiden kuvaaminen pitoisuuden puoliintumisajoilla tekee mallin soveltamisesta suoraviivaista. Eri vapautumisesteiden tehokkuutta voidaan helposti arvioida vertaamalla vapautumisesteisiin liittyviä pitoisuuden puoliintumisaikoja. Pitoisuusvuon vaimenemista koko loppusijoitussysteemissä hallitsee vapautumiseste, jossa pitoisuuden puoliintumisaika on pisin. Kulkeutuvien nuklidien radioaktiivista puoliintumisaikaa voi myös verrata pitoisuuden puoliintumisaikoihin vapautumisesteissä. Kaikki vapautumisesteet, joissa pitoisuuden puoliintumisaika on pidempi kuin nuklidin radioaktiivinen puoliintumistaika ovat tehokkaita vapautumisesteitä kyseessä olevalle nuklidille, vaikkakin pisimmän pitoisuuden puoliintumisajan vapautumiseste hallitsee koko systeemin käyttäytymistä.

Radionuklidien vapautumista polttoainematriisista ei ole tässä raportissa käsitelty vapautumisesteenä. Radionuklidien liukenemisen käsittely vapautumisesteenä on kuitenkin tässä raportissa esitetyn yksinkertaistetun mallin yhteydessä helppoa. Polttoainematriisin liukenemisaikaa voidaan verrata suoraan eri vapautumisesteiden aikavakioihin.

Raportissa esitettyä yksinkertaistettua mallia on verrattu numeeristen kulkeutumismallien antamiin tuloksiin kolmelle nuklidille: C-14, I-129 ja Pu-239. Tulosten perusteella yksinkertaistettu malli antaa kohtalaisen yhtäpitävät tulokset numeeristen simulointien kanssa.

Avainsanat - Keywords

Radionuklidien kulkeutuminen, loppusijoitustila, vapautumisesteet, toimintakykyanalyysi.

ISBN
ISBN 978-951-652-201-5

ISSN
ISSN 1239-3096

Sivumäärä – Number of pages
92

Kieli – Language
Englanti

PREFACE

During the course of the work many helpful discussions took place within Posiva's safety case assessment group and the authors would like to thank all the members of the assessment group for their comments and input. Especially, the comments from Dr. Paul Smith and Dr. José Luis Cormenzana on an early draft of the report were very helpful.

The authors of the report are particularly thankful to Professor Jussi Timonen and Mr. Mikko Nykyri for their thorough reviewing of the final draft of the report. Their comments and suggestions were very valuable and improved the report significantly.

TABLE OF CONTENTS

1 INTRODUCTION

Geological disposal of spent nuclear fuel in Finland is being planned on the basis of the KBS-3 concept. This disposal concept is based on a series of transport barriers that will hinder the migration of radionuclides if a waste canister loses its integrity. The repository is excavated deep in the bedrock. Waste is planned to be encapsulated in copper canisters that will be disposed of in vertical deposition holes drilled down from the floors of the deposition tunnels in KBS-3V. There is also a horizontal variant of the concept, called KBS-3H, which is not specifically handled in this report, although the concepts of the report mostly apply to it, too. The space between the waste canister and the surrounding rock face of the deposition hole will be filled with compacted bentonite clay (later called as the buffer). The tunnels will be backfilled using a mixture of crushed rock and bentonite or other material containing swelling clay (later called as the backfill or the tunnel backfill).

A detailed migration analysis of the whole multi-barrier system requires numerical modelling. Based on an integrated model response of the whole system, it is difficult to evaluate the importance of different transport barriers on the performance of the repository system as a whole. Understanding the relative importance of the different barriers and processes with varying release rates through them, makes it easier to judge for example the impact of various uncertainties on the release rates.

In this study we analyse the performance of the individual transport barriers, and that of the whole system of these barriers. The goal is a simplified description of the key factors in the multi-barrier system. Earlier studies that describe transport barriers by analytical and simplified methods have been carried out, such as Nilsson et al. (1991). The approach there is to represent the resistances to the mass transfer of radionuclides with an analogous network of resistances. The model embodies transport by diffusion from the defective canister into a fracture that intersects the deposition hole. Contrary to the present model, the Nilsson et al. (1991) model is a steady state model, but it includes sub-models for details of the system, which are not explicitly considered in the present model, e.g. different types of damage of the canister, the mass transfer resistance created by possible penetration of the buffer or backfill material into a fracture and diffusion from the buffer through the rock matrix to the ceiling or floor of the rock fracture. Additional resistances, like the aforementioned penetration of the buffer material into the fracture, can easily be incorporated also in the present model.

The description of mass transfer in the repository near field by equivalent flow rates have recently been reconsidered by Neretnieks et al. (2010), which confirmed that the inaccuracy of the simplified concept of equivalent flow rate is small compared to uncertainties in the actual flow rates and properties of the transport barriers.

Romero et al. (1991) have developed a simplified compartment model that takes advantage of supplementing analytical and semi-analytical solutions with simplifications in the model. The present model resembles very closely the compartment model of Romero et al. (1991). However, the present model simplifies the description of the transport barrier system even further. Each transport barrier is described by a single well-mixed compartment, and back coupling of the mass transfer along the release path is considered to be insignificant and it is neglected. This leads to

a system which is analogous with a branching radioactive decay chain. The system is represented by four compartments, because each barrier is represented by a single compartment. As a fundamental extension, the present model also studies the whole release path to the biosphere, including also the flow path through fractures in the geosphere. It is also studied how well the properties of the transport barrier in the geosphere release path can be represented using an equivalent mixing tank model. And, in addition, all mass transfer coefficients between the compartments are estimated analytically. The goal is to describe the performance of the transport barriers by their temporal characteristics, and to find a common conceptualisation basis for all of the barriers. Computations in the present study are based on the assumption that the engineered transport barriers function as they are planned to function and that the mass transfer in the repository near-field is dominated by molecular diffusion.

The relevance of the simplified description and the extraction of the key factors depends on the ability to reproduce the solute release rates that are consistent with detailed numerical computations. The end result is then a good understanding of the multi-barrier system as a whole and its individual components.

2 MULTI-BARRIER SYSTEM

The multi-barrier system in the KBS-3V disposal concept includes a copper canister, bentonite buffer, tunnel backfill and the geosphere. The geosphere is a natural barrier that secures stable and predictable chemical, hydraulic and mechanical conditions which are used as a basis for the technical design of other barriers, and also as a basis for the performance assessment of the repository system for the required period of time.

The multi-barrier system supports the endurance of the waste canister by restricting fluxes of corroding species onto the canister surface. Groundwater flow is confined outside the deposition holes due to the barrier system, and the barriers can also protect waste canisters mechanically by absorbing moderate rock movements.

The present report focuses only on the role of the multi-barrier system related to radionuclide releases. One important function of the multi-barrier system is to retard and limit radionuclide releases if a waste canister loses its integrity. Retardation means here that a release starting at some time at the inlet part of a component appear later at the outlet. This we also call a time shift in the following. Limitation means that the maximal release rate is lowered, but the duration of the release is lengthened. These temporal features of the release determine the performance of the individual barriers. The former feature is most important for short-lived radionuclides and the second one is essential for long-lived nuclides.

2.1 Migration pathway

A flow chart of solute transport along the release path through the different transport barriers is shown in Figure 2-1. The behaviour of this system is studied in the saturated conditions that are relevant for the long term safety analysis.

The barrier system forms a chain of barriers, in which the mass is transferred only between neighbouring barriers. The main features of the studied migration model are the following:

- All barriers are fully saturated by water.
- Mass transfer between barriers is limited by the “upstream” barrier and the mass flux between two barriers is determined by assuming zero concentration in the target barrier, i.e. no counter pressure is caused by the downstream barrier to the mass flux.
- The system is conceptualised as a system of reservoirs, in which capacities are connected by resistances that limit the mass fluxes.

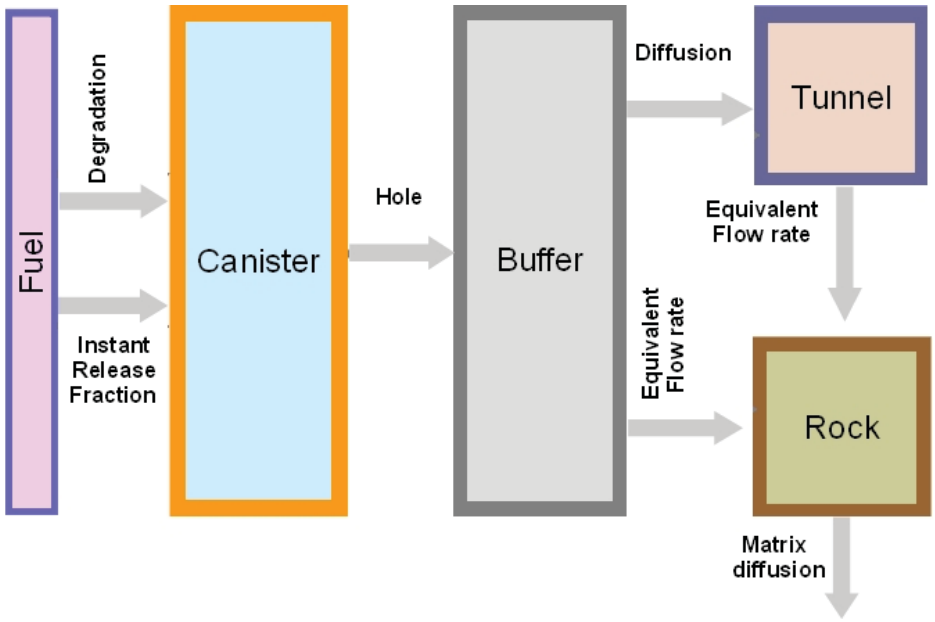

Figure 2-1. *Flow chart of solute mass transfer between the migration barriers.*

2.2 Dominating transport barriers

The main functions of the transport barriers are either to attenuate (limit) solute release rates or to retard (delay) the transport through them, or both, once a disposal canister has started to leak. The present study aim at formulating a simplified representation of the main transport resistances and capacities of the components of the repository system that forms a series of multiple transport barriers.

The response function of a transport barrier is represented by two time constants: 1) the delay between the start of inflow to the barrier and the outflow from the barrier and 2) the attenuation of the release rate, characterised by spreading in time of the solute pulse when passing through the transport barrier. Retardation in the transport times of the solute leads to attenuation of the release rates for the radioactively decaying species that have short half-lives or that are strongly sorbing. Spreading of the solute pulse attenuates also the release rates of the long-lived nuclides.

The analysis of the barrier system is first carried out by the studying release rates of a non-decaying and non-sorbing tracer. The concept of response function allows an easy extension of the analysis to decaying and sorbing species. Application of a simplified response function of the total repository system is demonstrated for a few radionuclides that are important also in the performance assessment: Pu-239 (sorbing and solubility limited nuclide), C-14 (non-sorbing nuclide) and I-129 (anion and dominating nuclide in the previous performance assessments).

Potential release pathways are studied by analysing first the whole multi-barrier system and then assessing each transport barrier one at a time. The aim is to identify a

dominating transport barrier or barriers that can be used to understand the most essential factors in radionuclide migration and also to estimate uncertainties in the transport analysis.

3 RESPONSE FUNCTION OF THE BARRIER SYSTEM

A characteristic feature of the multi-barrier system of a geological repository is that the reservoir capacities and mass transfer coefficients between the neighbouring transport barriers may differ significantly. This can lead to a situation in which the response function of the whole barrier system is essentially determined by one of the barriers. Other barriers of the multi-barrier system support and backup the performance of the main barrier, and also the performance of the whole multi-barrier system in case the main barrier fails. The sensitivity and uncertainty analyses of the whole multi-barrier system can be focused on a dominating barrier in each of the analysed cases.

3.1 Release rate out of the barrier system

Mass transfer between different components of the release pathways (Figure 2-1) are represented by linear processes (the influence of the solubility limits is discussed later). The source term of the radionuclides that emanate from the fuel matrix can be separated from the analysis of the solute migration through the barrier system. The release rate to the biosphere for a given source term $s(t)$ can be expressed as a superposition such that

$$r(t) = \int_0^t f_t(t-\tau)s(\tau)\,d\tau \quad , \tag{3-1}$$

where $f_t(t)$ is the total response function of the whole multi-barrier system. The behaviour of the barrier system is fully described by this response function.

3.2 Response functions of individual barriers

The release rate from an individual barrier can be calculated by convolving the inflow pulse to a barrier with the response function of the barrier, similarly as the outflow to the biosphere was calculated using the total response function of the whole barrier system and the source term resulting from dissolving fuel as the inflow. Analogously to (3-1), the release rate from a single barrier is given by

$$h(t) = \int_0^t f(t-\tau)g(\tau)\,d\tau \quad , \tag{3-2}$$

where *g(t)* is the inflow pulse to the barrier and *f(t)* is the response function of the barrier. It can be noted that the response function of the barrier, *f(t)*, is equivalent to the outflow from the barrier for a Dirac pulse input at t=0.

A convolution of two time series leads to a time series that is translated and spread in time compared to the original time series. For example, convolution of two Gaussian functions is also a Gaussian function, but the mean of the convolution is the sum of the means of the two convoluted functions and the variance is the sum of the two variances (e.g., Papoulis and Pillai 2002). Especially, it can be seen by direct substitution to Equation (3-2) that, if the response function is translated in time (e.g. $f(t) \rightarrow H(t-t_d)f(t-$

t_d), where H(t) is the Heaviside step function), then the functional form of the convolution remains unchanged but is translated by the same amount time. This shows that additional delays or time shifts in the response function of the barrier can be treated by simply adding the sum of the individual time shifts to the response function of the system.

Spreading caused by convolution is demonstrated here for two simple rectangular functions. Let $f(t)=1/(f_u-f_l)$ for $f_l<t<f_u$, where f_l and f_u are the lower and upper time limits, respectively, and elsewhere $f(t)=0$. Similarly let $g(t)=1/(g_u-g_l)$, for $g_l<t<g_u$, and elsewhere $g(t)=0$. Without restricting the problem we can also assume that $f_u-f_l<g_u-g_l$ (Figure 3-1). Functions $f(t)$ and $g(t)$ can be thought of, for example, as indicator functions for the spreading of the release and response pulses. Applying Equation (3-2) it can be seen that the convolution of the functions $f(t)$ and $g(t)$ is given by

$$h(t)=\begin{cases} 0, & t \le f_l + g_l , \\ \dfrac{t - f_l - g_l}{(f_u - f_l)(g_u - g_l)}, & f_l + g_l < t < f_u + g_l , \\ \dfrac{1}{g_u - g_l}, & f_u + g_l \le t \le f_l + g_u , \\ \dfrac{f_u + g_u - t}{(f_u - f_l)(g_u - g_l)}, & f_l + g_u < t < f_u + g_u , \\ 0, & t \ge f_u + g_u . \end{cases} \quad . \qquad (3\text{-}3)$$

The total width in time of the convoluted function is $f_u + g_u - f_l - g_l = (f_u - f_l) + (g_u - g_l)$, i.e. sum of the two individual widths. If one of the functions is much narrower than the other, then the shape and release rate of the resulting convoluted function follow those of the wider one, with some transients at the leading and tailing edges over a time interval that is comparable to the width of the narrower function. The resulting time shift in the middle of the leading edge transient is the sum of the time shifts of $f(t)$ and $g(t)$.

Convolution of two rectangular functions is illustrated in Figure 3-1. A case where the convoluted functions have different widths is shown to demonstrate how easily the wider function dominates the variance of the convolution. A limiting case of convoluting two functions of equal width is also shown. In this case the original inflow function slightly underestimates the width of the outflow function. In the assessment of the radionuclide migration this is in general a conservative approximation if short half-lives do not govern the leading edges.

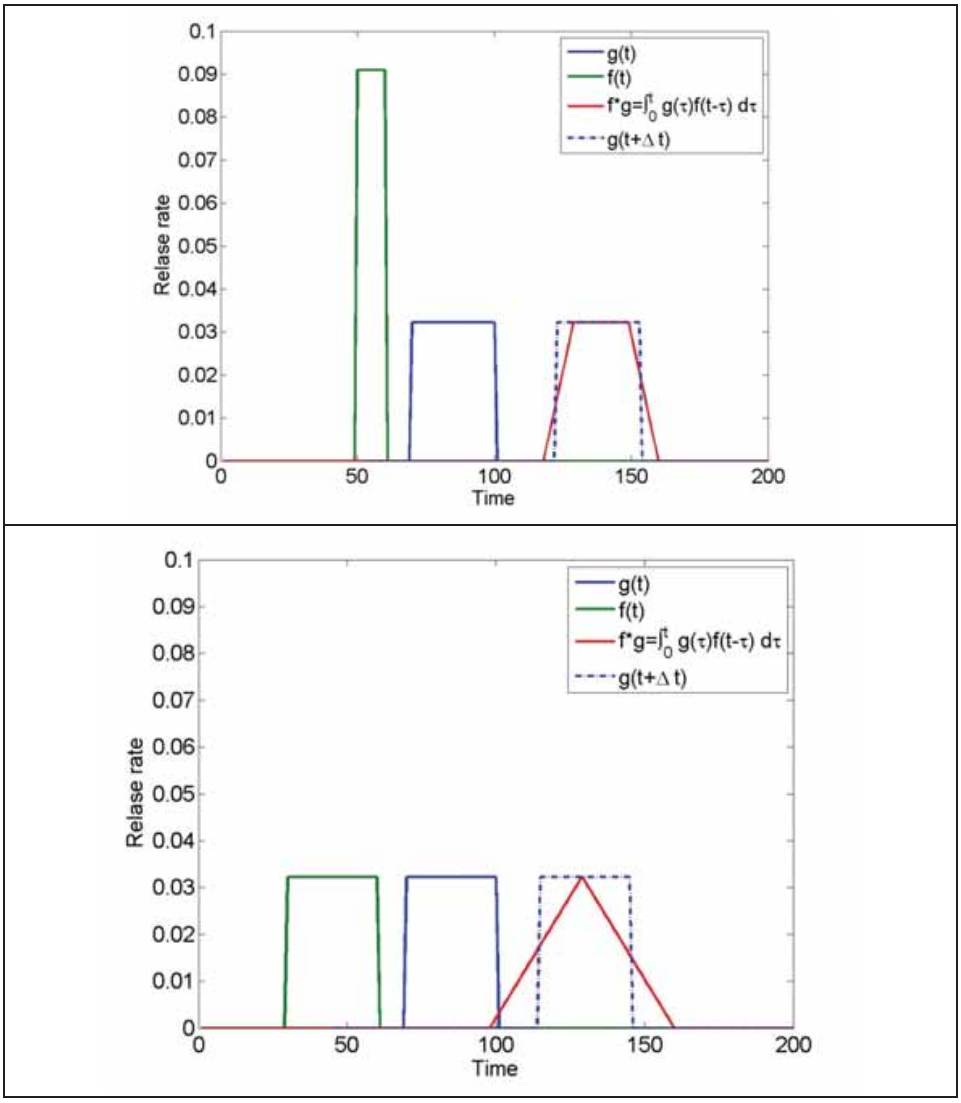

Figure 3-1. *Convolution of two rectangular functions. Variance of the convoluted function and the release rate is dominated by the wider function (upper figure) and the time shifts sum up. The lower figure shows the limiting case when the two convoluted pulses have equal widths. In that case the original pulse slightly underestimates the width of the convoluted pulse.*

Successive convolutions are applied to determine the response function for a system of several transport barriers that are connected in series. The previous example presented in Figure 3-1 can be interpreted as the response functions of two transport barriers in a series, where the inflow term to the first barrier has been a Dirac pulse at t=0 ($f(t)$ and $g(t)$ have both a unit mass in Figure 3-1). In cases such as in Figure 3-1 this means that

the transport barrier represented by the response function $g(t)$ dominates the duration and level of the release rate up to the situation when $f(t)$ would be broader.

The additive nature of the variance under the convolution operation leads easily to a situation where one of the convoluted functions dominates the total result of the convolution. This is illustrated by the example in Figure 3-2, where three functions are convoluted. All functions integrate to a unit mass and they can be regarded as simplified response functions for different transport barriers. The response functions are not very dissimilar. The relative widths (and average release rates) have ratios of 1:2:3. Still, the convoluted function that describes the system where all the three barriers are connected in series can be represented reasonably well using only the transport barrier that is represented by the widest response function. In Figure 3-2 this is demonstrated by translating the widest response function over the convolution function. When the difference between the response functions is increased, the influence of the narrower pulses on the convolution integral converges quite quickly to that of a Dirac pulse. This can be seen in the example of Figure 3-3 where the relative widths (and average release rates) of the pulses are 1:1:5.

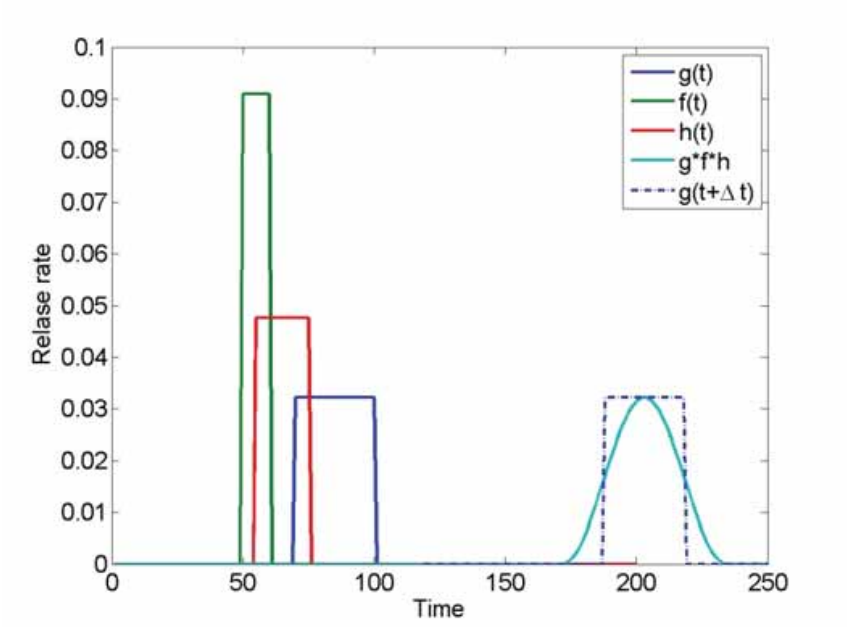

Figure 3-2. *Convolution of three pulses that have the width ratios 1:2:3. The convoluted function is compared with the widest function (g(t)) shifted in time (dashed line). The total time shift is the sum of the individual time shifts.*

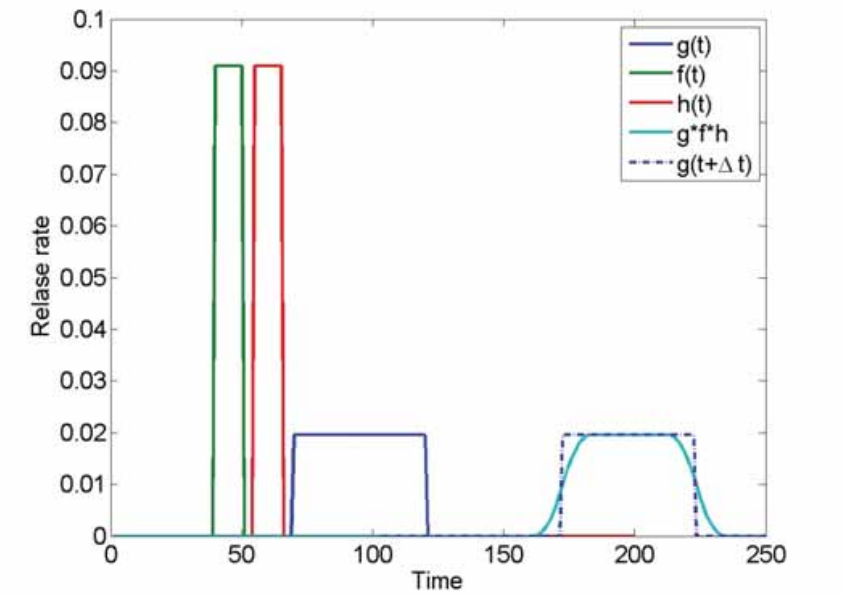

Figure 3-3. *Convolution of three pulses that have the width ratios 1:1:5. The convoluted function is compared with the widest function (g(t)) shifted in time (dashed line). The total time shift is the sum of the individual time shifts.*

4 A MULTI-COMPARTMENT MODEL

The mathematical treatment of the system can be further simplified by taking into account the characteristic behaviour of mass transfer between barriers. In many cases mass transfer between successive transport barriers is strongly restricted by the interfaces between these barriers, for example, a small hole in the canister, or a thin fracture intersecting the deposition hole or a section of the tunnel. The thereby restricted mass flow from a barrier to the next leads (because of diffusive mixing) to a homogenized concentration profile of the solute in the pore space of the individual transport barriers.

Well-mixed solute concentration profiles inside the transport barriers make it possible to describe the behaviour of these barriers by a multi-compartment system, in which the mass outflow depends linearly on the concentration (Figure 4-1). The behaviour of a compartment is essentially determined by the volume of its pore space and the mass flow out of that barrier. Due to the design of the repository system and the selected locations of the deposition holes, the pore volume of the next barrier in the system is usually much larger than the volume of the previous one. The system also tends to behave so that the mass transfer coefficient into a barrier is smaller than the one out of the barrier. This creates a very weak back coupling of the concentration in the target barrier to mass transfer from the preceding barrier. In the simplification of the barrier system, this is taken into account by assuming zero concentration in the target barrier when calculating the mass transfer. This is also a conservative assumption regarding mass fluxes.

The following sections represent different transport barriers as mixing tanks coupled by mass flux resistances that are used to build a multi-compartment model of the barrier system. The goal is to find typical time constants for the different transport barriers and to also evaluate the validity of the mixing tank approximation for different barriers.

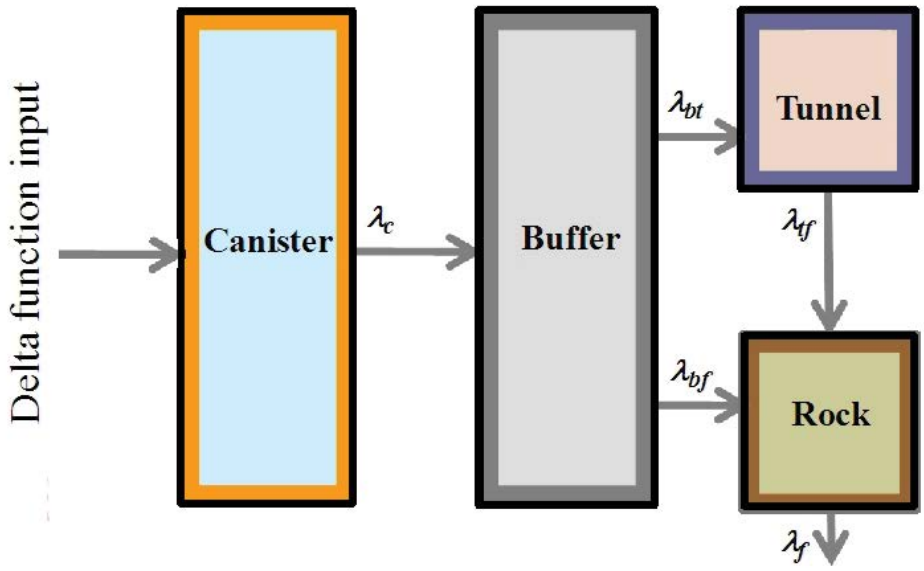

Figure 4-1. *A multi-compartment (mixing tank) model of the migration barrier system.*

4.1 Mathematical model with multiple compartments

4.1.1 Parameterisation of the compartments

With the concept and assumptions presented above the release rates from well mixed volumes are characterised by solute concentrations and mass transfer coefficients. This offers a systematic, compact and transparent way to represent typical transport characteristics of the barriers.

i) Half-time of the solute in the compartment: The equivalent flow rates together with the pore volumes of the barriers give the time constants of the different components. The half-time of the solute in the compartment is the only parameter needed to describe an ideal system of perfect mixing tanks, where the inverse of the mean lifetime is called the decay constant. Not only the engineered barrier system, but also the geosphere is represented by the mixing tank model as described in Section 4.6.

ii) Equivalent flow rate: The mass transfer coefficient can be expressed as equivalent flow rate discharging the compartment in question. The equivalent flow rate is an apparent volumetric flow rate. Combined with the solute concentration in the compartment, it gives the outflow of the solute mass.

iii) Delay time: In real transport barriers there is some delay before the outflow starts, because the solute should first reach the outlet location. This delay time is treated as a time shift in the solute release rate from the barrier, and it

affects the duration and level of the breakthrough curve only for strongly sorbing nuclides that have a short radioactive half-life.

The fact that the performance of individual barriers can be represented by the half-time of the solute and the sequential topology of the barrier system, makes it analogous to a chain of radioactive decays. This offers a straightforward way to solve the release rates of the whole barrier system.

The equivalent flow rate is a convenient quantity by which to measure the mass transfer capacity out of the barrier, because it makes possible to easily compare the diffusive and boundary layer resistances with each other, and also to put them in an overall context of the hydraulic environment deep in the rock.

Delay times have been added to the description of the barrier system in order to improve the applicability of the approach also to short lived nuclides. The compartment system can be represented as a series of successive convolutions between the response functions of the individual barriers. This means that the delay times of all barriers can simply be summed up and the response function of the system is shifted by the total delay time at the end of the calculation, as has been shown in Section 3.

4.1.2 Chain of transport barriers

As discussed above, release rates from one model compartment to the next are estimated by assuming zero concentration in the target compartment. Then the solute concentrations in the canister, buffer and a section of the tunnel can be represented by the following group of coupled equations (4-1)

$$\begin{aligned}
&\frac{d\,m_c}{dt} + \lambda_c m_c = \delta_0 \\
&\frac{d\,m_b}{dt} + (\lambda_{bf} + \lambda_{bt}) m_b = \lambda_c m_c * \delta_{t_{dc}} \\
&\frac{d\,m_t}{dt} + \lambda_{tf}\, m_t = \lambda_{bt} m_b * \delta_{t_{dbt}} \\
&\frac{d\,m_f}{dt} + \lambda_f\, m_f = \lambda_{tf}\, m_t * \delta_{t_{dtf}} + \lambda_{bf} m_b * \delta_{t_{dbf}} \quad ,
\end{aligned} \tag{4-1}$$

where * means convolution, $\delta_\tau = \delta(t-\tau)$, with δ the Dirac delta function, $\delta_{t_{dc}}$ is the delay time in the canister, $\delta_{t_{dbt}}$ the delay time from buffer to tunnel, $\delta_{t_{dbf}}$ the delay time from buffer to fracture and $\delta_{t_{dtf}}$ the delay time from tunnel to fracture. Other notations in Equation (4-1) include the decay constants of the solute: λ_c from canister to buffer, λ_{bf} from buffer to fracture, λ_{bt} from buffer to tunnel and λ_{tf} from tunnel to fracture. The mass transfer coefficients and decay constants are discussed in more detail in Sections 4.3-5. The initial conditions are $m_c(0)=0$, $m_b(0)=0$, $m_t(0)=0$ and $m_f(0)=0$. It can be seen that operation $*\delta_\tau$ creates a translation by time τ (i.e. delay)

$$(f * \delta_\tau)(t) = \int_0^t f(s)\delta_\tau(t-s)ds = \mathrm{H}(t-\tau)\, f(t-\tau) \quad , \tag{4-2}$$

where **H**(t) is the Heaviside unit step function.

We may construct an integral kernel for solving Equations (4-1). Let us assume that G_i is the Green's function of the differential operator L

$$L G_i = \frac{d G_i}{dt} + \lambda_i G_i = \delta(t) \quad , \tag{4-3}$$

and that there is a corresponding inhomogeneous equation

$$L G_j = \frac{d G_j}{dt} + \lambda_j G_j = f_j(t) \quad . \tag{4-4}$$

Solution to Equation (4-4) can be expressed in the form

$$G_j = G_i * f_j \quad , \tag{4-5}$$

which can be confirmed by direct substitution:

$$L(G_i * f_j) = \int_0^t \left(\frac{d G_i(t-\tau)}{dt} + \lambda_i G(t-\tau) \right) f_j(\tau) d\tau = \int_0^t \delta(t-\tau)\, f_j(\tau) d\tau = f_j(t), \tag{4-6}$$

where we have applied the Leibnitz integration rule and Equation (4-3).

The Green's function of Equation (4-3) and the solution in Equation (4-5) can be applied to solve Equations (4-1). Equations (4-1) do not contain a delay time in the fracture so the solute mass flow of the solute out of the system will be $m_{out} = \lambda_f m_f * \delta_{t_{df}}$, which gives the solution

$$\begin{aligned}
m_{out} &= \lambda_f m_f * \delta_{t_{df}} \\
&= \lambda_f (G_f * (\lambda_{tf} m_t * \delta_{t_{dtf}} + \lambda_{bf} m_b * \delta_{t_{dbf}})) * \delta_{t_{df}} \\
&= \lambda_f (G_f * (\lambda_{tf} (G_t * \lambda_{bt} m_b * \delta_{t_{dbt}}) * \delta_{t_{dtf}} \\
&\quad + \lambda_{bf} (G_b * \lambda_c m_c * \delta_{t_{dc}}) * \delta_{t_{dbf}})) * \delta_{t_{df}} \\
&= \lambda_f (G_f * (\lambda_{tf} (G_t * \lambda_{bt} (G_b * \lambda_c G_c * \delta_{t_{dc}}) * \delta_{t_{dbt}}) * \delta_{t_{dtf}} \\
&\quad + \lambda_{bf} (G_b * \lambda_c G_c * \delta_{t_{dc}}) * \delta_{t_{dbf}})) * \delta_{t_{df}} \\
&= \lambda_f \lambda_{tf} \lambda_{bt} \lambda_c G_f * G_t * G_b * G_c * \delta_{t_{dc}} * \delta_{t_{dbt}} * \delta_{t_{dtf}} * \delta_{t_{df}} \\
&\quad + \lambda_f \lambda_{bf} \lambda_c G_f * G_b * G_c * \delta_{t_{dc}} * \delta_{t_{dbf}} * \delta_{t_{df}}
\end{aligned} \quad , \tag{4-7}$$

where G_f, G_t, G_b, G_c are Green's functions (and in this case also response functions) for the fracture, section of the tunnel above the deposition hole, buffer and canister, respectively. The solution of Equation (4-7) demonstrates also that the response function of the whole release path is created by successive convolutions between the response functions of the barriers. It can also be found from Equation (4-7) that the solution includes translations in time, $*\delta_{t_{d1}} = *\delta_{t_{dc}} * \delta_{t_{dbt}} * \delta_{t_{dtf}} * \delta_{t_{df}}$ and $*\delta_{t_{d2}} = *\delta_{t_{dc}} * \delta_{t_{dbf}} * \delta_{t_{df}}$ for the two branches of the release path, respectively. These translations in time are the summed delay times of the barriers along the respective release paths, as already discussed in Section 3. The solution of Equation (4-7) is given in closed form in Appendix A.

The verification cases considered in this report were evaluated using a recursive solution to an arbitrarily long chain of barriers, which lends itself quite easily to possible changes in the topology of the compartment model. In this approach the response functions were first determined without the delay times, which were added at the end using the time shifts in Equation (4-7). Equations (4-1) can be expressed (without the delays) in the general form

$$\frac{d\,m_i}{dt} = -(\lambda_i + k_i)m_i + \lambda_{i-1}m_{i-1} \quad , \tag{4-8}$$

where the decay constant of member i is composed of two components: λ_i that will produce the next member $i+1$ of the chain, and an additional discharge term k_i. The additional discharge term was here used to describe branching of the release path to one via buffer to fracture and to another via buffer to tunnel.

The system of Equations (4-8) can be solved using the known solution of the Bateman equations

$$\frac{d\,m_i}{dt} = -\lambda_i m_i + \lambda_{i-1}m_{i-1} \quad . \tag{4-9}$$

The solution to Equations (4-9) is given by (American Nuclear Society 1987)

$$m_i(t) = \sum_{j=1}^{i} a_{ij} e^{-\lambda_j (t-t_0)} \quad , \tag{4-10}$$

$$a_{\mathrm{pq}} = \begin{cases} m_{0\,p} - \sum_{n=1}^{p-1} a_{pn} & \text{, if } p = q \\ \dfrac{\lambda_{p-1}}{\lambda_p - \lambda_q} a_{(p-1)q} & \text{, if } q < p \end{cases}$$

where m_{0p} is the amount of mass of nuclide p at time t_0.

By applying Laplace transforms, it can be shown that the solution of Equation (4-9) is formally equivalent to that of Equation (4-8) if the λ_n and (initial conditions) m_{0n} in Equation (4-10) are replaced by λ_n' and $m_{0n}^{'}$ (e.g., Poteri and Vieno 1989) such that

$$\lambda_n^{'} = \lambda_n + k_n$$
$$m_{0n}^{'} = \prod_{p=1}^{i-1} \frac{\lambda_p}{\lambda_p + k_p} m_{0n} \quad . \tag{4-11}$$

The system of Equations (4-8) is solved by applying Equations (4-10) with (4-11). The solution Equation (4-10) is not defined for nuclides that have equal decay constants, $\lambda_i = \lambda_j$. In practice, this case is rare and it can be easily solved by slightly changing some of the λ's.

4.1.3 Delay time

In an ideal well mixed system, the outflow of the solute begins immediately when there is mass in the system. In real transport barriers there is some delay before the outflow start, because the solute should reach the outlet location. This delay time may be important for strongly sorbing nuclides and it ought to be included in the simplified model. The previous section shows that the multi-compartment model can be solved by successive convolutions of the barrier response functions. This means that the delay times of the barriers can be simply added together to get the total delay time of the whole barrier system.

Delay time in the buffer and tunnel is determined by diffusion, and in the geosphere mainly by matrix diffusion, sorption and to a lesser extent by advection. Advective delay in the geosphere needs not to be taken into account in the present approach. It can be added separately to the sum of the delay times. Matrix diffusion is a process in which molecular diffusion enables solute particles to visit the pore space of the rock matrix next to the flowing fractures (Neretnieks 1980). In practice, groundwater in the pores of the rock matrix is stagnant and diffusion of the solute to the pore space of the rock matrix can cause considerable retention in the migration of the solute.

Delay time in the geosphere

Delay in the geosphere is based on the breakthrough curve of the unlimited matrix diffusion for a pulse input (e.g. Cvetkovic et al. 1999; Kekäläinen et al. 2011),

$$f_r(t) = \frac{d\, m_r(t)}{dt} = \frac{u}{\sqrt{\pi (t - t_w)^3}} e^{-\frac{u^2}{(t - t_w)}} \quad , \tag{4-12}$$

where parameter $u = \varepsilon \sqrt{D_p R_p} WL / Q$ is the transport resistance and t_w is the advective delay (if surface sorption is also included in the model then t_w is replaced by $R_a t_w$, with R_a the retardation coefficient of surface sorption). Transport resistance is thus determined by porosity ε, pore diffusivity D_p, retardation coefficient R_p (in the pore system of the rock matrix), transport channel width W, length L and flow rate Q. Delay

time is the sum of advective delay time ($R_a t_w$) and retention caused by matrix diffusion. Most of the past performance assessments have omitted the advective delay that usually contributes very little to the total delay.

The delay time caused by matrix diffusion in the geosphere transport is based in this work on reaching a prescribed level of the breakthrough curve. The maximum release rate in the breakthrough takes place at time $t = 2/3u^2$, when the advective delay is omitted (t_w=0). Delay time in the geosphere is determined by the time when the release rate is greater than an arbitrary fraction, 1/c, of the maximum release rate. This is calculated from equation $f_r(t) = f_r(2/3u^2)/c$ by assuming that t_w=0. The two solutions to this equation are

$$t_e = -\frac{2u^2}{3\,\mathrm{W}_{-1}\left(-\frac{1}{c^{2/3}e}\right)}, \qquad t_l = -\frac{2u^2}{3\,\mathrm{W}_{0}\left(-\frac{1}{c^{2/3}e}\right)} \qquad (4\text{-}13)$$

where t_e is the early time solution, i.e. before the time of the maximum release rate, and t_l is the late time solution caused by tailing of the breakthrough curve. W_0 and W_{-1} are the branches of the Lambert W function (e.g. Weisstein 2003) defined as $W_0(0) = 0$, $W_0(-1/e) = W_{-1}(-1/e) = -1$ and $W_{-1}(0^-) = -\infty$. To avoid overestimation of the delay time, a small fraction of the maximum release rate (1/c=1/300) is used to indicate the delay time to avoid underestimating the mass fluxes of short lived nuclides. For c=300 in Equation (4-13), we find $t_e \approx 0.1u^2$. The selected delay time is shown in Figure 4-2.

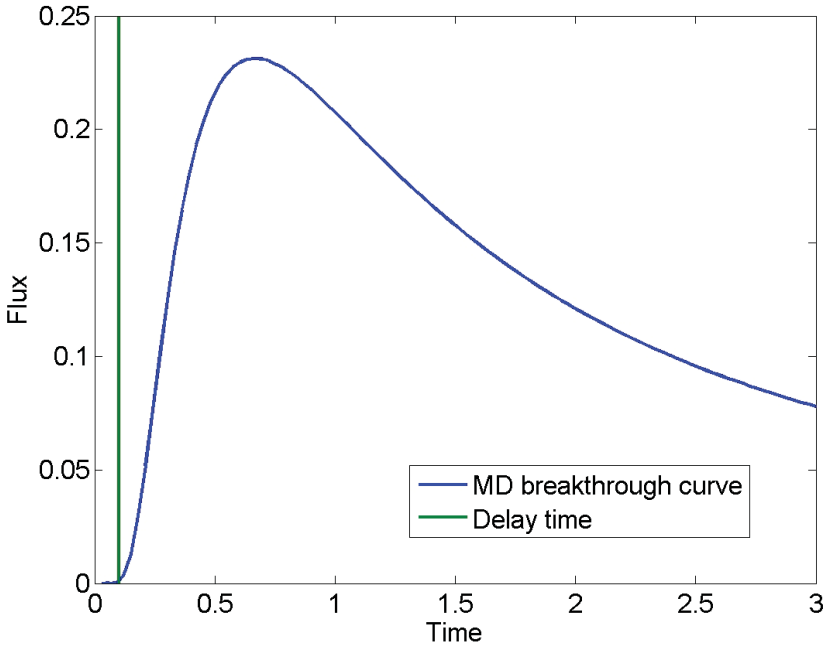

Figure 4-2. *Dimensionless breakthrough curve of matrix diffusion. The delay time* $t_e = 0.1u^2$ *of the geosphere, which corresponds to a release rate that is about 1/285 of the maximum release rate, is also indicated.*

Delay time in the buffer and tunnel

Delay time in the buffer and tunnel is estimated using two simple one-dimensional approaches: i) diffusion time from a point source to a zero concentration boundary, and ii) spreading of a solute mass by diffusion in an infinite medium.

It is convenient to treat the problem in the dimensionless form using variables $\tau = t\ D/s^2$ and $\xi = x/s$, where D is the diffusion coefficient and *s* is, for example, the distance from outflow point to the source. In one dimensional diffusion, the distribution of solute after an instantaneous release of unit mass at τ=0 and $\xi = \xi_0$ is given by (Carslaw and Jaeger 1959)

$$f(\xi,\tau;\xi_0) = \frac{\exp\left(-\frac{(\xi-\xi_0)^2}{4\,\tau}\right)}{2\sqrt{\pi\,\tau}} \quad , \qquad (4\text{-}14)$$

In the first option, the boundary condition of zero concentration is constructed by introducing a mirror source of the original source. Combination of a source at ξ=1 and a mirror source at ξ=-1 gives zero concentration at ξ=0. The mass flux of the solute at ξ=0 is then given by

$$j(\tau) = -\frac{d}{d\xi}\left(f(\xi,\tau;1) - f(\xi,\tau;-1)\right)\Big|_{\xi=0} \quad . \tag{4-15}$$

The delay before the outflow starts can be estimated based on the cumulative mass flux,

$$m_c(\tau) = \int_0^\tau j(\tau')d\tau' = \mathrm{erfc}\left(\frac{1}{2\sqrt{\tau}}\right) \quad . \tag{4-16}$$

Based on Equation (3-1), this result also gives the solute mass flux for a fixed continuous unit source at x=s. The dimensionless delay time is then given by

$$\tau_d = t\frac{D}{s^2} = \frac{1}{4\left(\mathrm{erfc}^{-1}(m_c)\right)^2} \quad , \tag{4-17}$$

where erfc^{-1} denotes the inverse function of the complementary error function and m_c is a suitable level of the cumulative mass flux. The delay time for both continuous and pulse sources can be defined by this equation. A short delay time was chosen, corresponding to a cumulative mass flux of 1/10 000 (m_c=10^{-4}) for a pulse source, to avoid underestimating the mass fluxes of short lived nuclides. This choice gave a delay time of $t_d\ D/s^2 \approx 0.033$. It is also interesting to note that the mass flux resulting from Equation (4-15) is of the same form as Equation (4-12) for the breakthrough curve of matrix diffusion with u=1/2. Using this relation and the chosen definition for the geosphere delay, t_d=$0.1\cdot u^2$, we find that $t_d\ D/s^2 \approx 0.025$. This result shows that the definitions of the delay times lead to slightly longer delay times in the near-field transport of the repository than in the far-field transport. The chosen delay time together with two diffusive breakthrough curves is shown in Figure 4-3.

The second approach to finding the delay time is to determine when the concentration begins to raise at the outlet. This time is estimated for a case where a fixed unit concentration is fixed at the inlet of the barrier, and the starting point in the increase in concentration at the outlet is estimated by diffusion in an infinite medium. In the dimensionless form the solution for the concentration is given by

$$c(\xi,\tau) = \mathrm{erfc}\left(\frac{\xi}{2\sqrt{\tau}}\right) \quad . \tag{4-18}$$

At the outlet $\xi = 1$, this solution leads to the same solution as Equation (4-16) above

$$c(1,\tau) = \mathrm{erfc}\left(\frac{1}{2\sqrt{\tau}}\right) \quad . \tag{4-19}$$

The same delay time results when a constant concentration is assumed at the source location and concentration at the outlet is followed, or a continuous source is assumed at the location of the source and mass flux at the outlet is followed.

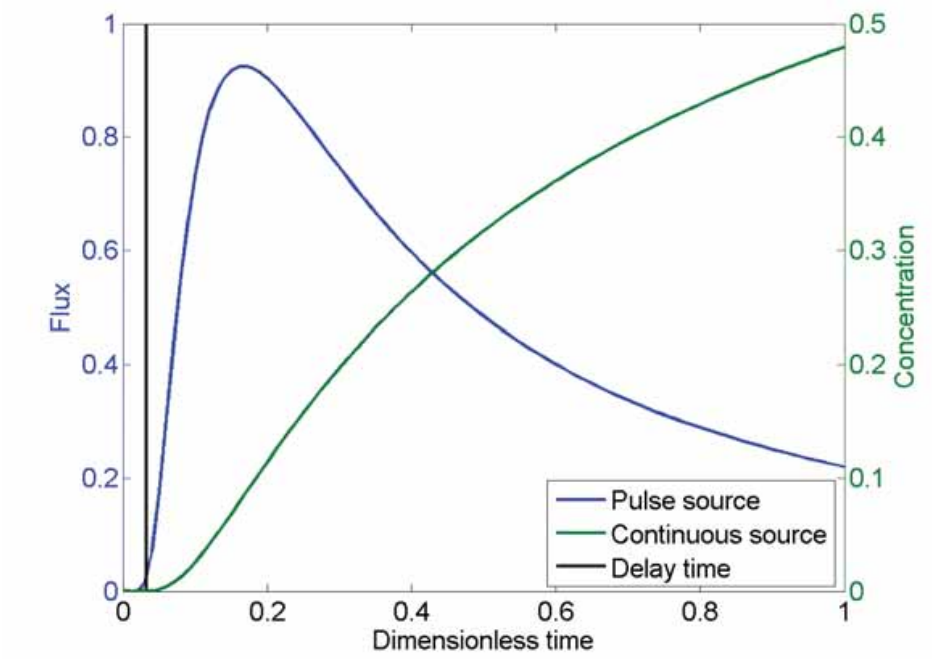

Figure 4-3. *Delay time (t D/s^2 = 0.033) for the dimensionless mass flux of the solute at the outlet after a release of unit mass at the inlet, and for concentration at the outlet with a unit concentration at the inlet (the concentration curve has an equal functional form to that of the cumulative mass flow at the outlet after a release of unit mass).*

4.1.4 Sorbing nuclides

Sorption increases the bulk capacity available for the nuclide. Let us consider, for example, the mass balance in the diffusion equation

$$\frac{\partial C_t}{\partial t} = \varepsilon \nabla \cdot \left(D_p \nabla C_w \right) , \qquad (4\text{-}20)$$

where C_t is the total bulk concentration, C_w the concentration in the mobile water phase, ε the porosity and D_p the pore diffusivity. Taking into account that $C_t = (1-\varepsilon)\rho C_s + \varepsilon C_w$, where C_s is the sorbed concentration, ρ the density of the medium, and $K_d = C_s / C_w$, Equation (4-20) can be expressed in the form

$$\left(\varepsilon + (1-\varepsilon)K_d \rho\right)\frac{\partial C_w}{\partial t} = \varepsilon \nabla \cdot \left(D_p \nabla C_w \right) \quad . \qquad (4\text{-}21)$$

This result shows that the capacity of the pore volume coupled to the temporal variation is increased from ε by term related to the sorbed mass of the solute, i.e. by $(R_p - 1)\varepsilon$

with $R_p = 1 + \frac{(1-\varepsilon)K_d \rho}{\varepsilon}$ the retardation coefficient. The total capacity of the pore volume for a sorbing nuclide is increased by the retardation coefficient

$$V_{pore}^{sorb} = R_p \, \varepsilon V_{bulk} \quad . \tag{4-22}$$

This means that sorbing nuclides can be modelled using the same equivalent flow rates that have been estimated for the non-sorbing nuclides, but increasing the pore volume capacity of the transport barrier by the retardation coefficient when determining the time constant of the barrier. Equation (4-21) shows also that the delay time for a sorbing nuclide is the product of the retardation coefficient and the delay time of a non-sorbing nuclide.

4.2 Fuel degradation

The present study does not consider fuel degradation as a transport barrier. The role of the temporal characteristics of it is, however, equivalent to that of a barrier. Dissolution of fuel matrix into groundwater is the source term of radionuclides into the waste canister which is the first transport barrier. Dissolution takes place by two processes: an instant release of degradation products and gradual leaching of the fuel matrix. The release from fuel is well represented by a Dirac pulse, which means that the outflow of the instantly released radionuclides from the multi-barrier system equals the response function of the system. Gradual leaching of fuel matrix is described using a constant release rate and a rectangular-shaped release pulse based on the inventory of the radionuclide. Safety assessment calculations have typically applied leaching times of 10^6 or 10^7 years, which corresponds to a constant leach rate of (10^{-7}–10^{-6})/a.

4.3 Waste canister

4.3.1 Mass transfer coefficient

One of the basic cases in safety analysis is the following. Mass transfer from the canister to the bentonite buffer takes place by diffusion through a small hole in the canister (Figure 4-4). The mass transfer coefficient is estimated by combining steady state diffusion through the hole with subsequent spreading of the solute into the bentonite.

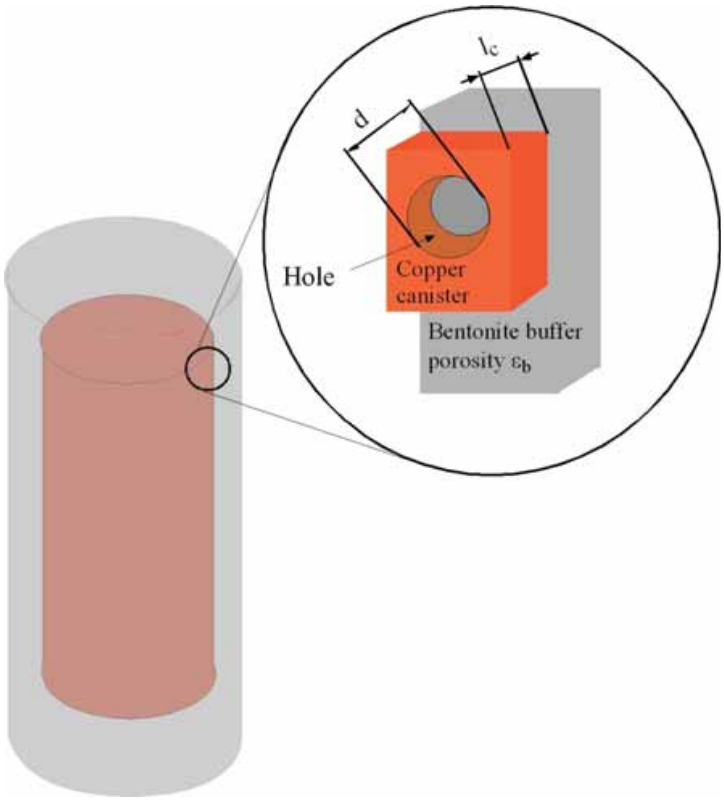

Figure 4-4. *Diffusion through a small hole in the canister wall.*

The rate of mass flow of the solute through the hole in the canister is determined based on the one dimensional steady state diffusion,

$$\frac{d\, m_{ch}(t)}{dt} = -\pi\, r_h^{\,2} D_w \frac{C_0 - C_1}{l_c} = -q_{ch}(C_0 - C_1), \tag{4-23}$$

where D_w is the molecular diffusion coefficient in water, C_0 is the concentration in the canister, C_1 is concentration in the bentonite side of the hole, πr_h^2 the area and r_h the diameter of the hole, and q_{ch} the equivalent flow rate through the hole.

The rate of mass flow through the hole to the bentonite is determined by assuming steady state radial diffusion from the canister wall to the bentonite. Diffusion of the solute to the bentonite through the hole is assumed to be into the half space (a solid angle of 2π) outside the canister wall. In this way we find that

$$\begin{aligned} &\frac{d\, m_{hm}(t)}{dt} = 2\,\pi\, r^2 D_{eb} \frac{dC}{dr} \\ &\Rightarrow \frac{d\, m_{hm}(t)}{dt} = -\frac{2\pi\, D_{eb}\, R_1\, R_2}{R_2 - R_1}(C_1 - C_2) = -q_{hm}(C_1 - C_2) \end{aligned}, \tag{4-24}$$

where D_{eb} is the effective diffusion coefficient in bentonite, R_1 the inner and R_2 the outer radius of the hemispheric volume of bentonite, C_1 the concentration on the bentonite side of the hole (distance R_1 from centre of the hole) and C_2 the concentration in bentonite at a distance of R_2 from the centre of the hole. In practice, R_1 is the radius of the hole and a zero concentration is assumed at a distance of R_2. q_{hm} is the equivalent flow rate on the bentonite side of the hole.

Connecting the mass transfer coefficients in series for the hole and the bentonite on the other side, we find that

$$\frac{d\ m_c(t)}{dt} = -\frac{q_{ch}\ q_{hm}}{q_{ch}+q_{hm}}\left(C_0 - C_2\right) \approx -\frac{q_{ch}\ q_{hm}}{q_{ch}+q_{hm}} C_0 = -\frac{1}{V_c}\frac{q_{ch}\ q_{hm}}{q_{ch}+q_{hm}} m_c = -\lambda_c m_c, \quad (4\text{-}25)$$

where q_{ch} and q_{mh} are the equivalent flow rates through the hole in the canister and on the bentonite side of the hole, V_c is the void volume in the canister, λ_c the decay constant of the solute in mass transfer through the hole, and m_c the solute mass inside the canister. It has been assumed that concentration is zero in bentonite at a distance of R_2 from the hole (see Equation (4-24)).

Typical values for the different parameters and mass transfer coefficients which were applied in the case studies are shown in Tables 4-1 and 4-2

Table 4-1. *Typical values for non-sorbing nuclides of the mass transfer coefficients from the canister to buffer.*

	Notation	Value	Unit	Value	Unit
Hole					
Diameter	d	1	mm		
Diffusion coefficient	D_w	$2 \cdot 10^{-9}$	m^2/s		
Canister thickness (copper overpack)	l_c	5	cm		
Equivalent flow rate	$q_{ch} = \frac{\pi r_h^2 D_w}{l_c}$	$3.14 \cdot 10^{-14}$	m^3/s	0.99	mL/a
Mouth of the hole					
Distance	$R_1=r_h$	0.5	mm		
Distance	R_2	5	cm		
Effective diffusion coefficient in bentonite (neutral)	D_{eb}	$1.2 \cdot 10^{-10}$	m2/s		
Effective diffusion coefficient in bentonite (aninon)	D_{eb}	$1 \cdot 10^{-11}$	m^2/s		
Equivalent flow rate (neutral)	$q_{hm} = \frac{R_1 R_2}{R_1 + R_2} 2\pi D_{eb}$	$3.7 \cdot 10^{-13}$	m^3/s	12	mL/a
Equivalent flow rate (anion)	$q_{hm} = \frac{R_1 R_2}{R_1 + R_2} 2\pi D_{eb}$	$3.1 \cdot 10^{-14}$	m^3/s	1	mL/a
Hole and mouth of the hole					
Equivalent flow rate (neutral)	$q_c = \frac{q_{ch} q_{hm}}{q_{ch} + q_{hm}}$	$2.9 \cdot 10^{-14}$	m^3/s	0.9	mL/a
Equivalent flow rate (anion)	$q_c = \frac{q_{ch} q_{hm}}{q_{ch} + q_{hm}}$	$1.6 \cdot 10^{-14}$	m^3/s	0.5	mL/a
Canister Volume	V_c	0.7	m^3	700	L
Solute decay constant (neutral)	$\lambda_c = \frac{q_c}{V_c}$	$1.3 \cdot 10^{-6}$	1/a		
Solute decay constant (anion)	$\lambda_c = \frac{q_c}{V_c}$	$7 \cdot 10^{-7}$	1/a		
Half-time (neutral)	$T_{1/2} = \frac{\ln(2)}{\lambda_c}$	530 000	a		
Half-time (anion)	$T_{1/2} = \frac{\ln(2)}{\lambda_c}$	980 000	a		

Table 4-2. *Equivalent flow rates and half-lives of the solute concentration in the canister for different nuclides.*

Nuclide	**Equivalent flow rate**	**Retardation coefficient**	$T_{1/2}$
C-14	0.9 mL/a	1	530 000 a
I-129	0.5 mL/a	1	980 000 a
Pu-239[*)]	0.9 mL/a	1	530 000 a

[*)] no solubility limit

4.3.2 Delay time

To support comparison with other transport barriers the delay times through the hole were estimated for different nuclides (Table 4-3). The delay time is very short for all tracers, because diffusion in bentonite on the other side of the hole is not included in the delay time of the canister.

Table 4-3. *Delay times from the canister to buffer.*

Parameter		**Notation**	**Value**
Distance		s	0.05 m
Diffusion coefficient		D_w	2e-9 m^2/s
Retardation coefficient	**C-14**	R_p	1
Delay time	**C-14**	$t_d \approx R_p \, s^2 0.033 / D_w$	11 h
Retardation coefficient	**I-129**	R_p	1
Delay time	**I-129**	$t_d \approx R_p \, s^2 0.033 / D_w$	11 h
Retardation coefficient	**Pu-239**	R_p	1
Delay time	**Pu-239**	$t_d \approx R_p \, s^2 0.033 / D_w$	11 h

4.3.3 Solubility limited nuclides

The release rate of gradual leaching is limited by the leaching of fuel matrix. The same amount of fuel matrix is dissolved per year, but the amount of radionuclides in that part of the fuel matrix decreases because of radioactive decay. Solubility limited release differs from that of gradual leaching so that the strength of the source remains constant and is determined by the concentration of the nuclide in the saturated water phase and the equivalent flow rate.

A simple approximation of the possible onset of solubility limitation is determined based on the inventory of the nuclide and fuel dissolution rate. Solubility limit is assumed to determine the release rate if the latter is smaller than the one caused by fuel dissolution in the beginning of the release.

Solubility limitation also influences the behaviour of canister interior as a transport barrier. Basically, each transport barrier is represented by an equivalent flow rate and a half time that is determined by the pore volume of the barrier. In the case of solubility

limited release, the release rate from the canister is determined only by the equivalent flow rate and the solubility limit. The volume capacity of the canister has no effect on the release rate in this situation. When transport through the barrier system is considered, this fact is taken into account by applying a very short half time for the canister in Equation (4-1). It also means that processes that take place after concentration decreases below the solubility limit are taken into account only approximatively in the present simplified approach. In practice, it is assumed that fuel degrades immediately. This overestimates slightly the duration of solubility limitation when the degradation rate is low and the radioactive half-life of the nuclide is short. The tailing of the released inventory when concentration is below the solubility limit is evaluated by representing the canister with a mixing tank model that is mimicked by the source term.

The solubility limited release rate is determined such that

$$f_{csl} = M\, N_A \lambda\, q_c = A_{\max}\, q_c \quad , \tag{4-26}$$

where f_{csl} is the activity release rate, M the solubility limit, N_A the Avogadro's number, λ the nuclide's decay constant, A_{max} the solubility limited volumetric activity of the nuclide, and q_c [m^3/a] the equivalent flow rate through the hole and bentonite side of the hole.

Solubility limitation ends when the whole inventory of the nuclide in the canister is decreased enough by radioactive decay and by solubility limited release through the hole in the canister (for simplicity it is assumed that there is no production of the nuclide). In the case the nuclide is produced, its decay chain and the release rates of the parent nuclides need also to be modelled. Here the number of nuclides in the canister is given by

$$\begin{aligned} &\frac{dN(t)}{dt} = -\lambda N(t) - q_c\, A_{\max} \\ &\Rightarrow N(t) = \exp(-\lambda t)\left(\frac{q_c\, A_{\max}}{\lambda} + N(0) \right) - \frac{q_c\, A_{\max}}{\lambda} \end{aligned} \quad , \tag{4-27}$$

where t is time, q_c the equivalent flow rate through the canister and the bentonite side of the hole, A_{max} the solubility limited volumetric activity of the nuclide, λ its decay constant, and $N(0)$ its inventory in the beginning. The duration of the solubility limited source, t_s, can be solved from $N(t_s) = A_{\max} V_c$ and we find that

$$t_s = \ln\left(\frac{A_{\max} q_c + N(0)\lambda}{A_{\max} q_c + A_{\max} V_c \lambda} \right) \Big/ \lambda . \tag{4-28}$$

After time t_s the concentration of the nuclides in the canister is less than the solubility limit. Release from the canister after t_s is determined by representing a simple mixing tank model by the tail of the source term.

A simple approximation of the possible solubility limited release can be found by the following steps (for radioactive nuclides):

1. Determine the release rate using the initial inventory and the fuel dissolution rate: $f_{cd}(0) = N(0)\,r_d$, where $N(0)$ [Bq] is the inventory and r_d [1/a] the fuel dissolution rate.

2. Determine the solubility limited release, f_{csl}, using Equation (4-26).

3. If $f_{csl} < f_{cd}(0)$ apply the solubility limited release, i.e. a constant release of f_{csl} for $t < t_s$ with $t_s = \ln\left(\frac{C_{\max} q_c + N(0)\lambda}{C_{\max} q_c + C_{\max} V_c \lambda}\right) \Big/ \lambda$. The release rate from the canister is determined by the equivalent flow rate through the hole in canister and the solubility limited concentration of the nuclide. For the half time of the canister we assign a small value because its volume does not affect the release rate when the solubility limit is operative. However, the volume of the canister and the corresponding half time determine the tail of the release rate for $t > t_s$, while the half times in Equation (4-1) are constant and they must be small when $t < t_s$. A practical solution to approximate the release rates at the late times $t > t_s$ is to represent them with an appropriate source term that mimics the release rate from a well-mixed canister: $f_{csl}(t > t_s) = C_{\max} q_c \exp(-(t - t_s)\, q_c / V_c)$. It is also assumed that short-lived early transients before the solubility limit is reached can be neglected. This assumption causes a slight overestimation of the mass fluxes out of the canister during the early transient.

4. If $f_{csl} \geq f_{cd}$ apply the release rate based on fuel dissolution, i.e. $f_{cd}(t) = N(0)\exp(-\lambda t) r_d$ for $t < t_s$ with $t_s = 1/r_d$, where r_d is the dissolution rate of the fuel.

In practice all computations are such that the radioactive decay is taken into account only at the end: The release rates are then multiplied by exponential decay factors. In this approach the source terms above (f_{csl} in Equation (4-26) and f_{cd} in point 4 above) need to be multiplied by the corresponding inverse of the exponential decay factor, $\exp(\lambda t)$, where λ is the decay constant of the radioactive decay.

In the case of concurrent release of isotopes of the same element the situation becomes more complex. The solubility limited concentration of the element is a superposition of the concentrations of the different isotopes. The relative concentrations of the isotopes are time dependent. For the rate of change of the *i*th isotope of the *m* possible isotopes we thus have the expression

$$\frac{dN_i(t)}{dt} = -\lambda_i N_i(t) + \lambda_{i-1}^{M} M_{i-1}(t) - q_c C_{\max} \frac{N_i(t)}{\sum_{j=1}^{m} N_j(t)} \quad , \qquad (4\text{-}29)$$

where M_{i-1} and λ_{i-1}^{M} refer to the parent of isotope N_i. These equations need to be solved numerically in parallel with transport modelling of all the decay chains, where different isotopes of the element appear. This task is outside the scope of the present study.

4.3.4 Response functions

The response function of the waste canister was studied using the typical parameters given in Tables 4-1 and 4-2. It was determined applying Equation (4-25) as well as with the numerical REPCOM model (Nordman and Vieno 1994). The two response functions are in good agreement (Figure 4-5).

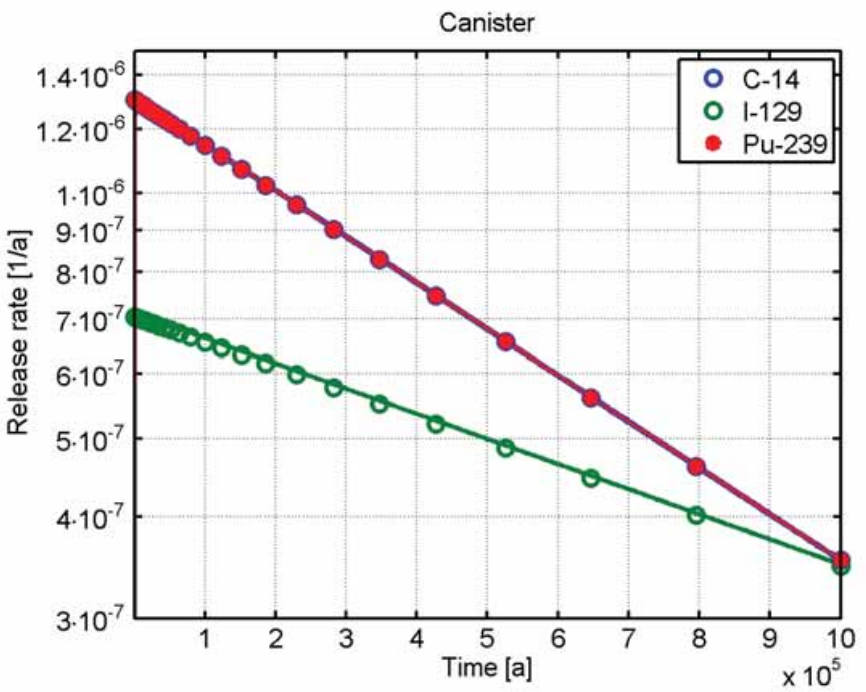

Figure 4-5. *The response function of the canister for three different nuclides as determined from Equation (4-25) (circles) with the estimated diffusive delay times, and by using the REPCOM model (solid lines). Response functions are shown without radioactive decay.*

4.4 Buffer

The space in the deposition hole around the waste canister is filled using bentonite clay. Solute transport through the buffer material may take two different routes: there is always a connection from the deposition hole to a section of the deposition tunnel above it and it is possible that the deposition hole is intersected by a water conducting fracture.

Solute transport along the two parallel release pathways, from the buffer to the fracture and from the buffer to a section of the deposition tunnel, is discussed in the corresponding sections below.

4.4.1 Mass transfer coefficient

From buffer to fracture

We assume that a subhorizontal fracture intersects the deposition hole (Figure 4-6). Hydraulic conductivity of the bentonite buffer is very low, and in practice the groundwater flows around the deposition hole filled by the buffer. Mass transfer from the bentonite buffer into the groundwater flowing in the fracture takes place by solute diffusion. Thereby a concentration profile is formed in the fracture from the buffer surface at the perimeter of the deposition hole outwards into the fracture.

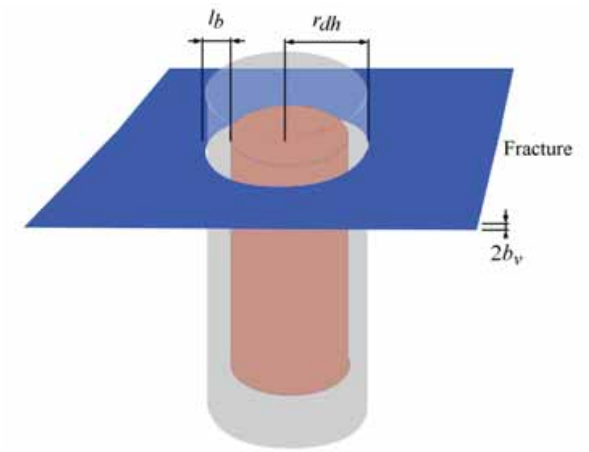

Figure 4-6. *Mass transfer from the buffer material in the deposition hole into a fracture that intersects the deposition hole will result in a concentration profile in the fracture around the hole. Groundwater flowing along the fracture will transport the solute mass into the geosphere.*

Mass transfer of the solute carried away by the groundwater flow in the intersecting fracture can be represented by an equivalent flow rate given by (e.g. Neretnieks 1982)

$$\frac{d\,m_b(t)}{dt} = -2\pi\, r_{dh}\, 2b_v \sqrt{\frac{4 D_w v}{\pi^2 r_{dh}}}\,\frac{m_b}{\varepsilon_b V_b} = -q_f C_b = -\lambda_{bf} m_b \quad , \qquad (4\text{-}30)$$

where q_f is the equivalent flow rate for the mass transfer from the buffer into the fracture, ε_b the porosity of the buffer, V_b its the volume, r_{dh} the radius of the deposition hole, $2b_v$ the volume aperture of the fracture, D_w the molecular diffusion coefficient in free water, and is the flow velocity in the fracture. A shorthand notation of λ_{bf} is used for the decay constant of the solute mass transfer from the buffer to the fracture.

Typical values for the different parameters and mass transfer coefficients are given in Tables 4-4 and 4-5.

Table 4-4. *Typical values for non-sorbing nuclides of the mass transfer coefficients from buffer to fracture.*

Parameter	Notation	Value	Unit	Value	Unit
Radius of the deposition hole	r_{dh}	0.88	[m]		
Fracture volume aperture	$2b_v$	$3{\cdot}10^{-4}$	[m]		
porosity of buffer (neutral)	ε_b	0.43			
porosity of buffer (anion)	ε_b	0.17			
Molecular diffusion coef.	D_w	$2{\cdot}10^{-9}$	[m^2/s]		
Groundwater flow velocity	v	$1.6{\cdot}10^{-8}$	[m/s]	0.5	m/a
Equivalent flow rate	$q_f = 2\pi r_{dh}\, 2b_v \sqrt{\frac{4D_w v}{\pi^2 r_{dh}}}$	$6.34{\cdot}10^{-12}$	[m^3/s]	200	mL/a
Volume of the buffer	V_b	15.3	[m^3]		
Solute decay constant (neutral)	$\lambda_{bf} = \frac{q_{bf}}{R_{pb}\varepsilon_b V_b}$	$3.0{\cdot}10^{-5}$	[1/a]		
Solute decay constant (anion)	$\lambda_{bf} = \frac{q_{bf}}{R_{pb}\varepsilon_b V_b}$	$7.7{\cdot}10^{-5}$	[1/a]		
Half-time	$T_{1/2} = \frac{\ln(2)}{\lambda_{bf}}$	23 000	[a]		
Half-time	$T_{1/2} = \frac{\ln(2)}{\lambda_{bf}}$	9 000	[a]		

Table 4-5. *Equivalent flow rates and half-lives of the solute concentration of three nuclides from buffer to fracture.*

Nuclide	**Equivalent flow rate**	**Pore volume**	**Retardation coefficient**	$T_{1/2}$
C-14	200 mL/a	6.6 m^3	1	23 000 a
I-129	200 mL/a	2.6 m^3	1	9 000 a
Pu-239	200 mL/a	6.6 m^3	14 300	$3.2{\cdot}10^8$ a

There is a small probability that the hole in the canister is adjacent to the fracture intersecting the deposition hole, so that diffusion distance through the bentonite buffer to the fracture is the minimum distance determined by the thickness of the buffer. In this case there will be an early transient in the mass transfer rate to the fracture, which could

be important for nuclides that are strongly sorbing and have a short radioactive decay time. Such a transient can be modelled by introducing an additional sub-compartment for the volume of buffer between the hole and the fracture, or by representing the buffer as a superposition of two response functions with different time constants. In order to maintain the generality of the discussion, the latter approach is applied in the present report. The shorter time constant represents the situation in which the concentration near the fracture has not yet reached the level of the well mixed concentration.

The early transient in the mass flux to the fracture is modelled by representing the response function of the buffer as a sum of a transient response (q_{tb}) and a well mixed response (q_{bf}) such that

$$\frac{d\,m_b(t)}{dt} = -\left(\left(1-\frac{m_{ftb}}{m_0}\right)q_{bf} + \frac{m_{ftb}}{m_0}q_{tb}\right)C_b = -\left(\left(1-\frac{m_{ftb}}{m_0}\right)\lambda_{bf} + \frac{m_{ftb}}{m_0}\lambda_{tb}\right)m_b \ , \qquad (4\text{-}31)$$

where the total released mass is divided between an early transient (m_{ftb}) and a well-mixed response (1-m_{ftb}) using the approach presented below.

The mass fraction of the early transient and the time constant of the transfer of this mass fraction is estimated as follows. The shortest diffusion distance from the canister surface to the fracture is the thickness of the buffer (l_b). The volume, where the concentration is clearly higher before equilibrium, is chosen so that the mass released during the transient phase is maximised. The hole in the canister is assumed to be in the lid (Figure 4-7). This means that the transient volume is composed of two dissimilar parts: the upper part is the deposition hole filled by the buffer material on top of the canister and the lower part is the buffer material that is located between the canister and the deposition hole. The transient volume is thus given by

$$V_{tb} = \pi\, r_{dh}{}^2\, s_{tb} - \pi(r_{dh}{}^2 - (r_{dh} - l_b)^2)\, s_{tb} \ . \qquad (4\text{-}32)$$

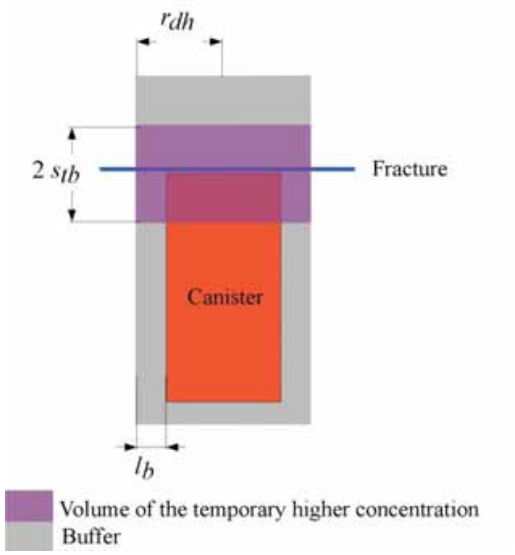

Figure 4-7. *Volume of the buffer with a higher solute concentration that creates the early transient in the mass flux to the fracture.*

The diffusion area from this volume of an initially high concentration to the rest of the buffer is thus

$$A_{tb} = 2\pi(r_{dh}{}^2 - (r_{dh} - l_b)^2) \quad . \tag{4-33}$$

The equivalent flow rate from the volume of increased concentration to the rest of the buffer is given by

$$q_{tb} = \frac{A_{tb}\, D_{eb}}{s_{tb}} \ , \tag{4-34}$$

where D_{eb} is the effective diffusion coefficient in the buffer and s_{tb} the diffusion distance defined by the vertical size of the volume (cf. Equation (4-32)). The time constant for diffusion between the defined volume and the rest of the buffer can be expressed in the form

$$\lambda_{tb} = \frac{q_{tb}}{\varepsilon_b R_{pb} V_{tb}} \ , \tag{4-35}$$

where R_{pb} is the retardation coefficient in the buffer. Mass flow to the fracture during the transient phase is determined by estimating the elevated solute concentration in the defined volume compared to the base case where the solute is well mixed over the whole buffer. Equilibration of the initially high concentration in that volume and the rest of the buffer is determined by considering only diffusion in the buffer and neglecting the mass transfer to the fracture at this point. This can be done because the

(equivalent) flow rate between these two parts (9500 mL/a) is much larger than that to the fracture (200 mL/a), see Table 4-7. This also means that the time constant in Equation (4-35) determines the duration of elevated concentration in the buffer next to the fracture, and thus also determines the time constant for the early transient phase.

Diffusional mass transfer between the two parts can be described by the equations

$$\begin{aligned}
\frac{dC_{tb}}{dt} &= -\frac{q_{tb}}{\varepsilon_b R_{pb} V_{tb}}\left(C_{tb} - C_{rb}\right) \\
\frac{dC_{rb}}{dt} &= \frac{q_{tb}}{\varepsilon_b R_{pb} (V_b - V_{tb})}\left(C_{tb} - C_{rb}\right), \\
C_{tb}(0) &= \frac{m_0}{\varepsilon_b R_{pb} V_{tb}},\ C_{rb}(0) = 0
\end{aligned} \tag{4-36}$$

where C_{tb} and C_{rb} are the concentrations in the volume of increased concentration and the rest of the buffer, respectively. V_b is the total volume of the buffer and a mass m_0 is initially released to the volume of increased concentration. Solution for the concentration in that (transient) volume is given by

$$C_{tb}(t) = \frac{m_0}{\varepsilon_b R_{pb} V_b}\left(1 + \exp\left(-\frac{q_{tb}\ V_b}{\varepsilon_b R_{pb}(V_{tb}V_b - V_{tb}^2)}t\right)\left(\frac{V_b - V_{tb}}{V_{tb}}\right)\right). \tag{4-37}$$

Equation (4-37) gives the concentration with respect to the well mixed condition, where a mass m_0 has been released to the whole buffer. The additional mass transferred from the buffer to the fracture because of the increased concentration in the discussed volume, is estimated by applying Equation (4-37) for the concentration and the equivalent flow rate from the buffer to the fracture, and we find that

$$\begin{aligned}
m_{tb} &= \int_0^\infty q_{bf} C_{tb}(t) \exp\left(-\lambda_{bf}\ t\right) dt \\
&= \frac{q_{bf}\left(q_{tb} + \varepsilon_b R_{pb}(V_b - V_{tb})\lambda_{bf}\right)}{\varepsilon_b \lambda_{bf}\left(q_{tb} R_{pb} V_b + \varepsilon_b R_{pb}^2 (V_b - V_{tb}) V_{tb} \lambda_{bf}\right)} m_0
\end{aligned} \tag{4-38}$$

Note that the time evolution of the concentration in the (transient) volume next to the fracture given in Equation (4-37) was determined assuming no mass outflow from the buffer. Applying this concentration in Equation (4-38) leads to the total released mass that is greater than m_0 by the transient mass fraction. The mass fraction of the transient is estimated to be $m_{ftb} = m_{tb} - m_0$.

The mass fraction of the transient release of mass given by Equation (4-38) is shown as a function of height of the transient volume (s_{tb}) in Figure 4-8. There is a minor difference between neutral and anionic species so that the maximum transient mass for neutral ions is obtained when height of the transient volume is s_{tb} = 1.26 m and

$s_{tb} = 1.21$ m for anions. The mean value of $s_{tb} = 1.24$ m was used for both anions and neutral ions.

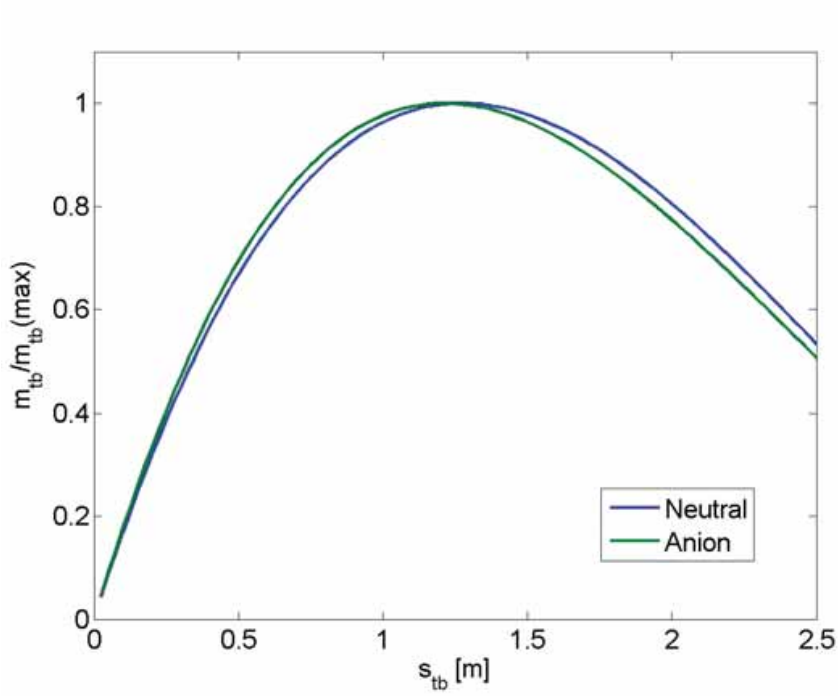

Figure 4-8. *The transient by released mass fraction divided by its maximum value as a function of a half of the height of the transient volume (s_{tb}).*

Table 4-6. *Specification of the buffer region in the transient phase between the hole in the canister and the fracture.*

Parameter	Notation	Value	Unit
Radius of the deposition hole	r_{dh}	0.88	[m]
Thickness of the buffer	l_b	0.35	[m]
Vertical half height of the sub-compartment	s_{tb}	1.24	[m]
Area of diffusion for the transient volume	$A_{tb} = 2\pi(r_{dh}^{\ 2} - (r_{dh} - l_b)^2)$	3.1	[m^2]
Volume of the transient behaviour	$V_{tb} = \pi\, r_{dh}^{\ 2}\, s_{tb} + \pi(r_{dh}^{\ 2} - (r_{dh} - l_b)^2)\, s_{tb}$	4.9	[m^3]
Total volume of the buffer	V_b	15.3	[m^3]

Table 4-7. *Estimated time constants and the nuclide masses released during the transient release of mass from the buffer into the fracture.*

Parameter	Notation	Unit	C-14	I-129	Pu-239
Solute decay constant for a well-mixed buffer	$\lambda_{bf} = \frac{q_{bf}}{R_{pb}\varepsilon_b V_b}$	[1/a]	$3.04 \cdot 10^{-5}$	$7.69 \cdot 10^{-5}$	$2.13 \cdot 10^{-9}$
Porosity	ε_b	[-]	0.43	0.17	0.43
Equivalent flow rate from the transient volume to the rest of the buffer	q_{tb}	[mL/a]	9 500	789	9 500
Equivalent flow rate from a well-mixed buffer to fracture	q_{bf}	[mL/a]	200	200	200
Effective diffusion coefficient	D_{eb}	[m^2/s]	$1.2 \cdot 10^{-10}$	$1 \cdot 10^{-11}$	$1.2 \cdot 10^{-10}$
Retardation coefficient	R_{pb}	[-]	1	1	14 300
Solute decay constant for the early transient from buffer to fracture	$\lambda_{tb} = \frac{q_{tb}}{\varepsilon_b R_{pb} V_{tb}}$	[1/a]	$4.4 \cdot 10^{-3}$	$9.4 \cdot 10^{-4}$	$3.1 \cdot 10^{-7}$
Half-time of the transient	$T_{1/2} = \frac{\ln(2)}{\lambda_{tb}}$	[a]	156	740	$2.2 \cdot 10^{6}$
Mass fraction of the transient release	$m_{ftb}/m_0 = m_{tb}/m_0 - 1$ and Eq. (4-38)	[-]	0.0096	0.11	0.0096

From buffer to tunnel

Mass transfer from the buffer to the tunnel takes place by diffusion along the deposition hole (Figure 4-9). This mass transfer by diffusion is handled analogously to that from the canister to the buffer. The main difference is that in this case the diffusion pathway is filled by the buffer material and its radius is larger.

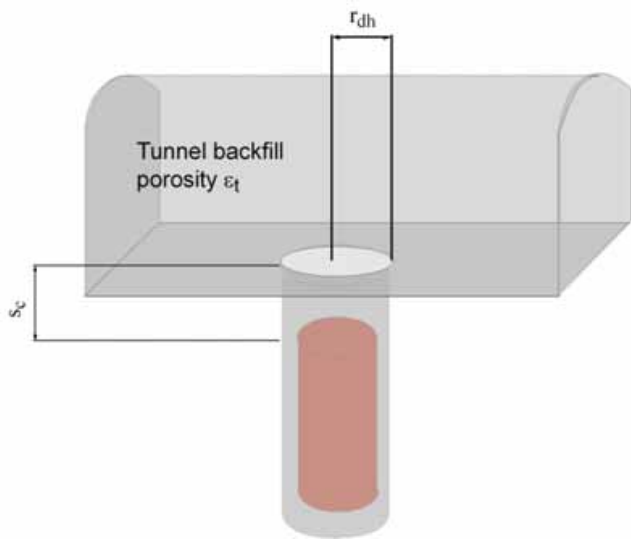

Figure 4-9. *Mass transfer by diffusion from the deposition hole to the tunnel.*

Mass transfer from the buffer to the tunnel is thus determined by

$$\frac{d\,m_{bt}(t)}{dt} = -\frac{\pi\left(r_{dh}\right)^2 D_{eb}}{s_c}\frac{m_b}{\varepsilon_b V_b} = -q_{bt}C_b = -\lambda_{bt}m_b \qquad , \tag{4-39}$$

where q_{bt} is the equivalent flow rate for the mass transfer from the buffer to the tunnel, ε_b the porosity of the buffer, V_b its volume, r_{dh} the radius of the deposition hole, D_{eb} the effective diffusion coefficient in the buffer, s_c the distance from the top of the canister to the floor of the tunnel, and λ_{bt} the decay constant of the solute mass transfer from the buffer to the tunnel.

Typical values for the different parameters and mass transfer coefficients that are applied in the computations are given in Tables 4-8 and 4-9.

Table 4-8. *Typical values for non-sorbing nuclides of the mass transfer coefficients from the buffer to the tunnel.*

Parameter	Notation	Value	Unit	Value	Unit
Radius of the deposition hole	r_{dh}	0.88	[m]		
Distance from the canister to the tunnel floor	s_c	2.5	[m]		
porosity of the buffer (neutral)	ε_b	0.43			
porosity of the buffer (anion)	ε_b	0.17			
Effective diffusion coefficient in the bentonite (neutral)	D_{eb}	$1.2\cdot10^{-10}$	[m^2/s]		
Effective diffusion coefficient in the bentonite (anion)	D_{eb}	$1.0\cdot10^{-11}$	[m^2/s]		
Equivalent flow rate (neutral)	$q_{bt} = \frac{\pi r_{dh}^{\,2} D_{eb}}{s_c}$	$1.2\cdot10^{-10}$	[m^3/s]	3 700	[mL/a]
Equivalent flow rate (anion)	$q_{bt} = \frac{\pi r_{bh}^{\,2} D_{eb}}{s_c}$	$9.7\cdot10^{-12}$	[m^3/s]	310	[mL/a]
Volume of the buffer	V_b	15.3	[m^3]		
Solute decay constant (neutral)	$\lambda_{bt} = \frac{q_{bt}}{R_{pb}\varepsilon_b V_b}$	$5.6\cdot10^{-4}$	[1/a]		
Solute decay constant (anion)	$\lambda_{bt} = \frac{q_{bt}}{R_{pb}\varepsilon_b V_b}$	$1.2\cdot10^{-4}$	[1/a]		
Half-time (neutral)	$T_{1/2} = \frac{\ln(2)}{\lambda_{bt}}$	1 200	[a]		
Half-time (anion)	$T_{1/2} = \frac{\ln(2)}{\lambda_{bt}}$	5 900	[a]		

Table 4-9. *Equivalent flow rates and half-lives of three solutes from the buffer to the tunnel.*

Nuclide	Equivalent flow rate	Pore volume	Retardation coefficient	$T_{1/2}$
C-14	3 700 mL/a	6.6 m^3	1	1 200 a
I-129	310 mL/a	2.6 m^3	1	5 900 a
Pu-239	3 700 mL/a	6.6 m^3	14 300	$1.8\cdot10^7$ a

4.4.2 Delay time

From buffer to fracture

Delay time in the buffer in mass transfer from the canister hole in the canister into the fracture is estimated using the diffusion time through the 35 cm thick layer of bentonite from the wall of the canister to the wall of the deposition hole (Table 4-10).

Table 4-10. *Delay times from the buffer into the fracture.*

Parameter		**Notation**	**Value**
Distance		l_b	0.35 m
Pore diffusion coefficient (neutral)		$D_{pb} = D_{eb} / \varepsilon_b$	$2.8 \cdot 10^{-10}$ m^2/s
Pore diffusion coefficient (anion)		$D_{pb} = D_{eb} / \varepsilon_b$	$5.9 \cdot 10^{-11}$ m^2/s
Retardation coefficient	**C-14**	R_{pb}	1
Delay time	**C-14**	$t_d \approx R_{pb}\, l_b^{\,2}\, 0.033 / D_{pb}$	0.46 a
Retardation coefficient	**I-129**	R_p	1
Delay time	**I-129**	$t_d \approx R_{pb}\, l_b^{\,2}\, 0.033 / D_{pb}$	2.2 a
Retardation coefficient	**Pu-239**	R_p	14 300
Delay time	**Pu-239**	$t_d \approx R_{pb}\, l_b^{\,2}\, 0.033 / D_{pb}$	6 600 a

From buffer into tunnel

Delay time in mass transfer from the canister hole to the tunnel floor is estimated using the diffusion time through the 2.5 m thick layer of bentonite in the deposition hole between the top of the canister and the floor of the tunnel (Table 4-11).

Table 4-11. *Delay times from the buffer to the tunnel floor.*

Parameter		**Notation**	**Value**
Distance		s_c	2.5 m
Pore diffusion coefficient (neutral)		D_p	$2.8 \cdot 10^{-10}$ m^2/s
Pore diffusion coefficient (anion)		D_p	$5.9 \cdot 10^{-11}$ m^2/s
Retardation coefficient	**C-14**	R_{pb}	1
Delay time	**C-14**	$t_d \approx R_{pb}\, s_c^{\,2}\, 0.033 / D_{pb}$	23 a
Retardation coefficient	**I-129**	R_{pb}	1
Delay time	**I-129**	$t_d \approx R_{pb}\, s_c^{\,2}\, 0.033 / D_{pb}$	110 a
Retardation coefficient	**Pu-239**	R_{pb}	14 300
Delay time	**Pu-239**	$t_d \approx R_{pb}\, s_c^{\,2}\, 0.033 / D_{pb}$	$3.4 \cdot 10^5$ a

4.4.3 Response functions

The simplified response functions of the mass transfer from the buffer into the fracture and from the buffer into the tunnel were compared with numerical simulation results obtained using both the REPCOM (Nordman and Vieno 1994) and COMSOL multiphysics (COMSOL 2009) models. The numerical models were constructed assuming that the hole in the canister is located in its lid. The fracture was assumed to be located next to the hole in the canister to have the smallest diffusion distance through the buffer (the thickness of the buffer) and the least mixing of the solute in the buffer. Therefore, the case used here for verification is the least favourable one for the simplified approach.

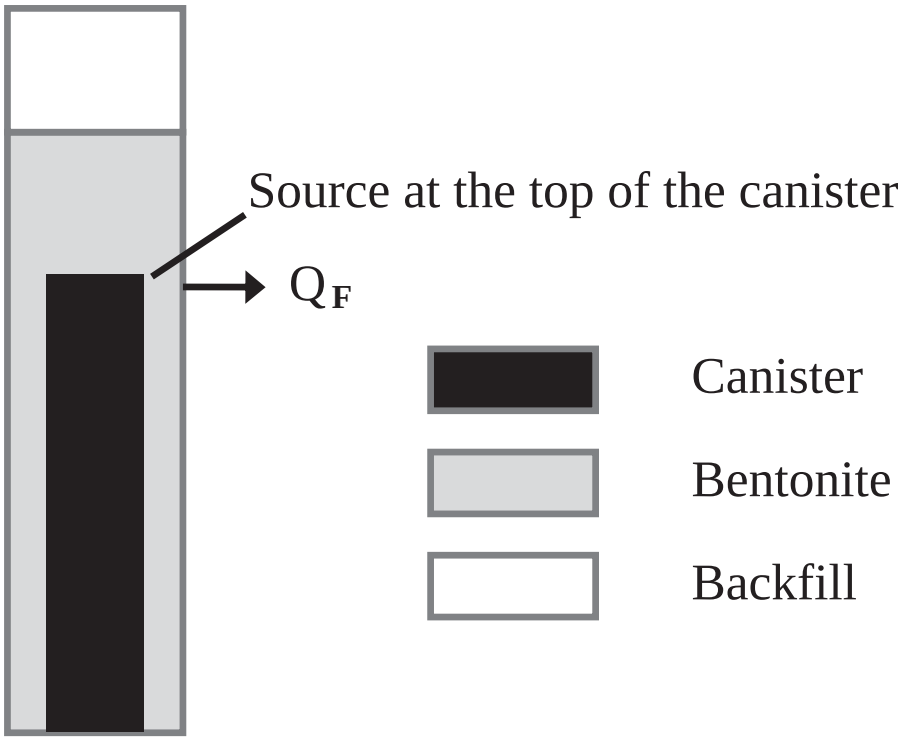

Figure 4-10. *Conceptual model used in the REPCOM and COMSOL computations. Q_F indicates the equivalent flow rate to the fracture and the location of the fracture.*

COMSOL simulations were applied to study issues connected to the physical diffusion process and geometrical representation of the diffusion problem. The model contained about 400,000 degrees of freedom that described in three dimensions the buffer material and the fracture intersecting the deposition hole. The properties of the fracture, groundwater flowing in the fracture, dimensions of the deposition hole, and properties of the buffer material for a neutral nuclide were taken from Table 4-4 to ensure that the same equivalent flow rate and time constants were applied in the COMSOL model as in the simplified model. The geometry of the COMSOL model is shown in Figure 4-11.

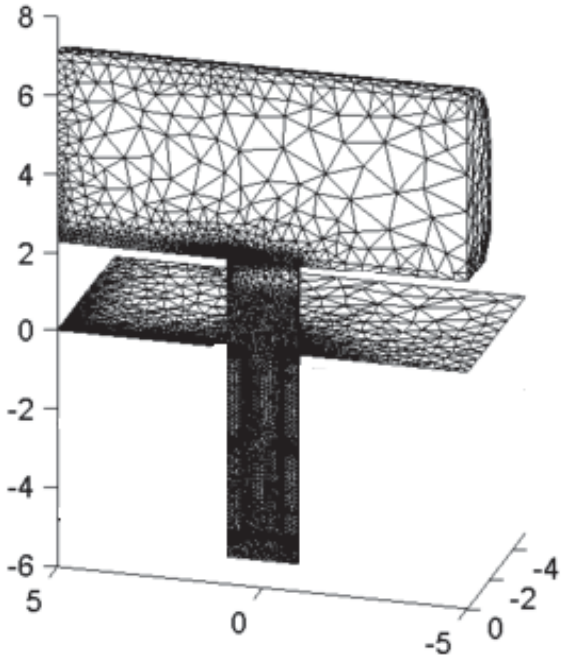

Figure 4-11. *Geometry of the COMSOL model.*

REPCOM is a compartment model that has been used previous performance assessments in the near field analysis of the repository. It is able to simulate diffusive solute transport in the buffer material of decay chains and solubility limited elements. The deposition hole and the buffer material were represented in a two dimensional axi-symmetric geometry by about 150 compartments. A close-up of the top of the canister in the REPCOM model is shown in Figure 4-12.

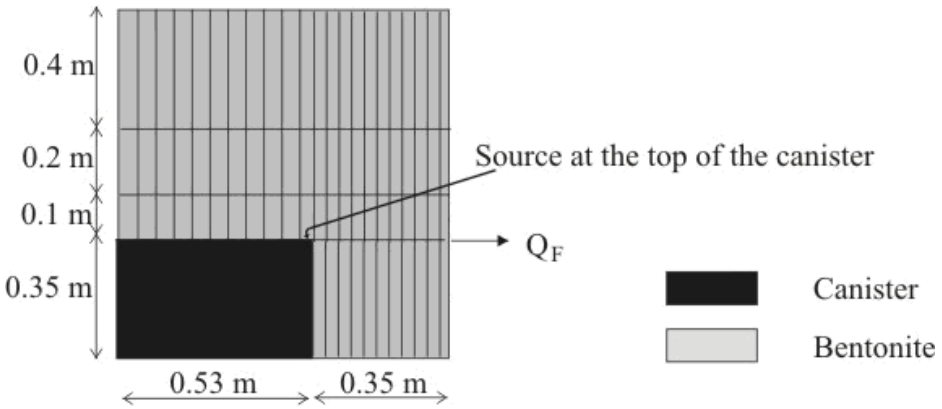

Figure 4-12. *Geometry of the REPCOM model.*

From buffer to fracture

Response functions determined by the different approaches described above are shown for the typical case in Figure 4-13. The simplified response function for a non-sorbing nuclide is characterised by a time constant of 9,000–20,000 years and a delay time of 2–9 years. Based on the simulations, well mixed conditions dominate the response function of non-sorbing nuclides after about 1,000 years (Figures 4-13 and 4-14).

Numerical simulations show that there is an early transient phase of the release rates. The main part of the transient is reproduced by both numerical methods. However, the geometrically more accurate COMSOL simulations also show a very quick and early transient phase that does not exist in the REPCOM simulations. The early and quick transient phase of the response function determined by COMSOL can be explained by the location of the defect in the canister with respect to the direction of the water flow in the fracture, and by the realistic water flow profile in the three dimensional COMSOL model. First, the nuclides spread quickly to the upstream location of the intersection between the fracture and the deposition hole, where the concentration of the nuclides is zero and nuclides are carried along the buffer surface by convection. The nuclides continue migrating with the flow near the buffer surface. This reduces the net release of nuclides in the downstream parts of the fracture intersection line causing a drop in the release rate. Eventually this initial behaviour levels off to the asymptotic behaviour. Numerical inaccuracy also affects the late time tailing of the response function in the COMSOL simulations.

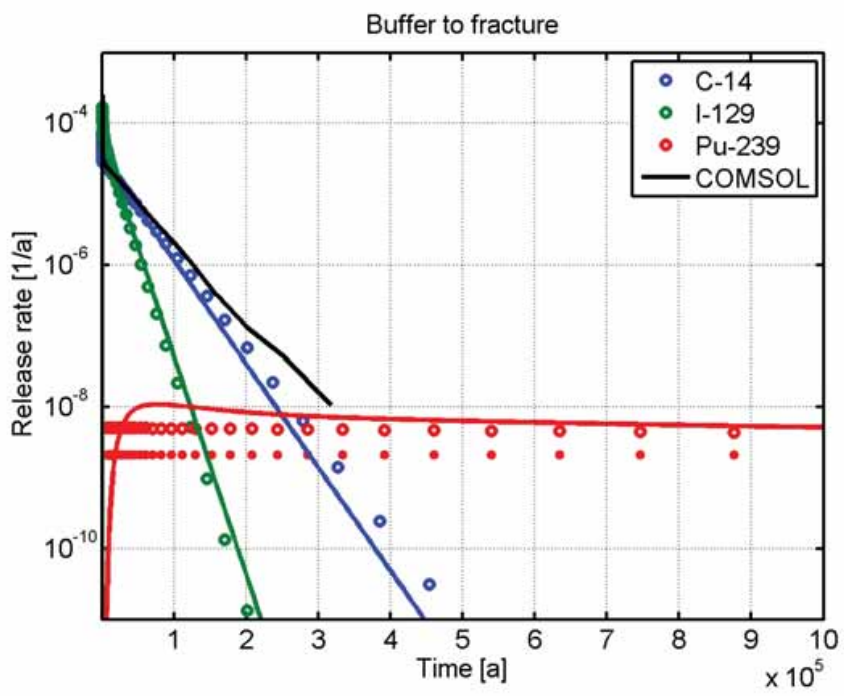

Figure 4-13. *Response functions of three nuclides from the buffer to the fracture, Equation (4-39). REPCOM results are shown by solid coloured lines and COMSOL result for a non-sorbing neutral nuclide (C-14) is shown by a black line. The well mixed model with the estimated transient part (Equation (4-31)) is shown by open circles. The well mixed model without the early transient (Equation (4-30)) is shown for Pu-239 by dots. All response functions are shown without radioactive decay.*

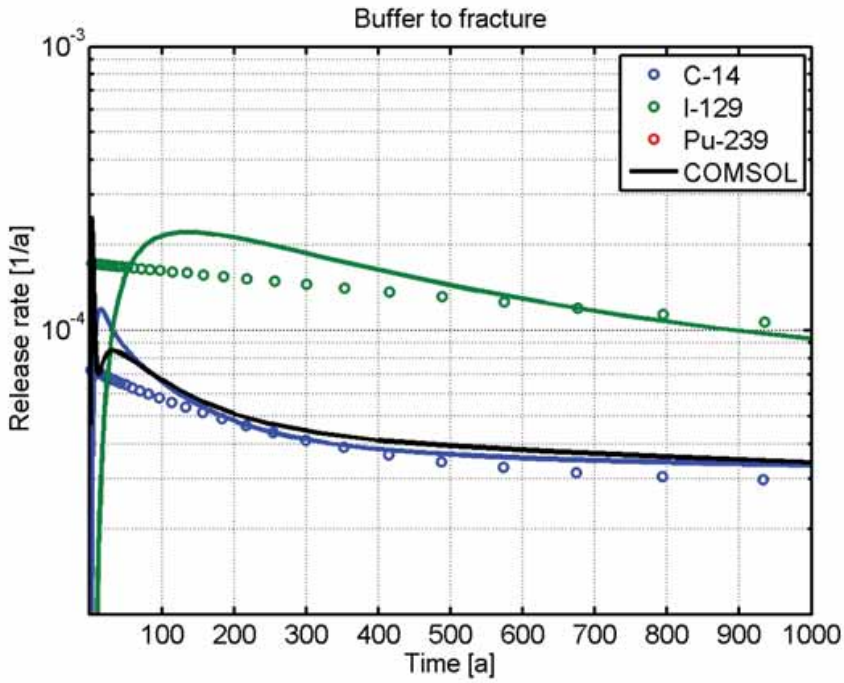

Figure 4-14. *Close-up of Figure 4-13 at early times showing a transient in the response functions of the non-sorbing nuclides. Results of REPCOM simulations are shown by solid coloured lines. Response functions from the buffer into the fracture as determined by Equation (4-31) are shown by open circles. The delay time of the diffusion in the buffer is greater for Pu-239 than the 1000 year time window of the figure.*

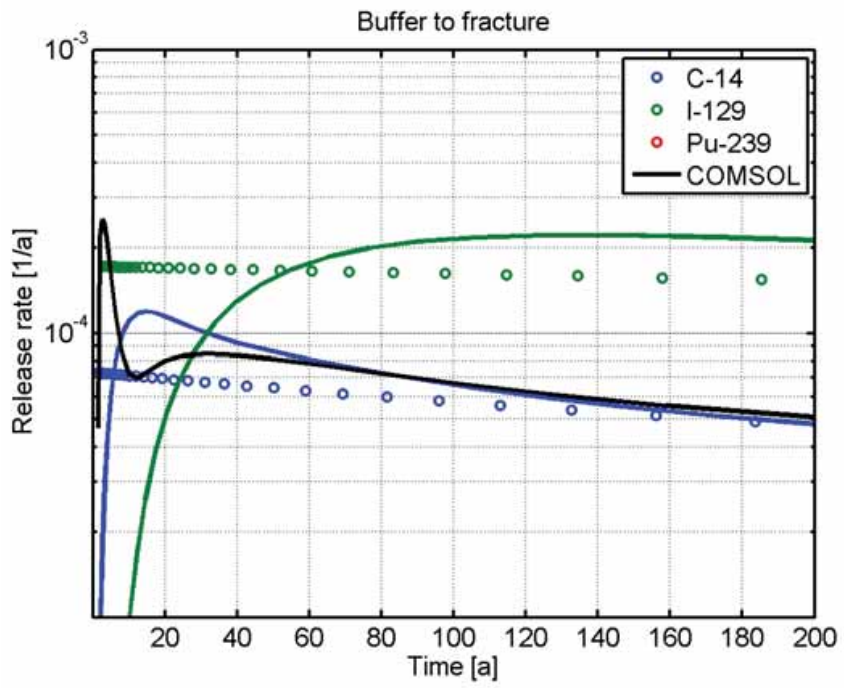

Figure 4-15. *Another close-up of Figure 4-13 showing the very early transient behaviour in the COMSOL simulations (black line) of a neutral non-sorbing nuclide (C-14). Results of REPCOM simulations are shown by solid coloured lines. Response functions from the buffer into the fracture as determined by Equation (4-31) are shown by open circles. The delay time of diffusion in the buffer is greater for Pu-239 than the 200 year time window of the figure.*

From buffer to tunnel

Response functions determined by the simplified and numerical approaches were compared for the typical case shown in Table 4-8. The simplified response function for a non-sorbing tracer was characterised by a time constant of 1,000–6,000 years and a delay time of 100–400 years.

Well mixed conditions dominate the response functions of non-sorbing nuclides after 2,000–4,000 years. In the COMSOL simulations we had some (numerical) difficulties with the long-time behaviour of the response function, but the early transient was quite similar in both numerical solutions. However, there was some difference in the timing of the transients at the COMSOL and REPCOM results, which became detectable for sorbing nuclides. The COMSOL simulations (scaled by the retardation coefficient of Pu-239, R_{pb}=14 300) indicate raising of the Pu-239 response function about 100,000 years later than the REPCOM simulations (cf. Figures 4-18 and 4-19).

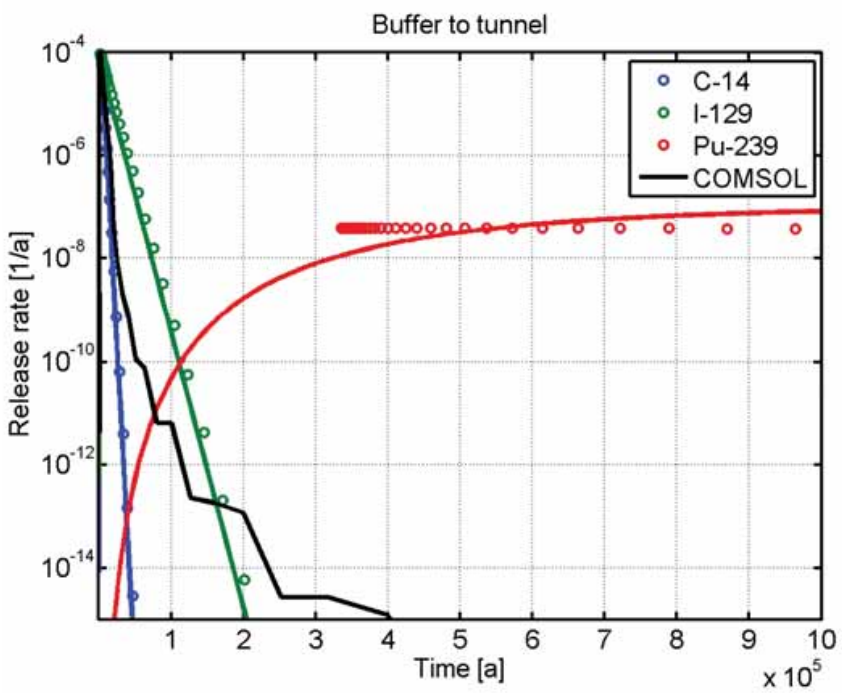

Figure 4-16. *Response functions from the buffer to the tunnel determined by the simplified model (circles) with the estimated diffusive delay times, and by the REPCOM model (solid line). Response functions are shown without radioactive decay.*

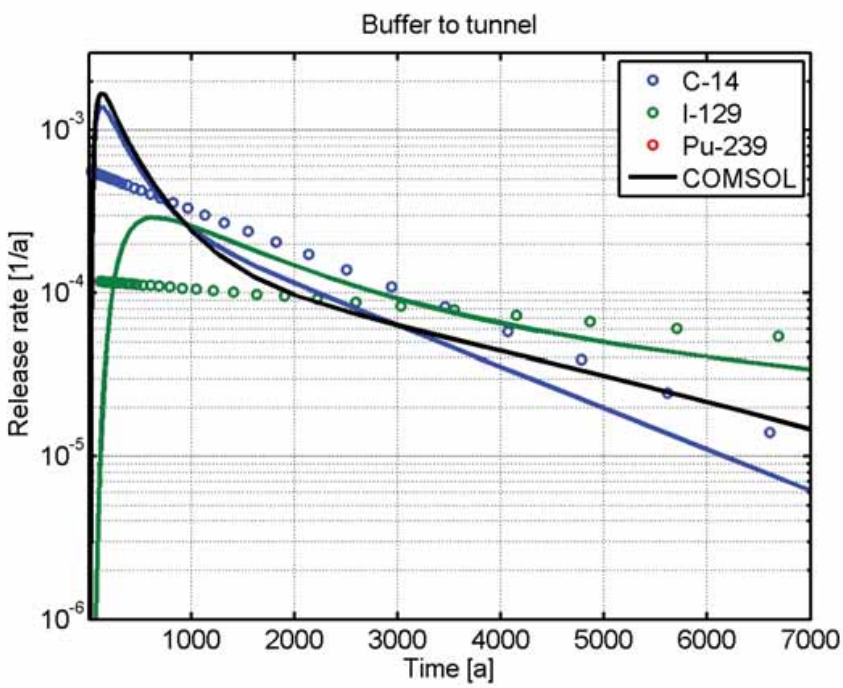

Figure 4-17. *Close-up of Figure 4-16 at early times showing the early transients of the response functions.*

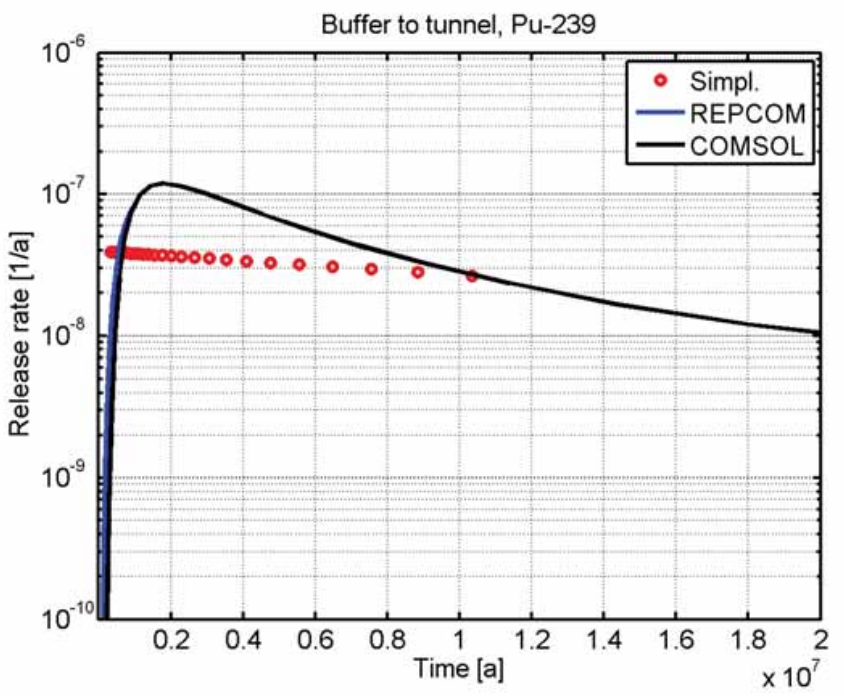

Figure 4-18. *Response functions from the buffer to the tunnel of Pu-239 determined by the simplified model (circles) with the estimated diffusive delay times, by the REPCOM model (solid blue line) and by COMSOL simulation results scaled by the retardation coefficient (R_{pb}=14 300) of Pu-239 (solid black line). Response functions are shown without radioactive decay.*

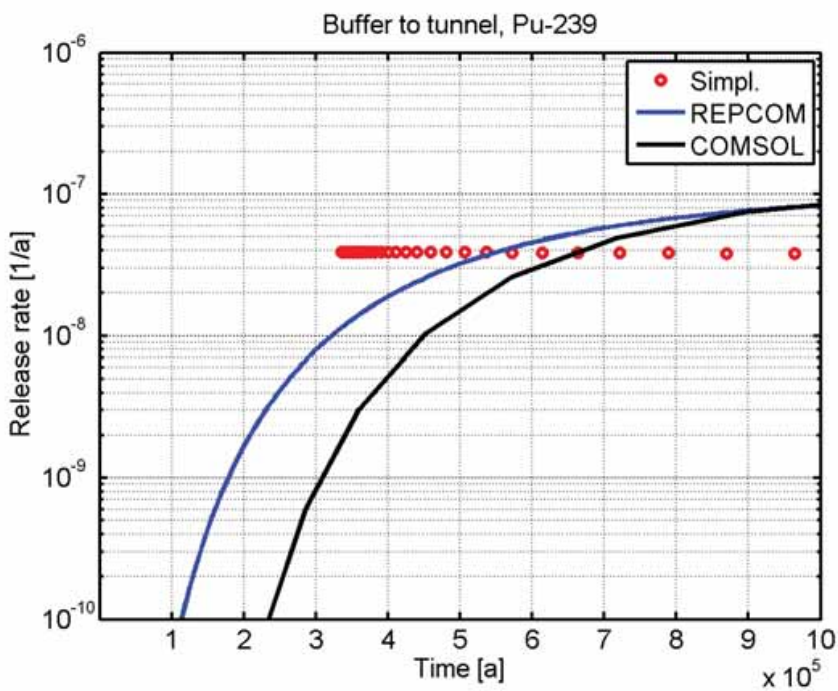

Figure 4-19. *Close-up of Figure 4-18 at early times showing response functions from the buffer to the tunnel of Pu-239 determined by the simplified model (circles) with the estimated diffusive delay times, by the REPCOM model (solid blue line) and by COMSOL simulation results scaled by the retardation coefficient (R_{pb}=14 300) of the Pu-239 (solid black line). Response functions are shown without radioactive decay.*

4.5 Tunnel section

Deposition holes will be bored in the floor of the deposition tunnels. One release pathway from a canister goes from that deposition hole to the tunnel above and eventually to the fracture intersecting the tunnel. The part of the tunnel above the deposition hole, which is included in the model, is called here the tunnel section. Typically, the length of the tunnel section is a few meters. Mass transfer from the tunnel section to the fracture intersecting the tunnel is estimated using the same model as for the mass transfer from the buffer surface to the fracture. It is assumed that the fracture intersects the whole tunnel (Figure 4-20).

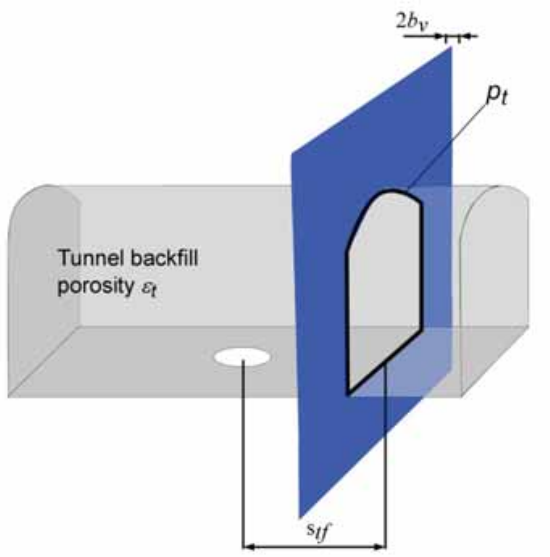

Figure 4-20. *Mass transfer from the tunnel to the fracture.*

4.5.1 Mass transfer coefficient

The hydraulic conductivity of the backfilled tunnel is assumed to be low compared to the transmissivity of the fracture so that groundwater flow goes around the tunnel section instead of flowing through it. Mass transfer from the tunnel backfill to the groundwater flow in the fracture is determined by the same equation (Equation (4-30)) as for mass transfer from the buffer to the fracture, but the length of the intersection of the fracture and deposition hole wall is replaced by that of the intersection of the fracture and tunnel wall,

$$\frac{d\,m_t(t)}{dt} = -p_t\,2b_v\sqrt{\frac{4D_w\,v}{\pi\,p_t/2}}\,\frac{m_t}{\varepsilon_t\,V_t} = -q_{tf}\,C_t = -\lambda_{tf}\,m_t \quad , \tag{4-40}$$

where q_{tf} is the equivalent flow rate for the mass transfer from the wall of the tunnel into the fracture, ε_t the porosity of the tunnel backfill, V_t the volume of the tunnel section, p_t the length of the intersection of the fracture and tunnel wall, $2b_v$ the volume aperture of the fracture, D_w the molecular diffusion coefficient in free water, v the flow velocity in the fracture, and λ_{tf} the decay constant of the solute mass transfer from the tunnel wall to the fracture.

Typical values for the different parameters and mass transfer coefficients used in the computations are shown in Tables 4-12 and 4-13. Layout of the repository tunnels and deposition holes for a real nuclear waste repository will follow criteria which aim to ensure a proper performance of the repository. According to the present plans (e.g. Hellä et al. 2009), the tunnel system should avoid large hydraulic structures that have a high transmissivity ($T \geq 10^{-5}$) and large size. Deposition holes will not be accepted if the inflow to the open deposition hole is more than 0.1 L/min. This inflow corresponds to

transmissivity of a fracture, which is roughly of the order of 10^{-9}–10^{-8} m^2/s (Smith, 2007). More transmissive fractures are allowed to intersect the deposition tunnel than the individual deposition holes. The computations in this report assume that the tunnel is intersected by a fracture that has a transmissivity of $T = 2.5 \cdot 10^{-7}$ m^2/s. This is about an order of magnitude higher than that allowed for the deposition hole, but still well below the typical transmissivity, $T=10^{-5}$ m^2/s, of the larger scale hydraulic structures. The Darcy flow velocity (volumetric flow) in the fracture intersecting the tunnel is estimated using an order of magnitude estimate for the gradient of the hydraulic head at Olkiluoto. This is roughly 0.005, based on the height of the island (about 18) m and the size of the island (about 5×2 km^2) (e.g. Posiva 2008). The actual average velocity of groundwater flow is smaller than the Darcy velocity because the apertures of the fractures vary and the resistance to the flow is determined by the smallest apertures, but the average flow velocity is determined by the volume of the fracture. The average volume aperture for a fracture is larger than the aperture that determines the flow resistance typically by a factor of C_v=5-20 (Gelhar 1987). A factor of C_v=15 was used when estimating the flow velocity in Equation (4-40).

Table 4-12. *Typical values for non-sorbing nuclides of the mass transfer coefficients from the tunnel to the fracture.*

Parameter	Notation	Value	Unit	Value	Unit
Perimeter of the tunnel	p_t	16	[m]		
Fracture volume aperture	$2b_v$	1.0	[mm]		
porosity of the tunnel backfill (neutral)	ε_t	0.23			
porosity of the tunnel backfill (anion)	ε_t	0.092			
Diffusion coefficient in water	D_w	$2 \cdot 10^{-9}$	[m^2/s]		
Velocity of groundwater flow	v	$1.25 \cdot 10^{-6}$	[m/s]	39	[m/a]
Equivalent flow rate	$q_{tf} = p_t 2b_v \sqrt{\frac{4D_w v}{\pi\, p_t / 2}}$	$3.2 \cdot 10^{-10}$	[m^3/s]	10 000	[mL/a]
Volume of the tunnel section	V_t	100	[m^3]		
Solute decay constant (neutral)	$\lambda_{tf} = \frac{q_{tf}}{R_{pt}\varepsilon_t V_t}$	$4.4 \cdot 10^{-4}$	[1/a]		
Solute decay constant (anion)	$\lambda_{tf} = \frac{q_{tf}}{R_{pt}\varepsilon_t V_t}$	$1.1 \cdot 10^{-3}$	[1/a]		
Half-time (neutral)	$T_{1/2} = \frac{\ln(2)}{\lambda_{tf}}$	1 600	[a]		
Half-time (anion)	$T_{1/2} = \frac{\ln(2)}{\lambda_{tf}}$	630	[a]		

Table 4-13. *Equivalent flow rates and half-lives of three solutes from the tunnel to the fracture.*

Nuclide	Equivalent flow rate	Pore volume	Retardation coefficient	$T_{1/2}$
C-14	10 000 mL/a	23	1	1 600 a
I-129	10 000 mL/a	9.2	1	640 a
Pu-239	10 000 mL/a	23	11 750	$1.9 \cdot 10^7$ a

4.5.2 Delay time

In principle the delay time for diffusive transport in the tunnel section can be estimated in the same way as for the buffer, i.e.,

$$t_{dt} \approx R_{pt}\, s_{tf}^{\,2}\, 0.033 / D_{pt} \quad , \qquad (4\text{-}41)$$

where D_{pt} is the pore diffusion coefficient in the backfill of the tunnel, R_{pt} the retardation coefficient and s_{tf} the diffusion distance. However, the tunnel section above the deposition hole has been treated as a mixing tank in the past performance assessments. This means that the delay time has been conservatively assumed to be zero. The simplified approach is now compared mainly against the numerical REPCOM/FTRANS simulations of the barrier system, which do not take into account the delay time in the tunnel section. Therefore, in the simplified approach here the delay time in the tunnel was also omitted.

If required, estimation of the delay time that could be used in the simplified approach would be straightforward. It can be based on a similar assessment of the diffusive delay as in the case of the delay through the buffer in the deposition hole from the top of the canister to the floor of the tunnel. This estimate would require parameterisation of the diffusion distance, pore diffusivity and retardation coefficient.

4.6 Bedrock

Migration through the bedrock is assumed to take place along a network of connected fractures. Transport and retention processes that are taken into account are advection with the groundwater flow, sorption on rock walls and matrix diffusion. The release path through the bedrock has been represented by an equivalent transport channel. The response function of the geosphere is determined by a parameter called transport resistance (u) and the advective delay time (t_w), as shown in Section 4.1.3.

4.6.1 Mass transfer coefficient

The response function for migration through the transport channel that is in contact with an infinite block of rock matrix is given by (e.g. Kekäläinen et al. 2011, Cvetkovic et al. 1999, cf. also Equation (4-12))

$$f_r(t) = \frac{d\, m_r(t)}{dt} = \frac{u}{\sqrt{\pi (t - t_w)^3}} e^{-\frac{u^2}{(t-t_w)}}, \qquad (4\text{-}42)$$

where $u = \sqrt{\varepsilon_m R_{pm} D_{em}} WL/Q$ is the transport resistance and t_w the water residence time (advective delay). The transport resistance is composed of rock matrix properties, $\sqrt{\varepsilon_m R_{pm} D_{em}}$, and properties of the flow field, WL/Q, where ε_m is the rock matrix porosity, D_{em} the diffusion coefficient of the effective diffusion in the rock matrix, R_p the retardation coefficient in the rock matrix, and the transport channel is characterised by width W, length L and flow rate Q. Dependence on the flow field of matrix diffusion, WL/Q, is called here the hydrodynamic control of retention (Cvetkovic et al. 1999).

Simplification of solute migration in the bedrock is realised by concentrating on the spreading and delay of the response function (i.e. solute breakthrough curve for a unit pulse input). The analytical form of the advection-matrix diffusion response function in Equation (4-42) is quite simple, but the motivation of the present section is to find a description of the geosphere barrier equivalent to those of the other barriers (i.e. the

time constant describing spreading and the delay time). The advective delay needs not to be included in this treatment. Advective delay in this system is pure translation in time. The release rate through the studied system of successive transport barriers can be calculated using the response function of the system, which is convoluted from the response functions of the individual barriers as discussed in Sections 3.1 and 4.1.1. The translation in time for this kind of convoluted system is the sum of the translations in time of the components of the system. Thus, also the geosphere response function can be calculated without advective delay. This delay can be taken into account as a component of the total delay (translation in time) of the whole system at the end of the calculations if needed.

A mixing tank approximation of the geosphere transport is based on both the maximum release rate and the half width of the response function in the case of an unlimited thickness of the rock matrix. By omitting the advective delay (t_w=0) in Equation (4-42), it can be found that the maximum release rate for a unit input pulse is given by

$$f_r\left(\frac{2}{3}u^2\right) = \frac{\sqrt[3]{\frac{3}{2\pi}}}{2e^{3/2}}u^2 \approx 0.23\,u^2 \quad . \tag{4-43}$$

The time to reach a fraction c of the maximum release was already determined in Equation (4-13). The half width of the release pulse (t_l-t_e) can be determined from Equation (4-13) by setting c=2. We find that

$$\mathrm{FWHM} = t_l - t_e = -\frac{2u^2}{3\,\mathrm{W}_0\left(-\frac{1}{2^{2/3}e}\right)} + \frac{2u^2}{3\,\mathrm{W}_{-1}\left(-\frac{1}{2^{2/3}e}\right)} \approx 1.8\,u^2 \quad . \tag{4-44}$$

The release rate of a unit mass in a mixing tank can be expressed in the form

$$F_m(t) = \lambda_f \exp\left(-\lambda_f t\right) , \tag{4-45}$$

where λ_f is the solute "decay constant" of the mixing tank. The maximum (release rate) of $F_m(t)$ is λ_f, and the half width of the pulse is $t_{1/2}$ = ln(2) / λ_f. From Equations (4-43) and (4-44) we find an approximative relation

$$\frac{1}{4.3\,u^2} < \lambda_f < \frac{1}{2.6\,u^2} \quad , \tag{4-46}$$

where the lower limit is based on the maximum release rate and the upper limit on the half width of the release pulse.

Both limiting values of λ_f above give a conservative estimate for the integrated response function (cumulative breakthrough curve for a unit pulse input), and the one based on the maximum release rate is closer to the response function of matrix diffusion. Figure 4-21 shows the analytical response functions of matrix diffusion and the two mixing tank approximations of it.

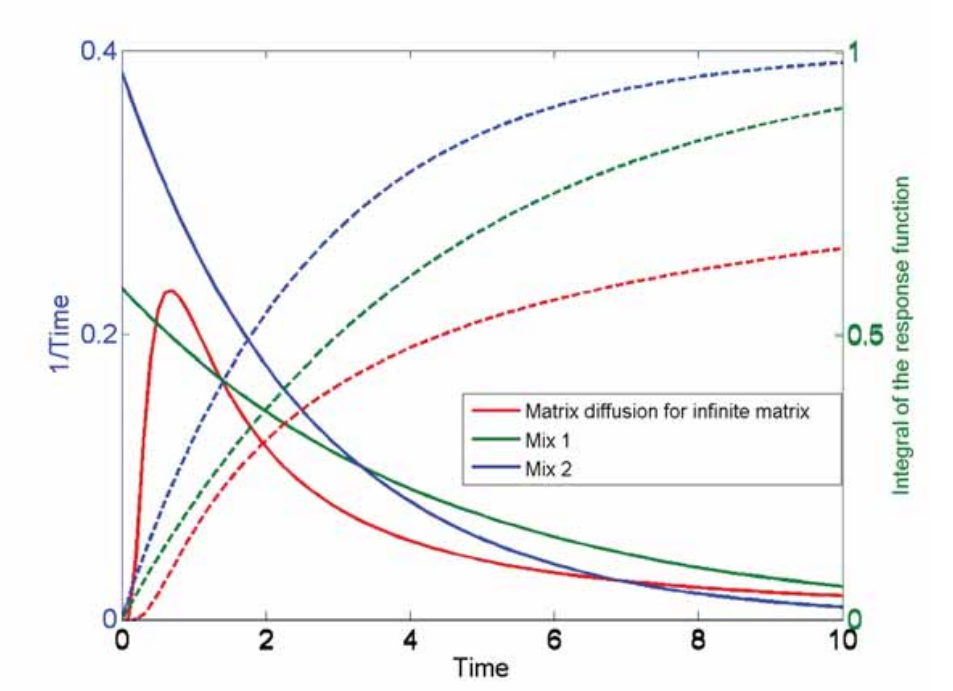

Figure 4-21. *Approximative solutions for the response functions of the geosphere described with mixing tank models based on the maximum release rate (Mix 1) and the half width of the release pulse (Mix 2). Response functions are expressed in terms of the dimensionless time (u^2=1). Release rates for instantaneous releases of unit pulse are shown by the solid lines, and the corresponding release rates are indicated on the y-axis on left hand side. Cumulative release rates are shown by the dashed lines and the corresponding release rates are shown on the y-axis on the right hand side.*

In reality the assumption of an unlimited rock matrix is an extreme case that is possibly the least favourable one for the mixing tank approximation. Figure 4-22 shows response functions for the limited and unlimited thickness of the rock matrix and in the corresponding mixing tank approximation based on the maximum release rate. It appears that the mixing tank model gives a rather accurate results at least up to the thickness of the rock matrix of about $L = 5/2\sqrt{D_{pm}\, u^2 / R_{pm}}$. For a very thin layer of rock, the retention caused by the immobile zones cannot be estimated accurately on the basis of parameter *u* only. The response function only produces a delay as the layer gets thinner. The pore volume of the limited matrix added to the volume of the flow channel determines the delay. For sorbing species the equilibrium sorption on the fracture and pore space surfaces is accounted for by means of a retardation factor.

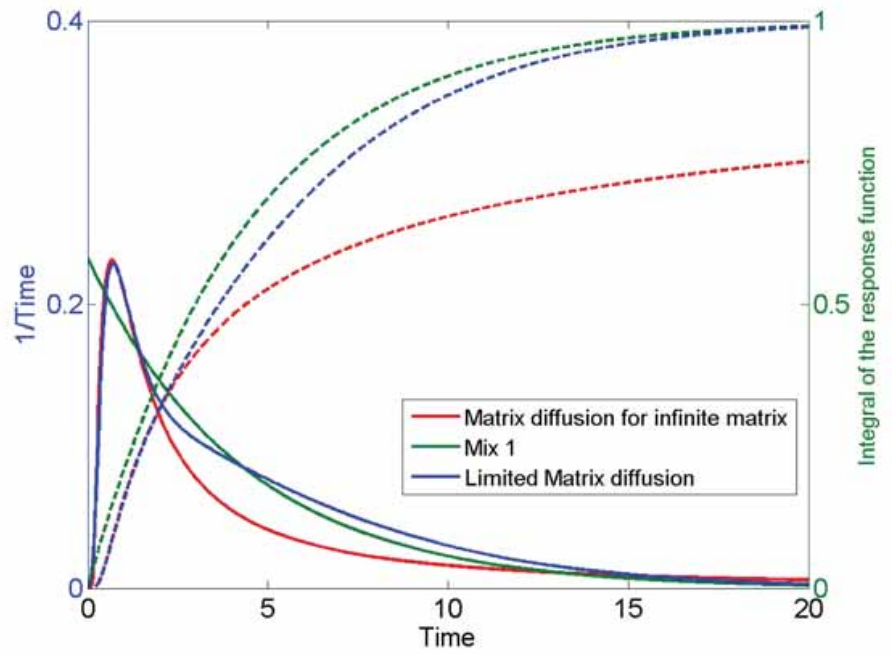

Figure 4-22. *Approximative solutions for the response functions of the geosphere with mixing tank model in the case of a limited thickness of the rock matrix* ($L = 5/2\sqrt{D_{pm}\, u^2}$). *The mixing tank model is based on the maximum release rate (Mix 1). Response functions are expressed in terms of dimensionless time* ($u^2=1$). *Release rates for instantaneous releases of unit pulse are shown by the solid lines, and the corresponding release rates are indicated on the y-axis on left hand side. Cumulative release rates are shown by the dashed lines and the corresponding release rates are shown on the y-axis on the right hand side.*

Typical values of the different parameters and mass transfer coefficients used in the computations are shown in Tables 4-14 and 4-15.

Table 4-14. *Typical values for non-sorbing nuclides of the mass transfer coefficients through the geosphere.*

Parameter	Notation	Value	Unit
Hydrodynamic control of retention	WL/Q	50 000	[a/m]
Porosity of the rock matrix (neutral)	ε_m	0.005	
Porosity of the rock matrix (anion)	ε_m	0.001	
Retardation coefficient	R_p	1	
Effective diffusion coefficient of the rock matrix (neutral)	D_{em}	10^{-14}	[m^2/s]
Effective diffusion coefficient of the rock matrix (anion)	D_{em}	10^{-15}	[m^2/s]
Transport resistance (neutral)	$u = \sqrt{\varepsilon_m R_{pm} D_{em}} WL/Q$	2.0	[$\sqrt{a}$]
Transport resistance (anion)	$u = \sqrt{\varepsilon_m R_{pm} D_{em}} WL/Q$	0.28	[$\sqrt{a}$]
Solute decay constant (neutral)	$\lambda_f = \frac{1}{4.3u^2}$	0.059	[1/a]
Solute decay constant (anion)	$\lambda_f = \frac{1}{4.3u^2}$	3.0	[1/a]
Half-time (neutral)	$T_{1/2} = \frac{\ln(2)}{\lambda_{bf}}$	12	[a]
Half-time (anion)	$T_{1/2} = \frac{\ln(2)}{\lambda_{bf}}$	0.24	[a]

Table 4-15. *Half-lives of three solutes in transport through the geosphere.*

Nuclide	**Retardation coefficient**	$u^2 = \varepsilon R_{pm} D_{em} (WL/Q)^2$	$\lambda_f = \frac{1}{4.3u^2}$	$T_{1/2} = \frac{\ln(2)}{\lambda_{bf}}$
C-14	1	3.9 a	0.06 1/a	12 a
I-129	1	7.9e-2 a	3.0 1/a	0.23 a
Pu-239	269 000*)	1 060 000 a	$2.2 \cdot 10^{-7}$ 1/a	$3.2 \cdot 10^{6}$ a

*) The retardation coefficient $R_{pm} = 1 + (1-\varepsilon) K_{dm} \rho / \varepsilon$ of Pu-239 is based on a rock matrix porosity of 0.005, on rock density of $\rho = 2700$ kg/m^3 and on K_d = 0.5 m^3/kg.

4.6.2 Delay times

The delay times through the geosphere shown in Table 4-16 are estimated based on the time when the release rate reaches 1/285 of the maximum release rate for a pulse input at $t_d = 0.1u^2$ (cf. Section 4.1.3).

Table 4-16. *Delay times for migration through the geosphere.*

Parameter		**Notation**	**Value**	**Unit**
Retardation coefficient	**C-14**	R_{pm}	1	[-]
Transport resistance	**C-14**	$u^2 = \varepsilon R_{pm} D_{em} (WL/Q)^2$	3.9	[a]
Delay time	**C-14**	$t_d = 0.1u^2$	0.39	[a]
Retardation coefficient	**I-129**	R_{pm}	1	[-]
Transport resistance	**I-129**	$u^2 = \varepsilon R_{pm} D_{em} (WL/Q)^2$	0.08	[a]
Delay time	**I-129**	$t_d = 0.1u^2$	0.008	[a]
Retardation coefficient	**Pu-239**	R_{pm}	269 000	[-]
Transport resistance	**Pu-239**	$u^2 = \varepsilon R_{pm} D_{em} (WL/Q)^2$	1 060 000	[a]
Delay time	**Pu-239**	$t_d = 0.1u^2$	106 000	[a]

*) The retardation coefficient $R_{pm} = 1 + (1-\varepsilon) K_{dm} \rho / \varepsilon$ of Pu-239 is based on a rock matrix porosity of 0.005, on rock density of ρ = 2700 kg/m^3 and on K_{dm} = 0.5 m^3/kg.

4.6.3 Response functions

The response functions of the simplified geosphere model are compared here with the analytically known response function of unlimited matrix diffusion. Comparison is made using the typical values for the geosphere parameters applied in performance assessments and shown in Table 4-14.

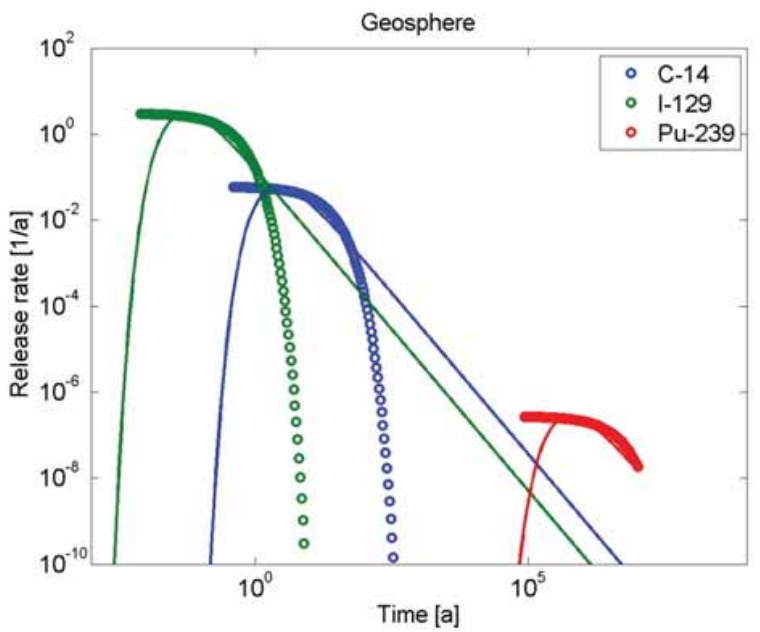

Figure 4-23. *Geosphere response functions (breakthrough curves) for three non-sorbing nuclides (cf. Tables 4-14, 4-15 and 4-16). Solid lines show the analytical breakthrough curves of unlimited matrix diffusion, and the simplified exponential expressions for the same breakthrough curves are indicated by open circles. Response functions are shown without radioactive decay.*

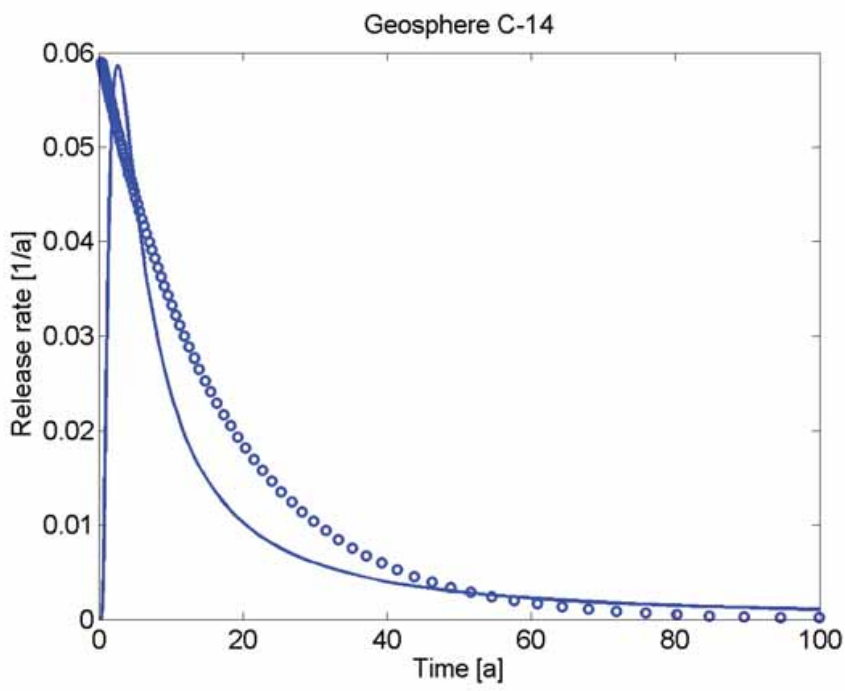

Figure 4-24. *The geosphere response function of C-14. Solid line shows the analytical result for the breakthrough curve of unlimited matrix diffusion and open circles indicate the simplified exponential representation of it. Response functions are shown without radioactive decay.*

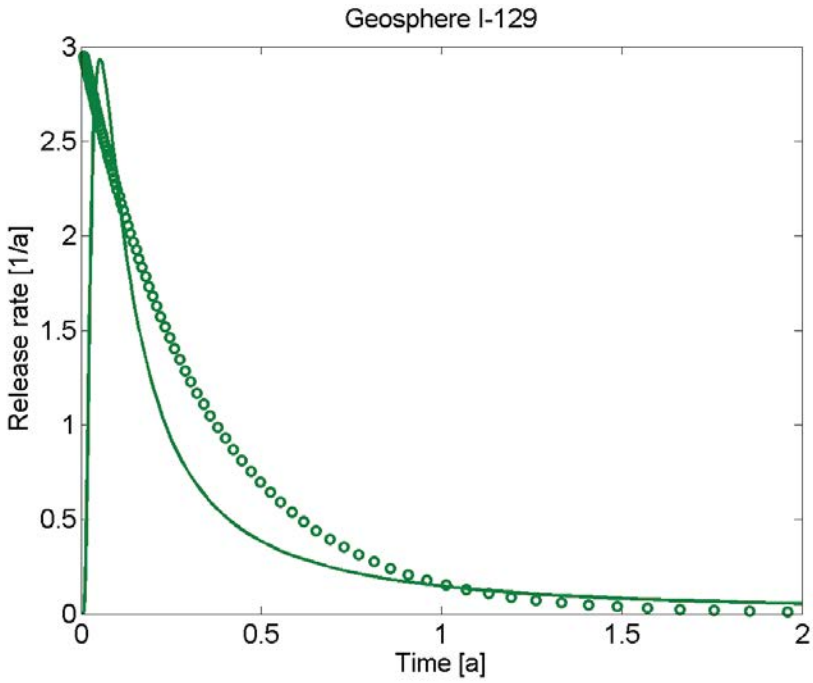

Figure 4-25. *The geosphere response function of I-129. Solid line shows the analytical result for the breakthrough curve of unlimited matrix diffusion and open circles indicate the simplified exponential representation of it. Response functions are shown without radioactive decay.*

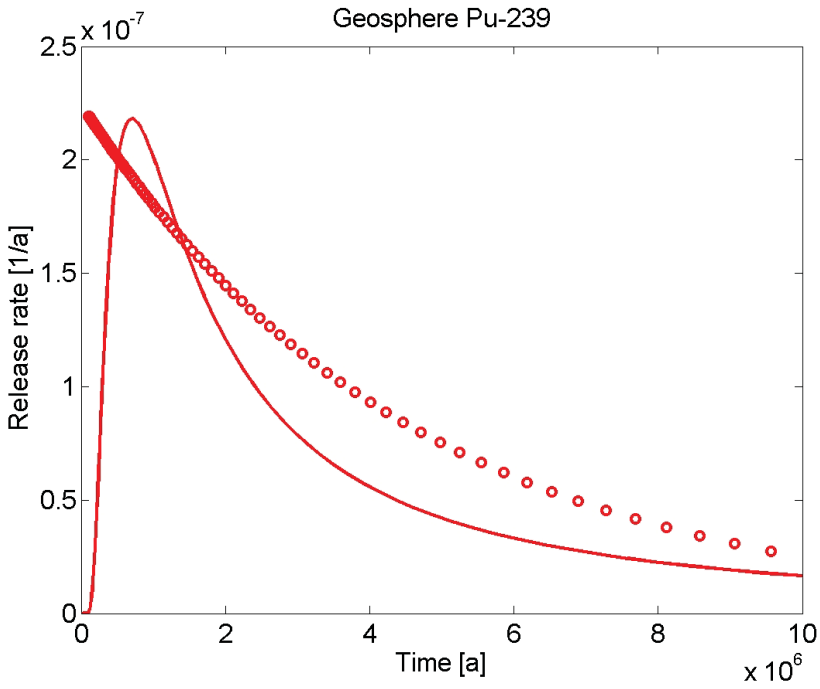

Figure 4-26. *The geosphere response function of Pu-239. Solid line shows the analytical result for the breakthrough curve of unlimited matrix diffusion and open circles indicate the simplified exponential representation of it. Response functions are shown without radioactive decay.*

5 SIMULATION OF RADIONUCLIDE MIGRATION FOR C-14, I-129 AND PU-239 EMANATING FROM A SINGLE CANISTER

Migration of nuclides through the whole repository system was computed for three representative nuclides (C-14, I-129 and Pu-239). The radioactive decay was taken into account by multiplying the resulting mass outflow at the end of the flow path by an appropriate decay factor.

Response functions for the individual barriers of these nuclides were already given in previous sections. Their release characteristics are described in the following:

C-14 A non-sorbing neutral nuclide, a fraction by instant release and another fraction by gradual leaching from the fuel to the water in a canister. The rate of leaching is determined by degradation of fuel and other parts of the fuel elements.

I-129 A non-sorbing anion, a fraction by instant release and another fraction by gradual leaching from fuel to the canister. The rate of leaching is determined by degradation of fuel.

Pu-239 A solubility limited sorbing nuclide, gradual leaching from the fuel to the canister. The rate of leaching is determined by degradation of fuel and the solubility of plutonium.

"Pu-239NS" A generic non-solubility limited variant of Pu-239, which is used to demonstrate the modelling of a sorbing nuclide.

Four different alternatives for the response functions of the system were constructed in order to investigate the influence of different details of the model on the overall performance of the simplified approach. The main motivation for using alternative models was that a nuclide that is strongly sorbing and also has a short decay time emphasises specific features of the total barrier system. The different alternative models used here are the following:

1. All barriers are modelled as well mixed volumes

2. All barriers are modelled as well mixed volumes, but the early transient from the buffer into the fracture is added to the buffer response function. The early transient in the mass flux from the buffer to the fracture is modelled by representing the buffer response function as a sum of transient response and well mixed response as explained in Section 4.4.1.

3. The geosphere is modelled using analytical response functions, and all near-field barriers of the repository are modelled as well mixed volumes. The response function of the whole system is determined as a convolution of the near-field and geosphere response functions.

4. The geosphere is modelled using analytical response functions, and the early transient from the buffer into the fracture is included in the model (combining cases 2 and 3). Using an analytical response function for the geosphere means

that the geosphere is not represented by the exponential response function of the compartment model with a solute half-time and a delay time, but the exact analytical response function of the infinite rock matrix in Equation (4-42) is used. This also means that the geosphere cannot be part of the decay chain analogy of the barrier system (Equation (4-1)). The decay chain analogy is applied up to the geosphere and the response function of the whole system is determined by convoluting the analytical response function of the geosphere with the response function estimated for the rest of the barrier system using the decay chain analogy.

The behaviour of the barrier system was first analysed by looking its response function without radioactive decay (Section 5.1). The response functions of the whole system were studied only for the model alternative 4.

The actual migration of nuclides through the barrier system for realistic source terms and radioactive decay is reported for all model alternatives in Section 5.3. The nuclide dependent source terms used are specified in Section 5.2, and the release rates determined by the simplified model are compared there with the corresponding numerical results using the REPCOM and FTRANS codes.

5.1 Response function of the repository system for C-14, I-129 and Pu-239

Response functions of the repository system are determined for the two release paths: 1) canister – buffer – fracture and 2) canister – buffer –section of the tunnel above the deposition hole – fracture. The response functions are determined using the best performing model that applies the “branching decay chains in series” – representation of the repository system (cf. Section 4.1) with the exceptions that the early transient from the buffer into the fracture is included in the model and that the geosphere is represented by the analytical response function (model alternative 4 above).

The properties of each transport barrier are given in Tables 4-1 to 4-16. The performance of the transport barriers in the simplified approach, i.e. that of well mixed barriers, is completely characterised by the time constant of the barrier and the time delay between the starting of inflow and outflow releases in the barrier (Table 5-1). A section of the tunnel above the deposition hole is modelled as a mixing tank without diffusive delay time, because this is the approach that has also been applied in the reference analyses using the REPCOM model.

Table 5-1. *Characteristics of the transport barriers for the release paths 1) canister – buffer – fracture and 2) canister – buffer –section of the tunnel above the deposition hole– fracture.*

Parameter	Nuclide	Canister	Buffer to fracture	Buffer to tunnel	Tunnel section	Geosphere
$T_{1/2}$ [a]						
	C-14	530 000	23 000 [2] 156	1300	1600	12
	I-129	980 000	9000 [2] 740	5900	640	0.23
	Pu-239	[1] 530 000	$3.3 \cdot 10^8$ [2] $2.2 \cdot 10^6$	$1.8 \cdot 10^7$	$1.9 \cdot 10^7$	$3.2 \cdot 10^6$
Delay time [a]						
	C-14	0.0013	0.46 [2] 0.46	23	0	0.39
	I-129	0.0013	2.2 [2] 2.2	110	0	0.008
	Pu-239	0.0013	6600 [2] 6600	$3.4 \cdot 10^5$	0	$1.1 \cdot 10^5$

[1] No solubility limitation.
[2] The early transient part of the response function of the buffer with transient mass fractions of 0.0096 (C-14), 0.11 (I-129) and 0.0096 (Pu-239).

Response functions of different nuclides for the barrier system are shown in Figures 5-1, 5-2 and 5-3. These response functions represent only the influence of the barrier system on the release rates and therefore radioactive decay is not taken into account. It can be noted that for C-14 and I-129 the response functions of the whole system are dominated by the widest response function, the one from the canister to the buffer. Therefore, the release rates of C-14 and I-129 for the whole system could be well approximated by taking into account only the canister to the buffer transport barrier in the small hole case. The Pu-239 response is strongly affected by sorption in the buffer, and therefore the one million year period of time considered in the analysis is still dominated by the early transient behaviour of the system. The Pu-239 response functions indicate that, if the computation time would have been longer, then also in this case the widest response function of the individual barriers would have dominated the total response of the system (i.e., the buffer to fracture response function).

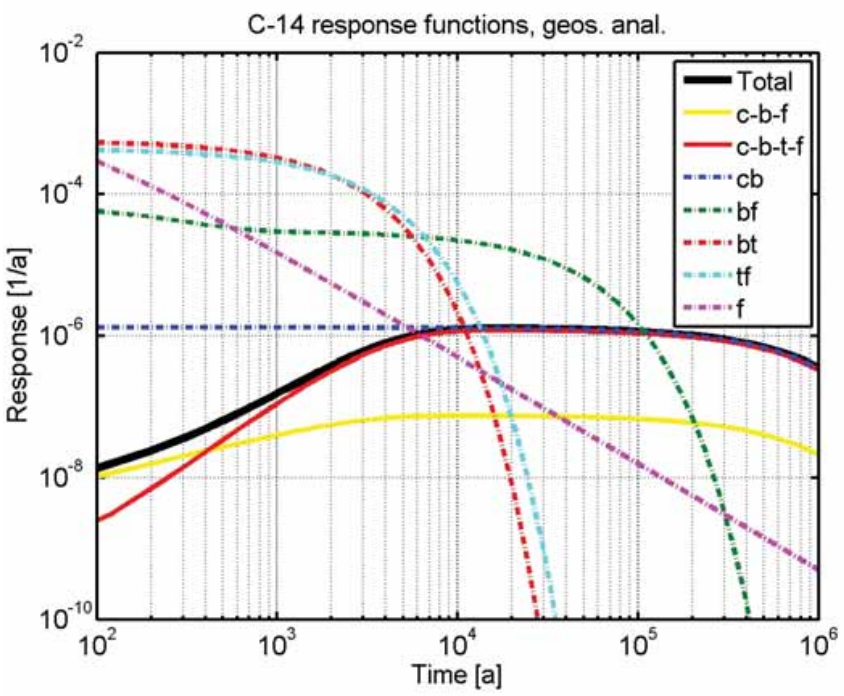

Figure 5-1. *C-14 response functions for individual barriers (cb: from canister to buffer, bf: from buffer to fracture, bt: from buffer to tunnel, tf: from tunnel section to fracture and f: geosphere), different pathways (c-b-f: pathway canister-buffer-fracture and c-b-t-f: pathway canister-buffer-tunnel section-fracture) and the total response function of the whole system (black line). The geosphere is represented by the analytical solution for the matrix diffusion model for infinite matrix.*

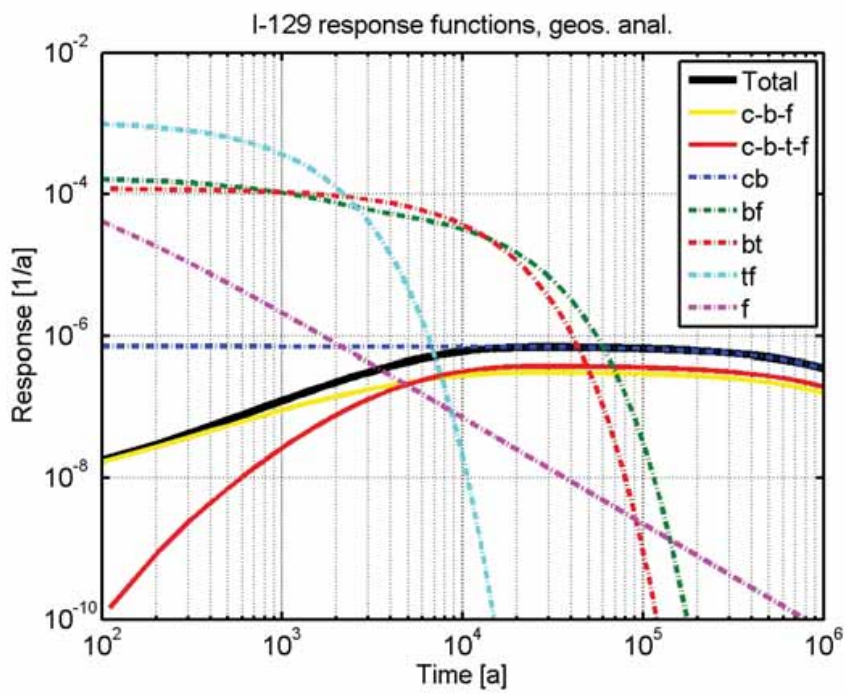

Figure 5-2. *I-129 response functions for individual barriers (cb: from canister to buffer, bf: from buffer to fracture, bt: from buffer to tunnel, tf: from tunnel section to fracture and f: geosphere), different pathways (c-b-f: pathway canister-buffer-fracture and c-b-t-f: pathway canister-buffer-tunnel section-fracture) and the total response function of the whole system (black line). The geosphere is represented by the analytical solution for the matrix diffusion model for infinite matrix.*

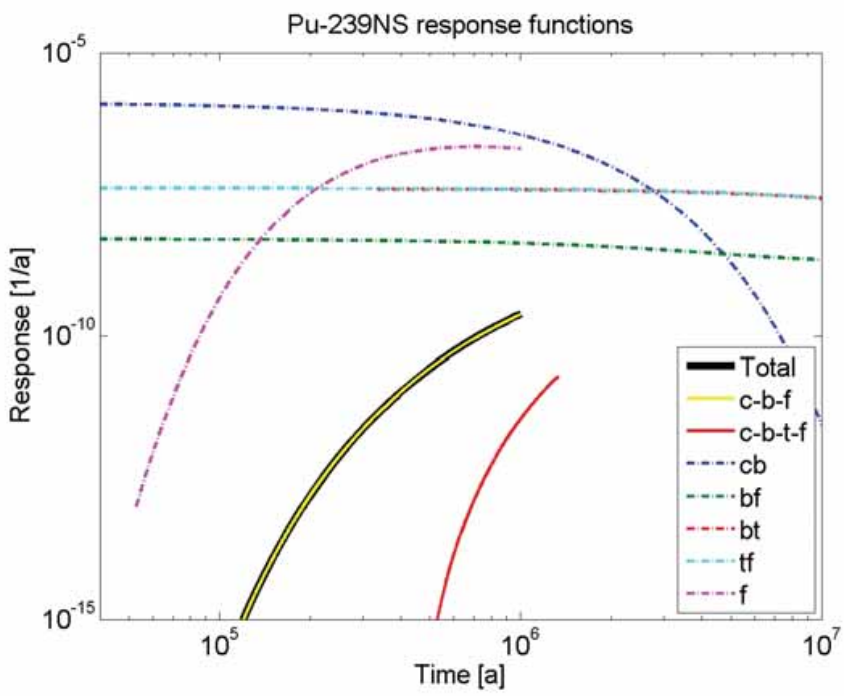

Figure 5-3. *Pu-239 response functions for individual barriers (cb: from canister to buffer, bf: from buffer to fracture, bt: from buffer to tunnel, tf: from tunnel section to fracture and f: geosphere) different pathways (c-b-f: pathway canister-buffer-fracture and c-b-t-f: pathway canister-buffer-tunnel section-fracture) and the total response function of the whole system (black line). The solubility limitation is not taken into account, because in the simplified approach it is a property of the canister source term. The geosphere is represented by the analytical solution for the matrix diffusion model for infinite matrix.*

5.2 Radionuclide sources

Three different source terms are available for the simulated radionuclides. In the case of C-14 and I-129 a portion of the radionuclide inventory is released instantly (the instant release fraction IRF). The whole inventory of Pu-239 and the remaining portions of the inventories of C-14 and I-129 are gradually leached according to the degradation rates of the fuel and other parts of the fuel assembly, and the release of Pu-239 is also limited by the solubility of plutonium in the groundwater intruding the canister.

The assumed leaching times for different parts of the fuel assembly are 10^6 years for the fuel matrix, 10,000 years for the metal parts of the assembly and 1,000 years for the cladding of the fuel rods. The leaching of the metal parts and cladding happens fast compared to the fuel matrix.

The solubility limited case of Pu-239 was determined by using Equation (4-26). Application of the equivalent flow rate given for Pu-239 in Table 4-1 (~0.9 mL/a), the initial inventory given in Table 5-2 below and a solubility limit of $1.1 \cdot 10^{-6}$ [mol/L] means that the solubility limited source for Pu-239 is active for about 484,000 a.

Table 5-2. *Source terms of three nuclides. Simulations have been done for 2.14 tons of uranium in a canister.*

Parameter	**C-14**	**I-129**	**Pu-239**
Initial inventory *)	27.8 GBq/tU	1.14 GBq/tU	10 500 GBq/tU
IRF portion	3.3 %	5 %	0 %
Gradual leaching	33 % during 1 000 a 33 % during 10 000 a 30 % during 10^6 a	95 % during 10^6 a	100 % during 10^6 a

*)Fuel type BWR Atrium 10x10-9Q bundle, no BA rods, enrichment 4.2 wt%, Void history 40 %, discharge burnup 40 MWd/kgU, cooling time 30 years (Anttila 2005)

5.3 Breakthrough curves to the biosphere

Nuclide dependent breakthrough curves for the instantly released portions of the inventories were determined by multiplying the response function by the instantly released fraction of the inventory (the IRF portions of the inventories for C-14 and I-129). For the rest of the inventories the source terms were defined as explained in the previous section. For C-14 and I-129 this meant gradual leaching from the fuel matrix. For Pu-239 this meant two alternative sources. One case was simulated to demonstrate transport of the sorbing nuclides in general. In that case there was no solubility limit for Pu-239, and the source term was determined by gradual leaching of the fuel matrix. In the second alternative the solubility limit of plutonium was taken into account, and the source term was limited by solubility. The nuclide dependent breakthrough curves were determined by convoluting the source term functions with the nuclide dependent response functions. Radioactive decay in the breakthrough curves was taken into account by multiplying the resulting breakthrough curve with an appropriate nuclide dependent exponentially decaying function.

Computed breakthrough curves are shown in Figures 5-4 to 5-7. In most cases there was good agreement between the breakthrough curves determined by REPCOM and the simplified model. Model results for the non-sorbing C-14 and I-129 were in practice identical with those of numerical simulations for all the alternative cases. It is evident that the early transients in different components of the system are not important for these nuclides.

Pu-239 provided a more complicated case because of the strong sorption and relatively short radioactive half-life. This was indicated in the modelling results so that in some cases the early transient dominated the release rates. The well mixed approximation of the geosphere response function strongly over-estimated the very early behaviour, which could be seen in the Pu-239 and Pu-239NS (the generic non-solubility-limited sorbing nuclide) release rates. The early transient mostly influenced highly sorbing

nuclides that had relatively short half-lives. Alternative models showed that transient effects can be compensated by introducing an early time contribution to the response function of the buffer and by applying a more precise response function in the geosphere. There was practically no release through the tunnel path of Pu-239, because the delay time from the buffer to the tunnel floor was very long ($3.4 \cdot 10^5$ a) compared to the radioactive half-life ($2.4 \cdot 10^4$ a) of Pu-239 (see also Figure 5-3).

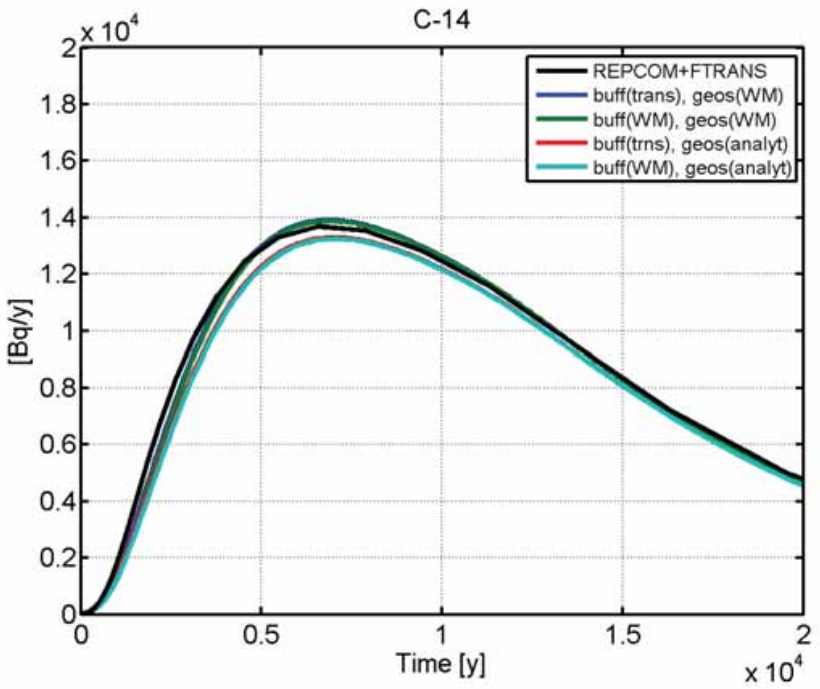

Figure 5-4. *C-14 release rates computed for different model alternatives. The notation buff(trans) indicates that the response function includes an early transient part, buff(WM) is determined by the well mixed buffer alone, geos(analyt) indicates that for the geosphere response function the analytical solution for matrix diffusion is used and geos(WM) denotes approximation of the geosphere response function by that of a well-mixed volume.*

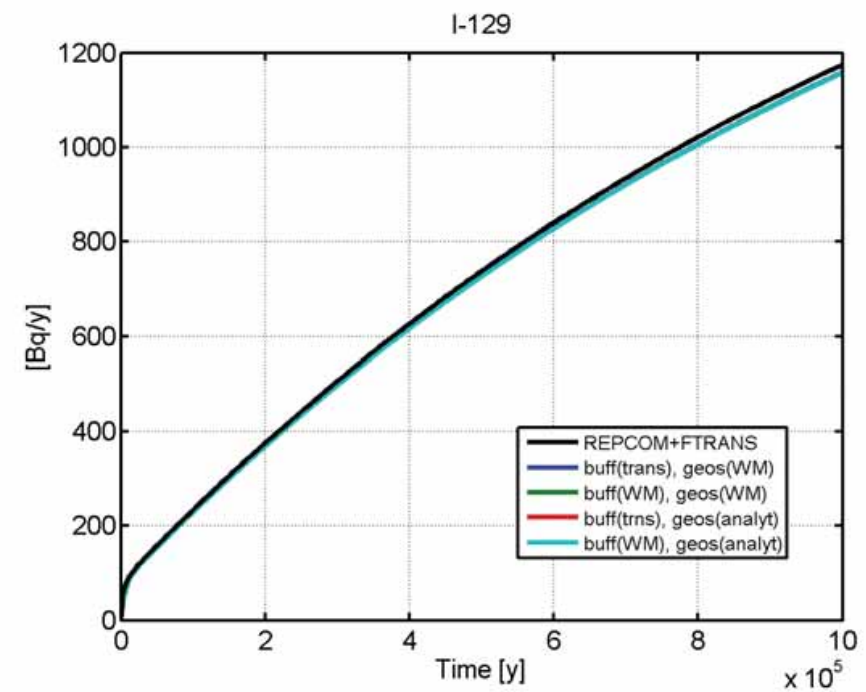

Figure 5-5. *I-129 release rates computed for different model alternatives. The notation buff(trans) indicates that the response function includes an early transient part, buff(WM) is determined by the well mixed buffer alone, geos(analyt) indicates that for the geosphere response function the analytical solution for matrix diffusion is used and geos(WM) denotes approximation of the geosphere response function by that of a well-mixed volume.*

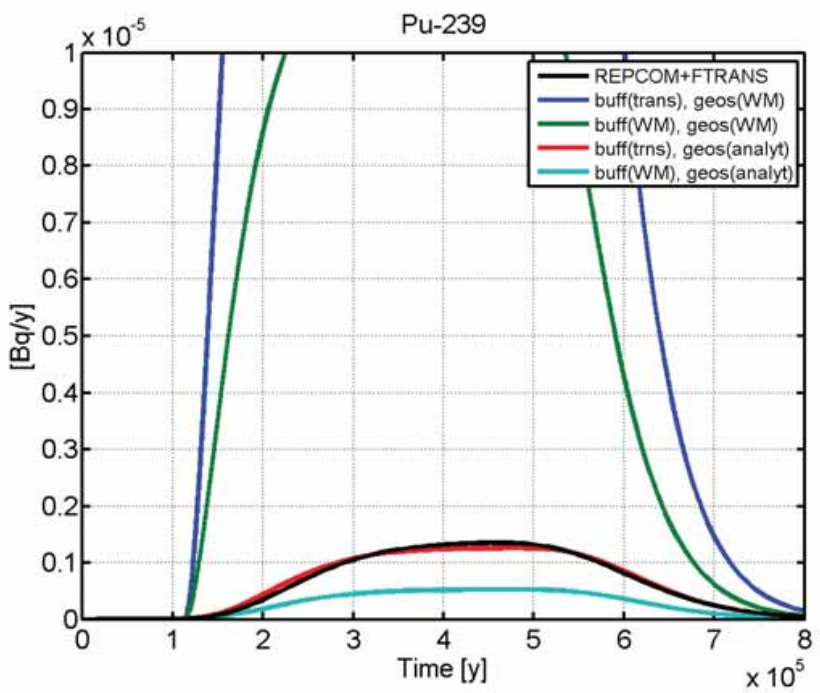

Figure 5-6. *Pu-239 release rates computed for different model alternatives. The notation buff(trans) indicates that the response function includes an early transient part, buff(WM) is determined by the well mixed buffer alone, geos(analyt) indicates that for the geosphere response function the analytical solution for matrix diffusion is used and geos(WM) denotes approximation of the geosphere response function by that of a well-mixed volume.*

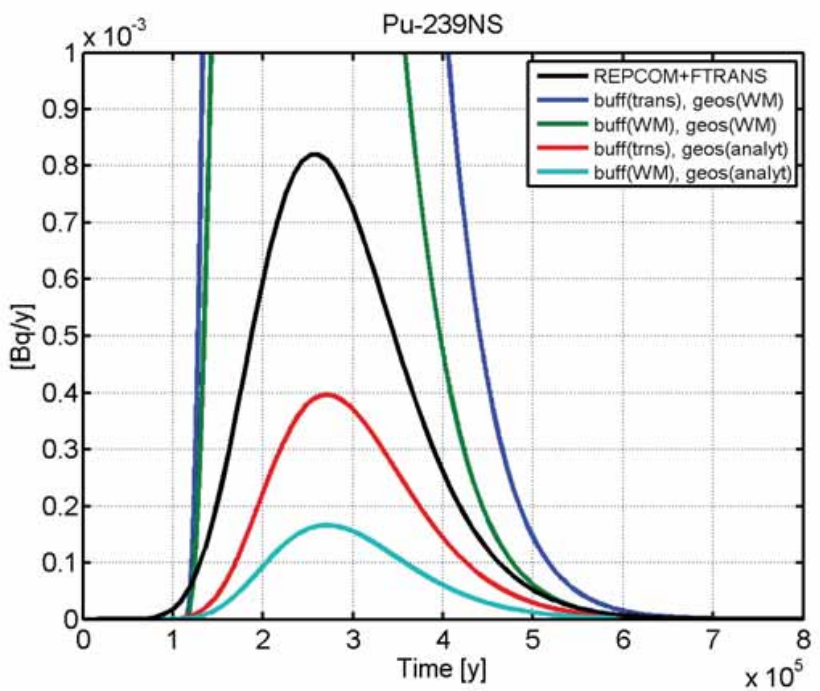

Figure 5-7. *Pu-239 release rates computed for different model alternatives. The notation buff(trans) indicates that the response function includes an early transient part, buff(WM) is determined by the well mixed buffer alone, geos(analyt) indicates that for the geosphere response function the analytically solution for matrix diffusion is used and geos(WM) denotes approximation of the geosphere response function by that of a well-mixed volume. The solubility limitation of Pu-239 is not taken into account.*

6 SUMMARY AND CONCLUSIONS

The repository system for the spent nuclear fuel is composed of multiple successive transport barriers. If a waste canister is leaking, this multi-barrier system retards and limits the release rates of radionuclides to the biosphere. Analysis of radionuclide migration in the previous performance assessments have largely been based on numerical modelling of the repository system. Importance of the different transport barriers to the performance of the whole repository system is then analysed by thorough numerical sensitivity analysis using numerical modelling of the whole system. This heavy machinery requires a large number of simulations and statistical handling of the modelling results, and the properties that lead to the observed behaviour of the system are not always clearly recognizable.

The simplified analytical approach introduced here provides a tool to analyse the performance of the whole system using simplified representations of the individual transport barriers. This approach is based on the main characteristics of the individual barriers and on the generic nature of the coupling between successive barriers.

In the case of the underground repository, mass transfer between successive transport barriers is strongly restricted by interfaces between these barriers, which leads to well-mixed conditions in them. The approach here simplifies the barrier system so that it becomes a very simple compartment model, where each barrier is represented by a single, or in the case of buffer by not more than two compartments. The compartment system could be solved by an analogy with a radioactive decay chain (see Section 4.1.2), because the feedback of any compartment to the previous one is weak. This model of well mixed compartments lends itself to a very descriptive way to represent and analyse the barrier system, because the relative efficiency of the different barriers in hindering solute transport can be parameterised by the solute's half-time in the corresponding compartments. It is also convenient to express the mass transfer between barriers by using an apparent volumetric flow rate called the equivalent flow rate (Section 4.1.1). The equivalent flow rate and pore volume of the barrier can be used to determine the decay constants of the solute, $\lambda = q/V$, for the barriers. The mass transfer coefficients and decay constants of the solute for different transport barriers of the underground repository are listed in Table 6-1.

Table 6-1. *Mass transfer coefficients for the inter-barrier transport.*

From To →	Canister	Buffer	Tunnel	Fracture
↓ **Buffer**	$q_{ch} = \frac{\pi r_h^2 D_w}{l_c}$ $q_{hm} = \frac{r_h r_u}{r_h + r_u} 2\pi D_{eb}$ $q_c = \frac{q_{ch} q_{hm}}{q_{ch} + q_{hm}}$ $\lambda_c = \frac{q_c}{V_c}$			
Tunnel		$q_{bt} = \frac{\pi r_{dh}^2 D_{eb}}{s_c}$ $\lambda_{bt} = \frac{q_{bt}}{R_{pb} \varepsilon_b V_b}$		
Fracture		$q_{bf} = 2\pi r_{dh} 2b_v \sqrt{\frac{4 D_w v_{dh}}{\pi^2 r_{dh}}}$ $\lambda_{bf} = \frac{q_{bf}}{R_{pb} \varepsilon_b V_b}$	$q_{tf} = p_t 2b_v \sqrt{\frac{4 D_w v_t}{\pi p_t / 2}}$ $\lambda_{tf} = \frac{q_{tf}}{R_{pt} \varepsilon_t V_t}$	
Biosphere				$u = \sqrt{\varepsilon_m R_{pm} D_{em}} WL / Q$ $\lambda_f = \frac{1}{4.3 u^2}$

The notations used in Table 6-1 are the following.

For the canister	
q_{ch}	the equivalent flow rate through the hole
q_{hm}	the equivalent flow rate on the bentonite side of the hole
q_c	the equivalent flow rate through the hole and bentonite side of the hole
r_h	the radius of the hole
r_u	the outer radius of the hole in the side fo the buffer
D_w	the molecular diffusion coefficient in free water
D_{eb}	the effective molecular diffusion coefficient in the buffer
l_c	the thickness of the canister wall
V_c	the volume of the canister
λ_c	the decay constant of the solute for the mass transfer from canister to buffer

For the buffer
q_{bf} equivalent flow rate from buffer to fracture
q_{bt} equivalent flow rate from buffer to tunnel
r_{dh} radius of the deposition hole
$2b_v$ volume aperture of the fracture
D_w molecular diffusion coefficient in free water
v_{dh} flow velocity of groundwater in the fracture
ε_b porosity of the buffer
V_b volume of the buffer
R_{pb} retardation coefficient in the buffer
λ_{bf} decay constant of the solute in mass transfer from buffer to fracture
λ_{bt} decay constant of the solute in mass transfer from buffer to tunnel
For the tunnel
q_{tf} equivalent flow rate from tunnel to fracture
p_t length of the intersection of the fracture and the tunnel wall
$2b_v$ volume aperture of the fracture
D_w molecular diffusion coefficient in free water
v_t flow velocity of groundwater in the fracture
R_{pt} retardation coefficient in the tunnel backfill
λ_{tf} decay constant of the solute in the mass transfer from tunnel to fracture
ε_t porosity of the tunnel backfill
V_t volume of the tunnel section
For the fracture
u transport resistance through the flow path
ε_m porosity of the rock matrix
R_{pm} retardation coefficient in the rock matrix
D_{em} effective diffusion coefficient in the rock matrix
WL/Q hydrodynamic control of retention (see Section 4.6.1)
λ_f decay constant of the solute in mass transfer along the flow path

In a real repository system there will be a delay between the start of the inflow and the start of the outflow from the barrier. In most of the cases this delay is caused by diffusion of the solute from the inflow location to the outflow location in the barrier. It can be important for the release rates of the short lived and sorbing radionuclides, and it was also included in the simplified representation of the barrier system.

The delay caused by a barrier was treated as a translation in time of the barrier's response function. Response function of the whole system was a convolution of the individual response functions of the barriers, which means that the delay caused by the

whole system was a sum of the delay times of the individual barriers. This means that it was possible to determine the response function of the whole system without any delay and then to translate the response function in time by the total delay caused by the barriers. The practical benefit of separating the actual response function, i.e. estimation of the solute's half-times in different barriers and the respective delays is that it makes the uncertainty analysis of the repository system more transparent. It also underlines the fundamental difference between the solute's delay time and half-time in a barrier. Half-time characterises how the barrier attenuates the release rate and disperses the pulse in time. Delay is just translation in time, which means that its effect on the release rate will depend on the half-life of the nuclide. In this report the delay times were selected based on quite early breakthrough times in order to avoid an excessive overestimation of them (Table 6-2).

Table 6-2. *Estimated delay times in the transport barriers.*

From To	→ Canister	Buffer	Tunnel	Fracture
↓ Buffer	$t_{dc} \approx l_c^{\,2} 0.033 / D_w$			
Tunnel		$t_{dbt} \approx R_{pb}\, l_b^{\,2} 0.033 / D_{pb}$		
Fracture		$t_{dbf} \approx R_{pb}\, s_c^{\,2} 0.033 / D_{pb}$	$t_{dtf} \approx R_{pt}\, s_{tf}^{\,2} 0.033 / D_{pt}$	
Biosphere				$t_{df} = 0.1 u^2$

Notations are the same as before or as given in the following.

t_{dc} the estimated delay in the canister
t_{dbf} the estimated delay in the buffer in transport to the fracture
t_{dbt} the estimated delay in the buffer in transport to the tunnel
t_{dtf} the estimated delay in the tunnel
t_{df} the estimated delay along the flow path (no advective delay is taken into account)
l_b the thickness of the buffer
s_c the distance from the canister to the floor of the tunnel
s_{tf} the diffusion distance along the tunnel section to the fracture intersecting the tunnel
D_{pb} the pore diffusion coefficient in the buffer
D_{pt} the pore diffusion coefficient in the tunnel backfil

Mass transfer between successive components of the release path was represented to a large extent by linear processes. In this case the release rate from an individual barrier could also be determined by convoluting the inflow pulse with the response function of the barrier. The total response of the system could be derived as a successive convolution of the response functions of all barriers. This already is an important characteristics of the system. The additive nature of variance under the convolution operation leads easily to a situation in which one of the convoluted functions dominates the result of the total convolution. This indicates that spreading of the outflowing

release pulse is often governed by the typical behaviour of one transport barrier, especially in a geological multi-barrier system where the reservoir capacities of and mass transfer coefficients between adjacent barriers may differ significantly. For example, the response function of I-129 is dominated by the response function of the canister as indicated in Figure 6-1 below, where the canister response (curve denoted by "cb") closely coincides with that of the whole system (curve denoted by "Total").

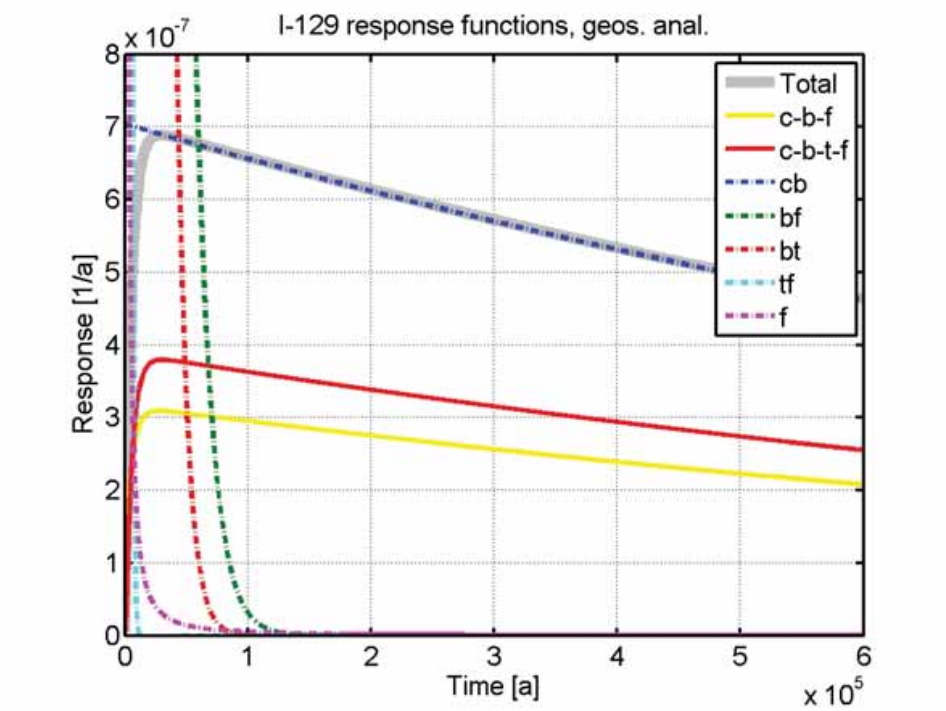

Figure 6-1. *I-129 response functions for individual barriers (cb: from canister to buffer, bf: from buffer to fracture, bt: from buffer to tunnel, tf: from tunnel section to fracture and f: geosphere), for different pathways (c-b-f: pathway canister-buffer-fracture and c-b-t-f: pathway canister-buffer-tunnel section-fracture). The total response function of the whole system is shown with the thicker gray line. The geosphere's response function is represented by the analytical solution for matrix diffusion model for infinite matrix (plotted in log-log scale in Figure 5-2).*

Characterisation of the repository system by the simplified approach is straightforward. Mass transfer between successive barriers can be defined by the equivalent flow rates (see Section 4.1.1) between these barriers, and the solute's half times in different barriers can be estimated by coupling the equivalent flow rates with the capacities (pore volumes) of the barriers. Characterisation of the repository system by the solute's half times is a compact, transparent and helpful way to represent the barrier system when selecting potentially safety-relevant radionuclides and analysing different scenarios. Although radioactive decay chains were not considered in this work, the achieved characterisation of the repository system for individual nuclides will also help to estimate their properties in the case of decay chains.

The release rates of radionuclides from a leaking waste canister may also be dominated by their source terms, instead of the repository barrier system. The spent nuclear fuel is a ceramic material that dissolves slowly when in touch with groundwater. The actual release rate from the system is a convolution of the response function of the system with the source function. The release rate of the radionuclide is thus determined by a series of convolutions between the different response functions of the transport barriers followed by convolution with the source term of the radionuclide. This means waste dissolution can also be treated as a barrier, in which the waste's dissolution time (or half of it) corresponds to the solute's half time in barrier. Solute's degradation time has been a million years in the verification simulations. This indicates that dissolution is a significant barrier, especially for non-sorbing nuclides that do not have a considerable fraction of instant release (IRF).

Some of the elements in spent nuclear fuel have quite limited solubility in water. This means that the source term is not determined by the dissolution rate, but the solubility limit. The possibility for the appearance of solubility limitation can tested by comparing the release rates from a canister based on the solubility limitation and the fuel dissolution rate. In this work it was conservatively assumed that solubility limit determines the release rate if it gives a smaller release rate than the fuel dissolution rate in the beginning of the simulation. For example, in the case of Pu-239, the solubility limit is about 10^{-6} mol/L and the equivalent flow rate for a hole in the canister is about 10^{-3} L/a. This gives a release rate that is about 550 Bq/a. The inventory of Pu-239 is about $2 \cdot 10^{13}$ Bq per canister, so the 10^{-6} 1/a degradation rate produces Pu-239 at a rate of $2 \cdot 10^{7}$ Bq/a into the water inside the canister. Solubility limitation will clearly hinder the release of Pu-239.

The validity of the simplified description was tested against numerical transport simulations for three representative nuclides: C-14, I-129 and Pu-239. The results of these simulations showed reasonable agreement with those of the simplified approach. For non-sorbing tracers, C-14 and I-129, the simplified description and numerical models produced essentially identical result. Strongly sorbing Pu-239 was a more challenging case in this respect. It has a short radioactive half-life compared to the relevant solute's half-times in the barriers, but slightly longer radioactive half-life than the estimated delay through the buffer to the fracture. This emphasised the importance of early transients in the pathway from the buffer to the fracture. However, also in this case the simplified approach was able to identify that the buffer is the most important transport barrier. In addition, a quite straightforward approximation of the transient behaviour was able to improve the results of analysis and to give reasonable agreement between the simplified approach and the performed numerical simulations. Delay time was not important for the release rates of C-14 and I-129, but for Pu-239 already the delay time indicated that the pathway from the buffer to the tunnel cannot lead to a high release rate (Table 5-1 and Figure 5-3).

The solute's half-times in different barriers (Table 5-1) can be compared with the radioactive half-lives of the nuclides. Already the first barrier along the release path in which the solute's half-time is longer than the nuclide's radioactive half-life will be an efficient transport barrier for that nuclide, although the barrier with longest solute half-time will be the most efficient barrier.

REFERENCES

Anttila M., 2005. Radioactive Characteristics of the Spent Nuclear Fuel of the Finnish Nuclear Power Plants. Posiva Oy, Olkiluoto, Finland. Posiva Working Report 2005-71.

Carslaw, H. S. and Jaeger, J. C., 1959. Conduction of Heat in Solids. Oxford University Press, Oxford, 2nd edition, 1959.

COMSOL, 2009. COMSOL Multiphysics webpage. URL http://www.comsol.com

Cvetkovic V., Selroos J.-O. and Cheng H., 1999. Transport of reactive tracers in rock fractures. J. Fluid Mech., 378, 335-356.

Gelhar, L. W., 1987. Applications of stochastic models to solute transport in fractured rocks. Swedish Nuclear Fuel and Waste Management Co. (SKB). Technical Report 87-05. Stockholm

Hellä, P. (ed.), Ikonen, A., Mattila, J., Torvela, T. and Wikström, L., 2009. RSC-Programme - Interim Report. Approach and Basis for RSC Development, Layout Determining Features and Preliminary Criteria for Tunnel and Deposition Hole Scale. Posiva Oy. Posiva Working Report 2009-29.

Kekäläinen, P., Voutilainen, M., Poteri, A., Hölttä, P., Hautojärvi, A. and Timonen, J., 2011. Solutions to and Validation of Matrix-Diffusion Models. Transport in porous media (2011) 87:125-149.

Neretnieks, I., 1980. Diffusion in the Rock Matrix: An Imporant Factor in Radionuclide Retardation. Journal of Geophysical Research, Vol. 85, No. B8, pp. 4379-4397.

Neretnieks, I., 1982. Leach rates of high level waste and spent fuel – Limiting rates as determined by backfill and bedrock conditions. New York, Elsevier Science Publishing Company Inc., Scientific Basis for Nuclear Waste Management V. pp. 557-568.

Neretnieks, I., Liu, L. and Moreno, L., 2010. Mass transfer between waste canister and water seeping in rock fractures. Revisiting the Q-equivalent model. Swedish nuclear fuel and waste management Co, Technical Report 91-48. Technical Report TR-10-42.

Nilsson, L., Moreno, L., Neretnieks, I. and Romero, L., 1991. A resistance network model for radionuclide transport into the near field surrounding a repository for nuclear waste (SKB, Near Field Model 91). Swedish nuclear fuel and waste management Co, Technical Report 91-30.

Nordman H. & Vieno T., 1994. Near-field model REPCOM. Nuclear Waste Commission of Finnish Power Companies (YJT), Helsinki, Finland. Report YJT-94-2.

Papoulis, A. and Pillai, S.U., 2002. Probability, random variables, and stochastic processes. McGraw-Hill Higher Education, 2002. ISBN 0-07-366011-6.

Posiva, 2008. Olkiluoto Site Description 2008, Part 1. Posiva Oy. Report Posiva 2009-01.

Poteri, A. and Vieno, T., 1989. Probabilistic system assessment code SYVAC/FI for safety analysis of nuclear waste disposal. Technical Research Centre of Finland, Research Notes 1018. (In Finnish).

Romero, L., Moreno, L. and Neretnieks, I., 1991. A compartment model for solute transport in the near field of a repository for radioactive waste (Calculations for Pu-239) Swedish nuclear fuel and waste management Co, Technical Report 91-48.

Smith, P., Johnson, L., Snellman, M., Pastina, B. and Gribi, P., 2007. Safety Assessment for a KBS-3H Spent Nuclear Fuel Repository at Olkiluoto, Evolution Report. Posiva Oy. Report Posiva 2007-08.

Transactions of the American Nuclear Society, Vol. 54(1987), pp. 106-107.

Vieno, T. and Nordman, H., 1999. Safety assessment of spent fuel disposal in Hästholmen, Kivetty, Olkiluoto and Romuvaara, TILA-99. Report Posiva 99-07.

Weisstein, E. W., 2003. Lambert's W-function, CRC Concise Encyclopedia of Mathematics, CRC Press (2003) pp. 1684–1685. (also in Weisstein, E. W. "Lambert W-Function." From MathWorld — A Wolfram Web Resource. http://mathworld.wolfram.com/LambertW-Function.html)

APPENDIX A: ANALYTICAL SOLUTION OF THE DECAY CHAIN MODEL

The solute concentrations in the canister, buffer and the section of the tunnel above the deposition hole ("tunnel section") can be described by the following group of coupled equations,

$$\begin{aligned}
&\frac{d\,m_c}{dt} + \lambda_c m_c = \delta_0 \\
&\frac{d\,m_b}{dt} + (\lambda_{bf} + \lambda_{bt}) m_b = \lambda_c m_c * \delta_{t_{dc}} \\
&\frac{d\,m_t}{dt} + \lambda_{tf} m_t = \lambda_{bt} m_b * \delta_{t_{dbt}} \\
&\frac{d\,m_f}{dt} + \lambda_f m_f = \lambda_{tf} m_t * \delta_{t_{dtf}} + \lambda_{bf} m_b * \delta_{t_{dbf}} \quad ,
\end{aligned} \tag{A-1}$$

where * means convolution, $\delta_\tau = \delta(t-\tau)$, with $\delta(x)$ the Dirac delta function, $\delta_{t_{dc}}$ is the delay time in canister, $\delta_{t_{dbt}}$ the delay time from buffer to tunnel, $\delta_{t_{dbf}}$ the delay time from buffer to fracture and $\delta_{t_{dtf}}$ the delay time from tunnel to fracture. Other notations in Equation (A-1) are for the solute's decay constants: λ_c from canister to buffer, λ_{bf} from buffer to fracture, λ_{bt} from buffer to tunnel and λ_{tf} from tunnel to fracture. The initial conditions are $m_c(0)=0$, $m_b(0)=0$, $m_t(0)=0$ and $m_f(0)=0$.

Solution to the mass out flow of the solute from the barrier system, $m_{out} = \lambda_f m_f * \delta_{t_{df}}$, was determined form Equations (A-1), and we found that

$$\begin{aligned}
m_{out} &= \lambda_f m_f * \delta_{t_{df}} \\
&= \lambda_f (G_f * (\lambda_{tf} m_t * \delta_{t_{dtf}} + \lambda_{bf} m_b * \delta_{t_{dbf}})) * \delta_{t_{df}} \\
&= \lambda_f (G_f * (\lambda_{tf} (G_t * \lambda_{bt} m_b * \delta_{t_{dbt}}) * \delta_{t_{dtf}} \\
&\qquad + \lambda_{bf} (G_b * \lambda_c m_c * \delta_{t_{dc}}) * \delta_{t_{dbf}})) * \delta_{t_{df}} \\
&= \lambda_f (G_f * (\lambda_{tf} (G_t * \lambda_{bt} (G_b * \lambda_c G_c * \delta_{t_{dc}}) * \delta_{t_{dbt}}) * \delta_{t_{dtf}} \\
&\qquad + \lambda_{bf} (G_b * \lambda_c G_c * \delta_{t_{dc}}) * \delta_{t_{dbf}})) * \delta_{t_{df}} \\
&= \lambda_f \lambda_{tf} \lambda_{bt} \lambda_c\, G_f * G_t * G_b * G_c * \delta_{t_{dc}} * \delta_{t_{dbt}} * \delta_{t_{dtf}} * \delta_{t_{df}} \\
&\qquad + \lambda_f \lambda_{bf} \lambda_c\, G_f * G_b * G_c * \delta_{t_{dc}} * \delta_{t_{dbf}} * \delta_{t_{df}} \quad .
\end{aligned} \tag{A-2}$$

The Green's function G of the operator L, which appears in this solution, was determined from the

$$L G_i = \frac{d\,G_i}{dt} + \lambda_i G_i = \delta(t) \quad , \tag{A-3}$$

with the result that

$$G_i = \mathrm{H}(t)\,\mathrm{Exp}(-\lambda_i t) \quad , \tag{A-4}$$

where **H**(t) is the Heaviside unit step function. Using the result Equation (A-4) in the solution of Equation (A-2), we find that

$$\begin{aligned} m_{out} = {} & \mathrm{H}(t-t_{d1})\lambda_c\lambda_{bt}\lambda_{tf}\lambda_f\left(\frac{\mathrm{Exp}\left[-(t-t_{d1})\lambda_c\right]}{(\lambda_{bt}-\lambda_c)(\lambda_{tf}-\lambda_c)(\lambda_f-\lambda_c)}\right. \\ & + \frac{\mathrm{Exp}\left[-(t-t_{d1})\lambda_{bt}\right]}{(\lambda_c-\lambda_{bt})(\lambda_{tf}-\lambda_{bt})(\lambda_f-\lambda_{bt})} + \frac{\mathrm{Exp}\left[-(t-t_{d1})\lambda_{tf}\right]}{(\lambda_c-\lambda_{tf})(\lambda_{bt}-\lambda_{tf})(\lambda_f-\lambda_{tf})} \\ & \left. + \frac{\mathrm{Exp}\left[-(t-t_{d1})\lambda_f\right]}{(\lambda_c-\lambda_f)(\lambda_{bt}-\lambda_f)(\lambda_{tf}-\lambda_f)}\right) \\ & + \mathrm{H}(t-t_{d2})\lambda_c\lambda_{bf}\lambda_f\left(\frac{\mathrm{Exp}\left[-(t-t_{d2})\lambda_c\right]}{(\lambda_{bf}-\lambda_c)(\lambda_f-\lambda_c)}\right. \\ & \left. + \frac{\mathrm{Exp}\left[-(t-t_{d2})\lambda_{bf}\right]}{(\lambda_c-\lambda_{bf})(\lambda_f-\lambda_{bf})} + \frac{\mathrm{Exp}\left[-(t-t_{d2})\lambda_f\right]}{(\lambda_c-\lambda_f)(\lambda_{bf}-\lambda_f)}\right) \end{aligned} \quad , \tag{A-5}$$

where the delay times for the two branches of the release path are given by

$$\begin{aligned} t_{d1} &= t_{dc} + t_{dbt} + t_{dtf} + t_{df} \\ t_{d2} &= t_{dc} + t_{dbf} + t_{df} \end{aligned} \quad . \tag{A-6}$$

LIST OF REPORTS

POSIVA-REPORTS 2012

POSIVA 2012-01	Monitoring at Olkiluoto – a Programme for the Period Before Repository Operation Posiva Oy ISBN 978-951-652-182-7
POSIVA 2012-02	Microstructure, Porosity and Mineralogy Around Fractures in Olkiluoto Bedrock *Jukka Kuva (ed.), Markko Myllys, Jussi Timonen*, University of Jyväskylä *Maarit Kelokaski, Marja Siitari-Kauppi, Jussi Ikonen,* University of Helsinki *Antero Lindberg,* Geological Survey of Finland *Ismo Aaltonen,* Posiva Oy ISBN 978-951-652-183-4
POSIVA 2012-03	Design Basis Report, DB-2012 ISBN 978-951-652-184-1
POSIVA 2012-04	Performance Assessment Report, PA-2012 ISBN 978-951-652-185-8
POSIVA 2012-05	Description of the Disposal System Report, DDS-2012 ISBN 978-951-652-186-5
POSIVA 2012-06	Biosphere Description Report, BSD-2012 ISBN 978-951-652-187-2
POSIVA 2012-07	Features, Events and Processes Report, FEP-2012 ISBN 978-951-652-188-9
POSIVA 2012-08	Formulation of Radionuclide Release Scenarios, FoS-2012 ISBN 978-951-652-189-6
POSIVA 2012-09	Assessment of Radionuclide Release Scenarios, RNT-2012 ISBN 978-951-652-190-2
POSIVA 2012-10	Biosphere Assessment Report, BSA-2012 ISBN 978-951-652-191-9
POSIVA 2012-11	Complementary Considerations Report, CC-2012 ISBN 978-951-652-192-6
POSIVA 2012-12	Synthesis Report ISBN 978-951-652-193-3

POSIVA 2012-13	Canister Design 2012 *Heikki Raiko* ISBN 978-951-652-194-0
POSIVA 2012-14	Buffer Design 2012 *Markku Juvankoski* ISBN 978-951-652-195-7
POSIVA 2012-15	Backfill Design 2012 ISBN 978-951-652-196-4
POSIVA 2012-16	Canister Production Line 2012 – Design, Production and Initial State of the Canister ISBN 978-951-652-197-1
POSIVA 2012-17	Buffer Production Line 2012 – Design, Production, and Initial State of the Buffer ISBN 978-951-652-198-8
POSIVA 2012-18	Backfill Production Line 2012 - Design, Production and Initial State of the Deposition Tunnel Backfill and Plug ISBN 978-951-652-199-5
POSIVA 2012-19	Closure Production Line 2012 - Design, Production and Initial State of Closure ISBN 978-951-652-200-8
POSIVA 2012-20	Representing Solute Transport Through the Multi-Barrier Disposal System by Simplified Concepts *Antti Poteri, Henrik Nordman, Veli-Matti Pulkkanen,* VTT *Aimo Hautojärvi,* Posiva Oy *Pekka Kekäläinen,* University of Jyväskylä, Department of Physics ISBN 978-951-652-201-5

PUBLICATION II

Retention properties of flow paths in fractured rock

In: Hydrogeology Journal 17(5), pp. 1081–1092.

doi: 10.1007/s10040-008-0414-y

Retention properties of flow paths in fractured rock

Antti Poteri

Abstract There is no straightforward way to extrapolate solute retention properties from typical site characterisation scales to typical scales in the performance assessment of the geological disposal of nuclear wastes. Solutes diffuse much deeper into the rock matrix under performance assessment flow conditions than under site characterisation flow conditions. The modelling approach applied in this study, associated with the Äspö Task Force, enables evaluation of the contribution of the individual immobile layers to the overall retention. This makes it possible to determine the influence of the immobile zone heterogeneity on solute retention under different flow conditions. It appears that there is a significant difference between the dominating immobile retention zones on site characterisation and performance assessment scales. Fractured rock is characterised by heterogeneity and in particular a large spread of hydraulic properties. This favours formation of the preferential flow paths by leading to a few dominating transport paths. Large hydraulic features are, on average, better hydraulic conductors than smaller ones. This causes spatial scale effects for the solute retention properties. In particular, the hydraulic properties at the early parts of flow paths are more favourable to retention than those at the later parts of the flow paths.

Keywords Fractured rocks · Solute transport · Äspö Task Force · Sweden

Introduction

The main characteristic of fractured rock is the great heterogeneity on all scales. In particular, this applies to the hydraulic properties. In practice, groundwater flow takes place only through the fractures. The rock mass between fractures is porous and saturated by water but it is not usually a conduit for groundwater flow. However, the immobile pore space in the rock matrix is important for solute transport and retention due to matrix diffusion (Neretnieks 1980).

The heterogeneous structure of fractured rock has significant effects on the groundwater flow and solute transport and retention processes. It affects the groundwater flow by favouring preferential flow paths that will govern not only the flow but also transport and retention characteristics. Observations from in situ experiments in fractured rock indicate that solute transport cannot be described accurately without considering distinct flow paths. Tracer experiments usually show fast initial arrival times, more than one peak in the breakthrough curves, and/or long tails and strong dependence on scale (Becker and Shapiro 2000; Nordqvist et al. 1996; Tsang et al. 1991). Modelling has shown that the preferential flow and transport paths run over long distances and reduce mixing, especially in the case of high transmissivity variance (Nordqvist et al. 1996).

Groundwater flow and solute transport in fractured rock has been studied at the Äspö Hard Rock Laboratory, Sweden, in the context of the geological disposal of nuclear waste. In spite of the intensive work on in situ tracer experiments there are untested properties that are important for the performance assessment of a nuclear waste repository. Many tests typically involve injection and pumping rates that are considerably higher than flow rates occurring under natural conditions, and the spatial scales of the tests are much smaller than should be applied in performance assessment. In practice, this cannot be avoided because tracers can only be recovered at the pumping borehole in in situ experiments if the experimental flow field is stronger than the background flow field. For the same reason, tracer tests need to be carried out in well conducting hydraulic structures and over short distances. In contrast, for performance assessment the overall retention of radionuclides is mainly dominated by the low transmissive fractures and transport paths are hundreds of meters long.

The present paper is based on the experiences of the Posiva-VTT (Posiva Oy - Technical Research Centre of Finland) modelling team participating in the Äspö Task Force on Modelling of Groundwater Flow and Transport of Solutes. Task 6 of the Äspö Task Force aimed to

Received: 17 September 2007 / Accepted: 24 November 2008

ASPO

A. Poteri (✉)
Technical Research Centre of Finland,
VTT,
P.O. Box 1000, 02044 VTT, Espoo, Finland
e-mail: antti.poteri@vtt.fi
Tel.: +358-20-7225059
Fax: +358-20-7226390

Hydrogeology Journal
Published online: 17 January 2009
DOI 10.1007/s10040-008-0414-y

provide a bridge between the site characterisation (SC) and performance assessment (PA) models and studied the significance of simplifications made in the performance assessment models (Hodgkinson et al. 2008). Task 6 was divided into a number of sub-tasks that concentrated on specific aspects of the transport through fractured rock. Gustafson et al. (2008) summarises the tasks involved.

This paper concentrates on the retention properties along transport paths and on the influence of heterogeneity of the retention properties under SC and PA flow conditions. The bases of the work are the simulations of Tasks 6D, 6E, 6F and 6F2 of the Äspö Task Force (Poteri 2006).

Transport model

Mathematical model

The solute transport model takes into account advection along the transport path, matrix diffusion and sorption in the immobile pore space. The model also takes into account heterogeneity of the immobile pore space. Immobile pore space is composed of layers describing, for example, fracture coating, fault gouge, altered rock and intact host rock. Surface sorption on the fracture walls is not included in the calculations because diffusion and sorption within the pore space of the fracture coating is modelled directly.

Transport paths are determined using particle tracking. In the transport modelling they are treated as independent one-dimensional conduits. Studied system of mobile and immobile pore space is illustrated in Fig. 1. Solute transport through a transport path is described by the advection-matrix diffusion equation

$$\begin{aligned} &\frac{\partial c_f}{\partial t} + v\frac{\partial c_f}{\partial x} - 2\frac{D_e}{2b}\frac{\partial c_m}{\partial z}\bigg|_{z=0} = 0 \\ &R_p\frac{\partial c_m}{\partial t} - D_p\frac{\partial^2 c_m}{\partial z^2} = 0 \end{aligned}, \qquad (1)$$

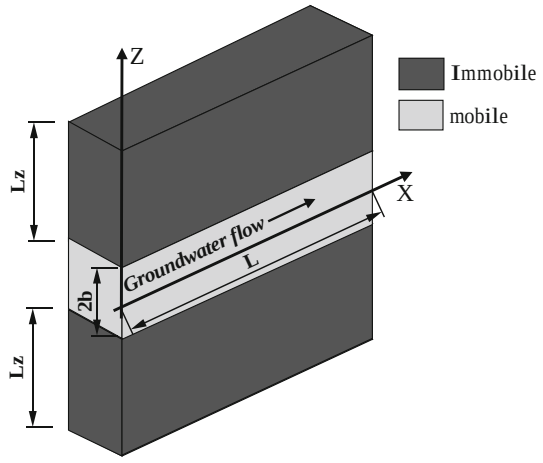

Fig. 1 Flow along a fracture that is surrounded by immobile pore space in the rock matrix

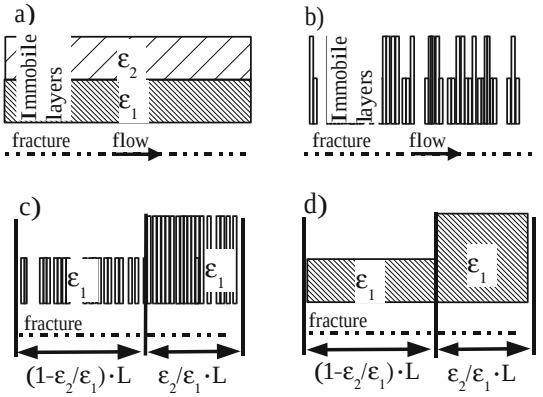

Fig. 2 Transport path along a fracture that is in contact with a heterogeneous immobile pore space. Immobile pore space is composed of two layers that have different porosities—$\varepsilon_2 < \varepsilon_1$ (**a**). Connected immobile porosity is represented by one-dimensional pipes (**b**). The pipes are rearranged to form two successive legs of flow path that both have one layer of immobile pore space (**c**–**d**)

where v is the flow velocity, $2b$ is the fracture aperture, R_p is the retardation coefficient in the immobile pore space, D_p is the pore diffusivity in the immobile pore space and D_e is the effective diffusion coefficient from fracture to immobile pore space. Solute concentrations in the pore water of the immobile pore space, c_m (x, z, t), and in the fracture, c_f (x, t), are coupled by the requirement that at the fracture wall c_m (x, 0, t) = c_f (x, t). The initial concentration is zero both in the immobile pore space and in the fracture.

At the end of the paper (see Appendix), it is shown that retention depends on three grouped parameters: $\beta = x/(v\,b)$ that describes the flow field, $\gamma = \varepsilon\sqrt{D_p R_p}$ that characterises the immobile zone and $t_d = L\sqrt{R_p/D_p}$ that parameterises the "diffusion time" through the immobile layer. This suggests that the solution for the case of several immobile layers can be constructed from an equivalent system of successive flow paths that are all composed of a single homogeneous immobile zone. However, it appears that this is not possible in a general case, but the approach is a good approximation for the situation that usually prevails in the fractured rock.

The case of layered immobile zones is modelled in the following way. The connected pores in the immobile layers can be conceptualised as pipes starting from the fracture but having different lengths. The local density of the individual pores gives the porosity of the immobile layers. Solute transport and retention along the flow path does not depend on the order of the immobile pores along the path. This means that the pores can be arranged by the length of the pore without changing the transport and retention properties. Figure 2 illustrates an example of two immobile zones. It can be noted that this approach can be applied only if $\varepsilon_2 < \varepsilon_1$. However, this is usually the case in fractured rock where the alteration of the host rock increases the porosity close to the fracture surface.

DOI 10.1007/s10040-008-0414-y

This approach can be extended to cases where, in addition to the porosity, diffusivity and sorption properties vary between the layers. According to Eq. (6), the solute transport depends on grouped parameters: $\beta = x/(v\,b)$, $\gamma = \varepsilon\sqrt{D_p R_p}$ and $t_d = L\sqrt{R_p/D_p}$. This means that it is possible to express differences in the grouped immobile retention property γ as corresponding differences in the porosity (ε) only and apply the same value for other parameters in all layers. In the case of two immobile layers, this means that porosity to be assigned for the second layer can be calculated from the grouped parameter γ of the second layer by requiring that D_p and R_p are the same as in the first layer, i.e. $\gamma_2 = \varepsilon_2\sqrt{D_{p2}R_{p2}} = \varepsilon_2'\sqrt{D_{p1}R_{p1}}$, where the numbers in subscripts refer to the immobile layer. If D_p and R_p of the second layer are changed then the "diffusion time" t_d of the second layer will also change. This can be compensated by making a corresponding change to the thickness of the second layer $L_2' = L_2\sqrt{D_{p1}/R_{p1}}\Big/\sqrt{D_{p2}/R_{p2}}$. It is noted that the requirement of $\varepsilon_2 < \varepsilon_1$ in Fig. 2 indicates in the more general case that $\gamma_2 < \gamma_1$.

It is straightforward to take the next step to a system that contains several immobile layers such that $\gamma_m < \gamma_n$ if the layer m is further from the fracture than the layer n (Fig. 3). The transport path is divided into as many legs as there are immobile layers. Starting from the layer that has the smallest γ (the layer that is furthest from the fracture) and using the argument above it can be seen that the location of leg m along the flow path is $(\gamma_{m-1}/\gamma_1, \gamma_m/\gamma_1)\cdot L$ and that the thickness of the immobile layer needs to be scaled to $L_m' = L_m\sqrt{D_{p1}/R_{p1}}\Big/\sqrt{D_{pm}/R_{pm}}$. This is illustrated for three layers in Fig. 3.

Advection and matrix diffusion equations can be solved in Laplace space for several layers of immobile pore space (e.g. Crawford and Moreno 2006). There is a slight difference between the approach applied in the present study, which assumes immobile pores as one-dimensional "pipes" of different lengths, and approaches that are based on the averaged pore structure allowing mixing between individual pores. It is also noted that geometry of the immobile pore space in the geological material is mostly unknown. It may be composed of micro-fractures that can be conceptualised as independent

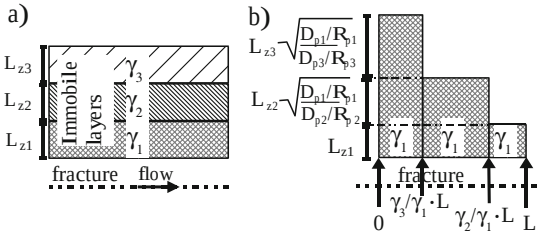

Fig. 3 A transport path with layered immobile pore space ($\gamma_1 > \gamma_2 > \gamma_3$) along the path (**a**) is divided into an equivalent system of successive transport paths that have homogeneous immobile pore space (**b**)

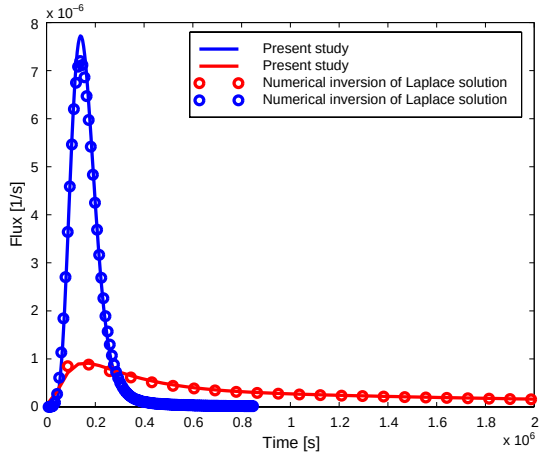

Fig. 4 Breakthrough curves calculated using approach of the present study (*solid lines*) and numerical inversion of the Laplace solution (*empty circles*) given by Crawford and Moreno (2006)

pipes as it has been done in the present study. However, in most of the cases, difference between the present approach and other approaches is insignificant. Comparison of the breakthrough curves using the approach of the present study and numerical inversion of the Laplace solution given by Crawford and Moreno (2006) shows quite good agreement between these two approaches (Fig. 4). Two cases are calculated for a non-sorbing tracer using a system of two immobile layers. The first layer is characterised by porosity 0.01 and effective diffusivity 10^{-11} m^2/s and the second layer is an infinite layer of porosity 0.001 and effective diffusivity 10^{-13} m^2/s. The two cases are calculated by varying thickness of the first layer from 5 mm to 5 cm.

An important property of the solution approach used in the present study is that it allows a straightforward way to determine contribution of the different immobile layers to the overall retention. This can be used to evaluate the importance of different heterogeneities under SC and PA flow conditions. This approach also enables the application of the efficient solutions of the homogeneous systems to heterogeneous systems.

Numerical implementation

Solute transport is calculated using an analytical model. Transport through a flow path is calculated by applying a one-dimensional lattice walk where the exchange of the solute particles between the mobile and immobile pore spaces and sorption are described by the waiting time distribution at the lattice points (Cvetkovic and Haggerty 2002). Cvetkovic and Haggerty (2002) calculate the waiting time distribution in the Laplace-transferred domain. Simulations in the present model are based on the calculations of the waiting time distributions of the diffusional solute particle exchange between the mobile and immobile pore space.

DOI 10.1007/s10040-008-0414-y

Modelling strategy

This paper focuses on the transport and retention properties of the fractured rock under SC and PA flow conditions. Task 6 of the Äspö Task Force offers a good platform for this study. The objectives of Task 6 are to: assess simplifications used in PA models; assess the constraining power of tracer (and flow) experiments for PA models; provide input for site characterisation programs from a PA perspective; and understand the site-specific flow and transport behaviour at different scales using SC models (Hodgkinson D (2007)). Most of the above objectives are addressed by modelling both the SC and PA aspects of the problem.

Task 6 is composed of several stages aiming at gradually increasing the reality and complexity of the flow system. Especially interesting for the scope of this paper are subtasks that address the heterogeneous structure of the immobile zones and fracture network (Tasks 6D, 6E, 6F and 6F2). These subtasks are modelled by applying a semi-synthetic hydrostructural model that gives a complete definition of the fracture network and immobile zones in the modelling domain. The semi-synthetic hydrostructural model is presented in the following section.

Task 6 is performed by modelling tracer transport in the semi-synthetic hydrostructural model both for the SC and PA flow conditions. The present study focuses on the retention properties and influence of the immobile zone heterogeneity on retention under different flow conditions.

In addition to the fracture network simulations, a simplified model of a complex hydraulic zone is examined. This helps to focus on specific features of the transport and retention processes. The simplified flow path model is presented in section Simplified model of a complex flow path.

Semi-synthetic hydrostructural model

Dershowitz et al. (2003) have developed a semi-synthetic hydrostructural model through a combination of deterministic and stochastic analyses of hydraulically significant structural features. The model contains 11 deterministic structures, 25 synthetic 100-m-scale structures and 5,660 synthetic background fractures in a 200×200×200 m volume of rock. At each scale, structures are described with regards to their geometric, hydraulic, and transport properties. Figure 5 shows the deterministic and stochastic fractures of the semi-synthetic hydrostructural model.

The structure of the immobile pore space next to the water conducting fractures is also specified in the semi-synthetic model. This microstructural model of the immobile zones is provided for the fractures at each scale. The fractures are attributed to two basic geological structure types: "fault" (type 1) and "non-fault" (type 2). The basic description and visualisation of the two types and their characteristic components (including intact unaltered wall rock, altered zone, cataclasite, fault gouge and fracture coating) are provided in Figs. 6 and 7. Transport parameters (porosity, formation factor and K_d) are assigned to the two structure types as shown in Table 1.

The semi-synthetic hydrostructural model is considered as the ultimate truth of the water conducting fractures in the modelled domain. It gives the exact locations, orientations and transmissivities of all fractures as well as the exact structure of the immobile pore space and sorption properties for the different types of groundwater.

Simplified model of a complex flow path

Large fracture zones are usually complex hydraulic features that are composed of several fractures. This means that the hydraulic structure of the zone is composed

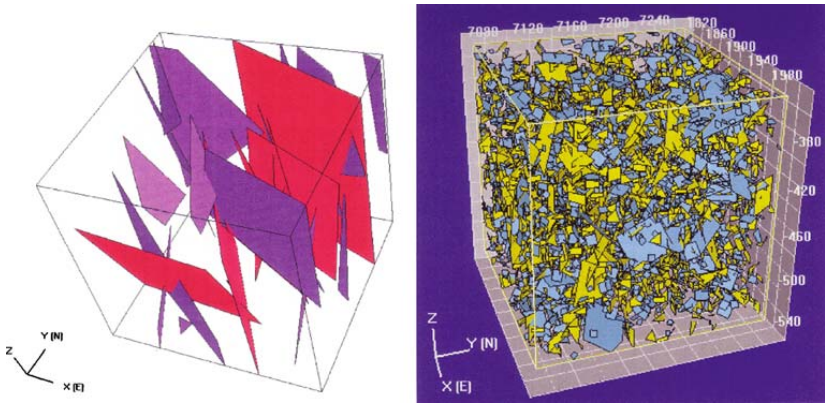

Fig. 5 Fractures of the semi-synthetic hydrostructural model. The 100-m-scale structures are on the *left* (synthetic is *mauve* and deterministic is *red*). Background fractures are on the *right*, coloured by set. The sub-horizontal fracture set is *blue* and the NNW striking fracture set is *yellow*. Coordinates *X*, *Y* and *Z* are presented in meters in the local Äspö coordinate system (from Dershowitz et al. 2003)

DOI 10.1007/s10040-008-0414-y

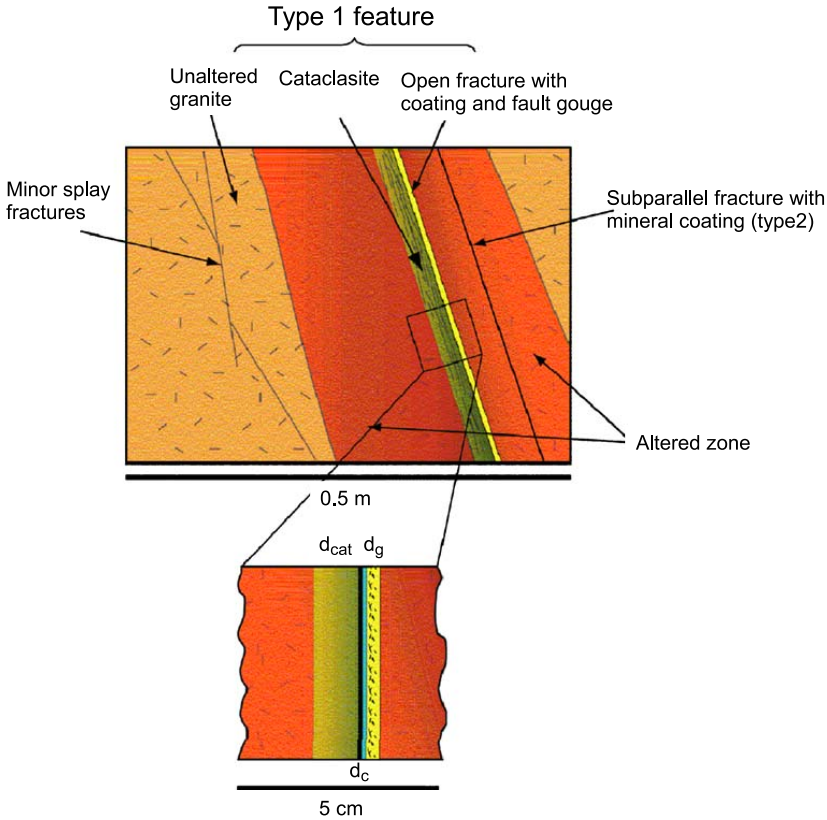

Fig. 6 Microstructural model of the type 1 fracture as defined in the semi-synthetic model (from Dershowitz et al. 2003)

of sub-parallel flow paths. Figure 8 illustrates a complex feature and a few transport paths through it. Fractures in the zone may have different retention characteristics. In the context of Task 6 this means the heterogeneous structure can be composed of both Type 1 and Type 2 fractures.Retention properties are studied by simplifying the complex system to a building block of the zone. The simplified system is composed of two fractures that are of different fracture type. The studied system of two parallel flow paths is illustrated in Fig. 9.

Preferential transport paths

Flow paths

Transport paths and retention properties along the paths are studied by a simulated tracer test for the SC flow conditions and by applying a low regional hydraulic gradient over the simulation region for the PA flow conditions. This section gives a short description of the simulated flow paths. The tracer test is modelled by simulating pumping of the borehole in one of the deterministic structures and releasing tracers in the injection borehole in the other deterministic structure at about 20 m distance from the pumping location. Flow paths are determined by particle tracking for 1,000 particles in the simulated flow field. Less than 10 fractures are active along the flow paths in the simulation and the water residence times from the injection to the pumping borehole vary from 110 to 180 h. Figure 10 shows the flow paths and fractures that are active in the simulation of the SC tracer test.

Transport under PA conditions is simulated using the same semi-synthetic fracture network, but applying a hydraulic gradient of about 0.5% over the modelled region. Tracers are released in the middle of the model along a 3-m-long line source in the same deterministic fracture as in the simulated SC tracer experiment. The simulated flow paths are determined by particle tracking for 100 particles that are spread over the source line. About 40 different fractures are visited by the flow paths and the water residence times along the paths vary from about 10 to about 140 years. Figure 11 shows the flow paths and some of the major fractures that are active for the transport in the PA flow field simulations.

SC and PA simulations show that only a small number of fractures are active in both cases, with more active fractures in the PA simulation. However, the transport

DOI 10.1007/s10040-008-0414-y

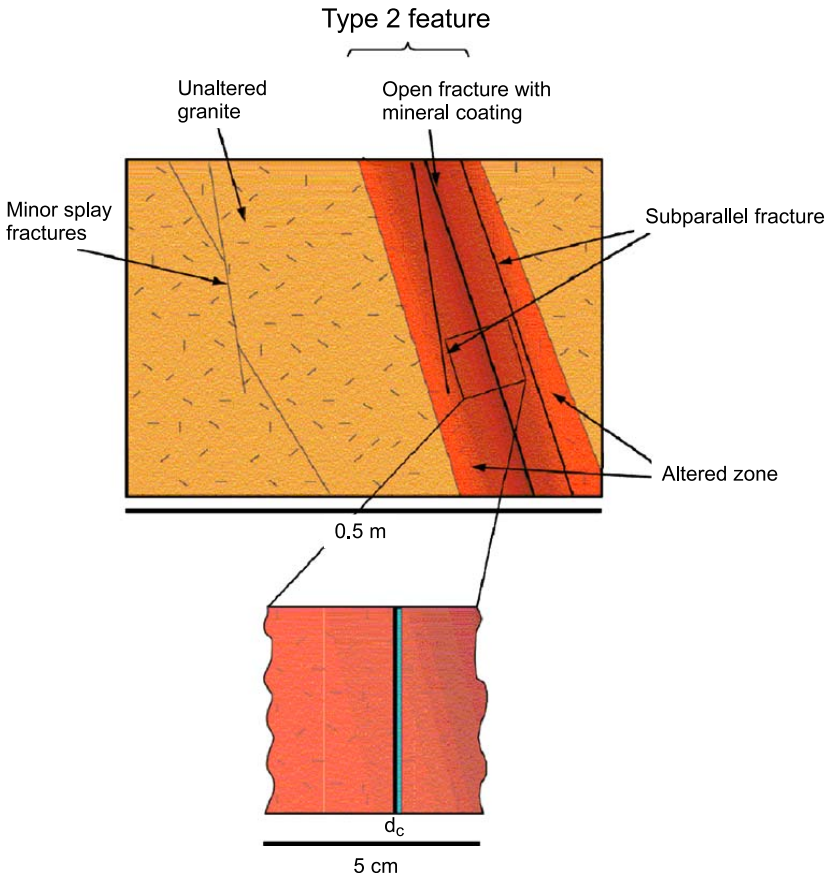

Fig. 7 Microstructural model of the type 2 fracture as defined in the semi-synthetic model (from Dershowitz et al. 2003)

distance in the PA simulations is much larger than in the SC tracer test simulation. The distance between the source and sink is about 20 m in the SC simulation and about 130 m in the PA simulations. Path lengths are correspondingly 60–70 m in the SC simulations and 250–300 m in the PA simulations. This indicates that once the transport has taken place along large fractures, then the smaller background fractures are not easily reactivated. It can also be noted that, in both simulations, a few preferential flow paths carry the main part of the flow.

Table 1 Geometric and transport parameters of the type 1 and type 2 fractures (from Dershowitz et al. 2003)

Rock type	Extent (cm)	Porosity %)	Formation factor (-)
Type 1 (fault)			
Intact wall rock	–	0.3	7.3e–5
Altered zone	20	0.6	2.2e–4
Cataclasite d_{cat}	2	1	4.9e–4
Fault gouge d_g	0.5	20	5.6e–2
Fracture coating d_c	0.05	5	6.2e–3
Type 2 (joint)			
Intact wall rock	–	0.3	7.3e–5
Altered zone	10	0.6	2.2e–4
Fracture coating	0.05	5	6.2e–3

Hydrodynamic control of retention

The focus of this study is on the retention properties along the flow paths. Retention properties are determined by the hydrodynamic control of retention, β (Eq. 6; Cvetkovic et al. 1999). This retention property is calculated as a part of

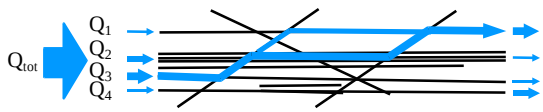

Fig. 8 The complex hydraulic structure is composed of several fractures. *Black lines* indicate fractures; *blue lines* are examples of the possible flow paths. The sizes of the *blue arrows* exemplify varying flow rates (from Poteri 2006)

DOI 10.1007/s10040-008-0414-y

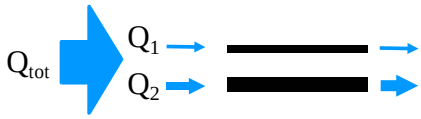

Fig. 9 The studied building block of the complex structure is a system of two parallel fractures (from Poteri 2006)

the particle tracking simulations by applying the following equation:

$$\beta = \sum_i \frac{2L_i}{q_i}, \qquad (2)$$

where the sum i is made over all the finite element model (FEM) elements of the numerical flow solution that the particle visits and $\beta_i = 2L_i/q_i$ is the contribution of the element i to the total β. Here, L_i is the length of the particle path over the element i and q_i is the two-dimensional Darcy velocity in the element i (i.e. Q/W, flow rate per fracture width).

Figure 12 shows the accumulation of the β along the flow routes in the case of the SC simulations. The solid lines show the cumulative β-factor as a function of the length of the flow path. Visited structures are indicated in the figure by coloured circles at the background of the solid lines. For example, from the slopes of the curves it can be concluded that there is a large β_i in structures 22D, 758C and 2403C (i.e. low flow rates).

Figure 13 shows the accumulation of β along the flow routes in the case of PA simulations. Generally the behaviour in the PA flow conditions is similar to that in the SC flow conditions. For a large part of the flow paths, β does not increase much after the first few tens of meters

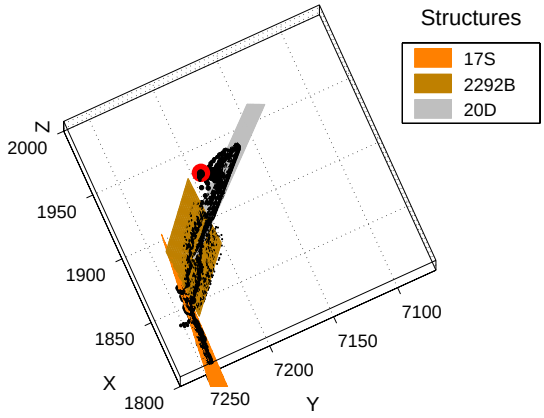

Fig. 11 Simulation results for the PA flow field simulations. Flow paths are shown by *black discs*. The sizes of the discs indicate the number of particles in the particle tracking, i.e. they are proportional to the flow rate. The source is marked by a *red disc* and some of the major hydraulic structures that connect the flow paths to the western boundary of the modelling region are indicated in the figure. Coordinates X, Y and Z are presented in meters in the local Äspö coordinate system (from Poteri 2006)

of the flow path. On the other hand, the spread between flow paths increases considerably after the first 50–100 m. The size scale of this behaviour is connected to the size of the hydraulic structures or fractures. The flat regions at the end of the flow paths indicate persistence of the flow paths to remain in the well conducting structures once the flow paths have entered large well conducting hydraulic structures. In a very few cases flow paths visit low conducting fractures between larger hydraulic structures. This can be seen as an almost vertical variation in the cumulative β.

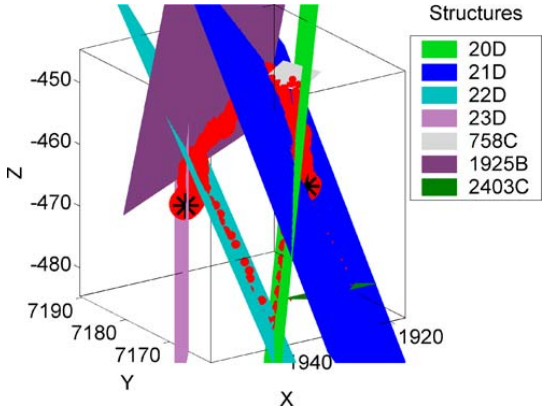

Fig. 10 Simulation results for the SC flow field simulations. Flow paths are indicated by *red discs*. The sizes of the discs are proportional to the number of the particles that follow the route. The legend indicates hydraulic structures that are visited by the flow paths. Source and sink are plotted by *black asterisks*. Coordinates X, Y and Z are presented in meters in the local Äspö coordinate system (from Poteri 2006)

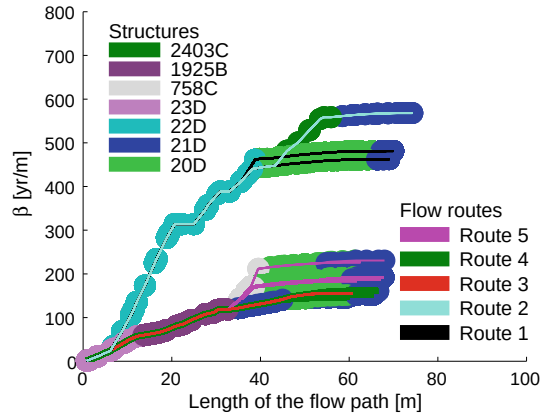

Fig. 12 Hydrodynamic control of retention (β) plotted as a function of the path length for the SC simulations. *Solid lines* show β and the *coloured discs* in the background indicate the visited structures. The major flow path (path number 4, *solid green line*) is plotted thicker than the others (from Poteri 2006)

DOI 10.1007/s10040-008-0414-y

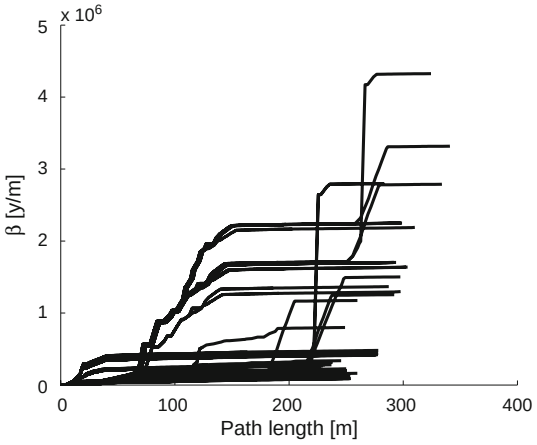

Fig. 13 Hydrodynamic control of the retention (β) plotted as a function of the path length for the PA simulations (from Poteri 2006)

It seems that the structure of the fractured rock has an important influence on the solute retention properties. Fractured rock is heterogeneous at all scales. In the semi-synthetic fracture network this is taken into account by the different size classes of the hydraulic features. In practice, this leads to a structure where a few fractures dominate flow and transport properties at each spatial scale. This is reflected in the hydrodynamic control of retention where the early part of the flow path tends to dominate the total β because later the flow paths accumulate in the large regional structures.

Simplified system of parallel transport paths

Preferential transport paths in the heterogeneous system are also studied using a very simple system that contains only two parallel fractures that have different structures of immobile zones in the rock matrix. Immobile zones of the fractures follow definition of the two fracture types presented in the section Semi-synthetic hydrostructural model. Focus of the analysis is on the retention properties of the heterogeneous system. Advective delay or other transport characteristics are not taken into account in the analysis. It is assumed that well-mixed conditions prevail at the inlet and outlet of the transport path. The flow properties are described by the hydrodynamic control of retention, β, and solute retention is studied from the superimposed tracer breakthrough curves of the two-fracture system. Conceptually, the system considered in this analysis is presented in Fig. 9.

The total flow rate going through the system of two fractures is kept fixed for all simulations. The total flow rate is divided between the fractures using the following divisions: all to one fracture, 8:1, 4:1, 2:1 and 1:1. The data used in the different calculation cases and the corresponding β's of the fractures are shown in Table 2.

Table 2 Calculation cases defined for the simplified two-fracture system

Case	β_1 [yr/m]	β_2 [yr/m]	Transport channel: width 0.1 m and length 20 m		Total flow rate
			$Q1$ [l/yr]	$Q2$ [l/yr	Q_{tot} [l/yr])
1	7,752	7,752	0.52	0.52	1.03
2	5,814	11,628	0.69	0.34	1.03
3	4,845	19,380	0.83	0.21	1.03
4	4,360	34,884	0.92	0.11	1.03
5	3,876		1.03		1.03
6	11,628	5,814	0.34	0.69	1.03
7	19,380	4,845	0.21	0.83	1.03
8	34,884	4,360	0.11	0.92	1.03
9		3,876		1.03	1.03

β_1 means F-factor to fracture 1 and β_2 means F-factor to fracture 2

Breakthrough curves are calculated for three different tracers: I-129 (iodine-129), Cs-137 (caesium-137) and Am-240 (americium-240). Figures 14, 15, 16 show the simulated breakthrough curves for the retention due to matrix diffusion and sorption. Note that advective delay is not included in the breakthrough curves because the analysis is focused on retention properties.

The results indicate that retention and the corresponding attenuation of the tracer discharge peak levels are very sensitive to the flow rate. The assumption of well mixed conditions at the inlet of the two-fracture system means that the tracer masses through the path are proportional to the flow rate. However, the inequality of the tracer mass going through the fractures cannot explain the results. Retention and attenuation of the release rates due to matrix diffusion have a significant influence on the results.

Examination of the I-129 breakthrough curves (Fig. 14) demonstrates that contribution of both the flow paths can be observed in the breakthrough curves only if the flow rate is almost evenly divided between the two flow paths.

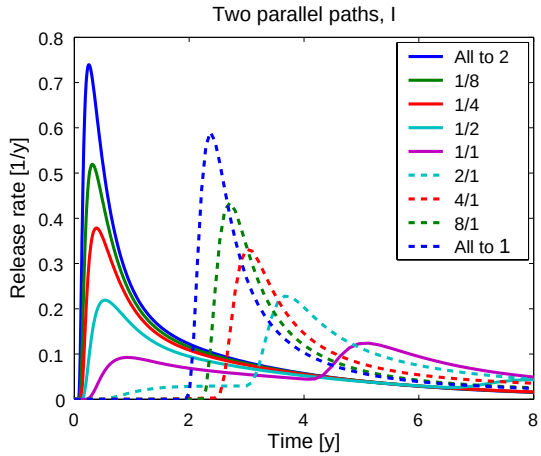

Fig. 14 Breakthrough curves for I-129 through the system of two parallel fractures. The *numbers in the legend* indicate division of the total flow rate between the type 1 and type 2 fracture ($Q1/Q2$) (from Poteri 2006)

DOI 10.1007/s10040-008-0414-y

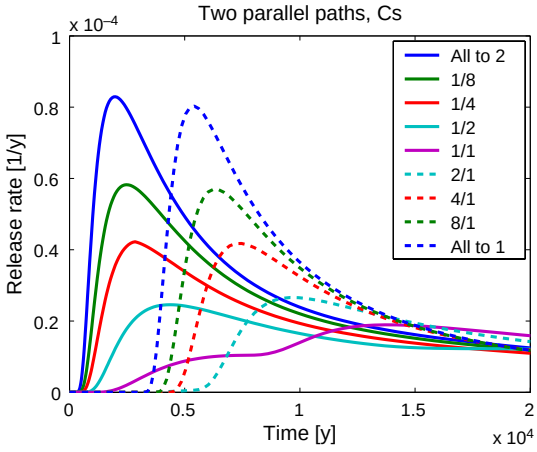

Fig. 15 Breakthrough curves for Cs-129 through the system of two parallel fractures. The *numbers in the legend* indicate division of the total flow rate between the type 1 and type 2 fracture ($Q1/Q2$) (from Poteri 2006)

Already an inequality of a factor of two in the flow rates means that one of the flow paths dominates the retention properties. This behaviour seems to be stronger for the sorbing tracers (Figs. 15 and 16). The reason is that in this analysis the additional delays provided by the small volumes of the porous immobile zones close to the fracture are not as significant for the overall retardation of the strongly sorbing tracers as they are for the non-sorbing tracers.

Influence of heterogeneity

SC and PA scale fracture network simulations of groundwater flow and flow paths have been presented in section Flow paths. Solute transport and retention along the flow paths have also been simulated using the approach presented in section Mathematical model The approach used for the solute transport calculations is especially suitable for studying the influence of the immobile zone heterogeneity on the retention because it provides a means to separate contributions of the different immobile zones from the overall retention. In the present paper, breakthrough curves are studied for a non-sorbing tracer (iodine) and a strongly sorbing tracer (americium).

Influence of the heterogeneity on solute retention is studied by focusing on the contribution of the individual immobile zones to the overall retention in typical SC and PA flow conditions. Tracer breakthrough curves and contributions of the individual immobile layers are shown in Fig. 17. The only difference between differently sorbing tracers appears to be scaling of the time axis and discharge rates. In contrast to sorption, flow conditions have a significant impact on the characteristics of the tracer transport. This can be observed when the contribution of the individual immobile zones to the overall breakthrough curves is examined. Typical to the PA flow condition is that contributions of the limited volume immobile pore spaces are narrow pulses. This indicates that those immobile pore spaces are fully saturated by the tracer and that the tracer concentration in those pore spaces is in equilibrium with the tracer concentration in the fracture. A consequence of this is that the characteristics of the breakthrough curve in PA conditions are determined by the very thick layer of unaltered rock. The limited volume immobile pore spaces that are saturated by the tracer cause only additional delay to the breakthrough curve. In the SC conditions kinetic behavior can be observed also in the contributions of the limited volume immobile pore spaces.

Simulation results can be interpreted so that the heterogeneity of the immobile zones has different impacts on the solute retention depending on the flow conditions. Under SC flow conditions, the high porosity immobile layers can be important components of the overall retention. For example, SC flow field simulations in Fig. 17 show that about half of the total retention time is caused by the fracture coating. This means that in order to predict or model SC scale retention properties one should be able to characterise immobile layers along the transport paths in a very detailed scale. On the other hand, under PA flow conditions retention properties are averaged over a much larger volume of the immobile layers. Heterogeneities caused by thin layers of high porosity immobile zones close to the fracture may not be important for the overall retention under PA flow conditions, although they may provide some additional delay to the solute transport. The fact that retention properties of the immobile zones are averaged over much larger volumes in the PA flow conditions than in the SC flow conditions facilitates PA scale transport analysis, but makes it impossible to validate the PA scale retention properties using SC scale tracer experiments.

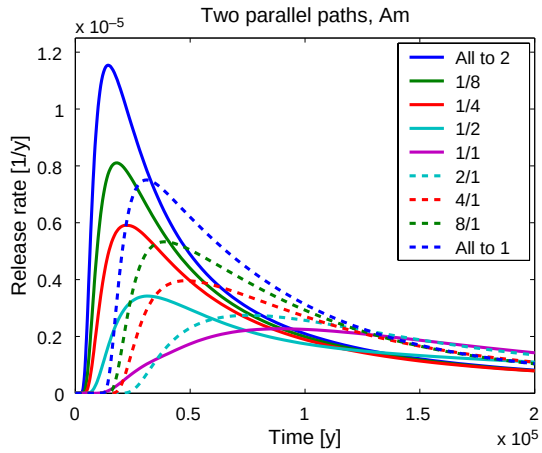

Fig. 16 Breakthrough curves for Am-240 through the system of two parallel fractures. The *numbers in the legend* indicate division of the total flow rate between the type 1 and type 2 fracture ($Q1/Q2$) (from Poteri 2006)

DOI 10.1007/s10040-008-0414-y

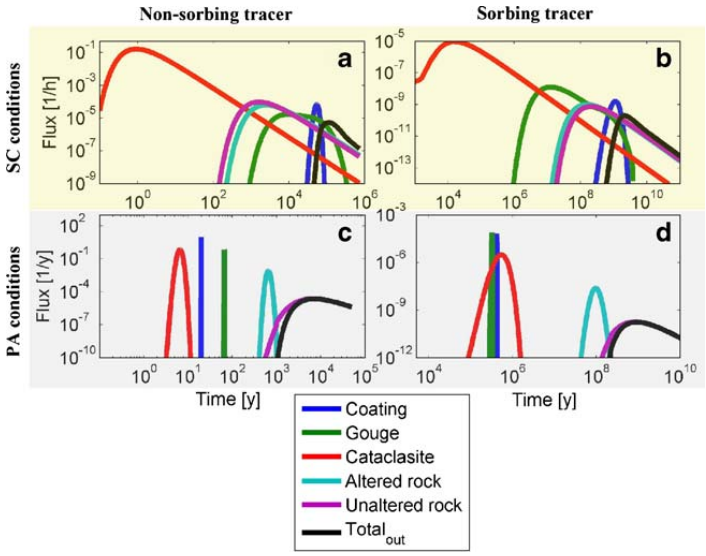

Fig. 17 Contributions of the individual immobile layers to the retention of the iodine and americium in the typical SC and PA flow conditions: **a** Iodine in SC flow field, **b** Americium in SC flow field, **c** Iodine in PA flow field and **d** Americium in PA flow field. Tracer breakthrough curves are indicated by *black lines*

Summary and discussion

Matrix diffusion is an efficient retention process that is able to significantly hinder the migration of radionuclides. The site specific potential for retention depends on the local flow conditions and the composition of the geological materials that contain the immobile pore spaces available for the matrix diffusion. Fractured rock is characterised by heterogeneity and a large spread of hydraulic properties. This leads to preferential flow paths and also significantly affects transport and retention properties along the flow paths. One of the effects is the spatial scale effect of the solute retention properties that is caused by the structure of the fractured rock. Large hydraulic features are, on average, hydraulically more conducting than the smaller ones. Flow paths tend to accumulate in the larger structures where the hydrodynamic control of retention is weaker than in the background fractures. This means that the early part of the flow path tends to dominate the total β of the whole flow path.

The special characteristics of the flow paths in fractured rock have also been observed in some other studies. Öhman et al. (2005) performed numerical studies on tracer transport through a stochastic continuum model. The study does not directly examine retention properties, but the results are in line with those of the present study. Block-size transit-time distributions have been modelled by discrete fracture network (DFN) modelling and different alternatives to up-scale the inter-block size transit time distributions have been studied. Persistent correlation, i.e. perfect correlation over a given number of blocks, gave the most promising results. Painter and Cvetkovic (2005) have developed a stochastic random walk process, a Markov-directed random walk (MDRW), which can be used to describe the transport and retention properties along the particle pathways. The statistics of the transport and retention properties are based on fracture network simulation results, which indicate a correlation in the transport properties between the successive segments along the particle trajectory. A particle that is in a high-velocity segment is more likely to indicate high velocity in the subsequent segment due to conservation of flux at the fracture intersections. According to Painter and Cvetkovic (2005), the correlation between successive segments along the particle trajectory is an important control on the breakthrough curves. The present study shows that the hydrodynamic control of retention can depend on the scale for different flow conditions if the rock is heterogeneous over all scales. The implication of this for radionuclide transport along the release paths from a repository is that the early parts of the flow paths are very important for the overall retention properties.

The modelling approach applied in the present study enables evaluation of the contribution of the individual immobile layers to the overall retention. This makes it possible to determine the influence of the immobile zone heterogeneity to the solute retention for different flow conditions. The role of the detailed scale heterogeneity in relation to the average retention properties is clearly different in the PA and SC flow conditions. For PA flow conditions the retention properties are averaged over much larger volumes of the immobile zones than for SC flow conditions. This facilitates PA scale transport analysis, because detailed scale heterogeneity is not of primary importance in these conditions. However, this makes it impossible to validate the PA scale retention by SC scale

DOI 10.1007/s10040-008-0414-y

tracer experiments. It also indicates that there is no straightforward way to extrapolate transport properties to the performance assessment scale from the observed transport properties in the site characterisation scale. The averaging of the immobile zone retention properties extend much deeper into the rock matrix under performance assessment flow conditions than for site characterisation flow conditions. This results in a significant difference between the dominating immobile retention zones for site characterisation and performance assessment scales.

Acknowledgements Dr. David Hodgkinson (Quintessa Ltd.) is thanked for his comments and suggestions regarding the manuscript. This study was funded by Posiva Oy, Finland.

Appendix: Grouped parameters in the matrix diffusion solution

Solute transport through a transport path is described by the advection-matrix diffusion equation

$$\begin{aligned} &\frac{\partial c_f}{\partial t} + v\frac{\partial c_f}{\partial x} - 2\frac{D_e}{2b}\frac{\partial c_m}{\partial z}\bigg|_{z=0} = 0 \\ &R_p\frac{\partial c_m}{\partial t} - D_p\frac{\partial^2 c_m}{\partial z^2} = 0 \end{aligned}, \tag{3}$$

where v is the flow velocity, $2b$ is the fracture aperture, R_p is the retardation coefficient in the immobile pore space, D_p is the pore diffusivity in the immobile pore space and D_e is the effective diffusion coefficient from fracture to immobile pore space. Solute concentrations in the pore water of the immobile pore space, c_m (x, z, t), and in the fracture, c_f (x, t), are coupled by the requirement that at the fracture wall c_m (x, 0, t) = c_f (x, t). The initial concentration is zero both in the immobile pore space and in the fracture.

The Laplace transform of Eq. (3) gives

$$\begin{aligned} &s\bar{c}_f + v\frac{\partial \bar{c}_f}{\partial x} - 2\frac{D_e}{2b}\frac{\partial \bar{c}_m}{\partial z}\bigg|_{z=0} = 0 \\ &R_p s\bar{c}_m - D_p\frac{\partial^2 \bar{c}_m}{\partial z^2} = 0 \end{aligned}, \tag{4}$$

where s is the variable of the Laplace domain. Equation (4) indicates that the solution could be sought using product $\bar{c}_m(x,z,s) = f(z)\bar{c}_f(x,s)$ with $f(0)=1$. This leads to the solution

$$\bar{c}_f(x,s) = C_0\,\mathrm{Exp}\left(-\frac{s\,x}{v} + \frac{2\,x\,D_e}{2bv}f'(0)\right), \tag{5}$$

where C_o is determined by the source term at the inlet of the flow path. For a step input c_o H (t), where H is the Heaviside step-function, it is $C_0 = c_0/s$ and for the Dirac pulse injection $\frac{M_0}{W(2b)v}\delta(t)$ it is $C_0 = \frac{M_0}{W(2b)v}$, where W is the width of the channel.

The structure of the immobile pore spaces is taken into account by the term $f'(0)$ of Eq. (4), which controls diffusion to the immobile zones. This property is used to construct the solution for a heterogeneous layered immobile pore space. One homogeneous layer of immobile pore space leads to the following equation:

$$\begin{aligned} &\frac{2\varepsilon D_p}{2b\,v}f'(0) = \\ &= -2\sqrt{s}\frac{x}{v2b}\varepsilon\sqrt{D_pR_p}\tanh\left(L\sqrt{s\,R_p/D_p}\right), \\ &= -\sqrt{s}\,\beta\,\gamma\,\tanh\left(L\sqrt{s\,R_p/D_p}\right) \end{aligned} \tag{6}$$

where the hydrodynamic control of retention, $\beta = x/(v\,b)$, specifies the flow conditions in the transport channel, $\gamma = \varepsilon\sqrt{D_pR_p}$ determines the properties of the immobile zone and L is the thickness of the immobile zone.

Equation (6) shows that the retention depends on three grouped parameters: β that describes the flow field, γ that characterises the immobile zone and $t_d = L\sqrt{R_p/D_p}$ that parameterises the "diffusion time" through the immobile layer.

References

Becker MW, Shapiro AM (2000) Tracer transport in fractured crystalline rock: evidence of non-diffusive breakthrough tailing. Water Resour Res 36(7):1677–1686

Crawford J, Moreno L (2006) Modelling of Task 6D, 6E and 6F, using CHAN3D. Äspö Hard Rock Laboratory, Äspö Task Force of modeling of groundwater flow and transport of solutes. Swedish Nuclear Fuel and Waste Management Co. International Progress Report, IPR-06-19, SKB, Stockholm

Cvetkovic V, Haggerty R (2002) Transport with multiple-rate exchange in disordered media. Phys Rev E 65:051308, May 2002

Cvetkovic V, Selroos JO, Cheng H (1999) Transport of reactive tracers in rock fractures. J Fluid Mech 378:335–356

Dershowitz W, Winberg A, Hermanson J, Byegård J, Tullborg E-L, Andersson P, Mazurek M (2003) TASK 6C, a semi-synthetic model of block scale conductive structures at the Äspö Hard Rock Laboratory, SKB International Progress Report IPR-03-13, SKB, Stockholm

Gustafson G, Gylling B, Selroos J-O (2008) The Äspö Task Force on groundwater flow and transport of solutes: bridging the gap between site characterization and performance assessment for radioactive waste disposal in fractured rocks. Hydrogeol J. doi: 10.1007/s10040-008-0419-6

Hodgkinson D (2007) Äspö Task Force on modelling of groundwater flow and transport of solutes: review of Tasks 6D, 6E, 6F and 6F2. Technical Report TR-07-03, Svensk Kärnbräsnlehantering AB, Stockholm

Hodgkinson D, Benabderrahmane H, Elert M, Hautojärvi A, Selroos J-O, Tanaka Y, Uchida M (2008) An overview of Task 6 of the Äspö Task Force: modelling groundwater and solute transport: improved understanding of radionuclide transport in fractured rock. Hydrogeol J. doi:10.1007/s10040-008-0416-9

Neretnieks I (1980) Diffusion in the rock matrix: an important factor in radionuclide retardation. J Geophys Res 85:4379–4397

Nordqvist AW, Tsang YW, Tsang CF, Dverstorp B, Andersson J (1996) Effects of high variance of fracture transmissivity on transport and sorption at different scales in a discrete model for fractured rocks. J Contam Hydrol 22:39–66

Öhman J, Niemi A, Tsang C-F (2005) A regional-scale particle-tracking method for nonstationary fractured media. Water Resour Res 41(3):W03016. doi:10.1029/2004WR003498

Painter S, Cvetkovic V (2005) Upscaling discrete fracture network simulations: an alternative to continuum transport models. Water Resour Res 41(2):W02002. doi:10.1029/2004WR003682

Poteri A (2006) Modelling of task 6D, 6E, 6F and 6F2 using the Posiva streamtube approach. Äspö Task Force on modelling of groundwater flow and transport of solutes. SKB International Progress Report IPR-06-17, SKB, Stockholm

Tsang CF, Tsang YW, Hale FV (1991) Tracer transport in fractures: analysis of field data based on a variable-aperture channel model. Water Resour Res 27(12):3095–3106

PUBLICATION III

Retardation of mobile radionuclides in granitic rock fractures by matrix diffusion

In: Physics and Chemistry of the Earth 33,
No. 14–16, pp. 983–990.

doi:10.1016/j.pce.2008.05.010

Physics and Chemistry of the Earth 33 (2008) 983–990

Contents lists available at ScienceDirect

Physics and Chemistry of the Earth

journal homepage: www.elsevier.com/locate/pce

Retardation of mobile radionuclides in granitic rock fractures by matrix diffusion

P. Hölttä [a,*], A. Poteri [b], M. Siitari-Kauppi [a], N. Huittinen [a]

[a] University of Helsinki, Laboratory of Radiochemistry, Department of Chemistry, P.O. Box 55, FIN-00014, Finland
[b] Technical Research Centre of Finland, P.O. Box 1000, FIN-02044 VTT, Finland

ARTICLE INFO

Article history:
Available online 7 June 2008

Keywords:
Block-scale experiments
Crystalline rock
Matrix diffusion
Migration

ABSTRACT

Transport of iodide and sodium has been studied by means of block fracture and core column experiments to evaluate the simplified radionuclide transport concept. The objectives were to examine the processes causing retention in solute transport, especially matrix diffusion, and to estimate their importance during transport in different scales and flow conditions. Block experiments were performed using a Kuru Grey granite block having a horizontally planar natural fracture. Core columns were constructed from cores drilled orthogonal to the fracture of the granite block. Several tracer tests were performed using uranine, ^{131}I and ^{22}Na as tracers at water flow rates 0.7–50 μL min^{-1}. Transport of tracers was modelled by applying the advection–dispersion model based on the generalized Taylor dispersion added with matrix diffusion. Scoping calculations were combined with experiments to test the model concepts. Two different experimental configurations could be modelled applying consistent transport processes and parameters. The processes, advection–dispersion and matrix diffusion, were conceptualized with sufficient accuracy to replicate the experimental results. The effects of matrix diffusion were demonstrated on the slightly sorbing sodium and mobile iodine breakthrough curves.

1. Introduction

In Finland, the repository for spent nuclear fuel will be excavated at a depth of about 500 m in the fractured crystalline bedrock in Olkiluoto at Eurajoki, the site proposed by Posiva Oy. The fractures provide the most effective transport paths even though most of the porosity derives from the pores. The diffusion of mobile radionuclides into the micro-fissures and pores is still regarded as the main mechanisms retarding radionuclide transport in crystalline rock (Neretnieks, 1980). Ground water flow in fractured rock is distributed unevenly causing strong channelling effects, where the water flow occurs mainly over a small proportion of the fracture surface (Tsang et al., 1991), and stagnant non-flowing areas. Only matrix diffusion can cause significant changes in the shape of a breakthrough curve as a function of either elution time or the diffusion coefficient. In the case of crystalline rock, the residence times of tracers have been too short for matrix diffusion to occur in short time scale laboratory experiments. In laboratory-scale experiments, the effects of matrix diffusion have been demonstrated by Callahan et al. (2000). They investigated solute transport in fractured saturated volcanic tuff, which is significantly more porous than crystalline rock, allowing matrix diffusion to occur in a reasonable time. The dominant matrix diffusion behaviour was demonstrated in porous ceramic columns, and demonstration of the effects of matrix diffusion in crystalline rock fracture column succeeded in a series of experiments where the experimental arrangements enabled very low water flow rates (Hölttä, 2002).

Performance assessment is directly concerned with the contribution of ^{129}I, ^{36}Cl, ^{79}Se, ^{14}C and ^{99}Tc in their long-term exposure risks. The elution times of non-sorbing tracers have been used usually to indicate the flow rate of the groundwater in the fracture. However, this knowledge and understanding about transport and retention processes can be utilized to evaluate the transport of mobile fission and activation products in the geosphere. Radionuclide transport through a natural fracture has been studied in many block-scale experiments (Drew et al., 1990; Cliffe et al., 1993; Vandergraaf et al., 1996, 1997; Park et al., 1997; Vilks and Baik, 2001; Vilks et al., 2003). Migration experiments in Kuru Grey granite block fracture and core columns were introduced to evaluate the simplified radionuclide transport concept used in assessing the safety of the underground waste repositories (Hölttä et al., 2004). The objectives were to examine the processes causing retention in solute transport, especially matrix diffusion, and to estimate the importance of retention processes during transport in different scales and flow conditions. In this paper, we present the modelling concept, scoping calculations, the results of tracer tests performed and demonstrate the effects of matrix diffusion.

* Corresponding author. Tel.: +358 9 19150142.
E-mail address: pirkko.holtta@helsinki.fi (P. Hölttä).

1474-7065/$ - see front matter © 2008 Elsevier Ltd. All rights reserved.
doi:10.1016/j.pce.2008.05.010

2. Experimental

Block-scale migration experiments were performed using Kuru Grey granite block which was obtained from Kuru Quarry, Tampereen Kovakivi Oy, Finland. The total porosity and the surface areas of mineral grains available for the migration of species were determined by the ^{14}C-PMMA method (Siitari-Kauppi, 2002). The pore aperture distribution was evaluated on the basis of Hg-porosimetry determinations. Pore apertures and geometry in the mineral phases were analyzed also by scanning electron microscopy (SEM) and the minerals were quantified by means of energy dispersive X-ray microanalysis (EDX). The specific surface area of the solid rock was determined by the BET Hg impregnation method. Determined values are given in Table 1 and detailed rock matrix characterization is reported in Hölttä et al. (2004, 2007).

An experimental set-up for a block is illustrated in Fig. 1a. The block contains a natural hydraulically conducting fracture (0.9 m × 0.9 m) intersected by nine vertical boreholes, which were equipped with injection or sealing packers. Water pools were installed on the vertical sides and top of the block in order to ensure the saturation of the block and to stabilize the hydraulic head on the vertical faces. The block was instrumented also at the outer vertical boundary of the block where the horizontal fracture intersects the faces of the block for the collection of the tracer. Hydrological properties of the fracture were characterized and flow paths are described in Hölttä et al. (2004). Estimated transmissivities are illustrated in Fig. 1b, which shows clearly the increase in transmissivity towards side 3. Evaluation of the water consumption tests from drill holes KR0 to KR6 show transmissivities that vary between 9×10^{-8} m^2 s^{-1} and 2×10^{-6} m^2 s^{-1} and the average parallel plate aperture of the fracture was about 0.1 mm. In parallel with the block-scale experiments core column experiments were performed to estimate the diffusion properties of Kuru Grey granite. Core columns (Fig. 1c) were constructed from cores drilled to the fracture and were placed inside a tube to form a flow channel representing an artificial fracture formed by the 0.5 mm gap between the core and the tube (Hölttä et al., 2007).

In a block, flow path tests with uranine dye tracer showed that migration took place through distinct channels (Hölttä et al., 2004). Drill hole KR1 was chosen for the tracer transport experiments because hydraulic characterization and qualitative uranine dye tracer tests indicated that it had the longest flow path of about 0.7 m. The water pool at the side 3 was divided into eight adjacent tracer collection cells based on the outflow positions of the main transport channels. The out flowing tracer was collected by pump-

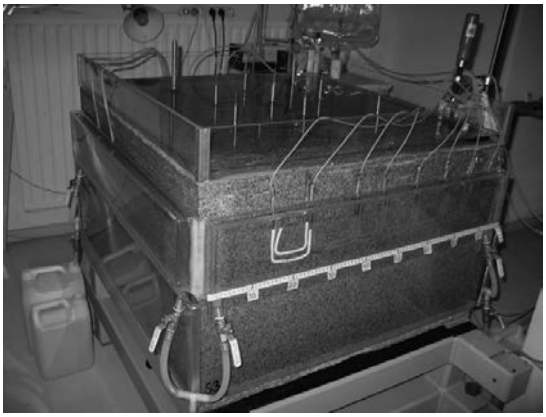

Fig. 1a. Kuru Grey granite block having a natural hydraulically conducting fracture (0.9 m × 0.9 m). The vertical bore–holes are equipped with injection or sealing packers. Water pools equipped with adjacent tracer collection channels ensure saturation and stabilize the hydraulic head around the vertical faces.

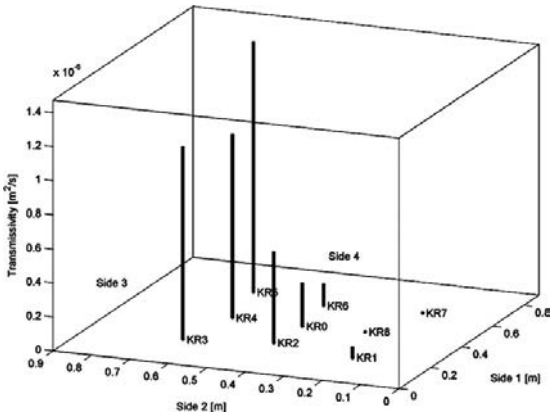

Fig. 1b. Local transmissivities in a natural fracture determined from the water pumping tests.

Table 1
Parameters applied in the modelling of the tracer experiments through the Kuru Grey granite borehole core and the natural fracture (0.9 m × 0.9 m)

Parameter	Core column	Block channel II	Block channel IV
Channel length (m)	0.685	0.75	0.80
Channel width (m)	0.044	0.06	0.035
Channel aperture (m)	7×10^{-4}	6.5×10^{-4}	5×10^{-4}
Matrix porosity (%)	0.04	0.5	0.5
Specific surface area (m^2 g^{-1})	0.03	0.03	0.03
Density (kg m^{-3})	2660	2660	2660
Average grain size (mm)	0.5–1.5	0.5–1.5	0.5–1.5
Average pore diameter (nm)	300–400	300–400	300–400
Flow rates (μL min^{-1})	Uranine: 3, 3, 6, 20 ^{22}Na: 3, 3, 6, 20 ^{131}I: 0.7, 4.2	Uranine: 7 (10) ^{22}Na: 7 (10) ^{131}I: 3.0	Uranine: 3 (10) ^{22}Na: 3 (10)
Width of the velocity profile (m)	0.022	0.03	0.024
Diffusivity in free water (m^2 s^{-1})	2×10^{-9}	2×10^{-9}	2×10^{-9}
Pore diffusivity (m^2 s^{-1})	Uranine: 6.6×10^{-11} ^{22}Na: 6.6×10^{-11} ^{131}I: 6×10^{-13}	Uranine: 6.6×10^{-11} ^{22}Na: 6.6×10^{-11} ^{131}I: 2×10^{-11}	Uranine: 6.6×10^{-11} ^{22}Na: 6.6×10^{-11}
K_d (m^3 kg^{-1})	^{22}Na: 6×10^{-4}	^{22}Na: 6×10^{-4}	^{22}Na: 6×10^{-4}
K_a (m)	^{22}Na: 2×10^{-5}	^{22}Na: 2×10^{-5}	^{22}Na: 2×10^{-5}

Fig. 1c. Experimental design used in core column experiments. Cores drilled to the fracture of the Kuru Grey granite, are placed inside a tube to form an artificial flow channel in a gap between the core and the tube.

ing and flushing collection channel areas. Several tracer tests were performed both in a block and core columns using uranine, HTO, ^{36}Cl, ^{131}I and ^{22}Na as tracers with injection flow rates of 0.7–50 μL min^{-1}. Flow channel dimensions, tracers and range of volumetric flow rate used in the experiments are summarized in Table 1.

3. Modelling

Transport of tracers through the flow channels in a core column or in a natural fracture was modelled using an advection–dispersion model based on the generalized Taylor dispersion. It was assumed that a linear velocity profile existed across the flow channel, from zero velocity to some maximum flow velocity, and that the flow field and molecular diffusion perpendicular to the flow dominate the transport of the tracer particles in the mobile pore space of the fracture (Hautojärvi and Taivassalo, 1994; Poteri et al., 2002). The exact shape of the velocity profile is important in the case of purely advective transport which is not the case in the present experiments and is not of interest in this. More essential is to describe the variation of the flow velocities. It is assumed that velocity variation exist also in the experiments carried out with the cores. The aperture between a core and tube is quite small and it is difficult to centre the rough surfaced core on the middle which can easily generate variable flow velocity for different streamlines in the circular slit around the core.

The mean concentration across the flow channel for a narrow box-function release is given by Eq. (1)

$$C_m = \frac{1}{2}\left(\operatorname{erf}\left[\frac{\frac{1}{2}X_s + X + \xi_1}{2\sqrt{\xi_2}}\right] + \operatorname{erf}\left[\frac{\frac{1}{2}X_s - X - \xi_1}{2\sqrt{\xi_2}}\right]\right);$$
$$\xi_1 = -\frac{1}{2}\tau;\ \xi_2 = \left(\frac{1}{(Pe)^2} + \frac{1}{120}\right)\tau - 8\sum_{n=0}^{\infty}\frac{1 - e^{-(2n+1)^2\pi^2\tau}}{(2n+1)^8\pi^8}; \quad (1)$$
$$\tau = \frac{Dt}{a^2};\ X = \frac{Dx}{a^2 v_0};\ X_s = \frac{Dx_s}{a^2 v_0};\ Pe = \frac{a v_0}{D}$$

where D is the molecular diffusion coefficient in water, a is the correlation length of the velocity variation approximated here as half of the flow channel width, x_s is the initial width of the tracer plume, v_0 is the maximum flow velocity, t is the time and x is the position along the channel. The solute discharge at the end of the transport channel for the delta function release and taking into account the matrix diffusion and sorption can be written as

$$j(t, t_w, u, R_a) = H(t - R_a t_w)\frac{u}{\sqrt{\pi}(t - R_a t_w)^{3/2}} e^{\frac{-u^2}{t - R_a t_w}}, \quad (2)$$

where parameter u determines the strength of the matrix diffusion, t_w is the groundwater transit time and R_a is the surface retardation coefficient. H is the Heaviside step function. The matrix diffusion property (u) is defined as

$$u = \varepsilon\sqrt{D_p R_p}\frac{WL}{Q} = \varepsilon\sqrt{D_p R_p}\frac{t_w}{2b}, \quad (3)$$

where t_w is the groundwater transit time, $2b$ is the channel aperture, D_p is the matrix pore diffusivity, ε is the matrix porosity and R_p is the retardation coefficient in the matrix. The last factor, $t_w/(2b)$, in Eq. (3) is also presented as WL/Q. This parameter represents the coupling of the matrix diffusion to the flow field by ratio Q/W, i.e. the flow rate per width and to the length of the channel L. Sorption was modelled as linear equilibrium sorption, both in the pore space of the rock matrix and on the outer surface of the core. Solute transport with matrix diffusion and sorption was calculated by integrating over the solute mass flux distribution according to Eq. (4)

$$k(t) = \int_0^t j(t, t_w, U_t t_w, R_a) b(t_w)\, dt_w, \quad (4)$$

where $b(t_w)$ is the solute mass flux distribution in the mobile pore space and $j(t, t_w, U_t, R_a)$ is the corresponding matrix diffusion breakthrough curve, Eq. (2).

The shape of the tracer breakthrough curve is affected, at least, by velocity variation over the flow channel, molecular diffusion in the flow channel, possible sorption and matrix diffusion. It could be very difficult to assess from an individual breakthrough curve whether matrix diffusion shows up in the experiment. A more robust approach is to analyse the dynamic behaviour of the tracer discharge when flow rate and tracer sorption properties are changed. Tests with the cores offer an opportunity to carry out a test with the same tracers and with the nearly identical rock matrix but under well-constrained flow geometry. A minor difference in the diffusion properties of the rock matrix could arise for example from possible alteration on the surface of the natural fracture.

The transport problem is characterized in the present modelling approach by parameters: the volume of the transport channel (V_c), correlation length of the velocity variation in the flow field (W_v), molecular diffusion in free water (D) and immobile pores of the rock matrix (D_p), distribution of flow velocities (linear velocity profile from zero velocity to v max), rock matrix porosity (ε), flow rate distribution in the flow channel (Q/W) and the channel length (L). Sorption properties of sodium were estimated from the K_d values determined for Syyry mica gneiss and unaltered tonalite (Hölttä, 2002). Commonly used literature value has been applied for the molecular diffusion coefficient in free water and pore diffusivity in a rock matrix is based on Archie's law for the formation factor $F = 0.71\varepsilon^{1.58}$ (Cheng and Cvetkovic, 2005). Measured data was

directly applied to describe rock matrix properties; the only calibration has been that in the fracture experiments rock matrix porosity was slightly increased from 0.4% to 0.5%.

Calibration aims at the consistency of the transport parameterisation in all modelled experiments with the same characterization of the transport path with emphasis on the matrix diffusion retention properties. Particularly, this applies to immobile zone retention properties, because all flow channels are dissimilar. Each channel is tested using different flow rates that facilitate the characterization of the flow channels. Early parts of the breakthrough curves and tests with the highest flow rates are not so much of interest because they are dominated by the advection. Focus of the calibration has been on the overall dynamic behaviour when flow rate and sorption properties change. In the fracture experiments the lengths of the transport paths are calculated from the locations of the injection and withdrawal points. Geometry of the transport channels is calibrated to give reasonable fit on retention in different tracer tests. In practice, this implies constraining of the channel widths. To some extent also early parts of the breakthrough curves were used to constrain volumes of the transport channels and correlation lengths of the velocity variation. Well mixed tracer concentration was assumed close to the injection drill hole KR1 where the transport paths diverged. Under this assumption, the flow rates of the transport channels were proportional to the recoveries collected from these channels. Division of the total flow rate between the channels was also subject to minor calibration. Tracer recoveries indicate that flow rate through the channel II is 73–75% of the injection flow rate. Calibrated value is that 70% of the total flow rate goes through the channel II. The only difference between modelled sodium and uranine breakthrough curves is the application of the measured K_d for sodium. In the case of core experiments the correlation length of the velocity variation was selected to be half of the channel width, i.e. 2.2 cm, to take into account that there are different flow velocities at different locations around the core circumference. The only calibration parameter in the core experiment was the aperture. The measured aperture, $2b = 0.5$ mm, do not account for the roughness of the surface of the core and the actual transport aperture may be larger. The calibrated aperture used is $2b = 0.7$ mm. Calibration of the transport aperture aimed at reasonable fit for different flow rates and tracers with emphasis to more retarded breakthrough curves, i.e. smaller flow rates. The modelled breakthrough curves for the tracer transport were convoluted with a response function of the tubing before being compared with the measured experimental breakthrough curves. The response function of tubing and other experimental equipment was determined by performing tracer tests without a core column or a natural fracture.

4. Results and discussion

First tracer tests in a block fracture were performed for uranine and ^{99m}Tc using injection flow rates of 350 μL min^{-1} and 230 μL min^{-1} (Hölttä et al., 2004). Obtained breakthrough curves were dominated by the advective field and the processes like diffusional mixing. Scoping calculations were carried out based on the geometrical dimensions and the hydraulic characterization of the fracture and preliminary tracer tests. In the scoping calculations for the sorbing tracer, the K_d value used, 7.1×10^{-6} m^3 kg^{-1}, was much smaller than the value of 6×10^{-4} m^3 kg^{-1} extracted from fits to experiments. In an ideal fracture, matrix diffusion is clearly observable for a non-sorbing tracer when the flow rate is 0.1 μL min^{-1} in a core column (Fig. 2a) and 1 μL min^{-1} in a block fracture (Fig. 2b).

Tracer tests analyzed in the present paper were performed for uranine and slightly sorbing sodium (^{22}Na) using flow rates 3–20 μL min^{-1} in a core column and 10–50 μL min^{-1} in a block. Measured and modelled breakthrough curves through the core column are presented for uranine in Fig. 3a and for ^{22}Na in Fig. 3b. Measured and modelled breakthrough curves of uranine and ^{22}Na through the block fracture are presented in Fig. 3c. Effects of the matrix diffusion in the breakthrough curves can be observed when results for non-sorbing and sorbing tracers are compared side by side. As explained in the model calibration the only difference between modelled breakthrough curves for uranine and sodium in the core column experiments is the non-zero K_d of the sodium. It should also be noted that K_d of the sodium has not been calibrated but it is estimated based on the measured data. The model explains the transport of the uranine for the lower flow rates well; the test

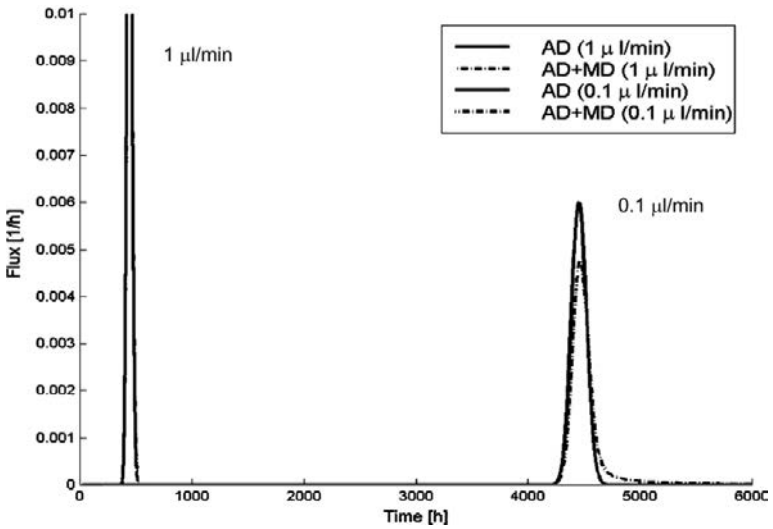

Fig. 2a. Scoping calculations for a core column tracer test based on the dimensions of an artificial flow channel and preliminary tracer experiments. Dotted lines are model results for advection–dispersion and matrix diffusion. Solid lines are for the advection–dispersion only.

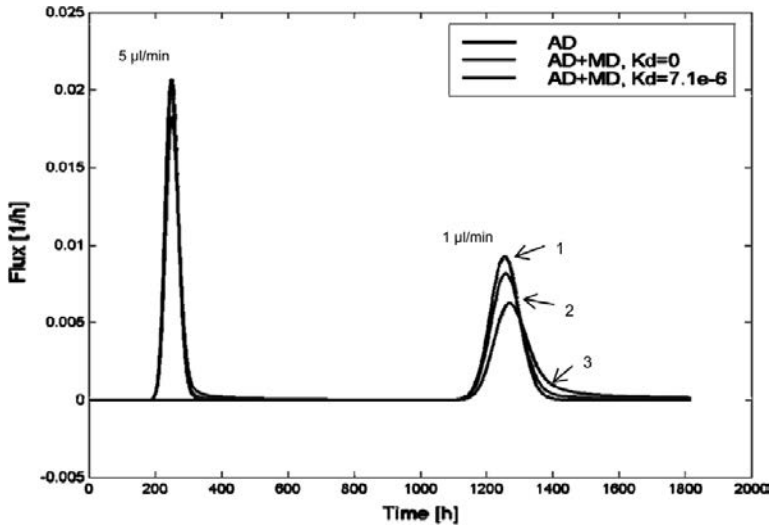

Fig. 2b. Scoping calculations for a tracer test in a natural fracture from injection hole KR1 to channel II based on the hydraulic characterization of the fracture, the estimation of flow paths and preliminary tracer experiments. Results are presented for advection–dispersion (1), matrix diffusion of non-sorbing tracer (2) and matrix diffusion of slightly sorbing tracer, $K_d = 7.1 \times 10^{-6}$ m^3 kg^{-1} (3).

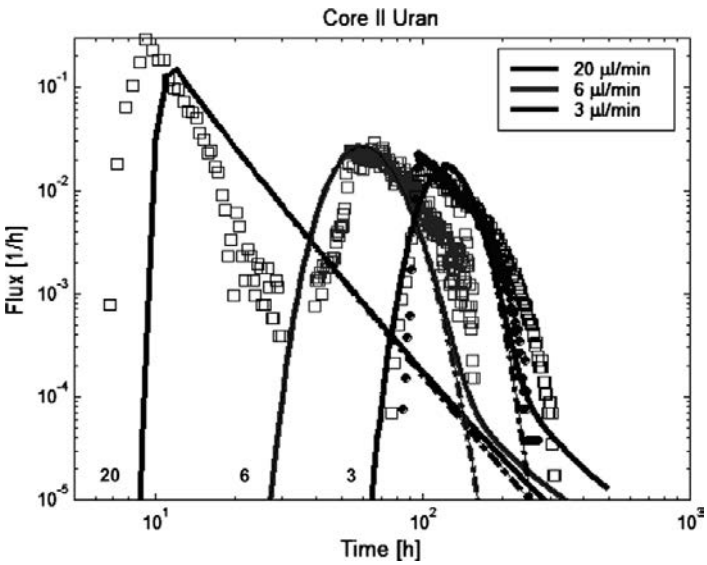

Fig. 3a. Modelled and measured breakthrough curves of uranine through a core column with flow rates of 20 µL min^{-1}, 6 µL min^{-1} and two experiments with flow rate of 3 µL min^{-1} (squares and full circles). Solid lines are model results for advection–dispersion and matrix diffusion. Dotted lines are for the advection–dispersion only.

with the highest flow is dominated by the velocity field in the experimental results and by the velocity profile in the modelled results and is not subject of main interest in the present study. Especially, it is observed that the model predicts matrix diffusion effects in the tailings of the breakthrough curves ($\sim t^{-3/2}$ tailing) beyond the range of measured data (Fig. 3a). Using exactly the same model to sodium breakthrough curves, only taking the sorption of the sodium into account, show very good agreement with the measured breakthrough curves (Fig. 3b). Sorption of the sodium enhances matrix diffusion showing clear difference in the tailings of the breakthrough curves. Fig. 3b includes also breakthrough curves that are modelled without matrix diffusion in order to facilitate the identification of the matrix diffusion effects. Results give strong evidence that sodium breakthrough curves are affected by matrix diffusion because: (i) the same model is able to reproduce advection–dispersion dominated the breakthrough of the uranine and even predicts that matrix diffusion effects are beyond the range of measured data, (ii) the same model is able to reproduce the breakthrough curves of the sodium; the only difference between these models being the sorption of sodium, even

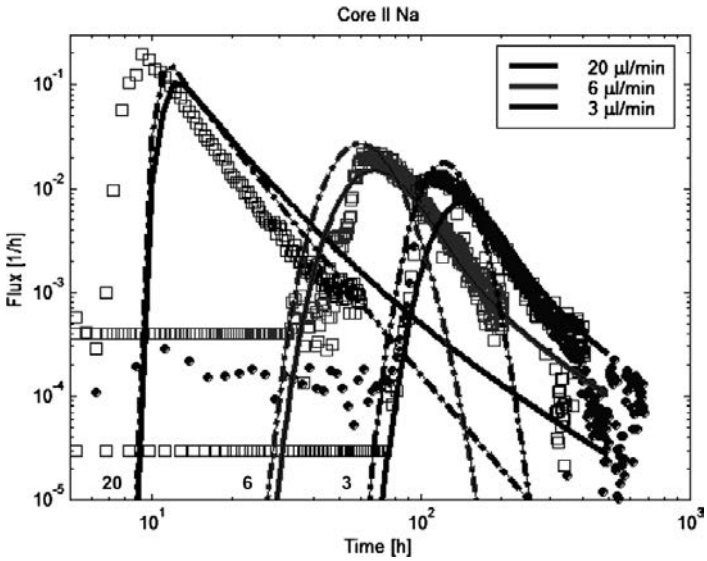

Fig. 3b. Modelled and measured breakthrough curves of ^{22}Na through a core column with flow rates of 20 μL min^{-1}, 6 μL min^{-1} and two experiments with flow rate of 3 μL min^{-1} (squares and full circles). Solid lines are model results for advection–dispersion and matrix diffusion. Dotted lines are for the advection–dispersion only.

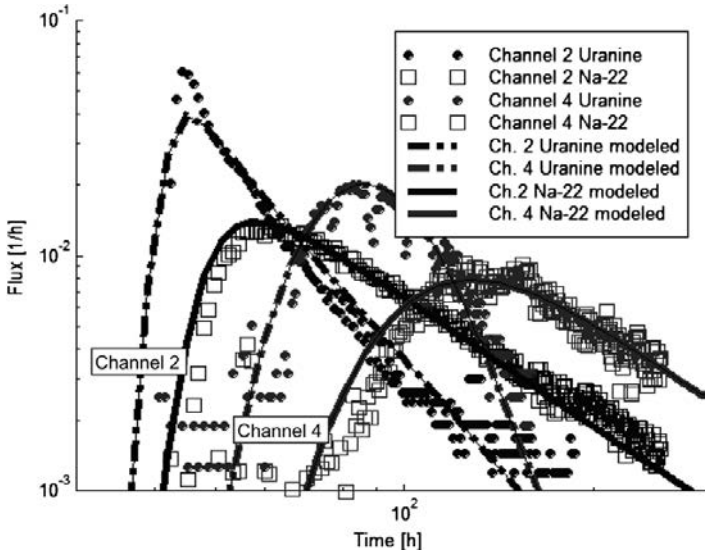

Fig. 3c. Modelled and measured breakthrough curves of uranine (full circles) and ^{22}Na (squares) through a natural fracture. All breakthrough curves are normalised to give a unit mass in the experimental time scale.

without calibration K_d of the sodium, and (iii) comparing modelled results for sodium with and without matrix diffusion supports the conclusion that tailings of the sodium breakthrough curves are affected by matrix diffusion.

An interesting question is how well the model used for explaining the experiments of the core columns will do with transport along a natural fracture. Fig. 3c shows experimental and modelled results for a fracture experiment. Two transport channels were active in the analyzed experiment that makes it possible to examine dynamic behaviour under changes of flow rate. Different sorption properties of the cocktail of two tracers make it possible look at matrix diffusion properties along the same flow path. The same model that was used to examine core column experiments was applied to the fracture experiment. The only difference in the retention parameters between the core column and fracture experiments was that porosity of the rock matrix was slightly increased from 0.4% to 0.5% in the model of the fracture experiment. The model reproduces the dynamic behaviour of the tracer

breakthrough very accurately when sorption properties are changed (Fig. 3c). There are strong indications that effects of the matrix diffusion were observed in the fracture flow experiment because: (i) when sorption properties are changed the dynamic behaviour of the breakthrough curves is well explained by the matrix diffusion model for both channels, i.e. for different flow rates, (ii) the same sorption properties for sodium as in the core column experiment explain the difference in breakthrough curves between uranine and sodium and (iii) the tailings of the sodium breakthrough curves follow $\sim t^{-3/2}$ which is typical for matrix diffusion. Note that the difference in the modelled breakthrough curves of uranine and sodium comes solely from the sorption properties of the sodium and that the same measured sorption values were applied as in the core column experiment.

A third set of tracer tests were performed for ^{131}I using flow rates 0.7–10 μL min^{-1} in a core column and 3–10 μL min^{-1} in a block. Examples of the measured and modelled breakthrough curves through the core column are presented in Fig. 4a and through the block fracture in Fig. 4b. The model used earlier for fracture column experiments (Hölttä, 2002) and the same transport parameterization that were used to examine uranine and sodium experiments were applied to independently interpret iodide results. In a core column, a D_e value of 6×10^{-13} m^2 s^{-1} gave the best overall fit between measured and calculated iodine break

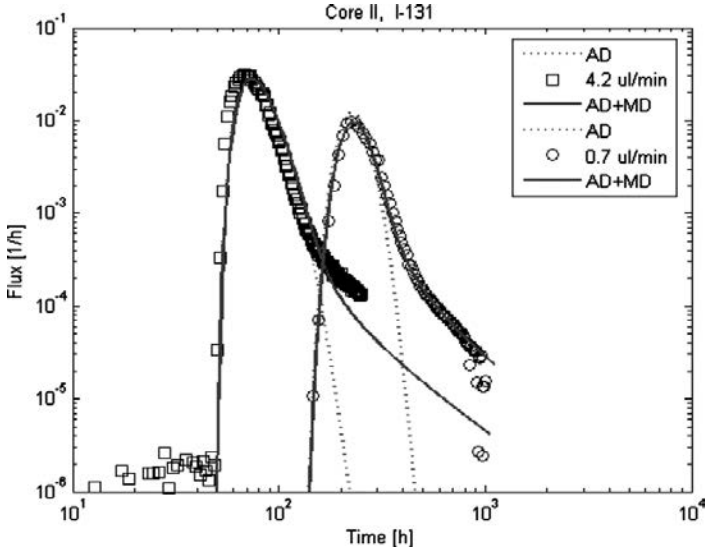

Fig. 4a. Modelled and measured breakthrough curves of ^{131}I through a core column. Solid lines are model results for advection–dispersion and matrix diffusion. Dotted lines are for the advection–dispersion only.

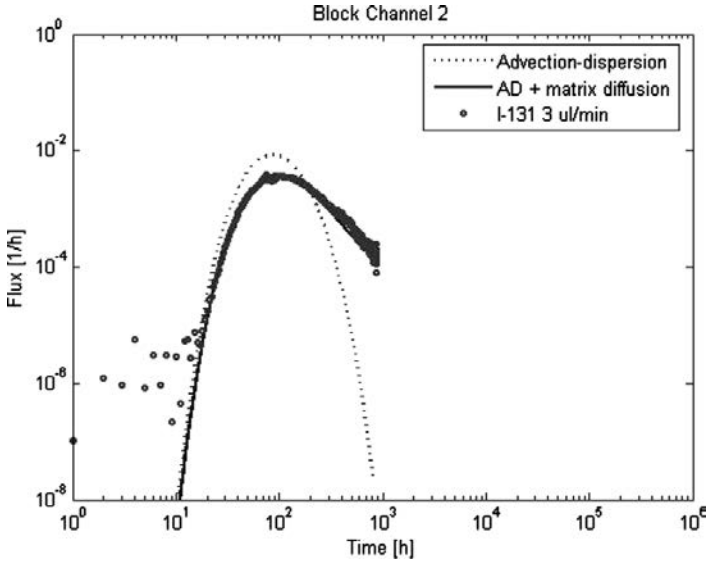

Fig. 4b. Modelled and measured breakthrough curves of ^{131}I through a natural fracture channel II. Solid lines are model results for advection–dispersion and matrix diffusion. Dotted lines are for the advection–dispersion only.

through curves. In a block fracture, a D_e value of 2×10^{-11} m^2 s^{-1} gave the best overall fit between measured and calculated iodine break through curves. This relatively high D_e value for low porosity granite possibly indicates diffusion also into the stagnant water areas of wide and ragged surfaces of a natural fracture. Comparing modelled results for iodide with and without matrix diffusion supports the conclusion that tailings of the iodide breakthrough curves are affected by matrix diffusion.

5. Conclusions

Block and core column migration experiments were performed to evaluate the simplified radionuclide transport concept used in assessing the safety of the underground waste repositories. Two different experimental configurations could be modelled applying consistent transport processes and parameters. The processes, advection–dispersion and matrix diffusion, were conceptualized with sufficient accuracy to reproduce the experimental results. The results provided show that it is possible to investigate matrix diffusion in low porosity crystalline rock at the laboratory scale. The effects of matrix diffusion were demonstrated on the slightly sorbing sodium and mobile iodine breakthrough curves. The modelled experiment builds confidence on the model predictions of the solute retention in groundwater flow. This understanding is transferable from the laboratory scale to in situ conditions though specific parameters can not be transferred directly to the spatial and temporal repository scale.

Acknowledgements

This work is part of the Finnish Research Programme on Nuclear Waste Management (KYT) funded by State Nuclear Waste Management Fund.

References

Callahan, T.J., Reimus, P.W., Bowman, R.S., Haga, M.J., 2000. Using multiple experimental methods to determine fracture/matrix interactions and dispersion of non-reactive solutes in saturated volcanic tuff. Water Resour. Res. 36 (2), 547–558.

Cheng, H., Cvetkovic, V., 2005. Evaluation of the BS2B sorbing tracer tests using the LASAR approach. TRUE Block Scale Continuation Project. Äspö HRL International Progress Report IPR-05-39, Svensk Kärnbränslehantering AB.

Cliffe, K.A., Gilling, D., Jeffries, N.L., Lineham, T.R., 1993. An experimental study of flow and transport in fractured slate. J. Contam. Hydrol. 13, 73.

Drew, D.J., Grondin, D.M., Vandergraaf, T.T., 1990. The Large Block Radionuclide Migration Facility. AECL Report TR-519 27.

Hautojärvi, A., Taivassalo, V., 1994. The Intraval Project – Analysis of the Tracer Experiments at Finnsjön by the VTT/TVO Project Team. Nuclear Waste Commission of Finnish Power Companies. Report YJT-94-24.

Hölttä, P., 2002. Radionuclide migration in crystalline rock fractures – Laboratory study of matrix diffusion. Doctoral Thesis, University of Helsinki. Report Series in Radiochemistry 20/2002, 55 p + Appendices (2002), (<http://ethesis.helsinki.fi>).

Hölttä, P., Poteri, A., Hakanen, M., Hautojärvi, A., 2004. Fracture flow and radionuclide transport in block-scale laboratory experiments. Radiochim. Acta 92, 775–779.

Hölttä, P., Siitari-Kauppi, M., Huittinen, N., Poteri, A., 2007. Determination of Matrix Diffusion Properties of Granitic Rock. In: Scientific Basis for Nuclear Waste Management XXX, Mater. Res. Soc. Proc., vol. 985, pp. 557–562.

Neretnieks, I., 1980. Diffusion in the rock matrix: an important factor in radionuclide retardation? J. Geophys. Res. 85 (B8), 4379.

Park, C.-K., Vandergraaf, T.T., Drew, D.J., Hahn, P.-S., 1997. Analysis of the migration of non-sorbing tracers in a natural fracture in granite using variable aperture channel model. J. Contam. Hydrol. 26, 97–108.

Poteri, A., Billaux, D., Dershowitz, B., Gomez Hernandez, J.J., Cvetkovic, V., Hautojärvi, A., Holton, D., Medina, A., Winberg, A., 2002. Final report of the TRUE Block Scale Project: 3. Modelling of flow and transport. Swedish Nuclear Fuel and Waste Management Company (SKB), Technical Report TR-02-15.

Siitari-Kauppi, M., 2002. Development of ^{14}C-polymethylmethacrylate method for the characterisation of low porosity media. Doctoral Thesis, University of Helsinki, Helsinki. Report series in Radiochemistry 17/2002, 156 p (<http://ethesis.helsinki.fi>).

Tsang, C.F., Tsang, Y.W., Hale, F.V., 1991. Tracer transport in fractures: analysis of field data based on a variable-aperture channel model. Water Resour. Res. 27 (12), 3095–3106.

Vandergraaf, T.T., Drew, D.J., Masuda, S., 1996. Radionuclide migration experiments in a natural fracture in a quarried block of granite. J. Contam. Hydrol. 21, 153–164.

Vandergraaf, T.T., Drew, D.J., Archambault, D., Ticknor, K.V., 1997. Transport of radionuclides in natural fractures: some aspects of laboratory migration experiments. J. Contam. Hydrol. 26, 83–95.

Vilks, P., Baik, M.-H., 2001. Laboratory migration experiments with radionuclides and natural colloids in a granite fracture. J. Contam. Hydrol. 47, 197–210.

Vilks, P., Cramer, J.J., Jensen, M., Miller, N.H., Stanchell, F.W., 2003. In situ diffusion experiment in granite: phase I. J. Contam. Hydrol. 61, 191–202.

PUBLICATION IV

Fracture flow and radionuclide transport in block-scale laboratory experiments

In: Radiochim. Acta 92, pp. 775–779.

http://dx.doi.org/10.1524/ract.92.9.775.55005

Radiochim. Acta **92**, 775–779 (2004)

Fracture flow and radionuclide transport in block-scale laboratory experiments

By P. Hölttä[1,*], A. Poteri[2], M. Hakanen[1] and A. Hautojärvi[3]

[1] University of Helsinki, Laboratory of Radiochemistry, Department of Chemistry, P.O. Box 55, FIN-00014 University of Helsinki, Finland
[2] Technical Research Centre of Finland, VTT Processes, P.O.Box 1000, FIN-02011VTT, Finland
[3] Posiva Oy, FIN-27160 Olkiluoto, Finland

(Received September 26, 2003; accepted March 8, 2004)

Migration / Crystalline rock / Block-scale experiments / Flow field

Summary. Block-scale migration experiments were introduced to evaluate the simplified radionuclide transport concept used in assessing the safety of underground spent nuclear fuel repositories. The experiments were aimed to demonstrate visually the fracture flow, and to determine the hydraulic characteristics of a natural planar fracture and the transport behaviour of non-sorbing and sorbing radionuclides. For drill holes orthogonal to the fracture and equipped with injection or sealing packers flow rates in this study were measured as a function of hydraulic head. The outflow positions of water at each four side of the block were determined using uranine dye tracer. Tracer tests were performed using uranine, ^{99m}Tc and ^{22}Na.

Transport of a non-sorbing tracer through one of the flow channels was interpreted using an advection-dispersion model that on the generalised Taylor dispersion.

Characterisation of the hydraulic properties of the fracture indicated that some drill holes were located in the region where the fracture was open and water conductive. No water conductivity was observed in two drill holes indicating closure of the fracture. Reasonably low flow rates obtained from three drill holes indicated their suitability for further radionuclide transport experiments. Elution times of technetium and uranine were fairly similar. Sodium was slightly retarded and was spread over a wider area than uranine and technetium. High water flow rates suggest that advective flow field dominated tracer transport. Experimental and calculated elution curves substantiate the suitability of our experimental set-up for further radionuclide transport experiments.

1. Introduction

Crystalline rock is being considered as a host medium for repository of highly radioactive spent nuclear fuel in Finland and elsewhere. The geosphere would act as the ultimate barrier retarding the migration of radionuclides to the biosphere if radionuclides are released through engineered barriers. In crystalline rock water flows through a fracture network and radionuclide transport is thought to proceed along water-carrying fractures. Retardation occurs both in the fractures and within the rock matrix. In order to understand the transport of dissolved radionuclides through rock it is necessary to consider both the fracture network geometry and the transport properties of the individual fractures. Ground water flow in fractured granite rock is distributed unevenly causing strong channelling effects, where the water flow occurs mainly over a small proportion of the fracture surface [1–3]. Stagnant water is also found in side fractures, micro fissures and in pores within the rock matrix. Block-scale experiments with natural fractures and only a few flow paths are important intermediate stages between small-scale fracture column and field experiments. The knowledge obtained from transport experiments in well-defined cm to m-scale laboratory conditions provides a basis for m- to km-scale field experiments performed to validate the radionuclide transport concept and to test the transferability of laboratory data to *in-situ* conditions.

Radionuclide transport has been studied in numerous laboratory-scale experiments in single fractures using the column method [4–7] and in block-scale fractures [8–14]. The influence of variable fracture aperture on the transport of non-sorbing solutes in a single fracture was investigated numerically by Grenier *et al.* [15], and the influence of specific surface area and fracture aperture on the transport of sorbing solutes in a fracture was investigated experimentally by Wels *et al.* [16]. Rock-block migration experiments were introduced to evaluate the simplified radionuclide transport concept used in assessing the safety of the underground waste repositories. Such experiments demonstrate visually the fracture flow, and determine the hydraulic characteristics of a natural planar fracture as well as the transport behaviour of non-sorbing and sorbing radionuclides. We describe below the experimental design utilising a large granite block and present hydraulic and first tracer test results.

2. Experimental

The $0.9 \times 0.9 \times 0.7$ m block of fine-grained, non-foliated and equigranular Kuru gray granite (Kuru Quarry, Tampereen Kovakivi Oy) composed of 36% potassium feldspar, 35% quartz, 21% plagioclase and 8% amphibole and mi-

*Author for correspondence (E-mail: pirkko.holtta@helsinki.fi).

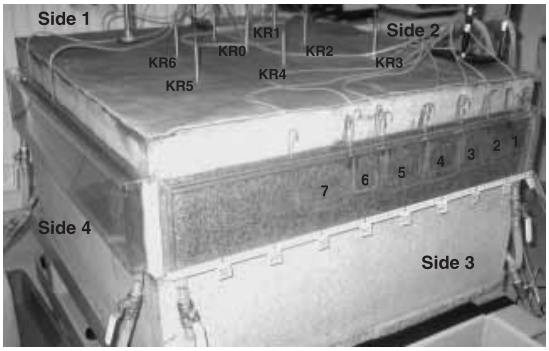

Fig. 1. A photograph of the granite block.

cas, has 0.2% total porosity and 2660 kg m^{-3} density. The single natural horizontal water-conducting planar fracture is located about 17 cm below the top of the block. A drill hole into the centre of the block with 3-cm diameter and eight additional drill holes with 2-cm diameter were drilled orthogonally to the fracture. The drill holes were equipped with injection or sealing packers. An experimental set-up is illustrated in a photograph of the granite block (Fig. 1).

2.1 Hydraulic characterisation of the fracture

Preliminary estimates of water conductivity in the fracture were obtained by observation of water consumption in tubes connected to the drill holes. The total water transmissivity of the fracture was determined by weighing the water consumption as a function of time. A hydraulic head controlled the water flow rate into the fracture through a drill hole. Hydraulic head values were determined as a difference in altitude between a fracture level and a water surface level in a container on scales. To determine channelling in the fracture, water was fed into the fracture from one drill hole at a time while the fracture in the other drill holes was plugged up with packers. Experiments were performed at different hydraulic head values. The outflow positions of water at all four sides of the block were detected and recorded by a video. The water mass flow distribution in different channels was determined by collecting the out flowing water from the main channels.

2.2 Tracer experiments

After hydraulic characterisation of the fracture, the block was surrounded with polymetacrylate pools filled with water (Fig. 1). A 5-mm wide water collection slit near the fracture was separated with a partitioning wall having openings at the bottom of the pool. The pools were constructed to maintain equal pressure conditions all around the fracture area and to avoid external disturbances. The outflow positions of water at all four sides of the block were determined using uranine dye tracer. Water was fed into the fracture from the drill holes labelled KR0, KR1, KR2 and KR5 using three different water flow rates, conrolled by hydraulic heads. A short uranine tracer pulse (5 μl) was injected into the water flow using an injection loop. The outflow points of the tracer were located by following the experiment with a video camera and later with digital camera.

Tracer experiments were performed using drill hole KR1 as the injection point and the tracer was collected from the opposite Side 3 in order to get as long flow path as possible. The fracture area in Side 2 was sealed up with rubber insulation in order to prevent tracer leakage from Side 2. Owing to no uranine leakage Sides 1 and 4 were not sealed. In Side 3 the water collection slit was separated into channels for collection of tracer. A peristaltic pump controlled water flow rate in the tracer transport experiments. Water was fed into the fracture from the drill hole KR1 using different flow rates of 0.2–0.5 ml min^{-1}. A short tracer pulse (50 μl) was injected into the water flow using an injection loop (Rheodyne). Out flowing tracer was collected by pumping and flushing collection channel areas. Uranine and ^{99m}Tc were used as non-sorbing tracers and ^{22}Na as a slightly sorbing tracer. Absorbance of uranine was measured by UV/VIS spectrophotometer and gamma activities of ^{99m}Tc and ^{22}Na were detected using a Wizard gamma counter.

3. Results and discussion

3.1 Hydraulic characterisation of the fracture

No water was consumed by drill holes KR7 and KR8 indicating that these holes were located in an area where the fracture was closed. Table 1 presents the measured water flow rates as a function of the hydraulic head. Hydraulic characterisation of the fracture is based on these measurements.

Pumping of the fracture by applied over-pressure in the drill holes was approximated by a two-dimensional radial flow field. The hydraulic head at distance r from the drill hole is given by Eq. (1)

$$h(r) = h_w - \frac{Q}{2\pi T} \ln\left(\frac{r}{r_w}\right) , \quad (1)$$

where h_w is the hydraulic head in the drill hole, Q is the flow rate, T is the fracture transmissivity and r_w is the ra-

Table 1. Water flow rates (ml min^{-1}) measured from different drill holes using different hydraulic heads (cm).

Hydraulic head/cm	Drill hole water flow rate/ml min^{-1}						
	KR0	KR1	KR2	KR3	KR4	KR5	KR6
24	4.9	1.9	16	35		26	2.2
23							1.2
22	3.9	1.6			19		1.2
21							1.1
20	3.5	1.5	13	27	16	17	1.1
18	2.9	1.5	12			15	1.0
16	2.2	1.3		27	12		0.8
14	1.8	1.1	9.1			12	
12	1.3	1.0	6.7	20	7.5		
10	0.7	0.8				7.9	
8		0.6	5.5	13	3.8	1.8	
6		0.4	4.1			0.6	
4		0.3	2.9	6.7			
2			1.8	3.2			
1			1.2				

dius of the drill hole. The hydraulic head is zero at the outer boundary of the rock block. Radial flow analysis is applied to interpret the tests by assuming that $h(r_0 = 0)$, where r_0 is the distance from the drill hole to the nearest side of the rock block. This may slightly underestimate the transmissivity for the drill holes that are located asymmetrically near to one of the sides. However, a radial flow field corresponds to a linear dependency between the flow rate and the corresponding hydraulic head. This allows a straightforward estimation of the local transmissivity using Eq. (2)

$$T = C\frac{\ln\left(\frac{r_0}{r_w}\right)}{2\pi}, \qquad (2)$$

where C is the slope of the (h_w, Q)-plot.

Estimated local transmissivities were consistent with those detected visually, *i.e.* the fracture opens towards Side 3 and is closed in the corner between Sides 1 and 4. Transmissivities are between 9×10^{-8} m^2 s^{-1} and 2×10^{-6} m^2 s^{-1} and they show the pattern illustrated in Fig. 2. Fracture aperture contours in Fig. 3 were determined by a least squares fit of the linear extrapolation between the data points. Parallel plate aperture corresponding to the mean transmissivity was approximately 0.1 mm.

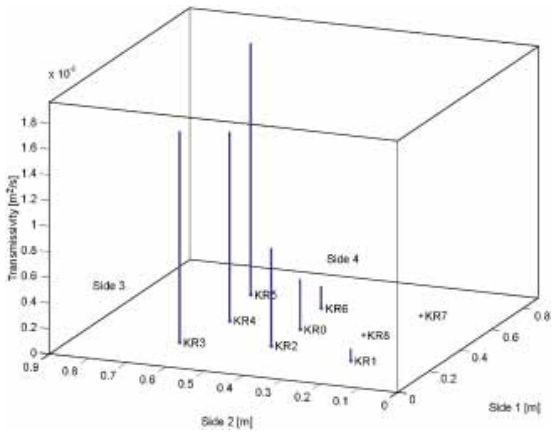

Fig. 2. Local transmissivities determined from the water consumption tests in the drill holes.

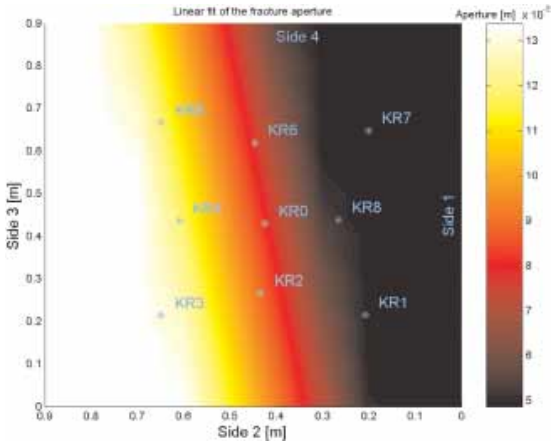

Fig. 3. Fracture aperture contours calculated from the transmissivities (linear fit).

3.2 Tracer tests

Drill hole KR1 was chosen for the tracer transport experiments because hydraulic characterisation and qualitative uranine dye tracer tests indicated that it had the longest flow path. Two different tracer tests were performed. The first test was performed using uranine and technetium. The injection flow rate to the drill hole was approximately 0.35 ml min^{-1}. The second test was performed using uranine, technetium and sodium with an injection flow rate of approximately 0.23 ml min^{-1}. The distance from the injection drill hole KR1 to the collection channels at Side 3 was 70 cm. Both tests showed breakthrough in collection channels 1–6 at the Side 3 (Fig. 1) and in total 80% of injected uranine and technetium was collected from Side 3. In both tests the elution times of technetium and uranine were similar. In some elution curves inadequate consistency arose from measurement problems due to the short half-life of ^{99m}Tc (6 h). In the second test only a slight retardation on sodium was found. The proportional recoveries from different collection channels are presented in Table 2.

Transport of a non-sorbing tracer through one of the flow channels was also modelled. Modelling was performed for channel 2 for both tracer tests. Both tests used an advection-dispersion model based on the generalised Taylor dispersion. It was assumed that a linear velocity profile existed across the flow channel, from zero velocity to some maximum flow velocity, and that the flow field and molecular diffusion perpendicular to the flow dominate the transport of the tracer particles. Hautojärvi and Taivassalo [17] give a more detailed discussion of the problem. The mean concentration across the flow channel for a narrow box-function

Table 2. Proportional recovery of injected uranine, technetium and sodium from different outflow channels in Side 3 with flow rates of 0.35 ml min^{-1} and 0.23 ml min^{-1}.

Outflow channel	Tracer		
	Uranine	^{99m}Tc	^{22}Na
0.35 ml min^{-1}			
1	0.01	0.03	–
2	0.19	0.19	–
3	0.25	0.24	–
4	0.23	0.24	–
5	0.12	0.11	–
6	0.03	0.02	–
7	0.01	0.002	–
0.23 ml min^{-1}			
1	0.19	0.20	0.12
2	0.22	0.21	0.14
3	0.23	0.24	0.10
4	0.17	0.09	0.12
5	0.01	0	0.04
6	0.01	0	0.05
7	0.001	0	0.04

release is given by Eq. (3).

$$C_m = \frac{1}{2}\left(\mathrm{erf}\left[\frac{\frac{1}{2}x_s + x + \xi_1}{2\sqrt{\xi_2}}\right] + \mathrm{erf}\left[\frac{\frac{1}{2}x_s - x - \xi_1}{2\sqrt{\xi_2}}\right]\right);$$

$$\xi_1 = \frac{1}{2}\tau; \quad \xi_2 = \left(\frac{1}{(\mathrm{Pe})^2} + \frac{1}{120}\right)\tau - 8\sum_{n=0}^{\infty}\frac{1 - \mathrm{e}^{-(2n+1)^2\pi^2\tau}}{(2n+1)^8\pi^8};$$

$$\tau = \frac{Dt}{a^2}; \quad x = \frac{Dx}{a^2 v_0}; \quad x_s = \frac{Dx_s}{a^2 v_0}; \quad \mathrm{Pe} = \frac{a^2 v_0}{D}, \qquad (3)$$

where D is the molecular diffusion coefficient in water (10^{-9} m^2 s^{-1} was used in the present analysis), a is the correlation length of the velocity variation (this is approximated here as half of the flow channel width), x_s is the initial width of the tracer plume (for a pulse release this is selected to be small compared to the length of the flow path), v_0 is the maximum flow velocity, is the time and is the position along the channel. The advection component dominated the advection-dispersion model with the flow rates used in this study. The advection-dispersion model of the present study is a purely advective transport characterised by a linear velocity profile over the flow channel.

The flow rate along the flow path that discharged to collection channel 2 was quantified by measuring the recoveries. It was assumed that the tracer mass flux in the different parallel flow channels was proportional to the flow rates of these flow channels. This means that well mixed conditions were assumed close to the injection drill hole KR1 where the different flow paths diverged. Under these assumptions the flow rates of the different flow channels were proportional to the recoveries collected from these channels. Measured recoveries from the collection channel 2 were 19% and 22% for the first and second tracer test, respectively. This yielded flow rates through the flow channel of 4 ml h^{-1} (0.19×0.35 ml min^{-1}) in the first tracer test and 3 ml h^{-1} (0.22×0.23 ml min^{-1}) in the second tracer test. The measured mean breakthrough times for the uranine were 2.5 hours for the first tracer test and 8.8 hours for the second tracer test. This means that the two tests gave slightly different volumes for transport channel 2, *i.e.* about 10 ml and 26 ml using data from the first and the second test, respectively. The variation in the parameters may indicate that the flow path itself may have been slightly different in the first test and in the second test.

After investigating the alternative flow channel geometry it appeared evident that the transport of uranine through flow channel 2 is best described by pure advection. The present analysis applies a linear velocity profile over the channel. This means that the tracer particles have an equal probability for any flow velocity between the minimum and the maximum values. Selecting the minimum flow velocity to be zero and the maximum flow velocity so that the mean flow velocity coincides with the measured average flow velocity, means that in the model the maximum flow velocity is about 0.56 m h^{-1} in the first test and 0.16 m h^{-1} in the second test. In both tests the length of the flow path was 0.7 m.

Modelling results for the uranine breakthrough curves are presented in Fig. 4. Experimental breakthrough curves

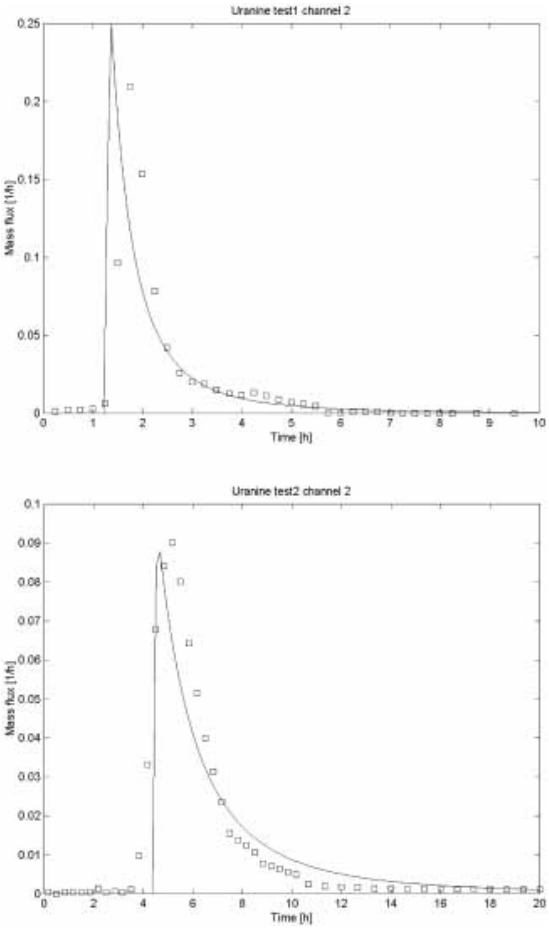

Fig. 4. Measured and modelled uranine breakthrough curves for the collection channel 2 in Side 3 with flow rates of 0.35 ml min^{-1} (upper) and 0.23 ml min^{-1} (lower).

were corrected by taking into account the time that the tracer resided in the tubing: 23 minutes in the first tracer test and 20 minutes in the second tracer test. This very simple model seems to be in quite good agreement with the measured breakthrough curves.

4. Conclusions

The hydraulic properties of the fracture have been characterised. Drill holes KR2-KR5 are located in the area where the fracture is open and water conductive. When the hydraulic head is used to control the water flow rate, than the flow rates from these drill holes are high and the residence times in the fracture are too short for tracer tests. No water conductivity was found in drill holes KR7 and KR8, indicating closure of the fracture in that area. Evaluation of the water consumption tests from drill holes KR0 to KR6 show transmissivities that vary between 9×10^{-8} m^2 s^{-1} and 2×10^{-6} m^2 s^{-1}. The average parallel plate aperture of the fracture was about 0.1 mm. Reasonable low flow

rates were obtained from drill holes KR0, KR1 and KR6. For further radionuclide transport experiments the longest flow paths can be obtained from the drill hole KR1 to Side 3.

Two sets of tracer tests were performed using flow rates of $0.35\,\mathrm{ml\,min^{-1}}$ and $0.23\,\mathrm{ml\,min^{-1}}$. Tracer breakthrough was detected from seven collection channels along Side 3. Elution times of technetium and uranine were quite similar and only slight retardation of sodium was found. It was also noted that sodium spreads over a wider area at Side 3 than do uranine and technetium. The reason for this behaviour is not yet known. However, the obtained elution curves indicate that the experimental set-up is suitable for radionuclide transport experiments. In these experiments the water flow rates were quite high. Modelling results indicate that in both tracer tests the transport was dominated by advective flow field. The study of interaction processes such as matrix diffusion requires lower flow rates in future experiments. The present experimental set-up can be modified for flow rates at least an order of magnitude lower.

Acknowledgment. Financing from Posiva Oy is gratefully acknowledged. We are obligated to Stewart Makkonen-Craig for revising the language of the manuscript.

References

1. Tsang, Y. W., Tsang, C. T., Neretnieks, I., Moreno, L.: Flow and tracer transport in fractured media: a variable aperture channel model and its properties. Water Resourc. Res. **24**(12), 2049 (1988).
2. Tsang, C. F., Tsang, Y. W, Hale, F. V.: Tracer transport in fractures: analysis of field data based on a variable-aperture channel model. Water Resourc. Res. **27**(12), 3095 (1991).
3. Neretnieks, I.: A stochastic multi-channel model for solute transport analysis of tracer test in fractured rock. J. Contam. Hydrol. **55**, 175 (2002).
4. Neretnieks, I., Eriksen, T. E., Tähtinen, P.: Tracer movement in a single fissure in granitic rock. Some experimental results and their Interpretation. Water Resourc. Res. **18**(4), 849 (1982).
5. Callahan, T. J., Reimus, P. W., Bowman, R. S., Haga, M. J.: Using multiple experimental methods to determine fracture/matrix interactions and dispersion of non-reactive solutes in saturated volcanic tuff. Water Resourc. Res. **36**(12), 3547 (2000).
6. Xu, S.: Effect of Uncertainty of Rock Properties on Radionuclide transport by Grounwater – Implications for Performance Assessments of the Repository of Spent Nuclear Fuel in Heterogeneous Bedrock. Doctoral Thesis, University of Uppsala, Uppsala, Sweden (2000).
7. Hölttä, P.: Radionuclie migration in crystalline rock fractures – Laboratory study of matrix diffusion. Doctoral Thesis, University of Helsinki. Report Series in Radiochemistry **20**, 55 (2002) + Appendices.
8. Drew, D. J., Grondin, D. M., Vandergraaf, T. T.: The Large Block Radionuclide Migration Facility. AECL Report TR-519 (1990) p. 27. .
9. Cliffe, K. A., Gilling, D., Jeffries, N. L, Lineham, T. R.: An experimental study of flow and transport in fractured slate. J. Contam. Hydrol. **13**, 73 (1993).
10. Vandergraaf, T. T., Drew, D. J., Masuda, S.: Radionuclide migration experiments in a natural fracture in a quarried block of granite. J. Contam. Hydrol. **21**, 153 (1996).
11. Vandergraaf, T. T., Drew, D. J., Archambault, D., Ticknor, K. V.: Transport of radionuclides in natural fractures: Some aspects of laboratory migration experiments. J. Contam. Hydrol. **26**, 83 (1997).
12. Vilks, P., Bachinski, D. B.: Colloid and suspended particle migration experiments in a granite fracture. J. Contam. Hydrol. **21**, 269 (1996).
13. Park, C.-K., Vandergraaf, T. T., Drew, D. J, Hahn, P.-S.: Analysis of the migration of non-sorbing tracers in a natural fracture in granite using variable aperture channel model. J. Contam. Hydrol. **26**, 97 (1997).
14. Vilks, P., Baik, M.-H.: Laboratory migration experiments with radionuclides and natural colloids in a granite fracture. J. Contam. Hydrol. **47**, 197 (2001).
15. Grenier, C., Mouche, E., Tevissen, E.: Influence of variable fracture aperture on transport of non-sorbing solutes in a fracture: a numerical investigation. J. Contam. Hydrol. **35**, 305 (1998).
16. Wels, C., Smith, L., Vandergraaf, T. T.: Influence of specific surface area on transport of sorbing solutes in fractures: An experimental analysis. Water Resourc. Res. **32**(7), 1943 (1996).
17. Hautojärvi, A., Taivassalo, V.: The Intraval Project – Analysis of the Tracer Experiments at Finnsjön by the VTT/TVO Project Team. Nuclear Waste Commission of Finnish Power Companies. Report YJT-94-24 (1994).

PUBLICATION V

Determination of matrix diffusion properties of granite

In: Mater. Res. Soc. Symp. Proc.
Vol. 985, 6 p.

Mater. Res. Soc. Symp. Proc. Vol. 985 © 2007 Materials Research Society 0985-NN11-11

Determination of Matrix Diffusion Properties of Granite

Pirkko Holtta[1], Marja Siitari-Kauppi[1], Nina Huittinen[1], and Antti Poteri[2]
[1]Laboratory of Radiochemistry, P.O. Box 55, University of Helsinki, FI-00014, Finland
[2]VTT Processes, P.O. Box 1608, VTT, FI-02044, Finland

ABSTRACT

Rock–core column experiments were introduced to estimate the diffusion and sorption properties of Kuru Grey granite used in block–scale experiments. The objective was to examine the processes causing retention in solute transport through rock fractures, especially matrix diffusion. The objective was also to estimate the importance of retention processes during transport in different scales and flow conditions. Rock–core columns were constructed from cores drilled into the fracture and were placed inside tubes to form flow channels in the 0.5 mm gap between the cores and the tube walls. Tracer experiments were performed using uranine, HTO, ^{36}Cl, ^{131}I, ^{22}Na and ^{85}Sr at flow rates of 1–50 $\mu L \cdot min^{-1}$. Rock matrix was characterized using ^{14}C–PMMA method, scanning electron microscopy (SEM), energy dispersive X–ray micro analysis (EDX) and the B.E.T. method.

Solute mass flux through a column was modelled by applying the assumption of a linear velocity profile and molecular diffusion. Coupling of the advection and diffusion processes was based on the model of generalised Taylor dispersion in the linear velocity profile. Experiments could be modelled applying a consistent parameterization and transport processes. The results provide evidence that it is possible to investigate matrix diffusion at the laboratory scale. The effects of matrix diffusion were demonstrated on the slightly–sorbing tracer breakthrough curves. Based on scoping calculations matrix diffusion begins to be clearly observable for non–sorbing tracer when the flow rate is 0.1 $\mu L \cdot min^{-1}$. The experimental results presented here cannot be transferred directly to the spatial and temporal scales that prevail in an underground repository. However, the knowledge and understanding of transport and retention processes gained from this study is transferable to different scales from laboratory to in–situ conditions.

INTRODUCTION

Crystalline rock is being considered as a host medium for the repository of highly radioactive spent nuclear fuel in Finland and elsewhere. The geosphere would act as the ultimate barrier retarding the migration of radionuclides to the biosphere if radionuclides were to be released through engineered barriers. In crystalline rock water flows through a fracture network and radionuclide transport is thought to proceed along water–carrying fractures. Retardation occurs both in the fractures and within the rock matrix. The experimental column method used in this study was a direct approach for determining the parameters affecting the fracture flow described in radionuclide transport models. Radionuclide transport has been studied in the Finnish program earlier using flow–through fracture and crushed rock columns [1, 2]. Fracture flow and radionuclide transport have been studied in block–scale experiments using Kuru Grey granite [3–5]. The objectives of those studies were to examine the processes causing retention in solute transport through rock fractures, especially matrix diffusion. The results can be used to estimate importance of retention processes during transport in different scales and flow conditions. Rock–core column experiments

were introduced to estimate the diffusion and sorption properties of Kuru Grey granite used in block–scale experiments. The results of this work will be used to estimate radionuclide transport times and retardation parameters in artificial fractures before conducting block–scale experiments in natural fracture. We describe below the rock matrix characterization and the experimental design utilising rock–core columns as well as present tracer test results and scoping calculations.

ROCK MATRIX CHARACTERIZATION

Kuru Grey granite was obtained from Kuru Quarry, Tampereen Kovakivi Oy, Finland. The total porosity and the surface areas of mineral grains available for sorption and migration of species were determined by the ^{14}C-PMMA method [6, 7]. Pore apertures and geometry in the mineral phases were analyzed by scanning electron microscopy (SEM), and the minerals and sorbed tracer were quantified by energy dispersive X-ray microanalysis (EDX). The specific surface area of the solid rock was determined by the B.E.T. Hg impregnation method. Kuru Grey granite is fine–grained, non–foliated and equigranular with composition of 36% potassium feldspar, 35% quartz, 21% plagioclase and 8% amphibole and micas. Its density given by Tampereen Kovakivi Oy is 2660 kg·m^{-3}. The total bulk porosity determined by water gravimetry and ^{14}C–PMMA method was 0.4 %. The average grain size determined by SEM was 0.5–1.5 mm. The specific surface area was 0.03 m^2·g^{-1} and the average pore diameter was 300–400 nm. A photo image of Kuru Grey granite and corresponding ^{14}C–PMMA autoradiograph showing the spatial porosity distribution is shown in Figure 1. Grain boundary porosity dominates, though intragranular porosity was observed in biotite and feldspar grains. Due to drilling the core and sawing the sample, the disturbed zone occupied a depth of 1 mm from the surface.

EXPERIMENTS

The experimental design for our rock–core column experiments is shown in Figure 2. Cores drilled perpendicular to the horizontal natural fracture of the Kuru Grey granite block were glued in series to form two longer rods, one (Core I) 74.5 cm long and the other (Core II) 68.5 cm long. In addition one short rod (Core III) of length about 28 cm was also employed in the experiments. Each rod, which had a diameter of 14 mm, was placed inside a plastic tube with an inner diameter of 15 mm, forming a flow channel in the 0.5 mm gap between the rod and the tube walls. The core-tube gap represents an artificial fracture. The volume of the flow channel in the 74.5 cm column was about 17 mL and that of the connecting tubing about 1.3 mL. Tracer experiments were performed using a peristaltic pump to control water flow rate. Water was fed into the columns at different flow rates of 1–50 µL·min^{-1}. A short tracer pulse (5 µL) was injected into the water flow using an injection loop (Rheodyne) and the out flowing tracer was collected. A large number of tracer tests were performed using different tracers and different rock cores. Uranine, HTO, ^{36}Cl and ^{131}I were used as non-sorbing tracers, ^{22}Na as a slightly sorbing tracer, and ^{85}Sr as a sorbing tracer. The optical absorbance of uranine at 491 nm was measured by UV/VIS spectrophotometer, beta activities of HTO and ^{36}Cl were determined by liquid scintillation counting and gamma activities of ^{22}Na, ^{85}Sr and ^{131}I were detected using a Wizard gamma counter. Synthetic granitic groundwater equilibrated with crushed rock material was used in all experiments.

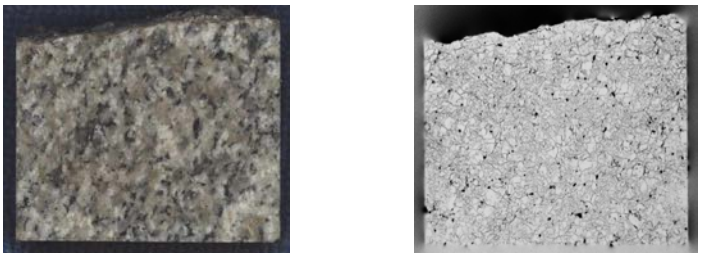

Figure 1. Photo micrograph of Kuru Grey granite and corresponding ^{14}C–PMMA autoradiograph showing the spatial porosity distribution.

Figure 2. Photograph of the experimental set-up.

RESULTS AND DISCUSSION

Several tracer tests were performed using uranine, HTO, ^{36}Cl and ^{131}I as non-sorbing, ^{22}Na as a slightly sorbing and ^{85}Sr as a sorbing tracer with injection flow rates 1–50 $\mu L \cdot min^{-1}$. All tracer tests were modelled to assess the influence of matrix diffusion in different tests. Solute mass flux through the transport channel was modelled by applying the assumption of a linear velocity profile and molecular diffusion. Coupling of the advection and diffusion processes was based on the model of generalised Taylor dispersion in the linear velocity profile. The model accounted for molecular diffusion both in the longitudinal direction and across the velocity profile. A detailed discussion of the problem and solution to the transport problem is given by Hautojärvi and Taivassalo [8].

Solute discharge at the end of the transport channel for the delta function release can be written as

$$j(t,t_w,u,R_a) = H(t-R_a t_w)\frac{u}{\sqrt{\pi}\left(t-R_a t_w\right)^{3/2}} e^{-\frac{u^2}{t-R_a t_w}} , \qquad (1)$$

where parameter u determines the strength of the matrix diffusion, t_w is the groundwater transit time and R_a is the surface retardation coefficient. H is the cumulative distribution function.The matrix diffusion property (u) is defined as

$$u = \varepsilon\sqrt{D_p R_p}\,\frac{W\,L}{Q} = \varepsilon\sqrt{D_p R_p}\,\frac{t_w}{2b} , \qquad (2)$$

where t_w is the groundwater transit time, $2b$ is the channel aperture, D_p is the matrix pore diffusivity, ε is the matrix porosity and R_p is the retardation coefficient in the matrix. The last part of the parameter u, $t_w/(2b)$, is also presented as WL/Q. This parameter represents the coupling of the matrix diffusion to the flow field by ratio Q/W, i.e. flow rate per width and to the length of the channel L. Sorption was modelled as linear equilibrium sorption, both in the pore space of the rock matrix and on the outer surface of the core. Solute transport with matrix diffusion and sorption was calculated by integrating over the solute mass flux distribution according to Equation (3).

$$k(t) = \int_0^t j(t,t_w,U_t\,t_w,R_a)b(t_w)dt_w , \qquad (3)$$

where $b(t_w)$ is the solute mass flux distribution in the mobile pore space and $j(t,t_w,U_t,R_a)$ is the corresponding sorption matrix diffusion breakthrough curve (Equation (1)).

This modelling work indicated that tests carried out with Core I had flow rates too high for clear indication of matrix diffusion. Tracer tests with the shortest core, Core III, were performed using a wide range of different tracers and flow rates. However, difficulties were faced in reproducing consistently the non-sorbing tracer breakthrough curves for different flow rates. Core II provided a consistent series of experimental results, and since it was longer than the Core III it emphasized the importance of matrix diffusion as a retention process. For this reason the main modelling effort focused on experiments performed using Core II. Breakthrough curves were modelled applying rock matrix characteristics and parameters estimated from previous experiments. The matrix pore diffusivity, D_p, was calculated from the rock porosity by applying Archie's law. The sorption properties of sodium were estimated from the values determined for Syyry mica gneiss and unaltered tonalite using fracture and crushed rock columns [2]. The modelled breakthrough curves were calculated by assuming instantaneous release of the tracer (Dirac's delta function). The influence of tubing and other experimental equipment on the breakthrough curves was determined by performing tracer tests without the rock column. The modelled breakthrough curves for transport through the rock column were convoluted with a response function of the tubing before being compared with the measured experimental break-through curves.

Examples of the modelled and observed breakthrough curves for uranine and ^{22}Na are presented in Figure 3. Especially interesting are the tailings of the low flow rate breakthrough curves. In the experimental breakthrough curves there appears to be clear differences in the tailings of uranine and ^{22}Na. In the modelled curves this behaviour is explained well by the stronger matrix diffusion effect in ^{22}Na breakthrough curves due to the sorption of ^{22}Na in the pore space of the rock matrix.

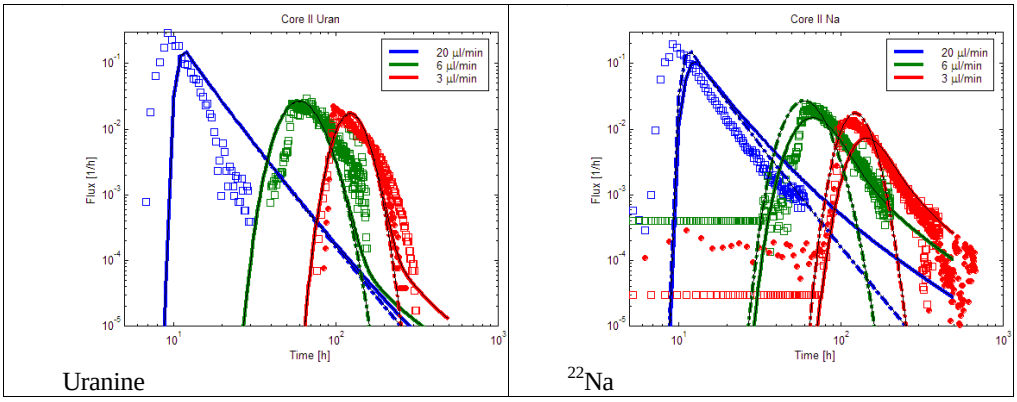

Figure 3. Modelled and measured breakthrough curves for uranine and ^{22}Na through the Core II column. Flow rates were 20 µL·min^{-1} (left), 6 µL·min^{-1} (middle) and 3µL·min^{-1} (right). Solid lines are modelled results for advection and matrix diffusion. Dotted lines are for the advection only.

The breakthrough curve for the highest flow rate was not well reproduced by the model. Reason for that was pump failure that resulted in the faster flow rate than set and used in model calculations. The breakthrough curve with the fastest flow rate, 20 µL·min^{-1}, was more advection–dispersion dominated than controlled by the matrix diffusion.

The matrix diffusion model applied in the modelling was based on the assumption of infinite rock matrix depth. The diameter of the borehole core was 14 mm and so it was necessary to estimate the possible influence of the limited thickness of the rock matrix to the breakthrough curves. One–dimensional calculations show that in the case of a non–sorbing tracer and limited rock matrix thickness, the breakthrough curve begins to deviate from the infinite rock matrix breakthrough curve at time $t \sim R_a t_w + R_p L_z^2 / D_p$, where t_w is the advective delay in the transport channel, R_a is the retardation coefficient for surface sorption, R_p is the retardation coefficient in the rock matrix, L_z is the thickness of the matrix, and D_p is the pore diffusivity. For a 5–mm layer of rock, the limited matrix thickness starts to influence a non-sorbing tracer breakthrough curve at around t ~ 240 h; for moderately-sorbing ^{22}Na, the breakthrough effect begins at t ~ 48 000 h. This means that it is possible that the uranine breakthrough curve shows some effects of the limitation in matrix thickness, but this is unlikely for ^{22}Na. Finite thickness would result in reflective boundary conditions in which tracer transport approaches a steady state. Then all the molecules statistically experience the same velocities having equal transport time within a Gaussian distribution [2].

Scoping calculations were made to estimate how slow flow rates are needed to show the effects of matrix diffusion for non–sorbing tracers. The scoping calculations at decreased flow rates were based on the geometrical dimensions and evaluation of existing models and column tests. These calculations show that matrix diffusion begins to be observable for a non–sorbing tracer when the flow rate is around 0.1 µL·min^{-1} for the column experiment. The advection–governed tests were sensitive to transport porosity (i.e. transport to hydraulic aperture ratio x hydraulic volume), and the shape of the curve was sensitive to correlation length in the velocity profile. In scoping calculations the channel geometry, i.e. the effective channel width that influences the matrix diffusion, was based purely on geometrical considerations.

CONCLUSIONS

Rock–core column experiments were performed to estimate the diffusion and sorption properties of Kuru Grey granite used in block–scale experiments. The experiments could be modelled by applying consistent parameterization and transport processes. The processes, advection–dispersion and matrix diffusion, were conceptualized with sufficient accuracy to replicate the experimental results. The results of the experiments provided evidence that it is possible to investigate matrix diffusion at the laboratory scale. The effects of matrix diffusion were demonstrated on the slightly sorbing tracer breakthrough curves. Based on scoping calculations matrix diffusion begins to be clearly observable for a non–sorbing tracer when the flow rate is below 0.1 $\mu L \cdot min^{-1}$. The modelled experiment builds confidence on the model predictions of the solute retention in groundwater flow. The experimental results presented here cannot be transferred directly to the spatial and temporal scales that prevail in the underground repository. However, this knowledge and understanding of the transport and retention processes is transferable to different scales from laboratory to in–situ conditions.

ACKNOWLEDGMENTS

This work is part of the Finnish Research Programme on Nuclear Waste Management (KYT2010) funded by the State Nuclear Waste Management Fund. The authors would like to thank Mr. Steward Makkonen-Craig for revising the language.

REFERENCES

1. I. Neretnieks, T. E. Eriksen, and P. Tähtinen, *Water Resourc. Res.* **18 (4)**, 849 (1982).
2. P. Hölttä, "Radionuclie migration in crystalline rock fractures–Laboratory study of matrix diffusion," Doctoral Thesis, University of Helsinki. Report Series in Radiochemistry 20/2002, 55 p. + Appendices (2002).
3. P. Hölttä, A. Poteri, M. Hakanen and A. Hautojärvi, *Radiochimica Acta* **92**, 775 (2004).
4. A. Poteri and P. Hölttä, Technical Research Centre of Finland Research Report. VTT/PRO1/1008/05, 37 p (2005).
5. A. Poteri and P. Hölttä, Technical Research Centre of Finland Research Report. VTT-R-03919-06, 25 p. (2006).
6. K-H. Hellmuth, M. Siitari-Kauppi and A. Lindberg, *Journal of Contaminant Hydrology* **13**, 403 (1993).
7. M. Siitari-Kauppi, "Development of ^{14}C-polymethylmethacrylate method for the characterisation of low porosity media," Doctoral Thesis, University of Helsinki. Report Series in Radiochemistry 17/2002, 156 p (2002).
8. A. Hautojärvi and V. Taivassalo, Nuclear Waste Commission of Finnish Power Companies. Report YJT-94-24 (1994).

Series title and number
VTT Science 42

Title	**Simplifying solute transport modelling of the geological multi-barrier disposal system**
Author(s)	Antti Poteri
Abstract	A simplified model was developed to represent radionuclide migration from a deep geological nuclear waste repository system to the biosphere. The modelled repository system is based on the concept of multiple nested transport barriers. The model can be used to assess migration and migration properties of single nuclides (no decay chains) through the repository system. Radionuclide transport processes included to the model are diffusion and sorption in the repository near-field and advection, matrix diffusion and sorption in the geosphere. A simplified approach to handle solubility limited release of the nuclide from the waste canister is included into the model. The model treats transport barriers as well-mixed volumes. It is also assumed that radionuclide outflow from a barrier can be calculated by negleting radionuclide concentration in the target barrier. Radionuclide transport through the simplified system can be calculated by applying formal analogy of the model to the mathematical model of the radioactive decay chain. Simplifying the barriers as well-mixed volumes suggests that they can be characterised by simple performance measures. Radionuclide outflow from the barrier can be represented by an equivalent flow rate, which is an apparent volumetric flow rate that combined with the radionuclide concentration in the barrier gives the outflow rate of the nuclide. Temporal behaviour of the release rate can be described by two time constants: i) compartment half-life of the nuclide concentration calculated by dividing capacity of the barrier (the total pore volume multiplied by the retardation factor) with the equivalent flow rate and ii) delay time for start of the outflow from barrier after beginning of the inflow to barrier. Performance of the simplified approach to produce actual release rates for different nuclides was tested by modelling C-14, I-129 and Pu-239 using data from the RNT-2008 radionuclide migration analysis. Accuracy of the simplified approach is challenged if the nuclide's half-life is not long compared to the time required for the development of perfectly mixed solute concentration field in the barrier. The nuclide and barrier combinations that are prone to this behaviour can be identified by comparing the estimated compartment delay time with the nuclide's radioactive half-life. The simplified model performed well for the C-14 and I-129, as expected based on the measures above. Early transients of the concentration field in the buffer and in the geosphere are important for the transport of Pu-239 in the calculated case. The simplified model gave results for Pu-239 that were roughly of the same order of magnitude than the corresponding numerical results.
ISBN, ISSN	ISBN 978-951-38-8097-2 (Soft back ed.) ISBN 978-951-38-8098-9 (URL: http://www.vtt.fi/publications/index.jsp) ISSN-L 2242-119X ISSN 2242-119X (Print) ISSN 2242-1203 (Online)
Date	October 2013
Language	English, Finnish abstract
Pages	63 p. + app. 141 p.
Name of the project	
Commissioned by	
Keywords	Nuclear waste, repository system, migration, modelling
Publisher	VTT Technical Research Centre of Finland P.O. Box 1000, FI-02044 VTT, Finland, Tel. 020 722 111

Julkaisun sarja ja numero
VTT Science 42

Nimeke	**Moniesteperiaatteeseen perustuvan geologisen loppusijoitusjärjestelmän yksinkertaistettu kulkeutumismalli**
Tekijä(t)	Antti Poteri
Tiivistelmä	Tässä työssä on kehitetty yksinkertaistettu malli kuvaamaan radionuklidien kulkeutumista geologisesta loppusijoitustilasta maanpinnalle. Mallinnettu loppusijoitusjärjestelmä perustuu moniesteperiaatteeseen. Mallin avulla on mahdollista arvioida yksittäisen nuklidin kulkeutumista ja kulkeutumisominaisuuksia loppusijoitussysteemissä. Kulkeutumisprosesseista malli sisältää loppusijoitustilan lähialueella diffuusion ja sorption sekä geosfäärissä kulkeutumisen pohjaveden virtauksen mukana, matriisidiffuusion ja sorption. Malliin on lisätty myös yksinkertaistettu kuvaus nuklidin liukoisuusrajoitteiselle vapautumiselle loppusijoituskapselista. Vapautumisesteet kuvataan mallissa hyvin sekoitettuina tilavuuksina ja massasiirron vapautumisesteestä ulos oletetaan riippuvan konsentraatiosta vain tarkasteltavassa vapautumisesteessä. Tällainen systeemi on matemaattisesti analoginen radioaktiivisen hajoamisketjun kanssa. Tätä analogiaa käytetään hyväksi laskettaessa radionuklidien kulkeutuminen loppusijoitussysteemin läpi. Hyvin sekoitetun tilavuuden malli mahdollistaa vapautumisesteen toiminnan kuvaamisen muutamalla tunnusluvulla. Nuklidin vapautumisnopeus loppusijoitusjärjestelmän vapautumisesteestä voidaan esittää ekvivalentin virtaaman avulla. Ekvivalentti virtaama on näennäinen tilavuusvirtaama, joka pitoisuuteen yhdistettynä antaa aineen massavirran. Vapautumisnopeuden aikakehitystä voidaan kuvata kahdella vapautumiseste- ja nuklidikohtaisella aikavakiolla: i) nuklidin pitoisuuden puoliintumisaika, joka voidaan laskea jakamalla vapautumisesteen nuklidikohtainen kapasiteetti (huokostilavuuden ja nuklidikohtaisen pidätyskertoimen tulo) nuklidin ekvivalentilla virtaamalla ulos vapautumisesteestä sekä ii) massan siirron viipymäaika vapautumisesteessä. Yksinkertaistetun mallin kykyä arvioida radionuklidien vapautumisnopeuksia testattiin mallintamalla nuklidien C-14, I-129 ja Pu-239 aktiivisuusvirrat yhdelle RNT-2008 kulkeutumisanalyysin laskentatapaukselle. Mallin tarkkuus heikkenee, jos nuklidin radioaktiivinen puoliintumisaika ei ole pitkä verrattuna aikaan, joka vaaditaan hyvin sekoitetun pitoisuuden saavuttamiseen vapautumisesteessä. Tällaiset nuklidit ja vapautumisesteparit on kuitenkin mahdollista tunnistaa vertaamalla nuklidin radioaktiivista puoliintumisaikaa ja massan siirron viivettä vapautumisesteessä. Malli tuotti vertailuna käytetyn numeerisen mallin kanssa yhtenevät tulokset nuklideille C-14 ja I-129, kuten edellä mainitun vertailun perusteella oli odotettavissa. Pu-239:n puoliintumisajan ja kulkeutumisnopeuden perusteella sen vapautumisnopeudet lasketussa tapauksessa sekä sijoitusreiän täyteaineesta että geosfääristä voivat määräytyä pitoisuuskentän transienttisesta käyttäytymisestä vapautumisesteessä. Mallin tuottamat tulokset vapautumisnopeudelle ovat kuitenkin tässäkin tapauksessa suunnilleen samaa suuruusluokkaa kuin numeerisen mallin tulokset
ISBN, ISSN	ISBN 978-951-38-8097-2 (nid.) ISBN 978-951-38-8098-9 (URL: http://www.vtt.fi/publications/index.jsp) ISSN-L 2242-119X ISSN 2242-119X (painettu) ISSN 2242-1203 (verkkojulkaisu)
Julkaisuaika	Lokakuu 2013
Kieli	Englanti, suomenkielinen tiivistelmä
Sivumäärä	63 s. + liitt. 141 s.
Projektin nimi	
Toimeksiantajat	
Avainsanat	Nuclear waste, repository system, migration, modelling
Julkaisija	VTT PL 1000, 02044 VTT, Puh. 020 722 111

Simplifying solute transport modelling of the geological multi-barrier disposal system

Spent nuclear fuel from Finnish nuclear power plants is planned to be disposed of in a geological repository hosted in deep crystalline bedrock. The plans in Finland are based on the Swedish KBS-3 concept, in which the waste is encapsulated into corrosion resistant copper canisters that are disposed of at about 400–500 m depth in the bedrock. The repository system is based on multiple nested transport barriers that should prevent possible future disturbances to impair tightness of the waste canisters and to limit radionuclide release rates to the biosphere in case there is a leaking waste canister.

Safety analysis of the deep underground repository needs to consider the possible release of radionuclides from the waste canister and the potential for subsequent migration of the radionuclides from the repository to the biosphere. Commonly, radionuclide migration in these analyses has been largely based on the application of a suit of nested numerical codes. Numerical models are a necessity when geometrically, physically and chemically detailed and complicated systems are modelled. A drawback of numerical models, however, is the difficulty in evaluating and elucidating the role and importance of individual transport barriers to hinder radionuclide migration as well as key processes and parameters with regard to the performance of the system as a whole. Understanding the main characteristics of the system is better achieved by the use of simplified concepts.

This thesis presents a simplified approach that can be used to study and demonstrate the main characteristics of the repository system that limit the radionuclide migration. Performance of the simplified approach to produce actual release rates for different nuclides has been tested against numerical modelling results.

ISBN 978-951-38-8097-2 (Soft back ed.)
ISBN 978-951-38-8098-9 (URL: http://www.vtt.fi/publications/index.jsp)
ISSN-L 2242-119X
ISSN 2242-119X (Print)
ISSN 2242-1203 (Online)